Regulation of the LAMMER Kinase Kns1, a TORC1 Effector and RNA Pol III Modulator in *Saccharomyces cerevisiae*

DISSERTATION ZUR ERLANGUNG DES
DOKTORGRADES DER NATURWISSENSCHAFTEN (DR. RER. NAT.)
DER FAKULTÄT FÜR BIOLOGIE UND VORKLINISCHE MEDIZIN
DER UNIVERSITÄT REGENSBURG

vorgelegt von
Simone Fabian

aus
Kaufbeuren

im Jahr
2024

Das Promotionsgesuch wurde eingereicht am: 06.06.2024

Die Arbeit wurde angeleitet von: Prof. Dr. Wolfgang Seufert

Unterschrift**:** _____

“Nothing in life is to be feared, it is only to be understood. Now is the time to understand more, so that we may fear less.”

– Marie Curie

Table of contents

1 ABSTRACT

The major regulator of cell growth, TORC1, mediates the stress response through conserved LAMMER kinases. In humans, these proteins play significant roles in the treatment of cancer and metabolic disorders. Human LAMMER kinases are well understood, but Kns1, a member of the LAMMER kinases in the yeast *S. cerevisiae*, is not yet well characterised in terms of its functions and regulation. Kns1 has the potential for various functions under unfavourable conditions, and its structure has not been resolved. An *in vivo* study confirmed that Kns1, a negative effector kinase of TORC1, directly phosphorylates Rpc53, a regulatory subunit of RNA polymerase III, under TORC1-inhibited conditions. Hyperphosphorylation of Rpc53 inhibits RNA polymerase III reinitiation, thereby reducing its activity.

This study investigated the regulation of Kns1 and its role in stress response. To gain a deeper understanding of its role, we examined the properties of the Kns1 protein. We employed various non-preferential carbon sources and mutants that replicated diminished global translation initiation, inhibited glycolytic flux, or blocked TORC1 activity to investigate the consequences on Kns1. The research unveils that Kns1 protein levels increase under stress, and elevated Rpc53 phosphorylation suggests a direct effect on RNA polymerase III activity. This study proposes that Kns1 protein levels rise due to the integrated stress response and altered carbon source availability, suggesting a novel regulation for Kns1-facilitated RNA polymerase III inhibition under unfavourable conditions.

The regulation of Kns1 is intricate and occurs rapidly under changing conditions. RNA sequencing data from prior studies have indicated increased mRNA levels in the presence of reduced global translation initiation, and preliminary findings from the current study suggest a similar trend for non-optimal carbon sources. The precise mechanism underlying the differential transcription remains unclear, but *KNS1* transcription is likely regulated by stress-dependent transcription factors and could include a carbon source-responsive element (CSRE). An increase in translation under non-optimal conditions, similar to Gcn4, is also possible. This study suggests that Kns1 is an unstable protein under favourable conditions but becomes slightly stabilised under stress response, supposedly due to an increase in autophosphorylation.

Overall, this study uncovered a new physiological role for Kns1 in the nutrient stress response, which is likely activated through increased transcription, changes in protein localisation, and stabilisation by autophosphorylation.

2 ZUSAMMENFASSUNG

Der Schlüsselregulator des Zellwachstums, TORC1, ist verantwortlich für die Stressantwort und vermittelt diese durch die konservierten LAMMER Kinasen. Diese Kinasen spielen beim Menschen eine bedeutende Rolle als Ziel für potenzielle Behandlungen von Krebs und Stoffwechselstörungen. Während die humanen LAMMER Kinasen ausführlich untersucht wurden, sind Funktion und Regulation der *S. cerevisiae* Kinase Kns1 noch nicht umfassend charakterisiert. Kns1 hat das Potenzial, unter ungünstigen Bedingungen verschiedene Funktionen zu übernehmen, und seine Struktur wurde bisher nicht aufgeklärt. Eine *in vivo* Studie bestätigte Kns1 als negativen Effektor von TORC1, und zeigte, dass Kns1 unter TORC1-inhibierten Bedingungen Rpc53, eine regulatorische Untereinheit der RNA Polymerase III, direkt phosphoryliert. Die Hyperphosphorylierung von Rpc53 hemmt die Reinitiation der RNA Polymerase III und reduziert somit ihre Aktivität.

Diese Arbeit untersucht die Regulation von Kns1 und dessen Rolle in der Stressantwort. Um ein tieferes Verständnis seiner Funktion zu erlangen, wurden die Proteineigenschaften von Kns1 analysiert. Verschiedene nicht bevorzugte Kohlenstoffquellen und Mutanten, die eine verminderte globale Translationsinitiation, einen gehemmten glykolytischen Fluss oder eine inhibierte TORC1 Aktivität nachahmen, wurden verwendet, um die Auswirkungen auf Kns1 zu untersuchen. Die Ergebnisse zeigen, dass die Kns1 Proteinmenge unter Stressbedingungen signifikant ansteigt. Die erhöhte Rpc53 Phosphorylierung weist außerdem auf eine direkte Beeinflussung der RNA Polymerase III Aktivität hin. Die Studie legt nahe, dass die Kns1 Proteinmengen aufgrund der „*integrated stress response*“ und veränderter Kohlenstoffquellenverfügbarkeit ansteigen, was auf eine neue Regulation von Kns1 in der Inhibition der RNA Polymerase III unter ungünstigen Bedingungen hinweist.

Die Regulation von Kns1 ist komplex und erfolgt schnell als Reaktion auf sich ändernde Bedingungen. RNA-Sequenzierungsdaten aus vorherigen Studien deuteten auf erhöhte mRNA-Level bei reduzierter globaler Translationsinitiation hin, und vorläufige Ergebnisse der aktuellen Studie zeigen einen ähnlichen Trend für nicht optimale Kohlenstoffquellen. Der genaue Mechanismus der spezifischen Transkription bleibt unklar, jedoch könnte die Transkription von *KNS1* durch stressabhängige Transkriptionsfaktoren oder durch ein kohlenstoffabhängiges Element („*CSRE*“) reguliert werden. Eine Zunahme der Translation unter nicht optimalen Bedingungen, ähnlich wie bei Gcn4, ist ebenfalls möglich. Die Studie legt nahe, dass Kns1 unter günstigen Bedingungen ein instabiles Protein ist, aber während der Stressantwort, vermutlich durch erhöhte Autophosphorylierung, stabilisiert wird.

Insgesamt deutet die Studie auf eine neue physiologische Rolle für Kns1 in der Nährstoffstressantwort hin, die wahrscheinlich durch erhöhte Transkription, Änderungen in der Lokalisierung des Proteins und Stabilisierung durch Autophosphorylierung aktiviert wird.

3 INTRODUCTION

Saccharomyces cerevisiae is a single-celled fungus that offers a streamlined approach to examining processes that are similar or even homologous to those found in multicellular organisms. The genome of *S. cerevisiae*, consisting of approximately 6,000 genes, is carried on 16 linear chromosomes and was first fully sequenced in 1996 (Goffeau *et al.* 1996). The non-motile, non-pathogenic yeast can be easily cultivated in both batch and continuous cultures (Busti *et al.* 2010). *S. cerevisiae* is a facultative anaerobic organism that utilises fermentation as the main energy production pathway, and its generation time is relatively short (approximately 90 min). It can survive as both haploid and diploid cells through mitotic division (Zeyl 2000). Yeast has become a highly valuable and well-understood model organism for studying eukaryotic genetics and population dynamics because of its easy manipulation and the wide range of available molecular techniques (Goffeau *et al.* 1996; Zeyl 2000; Busti *et al.* 2010). In *S. cerevisiae*, energy production is mainly dependent on glucose, which also serves as a crucial signalling molecule (Ashe *et al.* 2000). The behaviour of yeast cells is determined by the nutrient environment. When glucose levels are depleted, cells undergo various changes in gene expression and protein synthesis to compensate for the change in nutrients and adapt their growth rates (Busti *et al.* 2010; Broach 2012). Furthermore, cell cycle progression is highly dependent on energy availability, and fast entry into the cell cycle at the G_1/S transition only occurs when environmental conditions are sufficient (DeBerardinis *et al.* 2008; Busti *et al.* 2010; Broach 2012).

3.1 Overview of yeast growth

As described above, *S. cerevisiae* has a fast cell division cycle of approximately 90 min under optimal conditions (Busti *et al.* 2010). When sufficient nutrients are available and the intracellular protein composition is sufficient, cells undergo a cell cycle starting in the G_1 phase, going through the S and G_2 phases, and ending in mitosis, with each cell division leading to a duplication of cells (Busti *et al.* 2010; Suryadinata *et al.* 2010). In addition, growth behaviour can be altered depending on the nutrient availability. An accurate cell cycle requires energy, and only optimal conditions lead to a rapid increase in cell mass within colonies through exponential growth. However, adaptations to unfavourable conditions may lead to reduced growth rates. In summary, the viability of yeast cells is dependent on the connection between cell division and growth, and is adaptable to external and internal conditions (Futcher 1990). More precisely, only one cell cycle may occur for every mass doubling to ensure high viability.

3.1.1 Principles of cell cycle progression

The eukaryotic cell cycle, an evolutionarily conserved process from yeast to humans, leads to the generation of daughter cells from the genetic and cellular components of the mother cell (Suryadinata *et al.* 2010; Jiménez *et al.* 2015). One cell cycle consists of four phases: G_1, S, G_2, and M (Figure 3.1). In the G_1 phase, the first gap phase of each cell cycle, cells must reach a certain threshold of nutrients, small molecules, and organelles, as well as a critical cell size to start the cell cycle (Hartwell 1974; Dirick *et al.* 1995; Alberghina *et al.* 2004). Once the threshold is reached and cells pass the START checkpoint, they commit to the entire cell cycle (Hayles and Nurse 1986; Futcher 1990). This all-or-nothing reaction determines the fate of the cell for another round of cell division. In the subsequent S phase, the synthesis phase, DNA is replicated (Figure 3.1), resulting in the formation of sister chromatids connected by proteins in the cohesin complex, and a bud emerges (Hartwell 1974; Kalitsis *et al.* 2017). The bud expands, and the sister chromatids remain attached to one another in the subsequent gap phase G_2 (Figure 3.1). Lastly, in the M phase, mitosis, the mother cell is divided into two genetically identical cells (Jiménez *et al.* 2015). Mitosis comprises five steps: prophase, metaphase, anaphase, telophase, and cytokinesis (Yanagida 2014; McIntosh 2016). First, in prophase, chromosomes are condensed approximately two-fold with the aid of condensin complexes (Thadani *et al.* 2012; Kalitsis *et al.* 2017). The ring-like complexes consist of two structural maintenance of chromosomes proteins (Smc2 and Smc4) and three non-SMC subunits (Ycs4, Brn1, and Ycg1). The complexes encircle DNA, bind to histones H2A and H4 directly, preferentially at promoter motifs of RNA Pol III genes, and promote supercoiling of chromosomal DNA. Thus, the chromosomes are compacted, and structural integrity is maintained. During metaphase, chromosomes undergo complete condensation and sister chromatids are bound together by cohesin complexes (Figure 3.1). Cohesin complexes are ring-like structures such as condensins (Choudhary and Kupiec 2022). They consist of two structural maintenance of chromosomes proteins (Smc1 and Smc3) and two non-SMC proteins (Scc1 and Scc3), and are supported by regulatory proteins, such as Scc2 and Wpl1. The complexes are activated from the S phase through early anaphase to maintain sister chromatid cohesion. While sister chromatid cohesion is still in place, microtubules align at the kinetochore regions of the chromosome centromeres in a biorientation (Yanagida 2014; McIntosh 2016). The progression to anaphase leads to separase-mediated cleavage of the cohesin complexes, enabling sister chromatids to be separated by the spindle apparatus, aided by microtubules. In telophase, chromosomes are completely separated, decondensed, and the spindle apparatus depolymerises. Finally, cytokinesis (C) results in the formation of two genetically identical cells after the nucleus and the duplicated DNA is divided (Figure 3.1). However, daughter cells are smaller than mother cells. Once sufficient nutrients and cell size are reached, another cell cycle can start.

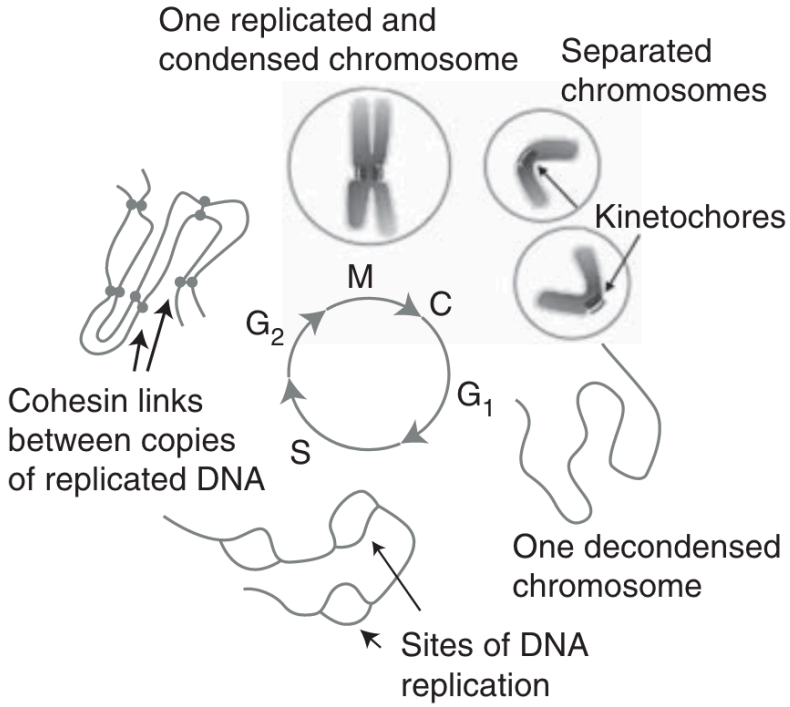

Figure 3.1 Phases of the eukaryotic cell cycle.

The eukaryotic cell cycle is a highly conserved process that consists of multiple steps. The start of the cell cycle is the G_1 phase. Here, the chromosomes are decondensed, and the cells ensure an accurate protein composition before they enter the cell cycle. During the G_1/S transition, an all-or-nothing reaction occurs. Once the cells enter the cell cycle, a complete round is required. In the S phase, the DNA is replicated. In the second gap phase (G_2), the established cohesin links between the replicated DNA copies maintain the cohesion of sister chromatids. After that, cells enter mitosis (M), where chromosomes are condensed, and sister chromatids are subsequently separated. In the final cytokinesis step (C), the genetic material is split into two to produce two genetically identical cells. Abbreviations: C, cytokinesis; G_1/G_2, gap 1/2 phase; M, mitosis; S, synthesis phase. Figure adapted from McIntosh (2016).

The duplication of genetic material is an important process that needs tight regulation and a high accuracy which is why the cell cycle is controlled by cyclin-dependent kinases (CDKs) (Suryadinata *et al.* 2010; Jiménez *et al.* 2015). These CDKs are expressed at a high level throughout the cell cycle and are regulated by interactions with their activating subunits, the so-called cyclins, which are differentially expressed at specific cell cycle phases. The only kinase in *S. cerevisiae* is Cdc28 which is regulated by six Clb proteins (Clb1-6) in the S, G_2, and M phases and by three Cln proteins (Cln1-3) in the G_1 phase (Dirick *et al.* 1995). As previously mentioned, the cell cycle is an important process; in particular, the G_1/S transition is critical for cell survival. This process is directly influenced by many environmental signals such as oxidative or replicative stress (Jiménez *et al.* 2015). When unfavourable conditions are sensed, cell cycle progression is slowed or even arrested to adapt to the conditions. Of special interest is nutrient availability, as their lack may lead to drastic problems and errors in important processes, such as DNA replication.

3.1.2 Adaptive growth response and the diauxic shift

While cell division is important for increasing the number of cells, cell growth is a fundamental process in all organisms (Conlon and Raff 2003). Except for the M phase, the cells grow during the entire cell cycle and double their mass before each division. Cell growth is tightly coordinated with cell cycle progression by the size checkpoints in the G_1 and G_2 phases, where a size threshold must be reached before the cell cycle continues. Growth rate is also influenced by nutrients (Conlon and Raff 2003). Cells can grow at a faster rate when they are provided with optimal conditions, as opposed to when they are subjected to unfavourable conditions. Upon transitioning from a nutrient-deficient environment to a nutrient-rich environment, the cell cycle is arrested and resumes only when the cells attain the appropriate size for the new environment. This process occurs within a single cell cycle, which demonstrates that cells can swiftly adapt their size threshold in response to external signals.

A proliferating cell culture, in which protein synthesis and cell division are in accordance with each other, is in exponential growth, as depicted in Figure 3.2 (Busti *et al.* 2010). In this growth phase, yeast cells preferably metabolize glucose by alcoholic fermentation despite oxygen for full oxidization would be present (section 3.2.1.2). Even though respiration is energetically more efficient, yeast favours fermentation, as it produces energy at faster rates. Additionally, yeast's high tolerance to the toxicity of the produced ethanol elevates its ecological niche and ensures successful survival compared to other microbes that utilise glucose as a carbon source. When glucose is limited and oxygen is available, yeast cells undergo a metabolic shift to process the ethanol produced during fermentation (Figure 3.2). This metabolic shift, known as the diauxic shift, results in a decrease in growth rate and derepression of glucose-specific genes (Busti *et al.* 2010; Galdieri *et al.* 2010). Global protein synthesis rates, both at the transcriptional and translational levels, are strongly reduced. Specific stress response genes are activated in response to nutrient depletion. One important gene that is expressed during this diauxic shift is the glucose-repressed enzyme Adh2, capable of converting ethanol as an energy source (section 3.2.1.3). In the post-diauxic phase, yeast utilises ethanol as the main energy source with an adapted respiratory metabolism and a slower increase in biomass (Figure 3.2). When ethanol levels in the medium decrease, and no other fermentable carbon source is available, the cells enter a stationary or quiescent phase and stop proliferating (Figure 3.2). Many signalling pathways are involved in the shift from exponential growth to diauxic and stationary phases. Here, protein kinase A (PKA), TOR, Snf1 and Rim15 are the main regulators that help to reprogram the transcription machinery in response to the lack of nutrients (section 3.2.2).

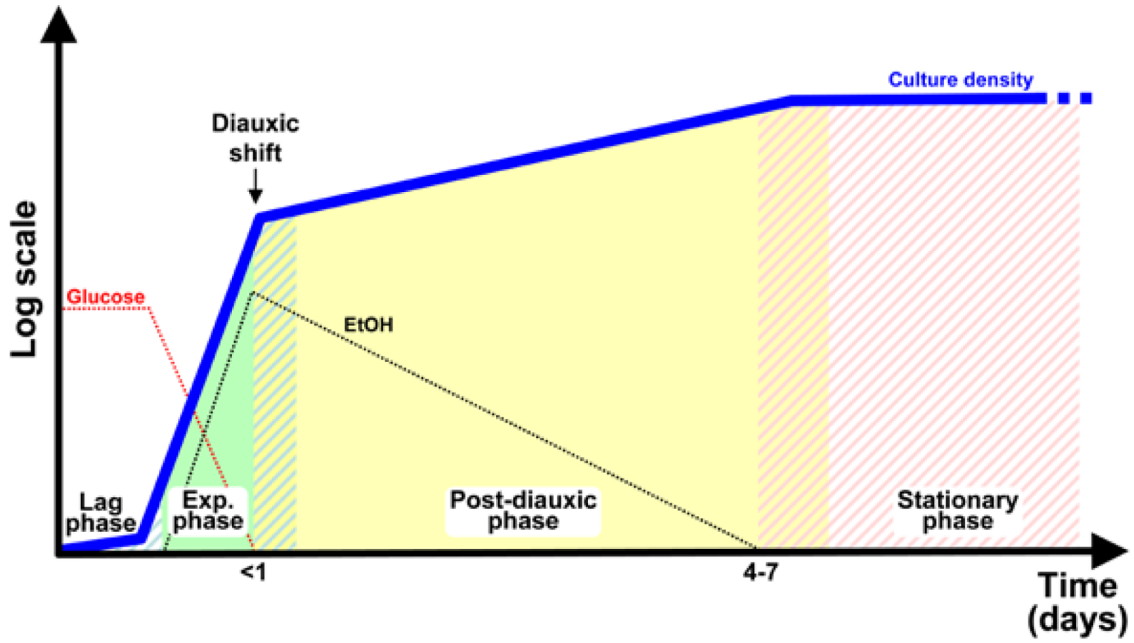

Figure 3.2 Cell growth in response to nutrient availability over time in *S. cerevisiae*.

The x-axis shows the time of growth in days, and the y-axis indicates the biomass on a log-scale (blue line). After a short lag phase, when yeast cells begin to recognise the available carbon sources, they quickly enter an exponential growth phase (green). In this phase, glucose is metabolized (red line), ethanol is produced (black line), and cells quickly gain biomass. Once glucose is depleted, cells switch from exponential growth to slow growth using ethanol. Yeast shifts from fermentation to respiration to gain energy. This switch is called a diauxic shift and includes a massive reprogramming of cells to adapt to nutrient starvation conditions. Ethanol is extensively used in the post-diauxic phase, but the increase in biomass is reduced (yellow). When ethanol is depleted and no other carbon source is available, the cells eventually enter the stationary phase (red). The cells enter a non-proliferating phase, and biomass accumulation stops. Abbreviations: EtOH, ethanol; Exp. phase, exponential phase. Figure from Busti *et al.* (2010).

Diploid yeast cells may also grow on non-fermentable carbon sources such as acetate or galactose (Mitchell 1994; Galdieri *et al.* 2010). When these cells are deprived of nitrogen, they eventually undergo meiosis and sporulation. This fine-tuned expression to use different carbon sources to gain energy is important for quick and precise long-term growth.

3.2 Metabolic pathways and regulatory mechanisms

Obtaining energy for growth and development is a highly important topic for every cell. Nutrients and their uptake and regulation are essential modulators of various cellular pathways (Vander Heiden *et al.* 2009; Busti *et al.* 2010; Conrad *et al.* 2014). Differentiated metabolic pathways are necessary to support cells with the required energy for all processes. Nutrient sensing, as part of metabolic pathways, is crucial to ensure that sufficient energy is provided for the building blocks of the cell. Ultimately, the goal is proliferation under conditions with abundant nutrients to increase the biomass (Figure 3.3). When nutrients are limited, cells use most of the available

resources for survival (Figure 3.3). The metabolic mechanisms that regulate nutrient utilisation may be as diverse as the nutrients themselves and can work independently.

While the differences in metabolism of proliferating and starved cells (section 3.1.2) are true for unicellular organisms, multicellular organisms regulate their metabolism slightly differently (Vander Heiden *et al.* 2009). Here, most cells grow under conditions of constant nutrient levels. Differentiated cells usually remain quiescent and do not take up nutrients from the environment. Therefore, their individual cell proliferation is blocked, and they use metabolic pathways similar to starvation conditions for unicellular organisms (Figure 3.3). Only when growth signals such as growth factors or hormones are present, cells start to proliferate, gain biomass, and produce lactate in the metabolic pathway (Figure 3.3). Interestingly, cancer cells develop genetic mutations that help them switch to proliferative metabolism, even without growth signals, and enter uncontrolled growth.

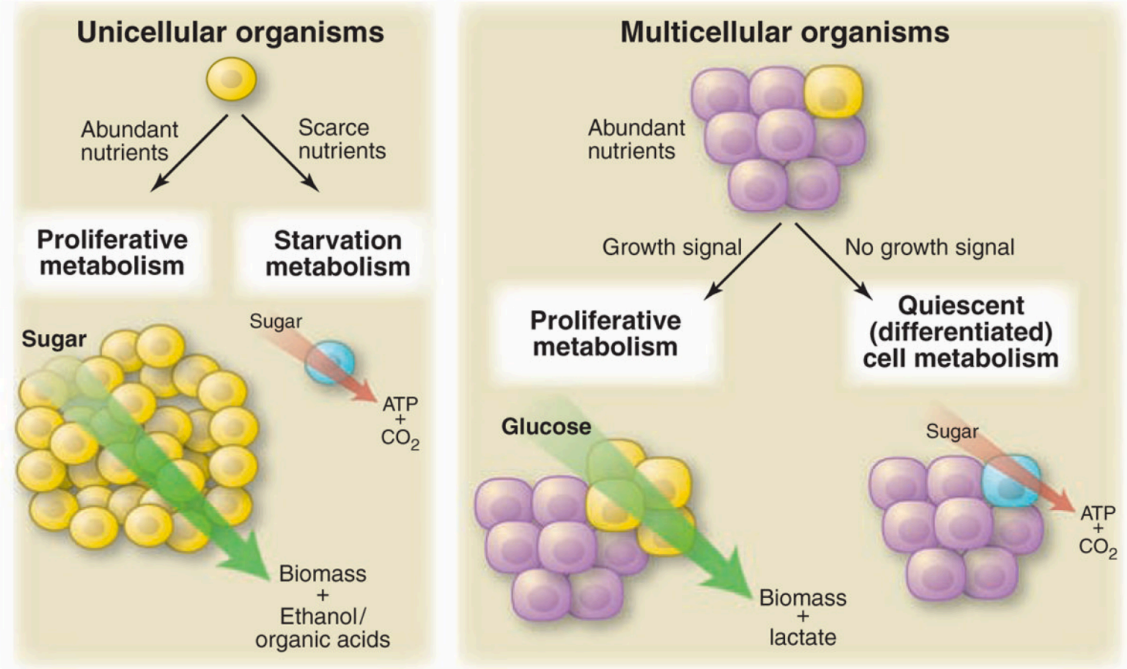

Figure 3.3 Metabolism in unicellular and multicellular organisms.

Unicellular organisms can switch between proliferative and starvation metabolism, depending on nutrient availability. When nutrients are present, sugar is metabolized to produce biomass, which, in turn, increases cell proliferation and ethanol production. When nutrients are depleted, the remaining sugar is metabolized to produce energy in the form of adenosine triphosphate (ATP) and CO_2. Multicellular organisms generally do not take up nutrients and remain quiescent, as long as no external growth signals are present. In this differentiated state, cells utilise sugars to gain energy (ATP) and CO_2. When growth signals are added, cells begin to proliferate, gain biomass, and produce lactate from glucose inputs. Figure from Vander Heiden *et al.* (2009).

3.2.1 Regulation of carbon source metabolism

S. cerevisiae is capable of utilising many different sugars as carbon sources; however, glucose is the preferred carbon source (Zimmermann and Scheel 1977; Gancedo 2008). The metabolism of the preferred sugar in yeast begins with the import of glucose and subsequent glycolysis, which serves as a fundamental starting point in energy production, which is described in more detail in section 3.2.1.1 (Barnett 2003; Pfeiffer and Morley 2014; De Alteriis *et al.* 2018). Glycolysis produces two molecules of adenosine triphosphate (ATP) and pyruvate, which can be further processed based on the availability of oxygen, resulting in the production of additional energy and the storage of ATP (Figure 3.4). Despite the availability of oxygen, yeast cells prefer to gain energy by alcoholic fermentation, producing and releasing ethanol as a waste product, although this process yields less energy than full oxidative phosphorylation via the tricarboxylic acid (TCA) cycle (Figure 3.4 and section 3.2.1.2) (Barnett 2003; Vander Heiden *et al.* 2009; Busti *et al.* 2010; Lunt and Vander Heiden 2011). Anaerobic fermentation only leads to the production of two ATP molecules per glucose molecule, whereas oxygen-dependent respiration yields 18 ATP per glucose (Pfeiffer and Morley 2014; De Alteriis *et al.* 2018). This phenomenon of using an energetically unfavourable process, known as the Crabtree or Warburg effect, is similar to the metabolism observed in cancer cells, where energy-inefficient metabolism is also favoured (Warburg 1956; De Deken 1966). However, when glucose is depleted, yeast cells can also shift to ethanol utilisation through the oxidative pathway by converting it to acetyl-coenzyme A (acetyl-CoA) (Figure 3.4, blue arrows and section 3.2.1.3) (Barnett 2003; Vander Heiden *et al.* 2009; Pfeiffer and Morley 2014; De Alteriis *et al.* 2018).

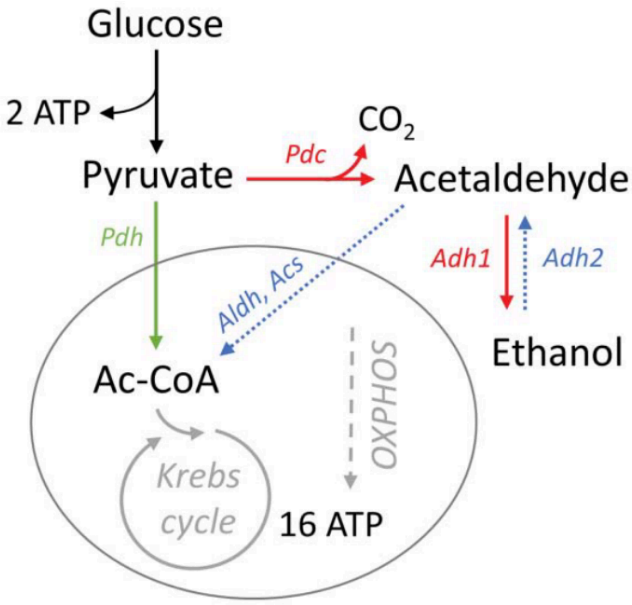

Figure 3.4 Overview of glucose metabolism in *S. cerevisiae*.

After importing glucose into the cells, the sugar is metabolized in glycolysis, producing two ATP as an energy output. The pyruvate product may be further catabolised by respiration (green arrow) or fermentation (red arrows). During fermentation, yeast cells convert pyruvate into ethanol via an acetaldehyde intermediate. The two enzymes Pyruvate decarboxylase (Pdc) and alcohol dehydrogenase (Adh1) are involved in this process. Fermentation does not produce further ATP but recycles NADH from glycolysis. This process is oxygen independent. Respiration fully metabolizes pyruvate to CO_2 via the TCA cycle (Krebs cycle) and oxidative phosphorylation (OXPHOS). Pyruvate dehydrogenase (Pdh) catalyses the conversion of pyruvate to acetyl-CoA, which then enters the TCA cycle. The entire process produces 16 more molecules of ATP but is oxygen-dependent. When glucose is depleted, ethanol can be used as an energy source. Ethanol is converted to acetaldehyde by using Adh2. Acetaldehyde is then further catalysed to acetyl-CoA which can enter the TCA cycle. This reaction is mediated by Aldh and Acs. Abbreviations: Ac-CoA, acetyl-CoA; TCA, tricarboxylic acid. Figure from De Alteriis *et al.* (2018).

Poor fermentable carbon sources can also be used in different metabolic pathways by *S. cerevisiae*. For instance, raffinose, a trisaccharide, must first be broken down in a process that requires the activity of an invertase, encoded by *SUC2*, and α-galactosidase (Atiyeh and Duvnjak 2003; Zhou *et al.* 2017a; b). First, raffinose is cleaved to produce fructose and melibiose (Figure 3.5 A). The disaccharide melibiose is composed of glucose and galactose and is subsequently hydrolysed into its components by α-galactosidase (Figure 3.5 C). Alternatively, α-galactosidase can cleave raffinose into sucrose and galactose (Figure 3.5 B). The resulting sucrose can then be hydrolysed into glucose and fructose (Figure 3.5 D). Fructose and glucose can then directly enter glycolysis, whereas galactose is first converted to glucose-6-phosphate via the intermediate glucose-1-phosphate before entering glycolysis. Finally, all components can fuel the TCA cycle and oxidative phosphorylation to gain energy. However, the utilisation of unfavourable carbon sources and the enzymes required for this process, such as Suc2, are repressed under glucose conditions.

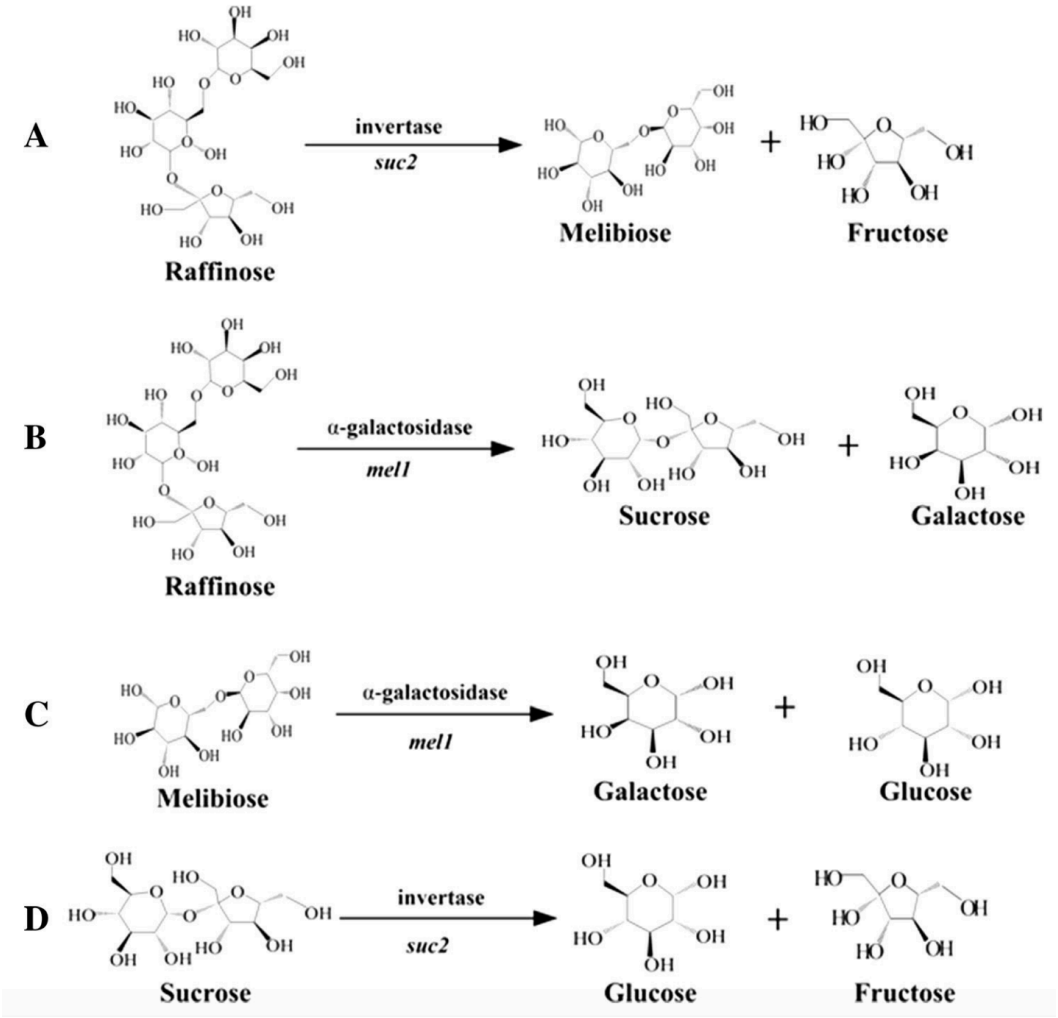

Figure 3.5 Metabolism of raffinose in *S. cerevisiae*.

A. Raffinose is cleaved to melibiose and fructose with help of the invertase Suc2. B. Raffinose alternatively can be metabolized to sucrose and galactose by the α-galactosidase Mel1. C. Melibiose produced from A can be further hydrolysed to galactose and glucose with the help of α-galactosidase Mel1, once again. D. The sucrose produced in B is further processed by the invertase Suc2 to glucose and fructose. Both the metabolic pathways lead to the production of glucose, fructose, and galactose from raffinose. Figure from Zhou *et al.* (2017a).

In contrast to raffinose, glycerol, a non-fermentable carbon source, cannot be utilised in glycolysis (Rønnow and Kielland-Brandt 1993; Klein *et al.* 2017; Xiberras *et al.* 2019). Instead, glycerol is coupled to respiration and degraded in two steps in the L-glycerol-3-phosphate pathway (Klein *et al.* 2017; Xiberras *et al.* 2019). First, glycerol kinase Gut1 converts glycerol to glycerol-3-phosphate (Figure 3.6). It is subsequently oxidised to dihydroxyacetone phosphate by the glycerol-3-phosphate dehydrogenase Gut2 (Figure 3.6). The second reaction is flavin adenine dinucleotide (FAD)-dependent and Gut2 is located on the outer surface of the inner mitochondrial membrane. The electrons from glycerol are thereby directly transferred to the respiratory chain via $FADH_2$. Furthermore, dihydroxyacetone phosphate can be used for glycolysis and gluconeogenesis. However, the enzymes necessary for the L-glycerol-3-phosphate pathway are repressed when glucose is available, limiting the utilisation of glycerol to conditions in which glucose levels are depleted.

To obtain a high energy yield, extracellular conditions must be monitored precisely, and fast and accurate regulation of gene expression has evolved to ensure continuous growth of *S. cerevisiae* (Busti *et al.* 2010). Glucose is not only the preferred carbon source for energy production, but it is also a signal molecule used to regulate various processes, as described more precisely in section 3.2.2.

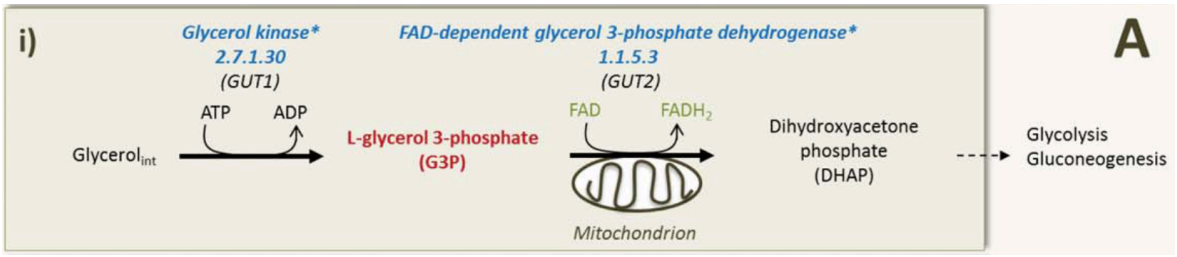

Figure 3.6 The L-glycerol-3-phosphate pathway of glycerol utilisation in *S. cerevisiae*.

Intracellular glycerol is first catabolised to L-glycerol-3-phosphate (G3P) with the aid of glycerol kinase (Gut1). G3P is then further processed in the mitochondria. Here, the FAD-dependent glycerol-3-phosphate dehydrogenase Gut2 converts G3P to dihydroxyacetone phosphate (DHAP). Glycerol electrons are directly transferred to $FADH_2$ in the respiratory chain. DHAP may also be used in glycolysis or gluconeogenesis for further energy production. Abbreviations: DHAP, dihydroxyacetone phosphate; G3P, L-glycerol-3-phosphate; $glycerol_{int}$, intracellular glycerol. Figure adapted from Klein *et al.* (2017).

3.2.1.1 Glycolysis: a key metabolic pathway

Glycolysis, the first step in glucose metabolism, breaks down glucose into two pyruvate molecules. During this process, two molecules of ATP and reduced nicotinamide adenine dinucleotide (NADH) are produced (Romano and Conway 1996; Barnett 2003; Richard 2003; Lunt and Vander Heiden 2011; Pfeiffer and Morley 2014). Glycolysis comprises ten biochemical reactions after glucose import, which are facilitated by a specific enzyme, as illustrated in Figure 3.7. Before glycolysis may take place, glucose is imported to the cells by many hexose transporters, for example, Hxt1 or Hxt2 (Kruckeberg 1996; Busti *et al.* 2010). The first step in glycolysis involves the phosphorylation of intracellular D-glucose to glucose 6-phosphate with the help of the enzyme hexokinase and the consumption of one ATP molecule. Glucose 6-phosphate is then converted into fructose 6-phosphate through reversible rearrangement, a process facilitated by glucose 6-phosphate isomerase. The next step involves the preparation of two three-carbon sugar phosphates. Fructose 6-phosphate is phosphorylated by phosphofructokinase with the aid of an ATP molecule to produce fructose 1,6-bisphosphate. The metabolic process wherein fructose 1,6-bisphosphate is cleaved into two three-carbon sugars is facilitated by aldolase. The final products of this reaction are dihydroxyacetone phosphate and glyceraldehyde 3-phosphate (Figure 3.7). Only glyceraldehyde 3-phosphate proceeds to the next stage of glycolysis. Therefore, the next step involves the conversion of dihydroxyacetone phosphate to glyceraldehyde 3-phosphate, which is accomplished by triose phosphate isomerase. The two molecules of glyceraldehyde 3-phosphate then undergo an oxidation reaction, leading to the initiation of the energy generation phase of glycolysis. The enzyme glyceraldehyde 3-phosphate dehydrogenase catalyses the conversion of glyceraldehyde 3-phosphate to 1,3-bisphosphoglycerate, also known as 3-phospho-D-glycerol phosphate, and generates one molecule of NADH for each molecule of glyceraldehyde 3-phosphate. Subsequently, phosphoglycerate kinase facilitates the production of 3-phosphoglycerate and one ATP molecule for every utilised 1,3-bisphosphoglycerate. Then, 3-phosphoglycerate is converted to 2-phosphoglycerate with the aid of the enzyme phosphoglycerate mutase. The elimination of water from 2-phosphoglycerate forms a high-energy bond in the resulting phosphoenolpyruvate. The enzymes responsible for this step are either enolase or phosphopyruvate hydratase. Glycolysis continues with the transfer of the high-energy bond to produce another molecule of ATP, and facilitates the formation of pyruvate from phosphoenolpyruvate with the aid of pyruvate kinase (Figure 3.7). The products of glycolysis can then be further processed based on the presence or absence of oxygen, with aerobic respiration or anaerobic fermentation as the two possible pathways.

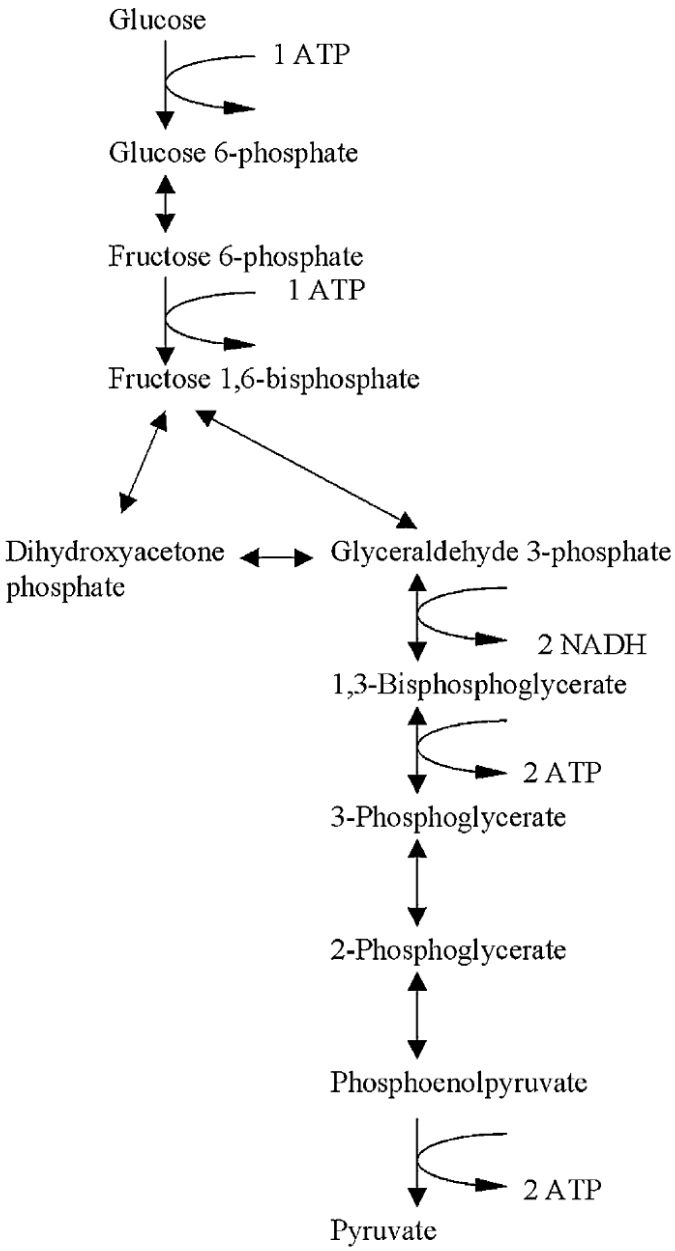

Figure 3.7 All steps of glycolysis in *S. cerevisiae*.

The metabolism of one glucose molecule in total requires two ATP molecules and generates four ATP molecules and two NADH molecules. Ten steps are required to produce pyruvate from glucose in an oxygen-independent manner. Each step is catalysed by a specific enzyme. A detailed description of this process is provided in the text. Figure from Richard (2003).

3.2.1.2 Fermentation and the Warburg effect

Adaptation to nutrient changes is of great importance to every organism. Unicellular organisms must constantly monitor their environment to adapt to changing conditions (Vander Heiden *et al.* 2009). A control system that tightly regulates metabolic mechanisms can differentiate between the fermentative and respiratory conditions. Yeast cells typically convert the two molecules of pyruvate generated during glycolysis (section 3.2.1.1) into ethanol through a process known as fermentation (Barnett 2003; Lunt and Vander Heiden 2011; Pfeiffer and Morley 2014). This process comprises two steps, as depicted in Figure 3.8 (right panel): first, pyruvate is catalysed to form acetaldehyde via pyruvate decarboxylase (Pdc in *S. cerevisiae*), and second, a tetrameric enzyme called alcohol dehydrogenase (Adh in *S. cerevisiae*) reduces acetaldehyde to ethanol. The ethanol and waste product CO_2 are then excreted from the cell, and NADH, which is produced during glycolysis, is recycled to oxidised NAD^+. Yeast cells prefer this oxygen-independent method of energy production even under aerobic conditions.

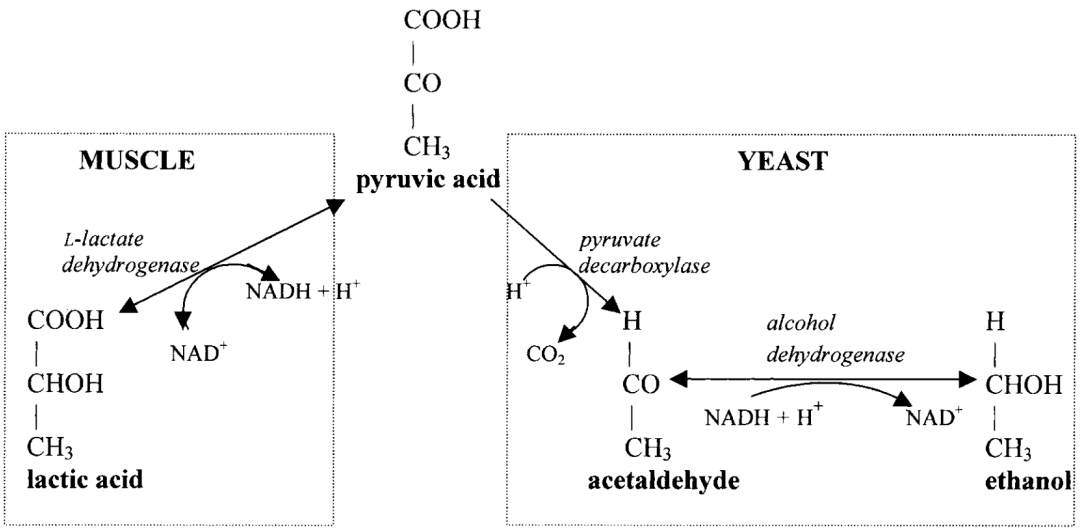

Figure 3.8 Fermentation of pyruvate from glycolysis in muscle and yeast cells.

Glycolytic pyruvate (pyruvic acid) is fermented to lactate in muscle cells by lactate dehydrogenase. This process is independent of oxygen. In yeast, pyruvate is fermented into ethanol in an oxygen-independent manner. This is a two-step process that involves an intermediate acetaldehyde. The enzymes that catalyse these steps are pyruvate decarboxylase and alcohol dehydrogenase. Ethanol and carbon dioxide are excreted from the cells. Furthermore, glycolytic NADH is recycled into NAD^+. Figure from Barnett (2003).

Mammalian cells, e.g. muscle cells, can utilise pyruvate in a similar process when oxygen is lacking (Barnett 2003; Pfeiffer and Morley 2014). Lactate dehydrogenase can convert pyruvate to lactate in an anaerobic environment using NADH (Figure 3.8, left panel). However, in the presence of oxygen, the differentiated tissues prefer oxidative phosphorylation (Vander Heiden *et al.* 2009). Here, following the metabolism of glucose to pyruvate in glycolysis, pyruvate enters the TCA cycle in the mitochondria and is fully oxidised to CO_2 (Figure 3.9, left panel). The NADH produced undergoes further oxidative phosphorylation to increase ATP output while maintaining minimum lactate production. Oxidative phosphorylation in differentiated tissues yields approximately 36 ATP per molecule of glucose, whereas anaerobic glycolysis and subsequent lactate production only yield 2 ATP per molecule of glucose.

In contrast to differentiated tissue, but similar to yeast, cancer cells typically undergo high levels of glycolysis and fermentation, even when sufficient oxygen is available (Barnett 2003; Vander Heiden *et al.* 2009; Galdieri *et al.* 2010; Lunt and Vander Heiden 2011). This process is known as the Warburg effect, named after its discoverer (Warburg 1956). Cancer cells convert approximately 85 % of glycolytic pyruvate to lactate instead of utilising mitochondrial oxidative phosphorylation (Figure 3.9, right panel). This so-called aerobic glycolysis generates only approximately 4 ATP molecules per molecule of glucose (Vander Heiden *et al.* 2009). An advantage of the Warburg effect is the availability of carbon atoms for conversion to macromolecular precursors, such as acetyl-CoA for fatty acid synthesis, glycolytic intermediates for amino acid synthesis, and other raw materials that promote cell growth (Vander Heiden *et al.* 2009; Lunt and Vander Heiden 2011).

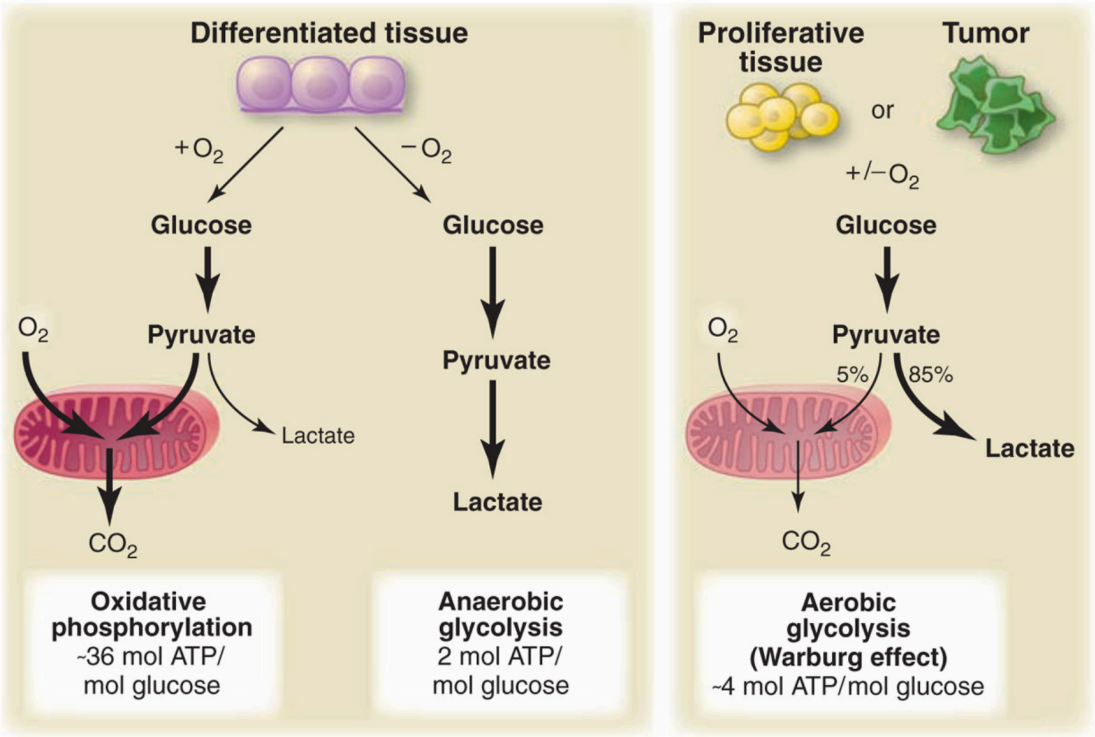

Figure 3.9 Metabolic options in differentiated cells and the Warburg effect in tumor cells.

Differentiated tissues undergo oxidative phosphorylation of glucose when sufficient oxygen is available (left panel). This leads to the full oxidation of pyruvate to CO_2 and a high energy yield of approximately 36 molecules of ATP per molecule glucose. When no oxygen is available, the cells switch to anaerobic glycolysis, converting glucose to pyruvate and lactate. This process yields only two molecules of ATP per molecule glucose. Tumour cells have been found to prefer glycolysis and the subsequent fermentation of glucose to lactate (right panel). Regardless of oxygen availability, oxidative phosphorylation is maintained at a minimal level, and 85 % of glycolytic pyruvate enters fermentation. Anaerobic glycolysis yields approximately four molecules of ATP per molecule glucose and is known as the Warburg effect. Abbreviation: mol, molecule. Figure from Vander Heiden *et al.* (2009).

3.2.1.3 Respiratory metabolism

Although yeast cells grow faster by fermentation, they can also utilise respiration when glucose levels decrease (Lunt and Vander Heiden 2011). Either ethanol produced during fermentation or other non-fermentable carbon sources like glycerol may be used in respiration (Rosa and Gábor 2006; Lunt and Vander Heiden 2011; Gasmi *et al.* 2014). Following aerobic glycolysis, a cell can produce high amounts of ATP through respiration (Dickinson and Schweizer 1999; Rosa and Gábor 2006; Vander Heiden *et al.* 2009; Van Rossum *et al.* 2016). Glycolytic pyruvate is transported into the mitochondria where it is converted to acetyl-CoA by the pyruvate dehydrogenase complex (PDH, Figure 3.10). Acetyl-CoA then enters the TCA cycle and is oxidised in multiple reaction steps, with the main goal of producing reducing equivalents for the electron chain (Figure 3.10). First, oxaloacetate and acetyl-CoA are condensated to citrate using citrate synthetase. Citrate is then converted to α-ketoglutarate by the intermediate isocitrate. The reaction to produce isocitrate is catalysed by aconitase,

and the subsequent oxidative decarboxylation to α-ketoglutarate is mediated by isocitrate dehydrogenase. α-Ketoglutarate is then metabolised to succinyl-CoA, which is further converted to succinate by CoA transferase Ach1. Succinate dehydrogenase converts succinate to fumarate. The next step in the TCA cycle is the conversion of fumarate to malate by fumarase, which is then oxidised to oxaloacetate by malate dehydrogenase, closing the circle. Glycolytic pyruvate can not only be imported to the mitochondria but also be converted to acetyl-CoA in the cytosol (Rosa and Gábor 2006; Van Rossum *et al.* 2016). This multi-step process is called the pyruvate dehydrogenase bypass and starts with the conversion of pyruvate to acetaldehyde by pyruvate decarboxylase (PDC, Figure 3.10). Acetaldehyde is then metabolised to acetate by acetaldehyde dehydrogenase (ALD), and finally acetate is converted to acetyl-CoA by acetyl-CoA synthetase (Acs1, 2, Figure 3.10). Acetyl-CoA is then used to catalyse the conversion of oxaloacetate to citrate mediated by Cit2, and the citrate produced is imported into the mitochondria in exchange for oxaloacetate from the TCA cycle (Figure 3.10). Mitochondrial citrate can fuel the TCA cycle. Alternatively, cytosolic acetyl-CoA may be transported into the mitochondria by the carnitine shuttle (Rosa and Gábor 2006; Van Rossum *et al.* 2016). The carnitine acetyltransferase CAT transfers the acetyl group of acetyl-CoA to carnitine (Figure 3.10). The produced acetyl-carnitine may then be transported to the mitochondria by the acetyl-carnitine translocase Crc1. Within the mitochondrial matrix, acetyl-carnitine is recycled into carnitine and acetyl-CoA. Acetyl-CoA can enter the TCA cycle and carnitine is exported from the mitochondria. Additionally, ethanol can be used directly to produce acetyl-CoA in the cytosol. It is converted to acetaldehyde by alcohol dehydrogenase ADH (Figure 3.10). Acetaldehyde is then metabolised to acetate, and finally to acetyl-CoA, which may enter the mitochondria to fuel the TCA cycle.

In summary, the oxidation of the TCA cycle releases a significant amount of energy, which is stored within the electrons of NADH (Dickinson and Schweizer 1999; Rosa and Gábor 2006; Van Rossum *et al.* 2016). The byproduct of this process is CO_2, which is released into the environment. NADH then transports and transfers electrons to the electron transport chain in the mitochondrial membrane, coupled with the single-subunit NADH:ubiquinone oxidoreductase (Rosa and Gábor 2006). This enzyme catalyses the transfer of two electrons from mitochondrial NADH to ubiquinone. The energy of NADH is, therefore, converted to phosphate-bond energy in ATP, and the respiration process produces 10 ATP molecules per acetyl-CoA (Rosa and Gábor 2006). Compared with fermentation, respiration is much more efficient (section 3.2.1.2).

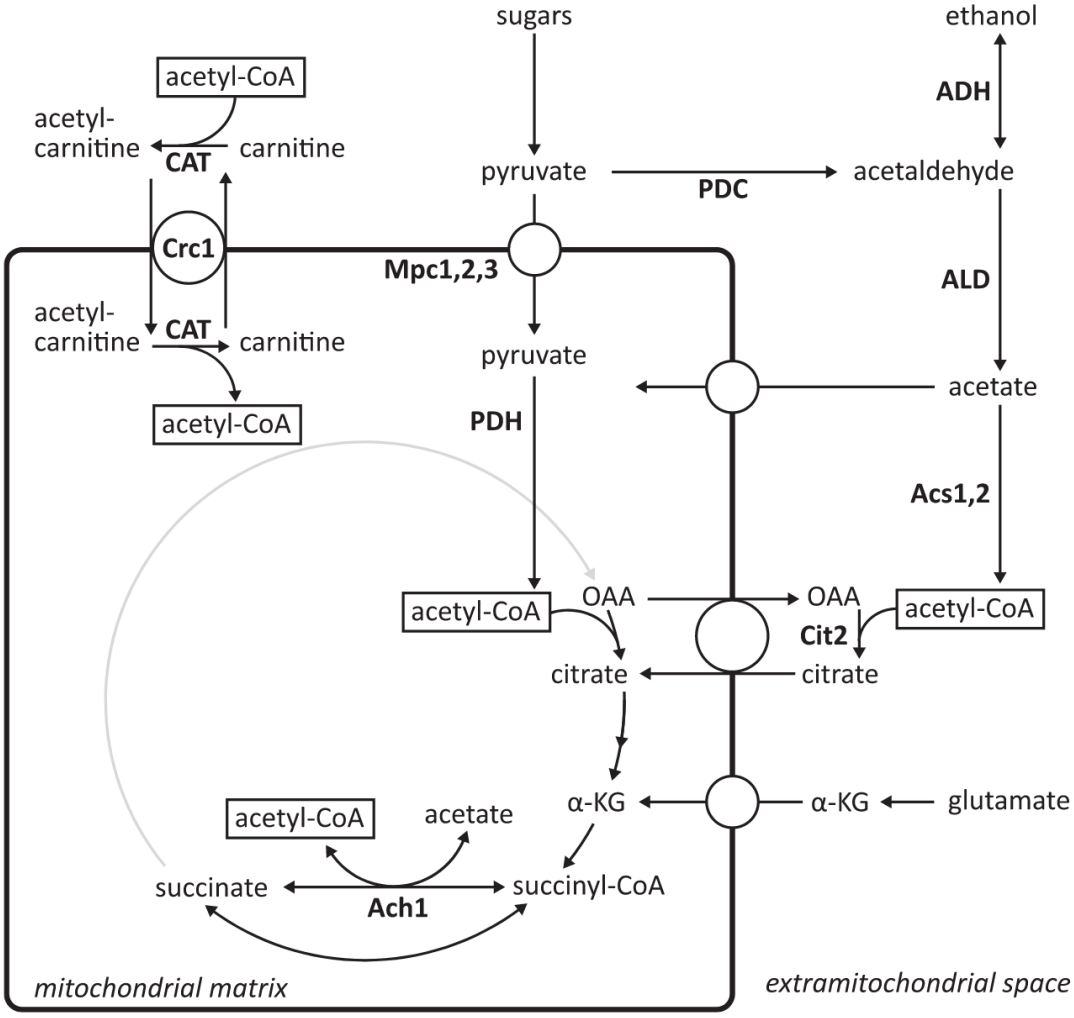

Figure 3.10 Respiratory pathway for energy production utilizing pyruvate in *S. cerevisiae*.

Glycolytic pyruvate may be imported into the mitochondrial matrix to enter the tricarboxylic acid (TCA) cycle. Pyruvate is converted to acetyl-CoA by pyruvate dehydrogenase (PDH), which is then oxidised in the TCA cycle in multiple steps (OAA to citrate to α-KG to succinyl-CoA to succinate to fumarate (not shown) to malate (not shown) to OAA). Cytosolic acetyl-CoA can also be used to fuel the TCA cycle. Pyruvate can be converted to acetyl-CoA in the pyruvate dehydrogenase bypass reaction, using Acs1, 2 in the final step. The conversion uses the intermediates acetaldehyde (with the help of PDC) and acetate (with the help of ALD). OAA and acetyl-CoA are then oxidised to citrate which finally enters the mitochondria and fuels the TCA cycle. Furthermore, cytosolic acetyl-CoA may enter the mitochondria with the aid of carnitine. Acetyl-carnitine produced in the cytosol may be shuttled by Crc1 and acetyl-CoA is recycled within the mitochondria. Abbreviations: α-KG, α-ketoglutarate; Acs1/Acs2, acetyl-CoA synthetase; Ach1, CoA transferase; ADH, alcohol dehydrogenase; ALD, acetaldehyde dehydrogenase; CAT, carnitine acetyltransferase; Cit2, citrate synthase; Crc1, acetyl-carnitine translocase; Mpc1/Mpc2/Mpc3, mitochondrial pyruvate carrier; OAA, oxaloacetate; PDC, pyruvate decarboxylase; PDH, pyruvate dehydrogenase complex. Figure from Van Rossum *et al.* (2016).

3.2.2 The role of glucose sensing and signalling in yeast metabolism

Glucose levels are not only important for the choice of the metabolic pathway used for energy production, but glucose also holds regulatory function (Barnett 2003; Santangelo 2006; Galdieri *et al.* 2010; Kim *et al.* 2013; Conrad *et al.* 2014). Glucose uptake induces the expression of genes relevant for glycolysis and fermentation. In contrast, genes encoding enzymes involved in respiration or metabolism of alternative carbon sources are repressed. The regulatory pathways are an interconnected network and glucose in the medium can be detected using specific sensors (Dickinson and Schweizer 1999; Santangelo 2006; Van Ende *et al.* 2019). Such sensors for extracellular glucose levels are Snf3 and Rgt2 (Santangelo 2006; Kim *et al.* 2013; Conrad *et al.* 2014; Van Ende *et al.* 2019). If sufficient glucose is available in the medium, the regulators Std1 and Mth1 are phosphorylated by Yck1 and Yck2, respectively (Figure 3.11). This phosphorylation then induces the ubiquitination by Grr1 and the subsequent degradation of Std1 and Mth1 by the proteasome. When the glucose levels decrease, Snf3 mediates the expression of high-affinity hexose transporters. If extracellular glucose cannot be sensed, Std1 and Mth1, together with Rgt1, inhibit the transcription of hexose transporters (*HXTs*; Figure 3.11). Gpr1 is an additional glucose sensor that interacts with the heterotrimeric G protein Gpa2 in the presence of glucose (Santangelo 2006; Van Ende *et al.* 2019). Thus, Gpa2 is activated, and cyclic adenosine monophosphate (cAMP) levels are increased (Figure 3.11). This in turn leads to protein kinase A (PKA) activation. Increased production of cAMP can also be mediated by Ras, which is activated by glycolysis, more precisely its intermediate fructose-1,6-bisphosphate (Santangelo 2006; Conrad *et al.* 2014; Peeters *et al.* 2017).

Genes involved in the metabolism of alternative carbon sources are regulated by the Snf1/Reg1 pathway and are only activated when glucose is not available (Treitel *et al.* 1998; Santangelo 2006; Conrad *et al.* 2014; Van Ende *et al.* 2019). The mechanism of glucose repression mediated by Mig1 depends on its phosphorylation status (Santangelo 2006; Conrad *et al.* 2014; Van Ende *et al.* 2019). If sufficient levels of glucose are available, Mig1 is localised in the nucleus in its dephosphorylated form, where it inhibits the expression of specific genes (Figure 3.11). If glucose is depleted, Snf1 phosphorylates Mig1, which is then inactivated and exported from the nucleus. Thus, glucose-repressed genes are derepressed. Additionally, in the absence of glucose, galactose can be imported into the cells by Gal2 (Van Ende *et al.* 2019). Intracellular galactose then binds to Gal3 which, in turn, facilitates its binding to Gal80 (Figure 3.11). Therefore, Gal80 cannot bind to Gal4 to inhibit its function. Gal4 is thereby active and promotes the transcription of *the GAL* and *MTH1* genes in the nucleus.

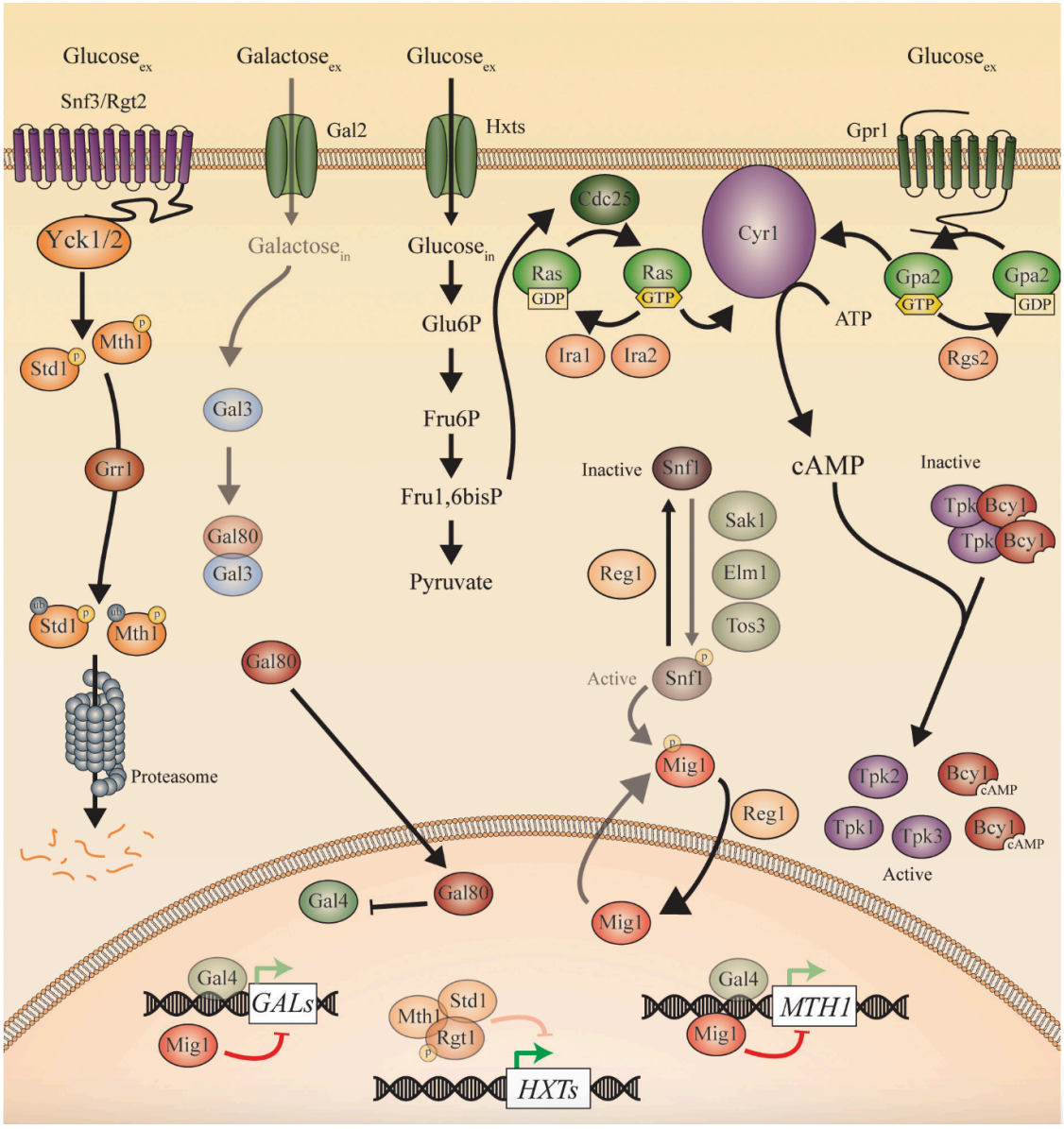

Figure 3.11 Glucose sensing and signalling network in *S. cerevisiae*.

Three main pathways are known to regulate glucose levels and mediate glucose-dependent transcription in yeast. The first pathway is the Snf3/Rgt2 pathway. The glucose sensors Snf3 and Rgt2 sense extracellular glucose levels. In the presence of glucose, Yck1/2 phosphorylates the regulators Std1 and Mth1. When phosphorylated, these regulators are ubiquitinated by Grr1 and degraded by the proteasome. In the absence of glucose, Std1 and Mth1, together with Rgt1, inhibited the expression of HXT genes encoding glucose transporters. The second pathway is the Ras/cAMP/PKA pathway, which increases intracellular cAMP levels and thereby activates PKA in response to glucose. On the one hand, a high glycolytic flux and high levels of the intermediate fructose-1,6-bisphosphate activate the GEF Cdc25 which exchanges GDP for GTP on the Ras proteins. Active Ras can then stimulate Cyr1 to convert ATP to cAMP. In contrast, an additional extracellular glucose signal is sensed by Gpr1. Under high-glucose conditions, Gpr1 activates GDP to GTP exchange on Gpa2. Gpa2, in its GTP-bound form, then stimulates Cyr1 which leads to an increase in cAMP levels. cAMP may then bind to the regulatory subunit Bcy1 of PKA, thereby facilitating its dissociation from the complex. The catalytic subunits Tpk1-3 are released and activated. The third glucose-sensing pathway involves Snf1/Reg1 repression. In the absence of glucose, the AMP kinase Snf1 is phosphorylated by Sak1, Elm1, and Tos3 and is thereby activated. Active Snf1 can then phosphorylate its targets, primarily Mig1. This phosphorylation prevents Mig1

from entering the nucleus. Under glucose conditions, Reg1 dephosphorylates and inactivates Snf1 which in turn leads to dephosphorylation of Mig1. Mig1 can then be imported into the nucleus to repress the transcription of *GAL* and *MTH1* genes. Additionally, galactose may enter the cells via Gal2 in the absence of glucose. Galactose can then bind to Gal3 which, in turn, binds to Gal80. Thus, Gal80 cannot bind to Gal4 which is thereby activated. Gal4 then functions as a transcription factor in the nucleus and activates the expression of *GAL* and *MTH1*. The desaturated arrows and proteins indicate conditions without glucose. Green arrows indicate activation and red arrows represent inhibition. Abbreviations: ex, extracellular; Fru1,6bisP, fructose-1,6-bisphosphate; Fru6P, fructose-6-phosphate; GEF, guanine exchange factor; Glu6P, glucose-6-phosphate; in, intracellular. Figure from Van Ende *et al.* (2019).

3.2.2.1 Signal transduction via the Ras/cAMP/PKA pathway

The Ras/cAMP/PKA pathway regulates the activity of PKA in response to glucose availability (Santangelo 2006; Gancedo 2008; Conrad *et al.* 2014; Peeters *et al.* 2017). Activation of cAMP synthesis is mediated by two pathways. The glucose sensor Gpr1 recognizes extracellular glucose levels and, in the presence of glucose, interacts with the heterotrimeric G protein Gpa2 intracellularly (Figure 3.12). Thus, the inactive GDP-bound form of Gpa2 is activated and Gpa2-GTP in turn activates adenylate cyclase Cyr1, which increases cAMP levels in the cell. In contrast, intracellular glucose is recognised by Ras (Figure 3.12). These Ras proteins are also G proteins, which are inactive in their GDP-bound state. The guanine exchange factor (GEF) Cdc25 activates Ras in response to glucose availability, more precisely by the availability of the glycolytic intermediate fructose-1,6-bisphosphate. Hydrolysis of Ras-GTP to Ras-GDP is accomplished by GTPases and is facilitated by GTPase-activating proteins (GAPs), Ira1 and Ira2. When Ras is in its active form, it activates Cyr1 which leads to an increase in cAMP levels. High levels of cAMP are reduced by phosphodiesterases Pde1 and Pde2 to regulate Ras/Gpr1 signalling (Figure 3.12). However, in the presence of glucose, intracellular cAMP levels increase up to 50-fold in a quick spike by the dual activation of Cyr1, which leads to the activation of PKA. PKA is a heterodimer consisting of two catalytic subunits encoded by Tpk1-3 and two regulatory subunits (Bcy1). The rapid cAMP spike leads to binding of cAMP to Bcy1, thereby inhibiting its regulatory function. The catalytic subunits Tpk1-3 are now dissociated from the complex and in their active kinase state (Figure 3.12).

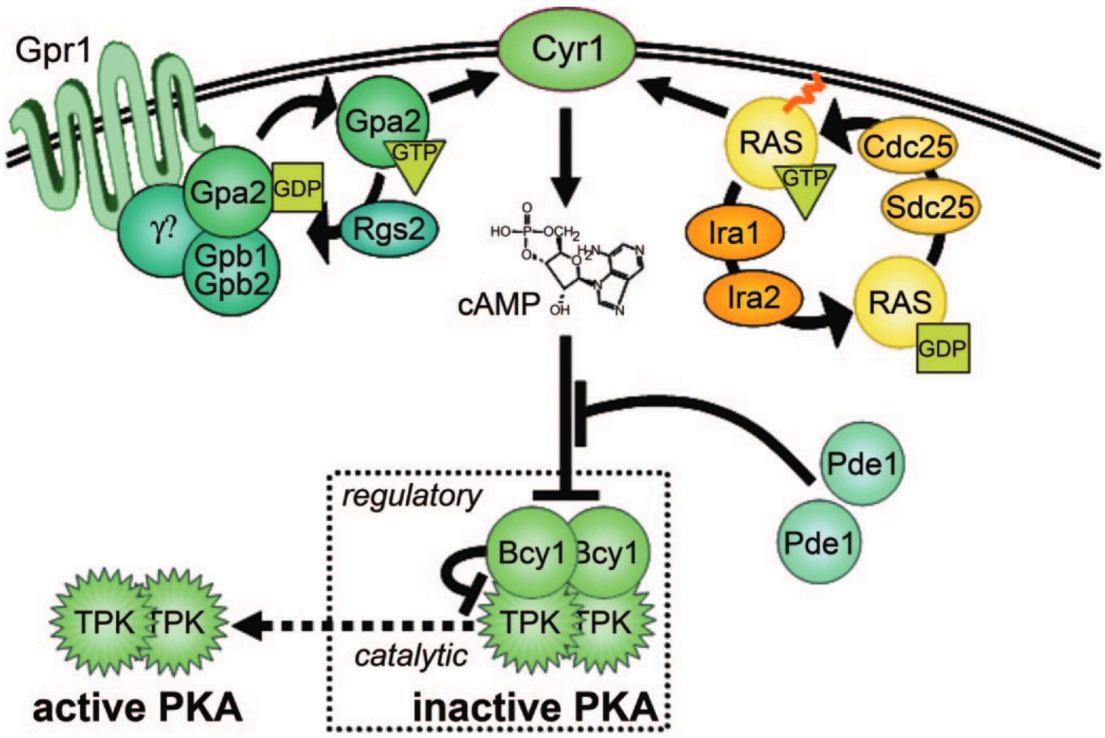

Figure 3.12 The Ras/cAMP/PKA pathway in *S. cerevisiae*.

High glucose levels lead to the activation of protein kinase A (PKA) via the secondary messenger cAMP. Extracellular glucose is recognised by the G protein and glucose sensor Gpr1. Gpr1 interacts with Gpa2 in its GDP-bound form. This interaction leads to the exchange of GDP with GTP, thereby activating Gpa2. Gpa2 then activates Cyr1, which is an adenylate cyclase. Rgs2 is responsible for the inactivation of Gpa2. Additionally, Cyr1 is activated by Ras-GTP, which is anchored in the membrane by a post-translationally added palmitoyl moiety (red squiggle). Ras is activated in response to intracellular glucose, more specifically fructose-1,6-bisphosphate, an intermediate of glycolysis. When fructose-1,6-bisphosphate is present, the guanine exchange factors Cdc25 and Sdc25 are activated which switches Ras from an inactive to an active state. Ira1 and Ira2 are responsible for inactivation of Ras. When Cyr1 is active, it increases the intracellular levels of cAMP. cAMP can then bind to Bcy1, the regulatory subunit of PKA, thereby inhibiting its activity. The catalytic subunits (Tpk1-3) are then free from the complex, and PKA is active. Pde1 and Pde2 antagonise this mechanism by converting cAMP into AMP. Figure from Santangelo (2006).

3.2.2.2 Glucose repression via the Snf1/Reg1 pathway

The derepression of many glucose-repressed genes, such as genes involved in alternative carbon source utilisation and respiration, relies on the serine-threonine protein kinase Snf1, a kinase that is highly conserved among eukaryotes, and the orthologue of the mammalian AMP-activated protein kinase, which becomes active under low glucose conditions (Ludin *et al.* 1998; Santangelo 2006; Tabba *et al.* 2010; Broach 2012). The essential step for the activation is the phosphorylation of the threonine residue in the activation loop of Snf1 (Santangelo 2006; Tabba *et al.* 2010; Broach 2012). Inactivation occurs by subsequent dephosphorylation via the protein phosphatase type I (PP1) Glc7 in complex with the regulatory protein Reg1. Here, the dephosphorylation rates are over 10-fold slower in low glucose than in high glucose

levels. In *S. cerevisiae*, Snf1 functions as a complex with Snf4 and Gal83, similar to the heterotrimeric Snf1 orthologue in mammals (Ludin *et al.* 1998; Santangelo 2006; Tabba *et al.* 2010; Kayikci and Nielsen 2015). Snf1 functions as the α subunit, Snf4 as the γ subunit and Gal83 as the β subunit. Snf4 is required for proper Snf1 kinase activity and Gal83 functions as a scaffold (Ludin *et al.* 1998; Santangelo 2006; Kayikci and Nielsen 2015). Under high glucose conditions, the Snf1 complex is targeted by Reg1 in its phosphorylated state (Santangelo 2006; Tabba *et al.* 2010; Conrad *et al.* 2014; Kayikci and Nielsen 2015; Van Ende *et al.* 2019). Reg1 forms a PP1 complex with the subunit Glc7, which is responsible for the dephosphorylation of the catalytic domain of Snf1 (Figure 3.13 #1). Activation of Snf1 is associated with a conformational change in a glucose-dependent manner (Ludin *et al.* 1998; Santangelo 2006). Under glucose conditions, the C-terminal regulatory domain of Snf1 interacts with the catalytic domain, thereby autoinhibiting kinase function (Figure 3.13 #2). In this unphosphorylated state, Snf1 is found exclusively in the cytoplasm (Tabba *et al.* 2010; Broach 2012). When glucose becomes limiting, Sak1, Elm1, or Tos3 phosphorylate the catalytic domain at conserved threonine 210 in the activation loop of Snf1 (Figure 3.13 #3). This phosphorylated residue is essential for kinase function. Additionally, Snf4 binds to the regulatory subunit of Snf1 when phosphorylated, which produces an open, active conformation of Snf1 and releases autoinhibition (Figure 3.13 #4). Under these conditions, Gal83 shuttles Snf1 to the nucleus (Santangelo 2006; Tabba *et al.* 2010). Std1 may also further activate Snf1 kinase function (Figure 3.13 #5). Furthermore, Snf1 now phosphorylates Reg1 and thereby stabilizes the interaction between Reg1/Glc7 and the Snf1 complex (Figure 3.13 #6). While Snf1 actively phosphorylates Reg1, Glc7 is dephosphorylating the latter (Figure 3.13 #7). Thus, constant binding and dissociation of Reg1/Glc7 from Snf1 is present which helps to sustain a quick response to changing carbon source levels. Upon addition of glucose signals, Glc7 can quickly remove the phosphorylation of Snf1 to switch the kinase complex to its inactive form (Figure 3.13 #1). The dynamic regulation of Snf1 and Reg1/Glc7 ensures a fast switch from inactive to active state and *vice versa*.

To derepress glucose-repressed genes under low glucose conditions, Snf1 has a multitude of downstream targets, mostly repressors, but also activators (Treitel *et al.* 1998; Santangelo 2006; Conrad *et al.* 2014; Kayikci and Nielsen 2015). One important target is Mig1, a Cys2His2 zinc finger protein that typically binds to GC-rich sequences and binds to at least 90 different genes to inhibit their transcription (Treitel *et al.* 1998; Carlson 1999; Santangelo 2006; Kim *et al.* 2013). Snf1 is responsible for the differential phosphorylation of Mig1 and its localisation in response to glucose levels (Figure 3.14). In the absence of glucose, when Snf1 is active, Mig1 is phosphorylated and thereby exported from the nucleus with aid of the exporter Msn5 (DeVit and Johnston 1999; Santangelo 2006). Thus, the expression of glucose-repressed genes is activated (Figure 3.14). When glucose is available and Snf1 gets inactivated, a dephosphorylation of cytoplasmic Mig1 follows, which results in a relocation of Mig1 to the nucleus (Figure 3.14). Subsequently, Mig1 binds to the recognition sites of

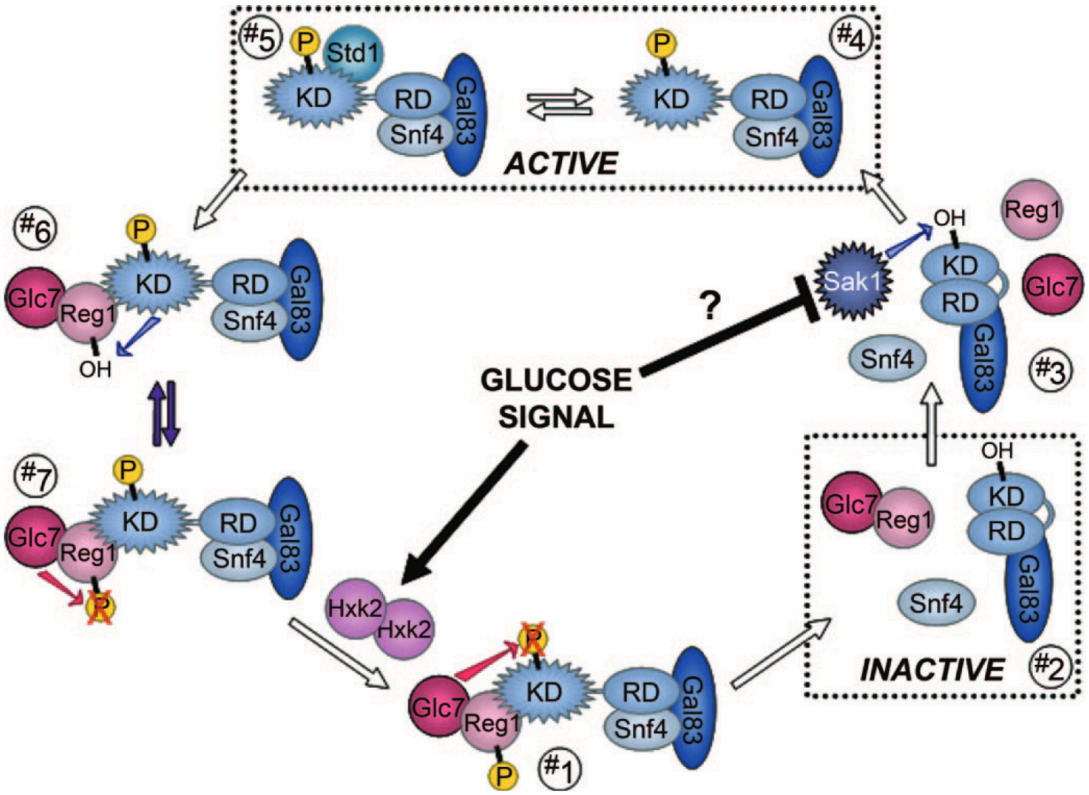

Figure 3.13 The interplay of Snf1 kinase complex and Reg1/Glc7 phosphatase.

Snf1 kinase can be switched on (*ACTIVE*) and off (*INACTIVE*) in response to Reg1/Glc7 activity. This response is mediated by the regulatory domain (RD) of Snf1. When the regulatory domain is bound to the kinase domain (KD), the kinase function is autoinhibited. This switch is important for the regulation of gene expression in the presence or absence of glucose. The Snf1 kinase complex consists of Snf1 (KD and RD) as the α subunit, Snf4 as the γ subunit, and Gal83 as the β subunit that also functions as a scaffolding for Snf1 and Snf4. The regulatory cycle begins when glucose is added to cells grown on an alternative carbon source (#1). Reg1/Glc7 dephosphorylates Snf1 in its kinase domain. This dephosphorylation releases Snf4, and the Snf1 domains interact, resulting in autoinhibition (#2). The Snf1 complex is also exported from the nucleus. When glucose is scarce, Sak1 phosphorylates Snf1 (#3) and the Snf1 complex is imported to the nucleus. Snf4 then binds to the regulatory domain of Snf1, which releases the kinase domain and activates Snf1 (#4). Std1 may also interact with the kinase domain, thereby further activating kinase (#5). Reg1 can then be phosphorylated by Snf1 (#6) which is necessary for stabilising the interaction between the Snf1 complex and Reg1/Glc7 (#7). This interaction is important for the inhibition of Snf1 via Reg1/Glc7, if glucose availability is increased. Additionally, Glc7 dephosphorylates Reg1, leading to its release from the Snf1. In the absence of glucose, Snf1 re-phosphorylates Reg1 in an interplay between the two. When glucose signals, for example, those mediated via Hxk2, are present, the Snf1 kinase complex is quickly inhibited, and the cycle can start anew. Red arrow: dephosphorylation, blue arrow: phosphorylation. Figure from Santangelo (2006).

specific genes and recruits the Ssn6-Tup1 complex which leads to transcriptional repression of these genes (Carlson 1999; Santangelo 2006; Broach 2012; Kayikci and Nielsen 2015). However, Snf1 can also regulate a variety of transcription activators required for the utilisation of non-fermentable carbon sources, such as Cat8 or Sip4, that both bind to carbon source responsive elements (CSRE) specifically to derepress the expression of these genes (Carlson 1999; Santangelo 2006; Broach 2012; Kayikci and Nielsen 2015)

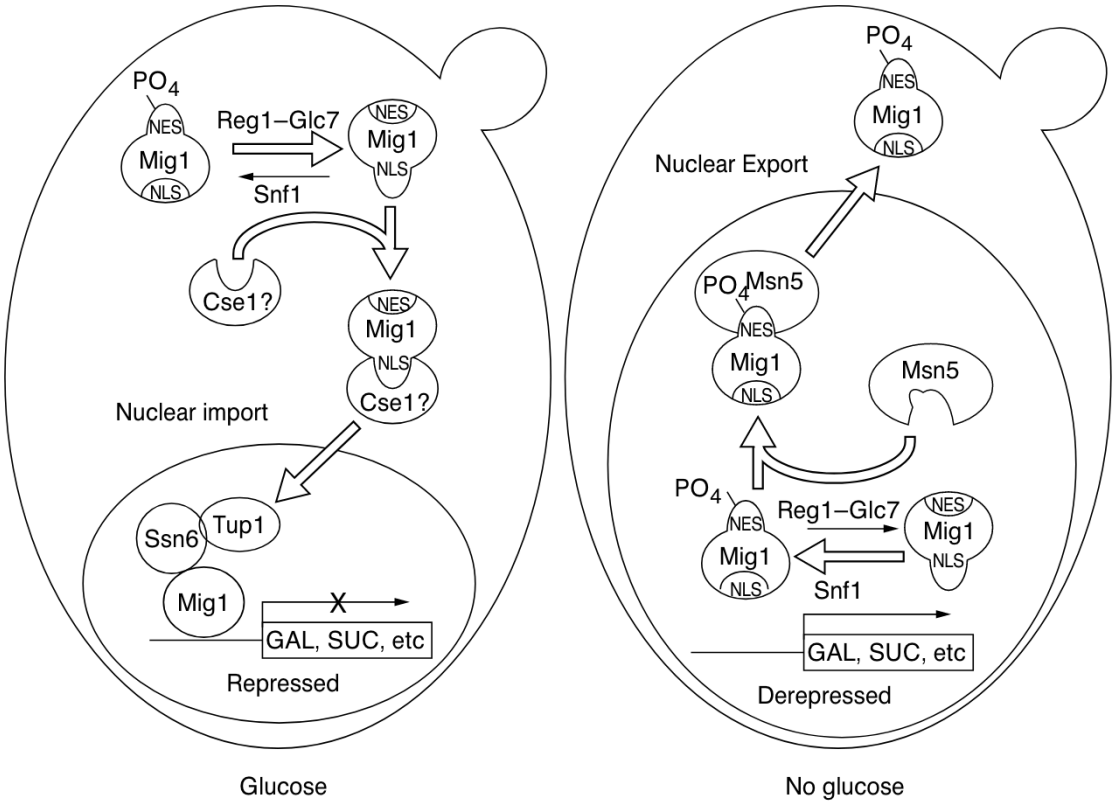

Figure 3.14 The import-export cycle of Mig1 in *S. cerevisiae*.

Left panel: Mig1 is dephosphorylated by Reg1/Glc7 when glucose is available. Thus, a nuclear localisation sequence (NLS) can be recognised by importin, most likely Cse1. The importin then shuttles Mig1 into the nucleus, where it binds to glucose-repressed genes and recruits Ssn6-Tup1 to block the expression of these genes. Right panel: When glucose is depleted, Snf1 is activated and enters the nucleus. Here, it phosphorylates Mig1, revealing its nuclear export sequence (NES). This sequence is recognised by Msn5, which exports Mig1 from the nucleus. Thus, glucose-repressed genes are derepressed and transcription can take place. Figure from DeVit and Johnston (1999).

3.3 Protein synthesis and homeostatic mechanisms

Protein expression is the process by which genetic information encoded in the DNA is transcribed into RNA and translated into proteins. This crucial mechanism involves many processes such as regulated synthesis, protein folding, and protein degradation (Dvir *et al.* 2001; Moore and Proudfoot 2009; Sonenberg and Hinnebusch 2009; Hinnebusch 2011; Sampaio-Marques and Ludovico 2018).

Protein synthesis begins with transcription (Figure 3.15), where the DNA sequence of a gene is transcribed into the corresponding mRNA by an RNA polymerase (Turowski and Tollervey 2016; Engel *et al.* 2018). In *S. cerevisiae*, three distinct RNA polymerases are utilised depending on their function. RNA polymerase I (RNA Pol I) is responsible for ribosomal RNA transcription, RNA polymerase II (RNA Pol II) is necessary for the transcription of protein-coding genes, and RNA polymerase III (RNA Pol III) transcribes non-coding genes such as tRNA and 5S rRNA. Transcription initiation involves assembly of the pre-initiation complex (PIC) at the promoter region, followed by RNA Pol II recruitment (Dvir *et al.* 2001). Transcriptional activators and repressors regulate gene expression by binding to specific DNA sequences, thereby promoting or inhibiting PIC assembly, respectively. After transcription, pre-mRNA undergoes processing, including capping and polyadenylation, to produce mature mRNA (Moore and Proudfoot 2009). While capping involves the addition of a 7-methylguanosine cap (m7G) at the 5' end of the mRNA, serving as protection from degradation and facilitating translation initiation, polyadenylation adds a poly(A) tail to the 3' end of the mRNA which is important for stability and export from the nucleus (Moore and Proudfoot 2009; Sonenberg and Hinnebusch 2009). Once the pre-mRNA is fully processed, the mature mRNA is exported from the nucleus to the cytoplasm, where translation initiation can begin (Figure 3.15). The ternary complex, consisting of eukaryotic initiation factor 2 (eIF2), GTP, and the initiation methionyl tRNA ($tRNA_i^{Met}$), is formed and binds to the 40S ribosomal subunit. Together with other eIFs, a 43S pre-initiation complex is formed (Sonenberg and Hinnebusch 2009; Jackson *et al.* 2010; Hinnebusch 2014). The 43S PIC scans the mRNA from the 5' direction until the start codon is recognised. When the start codon is found, the ribosome is recruited and eIFs are released. This allows proper ribosome assembly and translation elongation. During translation elongation, the ribosome moves in the 5' to 3' direction along the mRNA, and the corresponding aminoacyl-tRNAs are brought to the recognised codons promoted by elongation factors (eEFs). To produce a growing polypeptide chain, peptide bonds are formed between the adjacent amino acids (Schmeing and Ramakrishnan 2009; Voorhees and Ramakrishnan 2013; Hershey *et al.* 2019). Translation termination is signalled by the stop codon, which leads to the release of the newly synthesized polypeptide chain from the ribosome (Schmeing and Ramakrishnan 2009; Jackson *et al.* 2010). After translation, newly synthesised proteins may undergo various post-translational modifications (PTMs) to complete their functional forms (Figure 3.15) (Hochstrasser 2009; Holt *et al.* 2009; Henriksen *et al.* 2012; Biggar and Li 2015). Common PTMs include phosphorylation, acetylation, methylation, and ubiquitination, all of which influence protein stability, localisation, activity, and

interaction with other molecules. This is crucial, as it modulates cellular processes in signal transduction, metabolism, and cell cycle regulation.

Protein expression is a key factor in facilitating new protein synthesis, and protein homeostasis, also known as proteostasis, is essential for maintaining proper protein balance and ensuring optimal cellular function. The processes involved in maintenance include protein synthesis, folding, assembly, trafficking, and degradation (Sampaio-Marques and Ludovico 2018; Grandi and Bantscheff 2019; Chen *et al.* 2023). Regulation of protein synthesis, especially translation initiation, is the first step in ensuring the correct level of necessary proteins (Jackson *et al.* 2010; Hinnebusch 2011). Proteostasis includes protein folding and the corresponding quality control (Balch *et al.* 2008; Kraft *et al.* 2010; Sampaio-Marques and Ludovico 2018). Newly synthesised proteins undergo folding to acquire functional three-dimensional structures (Kraft *et al.* 2010; Walter and Ron 2011; Sampaio-Marques and Ludovico 2018). In this process, molecular chaperones are involved in helping the proteins fold correctly, preventing misfolding, and the formation of aggregates (Figure 3.15). Quality control mechanisms, such as the unfolded protein response (UPR) in the endoplasmic reticulum (ER), monitor protein folding, and target misfolded proteins for degradation (Figure 3.15). The localisation and trafficking of proteins to their specific cellular compartments also ensure an important balance (Kumar *et al.* 2002). Protein trafficking involves vesicular transport and targeting signals that direct proteins to their appropriate subcellular destinations as well as protein interactions that help shuttle the required protein into specific organelles. Finally, protein degradation is important for the maintenance of protein homeostasis (Kraft *et al.* 2010; Sampaio-Marques and Ludovico 2018; Grandi and Bantscheff 2019). Proteins are constantly degraded by proteolytic systems (Figure 3.15). The ubiquitin-proteasome system (UPS) targets ubiquitinated proteins for degradation by the 26S proteasome, whereas lysosomal degradation pathways, such as autophagy, degrade proteins and organelles via lysosomal fusion. The following chapters highlight the important aspects of protein expression and proteostasis that are relevant to this study.

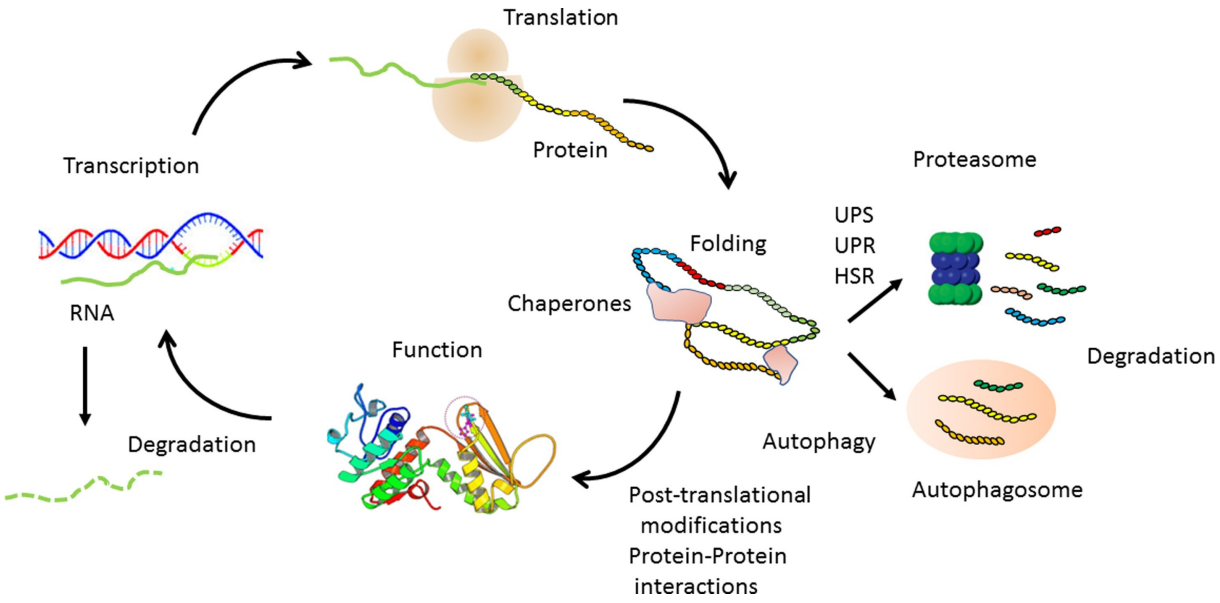

Figure 3.15 Main processes of protein homeostasis.

Protein homeostasis is necessary for maintaining correct protein concentrations and adapting the proteome to stress. There is a delicate interplay between protein synthesis and degradation. Processes involved are transcription and translation of proteins, their folding by chaperones, post-translational modifications for proper function, and degradation mediated by the proteasome or the autophagosome. Control mechanisms for folding include the ubiquitin-proteasome system for non-functional proteins, the unfolded protein response, and the heat shock response of misfolded proteins. Abbreviations: HSR, heat shock response; UPR, unfolded protein response; UPS, ubiquitin-proteasome system. Figure from Grandi and Bantscheff (2019).

3.3.1 Overview of transcriptional processes

Transcription is essential for the synthesis of RNA from DNA templates and is mediated by RNA polymerases (Turowski and Tollervey 2016). Depending on the RNA product, different polymerases can be utilised (Turowski and Tollervey 2016; Engel *et al.* 2018). The transcriptional mechanism is similar for all three RNA polymerases in *S. cerevisiae*, and consists of initiation, elongation, and termination (Engel *et al.* 2018). The transcriptional process in yeast is highly regulated and involves multiple proteins and regulatory elements that control gene expression and cellular functions. While the catalytic cores of the polymerases are similar, the associated transcription factors and structural features of the three polymerases differ (Figure 3.16).

3.3.1.1 Transcription by RNA Pol II

RNA polymerase II (RNA Pol II) consists of 12 subunits (Rpb1-12), as depicted in Figure 3.16 b, and is responsible for the transcription of coding mRNAs (Hampsey 1998; Wade and Struhl 2008; Hahn and Young 2011). Rpb1 and Rpb2 form the active site, while Rpb5, Rpb6, Rpb8, Rpb10, and Rpb12 are subunits shared with polymerases I and III. RNA Pol II contains a unique C-terminal domain (CTD) on Rpb1, which is important for PIC assembly and is targeted for phosphorylation. Transcription by RNA Pol II begins with initiation, followed by elongation and ends with termination (Erb and Van

Nimwegen 2011; Hahn and Young 2011; Engel *et al.* 2018). Transcription initiation begins with the assembly of the PIC in the promoter region of a target gene. The core promoter typically contains a TATA box sequence, situated approximately 80 bp upstream of the transcription start site (TSS), and recognised by the TATA-binding protein (TBP). Binding of TFIID, along with other general transcription factors such as TFIIA, TFIIB, and TFIIE, recruits RNA polymerase II to the promoter. TFIIB is crucial for the binding of RNA Pol II as it directly contacts it. This leads to the formation of an active open complex state of the transcription machinery, and thus the initiation of transcription. Once the transcription start site is found, transcription elongation continues (Wade and Struhl 2008; Kwak and Lis 2013).
Here, RNA Pol II synthesises an mRNA transcript using DNA as a template. Nucleoside triphosphates are added to the growing RNA in a 5' to 3' direction, complementary to the template DNA. Continuous RNA synthesis is achieved by the constant unwinding of DNA and re-annealing behind the transcription bubble. When a termination signal is reached, transcription termination occurs (Connelly and Manley 1988; Porrua and Libri 2015). Two termination mechanisms have been identified in *S. cerevisiae*. Polyadenylation-dependent termination involves cleavage of the nascent RNA transcript, followed by polyadenylation. Polyadenylation-independent termination relies on specific sequence motifs of the DNA template. Following transcription, the produced pre-mRNA is processed into a mature mRNA with an attached 5' m7G cap and 3' poly(A) tail before translation can take place (Das and Das 2013). The regulation of transcription is mainly mediated by transcription factors such as Mig1 or Cat8, which adapt the expression of genes to environmental conditions and stress situations (Hedges *et al.* 1995; Hiesinger *et al.* 2001; Turcotte *et al.* 2010).

3.3.1.2 Transcription by RNA Pol III

RNA polymerase III (RNA Pol III) consists of 17 subunits with specific roles (Figure 3.16 c), and is responsible for the transcription of small non-coding RNAs, including tRNAs and 5S rRNAs (Willis 1993; Pluta *et al.* 2001; Schramm and Hernandez 2002). While the transcriptional mechanism is similar to that of RNA Pol II (section 3.3.1.1), there are a few differences. RNA Pol III recognizes distinct promoter regions containing conserved sequence elements depending on the transcribed gene (Willis 1993; Schramm and Hernandez 2002; Orioli *et al.* 2012). tRNA genes have a type 2 promoter containing an A box positioned at +8 to +19 bp, and a B box motif positioned at +52 to +62 bp (Figure 3.17). 5S rRNA genes use type 1 promoters with an internal control region (ICR) (Figure 3.17). This ICR contains an A box at positions +50 to +60 bp, an intermediate element (IE) from +67 to +72 bp, and a C box, at +80 to +90 bp. Recognition of type 1 or type 2 promoter elements by the TFIIIB and TFIIIC transcription factor complexes is critical for Pol III recruitment and assembly of the transcription initiation complex (Willis 1993; Pluta *et al.* 2001; Orioli *et al.* 2012). TFIIIC, a large transcription factor, binds to promoter sequences and recruits initiation factor TFIIIB. TFIIIB is positioned upstream of the transcription start site and may recruit RNA Pol III. Once RNA Pol III is correctly recruited to the promoter, transcription is initiated and proceeds through the elongation phase. The elongation

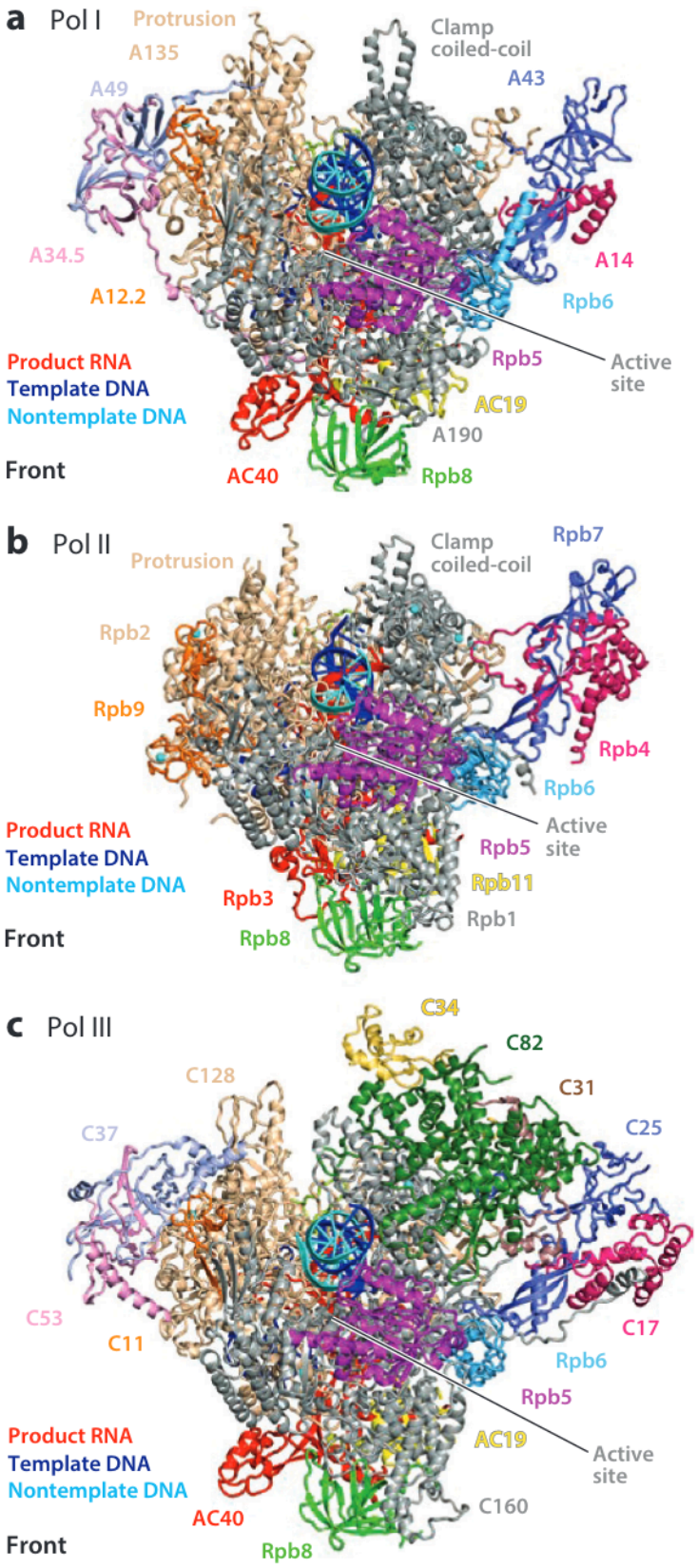

Figure 3.16 Structure of the three RNA polymerases as elongation complex in *S. cerevisiae*.

The elongation complexes of RNA Pol I (a), RNA Pol II (b), and RNA Pol III (c) are shown. The structures were resolved by X-ray crystallography or cryo-EM and are shown in front view. The general subunits, Rpb10 and Rpb12, are not visible, as they are positioned at the back. All other subunits are coded by colour, indicating their respective localisations. The

template (blue) and non-template DNA (cyan) are situated at the bottom of the active centre cleft and are tightly bound. This is also true for the RNA product (red). Abbreviations: EC, elongation complex; EM, electron microscopy; Pol, RNA polymerase. Figure adapted from Engel *et al.* (2018).

rate of RNA Pol III is rather fast, and the termination of transcription involves a combination of mechanisms (Landrieux *et al.* 2006; Orioli *et al.* 2012; Turowski and Tollervey 2016). These mechanisms include termination sequences within the DNA, which consist of four or more thymidine residues downstream of the 3' end of the RNA sequence, and termination factors, such as Rpc11 or Rpc53, which facilitate the release of the RNA transcript and coordinate the disassembly of RNA Pol III (Landrieux *et al.* 2006; Orioli *et al.* 2012).

The termination of transcription by RNA Pol III is directly coupled with the reinitiation of transcription (Landrieux *et al.* 2006; Boguta and Graczyk 2011). RNA Pol III is more likely to reinitiate on the same gene after the first round of transcription without being released from the DNA template mediated by a stably bound TFIIIB. This results in a higher initiation efficiency at a rate of 2 – 4 transcripts per gene and a 5-fold increase with reinitiation (Boguta and Graczyk 2011). Important for the correct recognition of termination signals and a fast reinitiation process are the factors Rpc11 and the heterodimer Rpc37/Rpc53, which are known to physically interact with each other (Landrieux *et al.* 2006; Orioli *et al.* 2012; Moir and Willis 2013; Shekhar *et al.* 2023). Rpc37/Rpc53 is located at the outer edge of the DNA-binding cleft (Figure 3.16 c), where DNA enters the complex, which allows for the correct recognition of the termination signals. A conformational change in the terminating sequence mediated by the Rpc37/Rpc53 subunit results in a high level of pausing of RNA Pol III, slowing down transcription and thus facilitating RNA release. Additionally, the complex is involved in promoter opening by interacting with the subunits of TFIIIB and TFIIIC. The subunits Rpc37 and Rpc53 have no paralogs in RNA Pol I or II highlighting their specific relevance in RNA Pol III transcription (Schramm and Hernandez 2002). Additionally, Rpc11 is crucial for facilitating the reinitiation of RNA Pol III, as it induces a conformational change in RNA Pol III (Landrieux *et al.* 2006; Moir and Willis 2013).

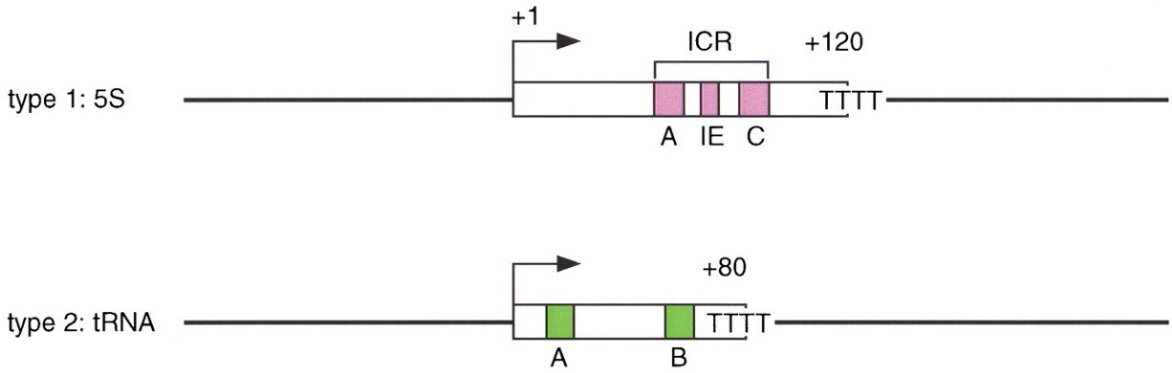

Figure 3.17 Types 1 and 2 RNA polymerase III promoter structures.

Type 1 promoters are usually present in 5S rRNA genes. These include an A box (+50 to +60 bp), an intermediate element (+67 tp +72 bp), and a C box (+80 to +90 bp). Together, these three motifs form an internal control region (ICR). tRNA genes contain a type 2 promoter with an A box (+8 to +19 bp) and a B box (+52 to +62 bp) motif. Abbreviations: A, A box; B, B box; C, C box; ICR, internal control region; IE, intermediate element. Figure adapted from Schramm and Hernandez (2002).

Transcription by RNA Pol III is also regulated by various factors, such as nutrient availability, cellular stress, and growth conditions (Pluta *et al.* 2001; Boguta and Graczyk 2011; Szatkowska *et al.* 2019). Maf1 has been identified as a key repressor of RNA Pol III activity in response to environmental conditions (Pluta *et al.* 2001; Lee *et al.* 2009; Boguta and Graczyk 2011; Moir and Willis 2013; Szatkowska *et al.* 2019). Under favourable growth conditions, Maf1 is phosphorylated by a variety of kinases, including TORC1, Sch9, and PKA, on corresponding consensus sites (for example, RR/KXS/T). Phosphorylated Maf1 is exported from the nucleus as Sch9 mediates interaction with exportin Msn5, and PKA inactivates the two NLSs to keep Maf1 in the cytoplasm (Figure 3.18). The N-terminal NLS is located close to the PKA/Sch9 phosphorylation site, whereas the C-terminal NLS lies within the conserved domain of the protein. Both NLSs are functional and sufficient for the localisation of Maf1. When Maf1 is exported from the nucleus, RNA Pol III is activated, enabling its transcription by reinitiation. If conditions are unfavourable, Maf1 is dephosphorylated by PP2A and other phosphatases and imported to the nucleus via activated NLSs (Figure 3.18). Further, nuclear dephosphorylation of Maf1 leads to shuttling to the nucleolus and an interaction with the RNA Pol III complex, where it inhibits the reinitiation of transcription (Figure 3.18). Maf1 also interacts with unbound RNA Pol III to prevent it from binding to the template.

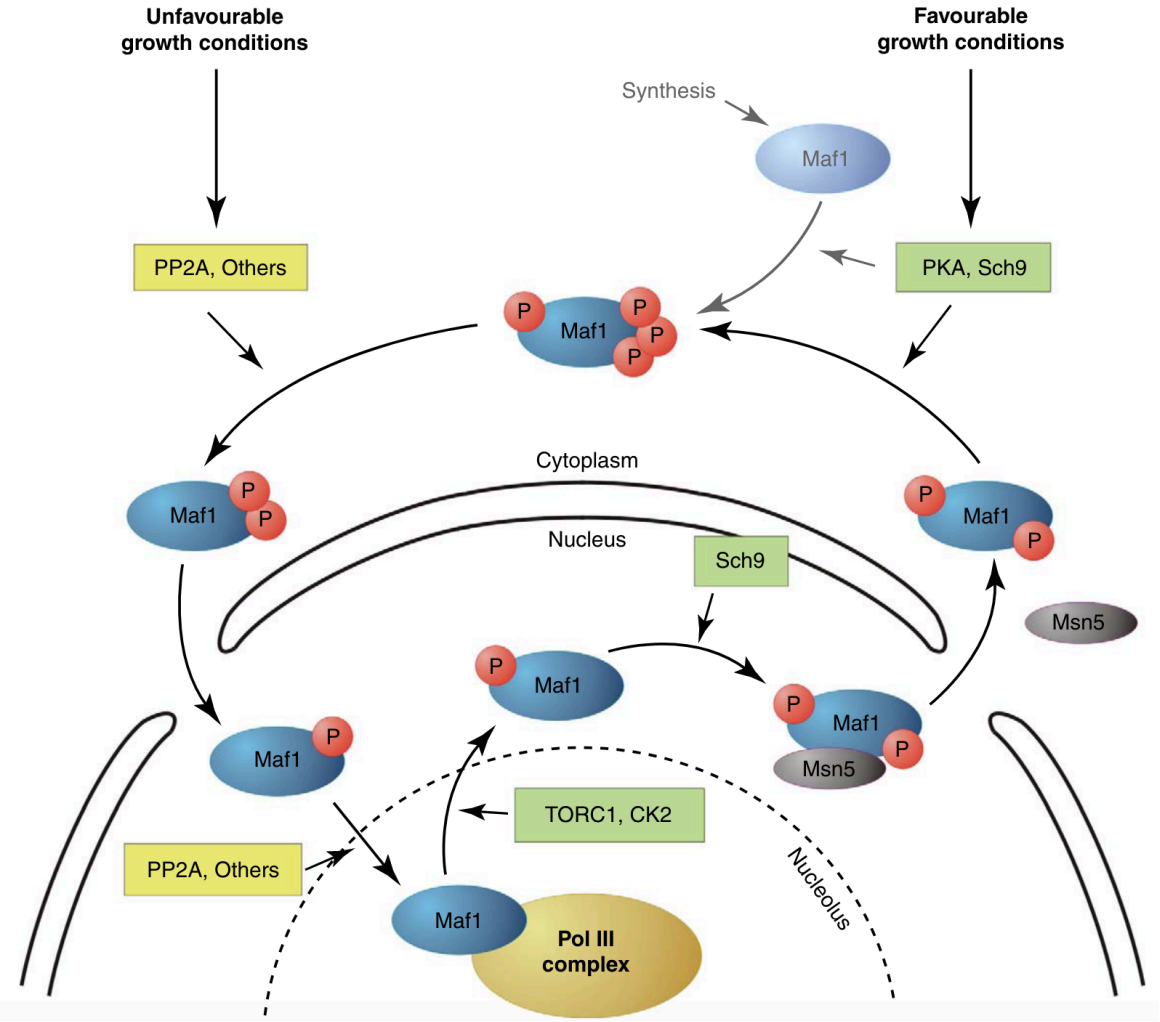

Figure 3.18 Mechanism of phosphorylation-dependent nuclear shuttling of Maf1.

Under favourable growth conditions, Maf1 is localised in the cytoplasm and phosphorylated by PKA and Sch9. This inactivates the nuclear localisation sequences. When conditions become unfavourable, PP2A, and other phosphatases dephosphorylate Maf1, leading to its import into the nucleus. Additional dephosphorylation of Maf1 enables the protein to enter the nucleolus and interact with RNA Pol III, thereby inhibiting its function. Once circumstances return to optimal growth conditions, TORC1 and CK2 phosphorylate nucleolar Maf1 which dissociates from RNA Pol III and thereby reactivates the polymerase. Maf1 exits the nucleolus. In the nucleus, Maf1 is further phosphorylated by Sch9 which enables its interaction with exportin Msn5. Maf1 is exported from the nucleus and is phosphorylated for inactivation. Abbreviations: PP2A, protein phosphatase 2A. Figure from Boguta and Graczyk (2011).

A second pathway for RNA Pol III inhibition involves direct phosphorylation of the subunit Rpc53 (Moir and Willis 2013; Lee *et al.* 2015; Turowski and Tollervey 2016). Kns1, a member of the LAMMER family kinases and negative effector of TORC1, acts as a priming kinase for Rpc53 hyperphosphorylation by Mck1 (Lee *et al.* 2012, 2015; Moir and Willis 2013; Turowski and Tollervey 2016). These kinases act in response to nutrient stress, where the phosphorylation of Rpc53 not only induces a change in terminator recognition, but also influences Rpc11 function, although the precise mechanisms have not yet been revealed (Figure 3.19). Together, this leads to an inhibition of RNA Pol III rebinding by reducing the affinity for TFIIIB, disrupting facilitated recycling, and hence promoting RNA Pol III dissociation from the DNA template at the terminator (Figure 3.19). If hyperphosphorylation of Rpc53 occurs together with Maf1 binding to RNA Pol III, reinitiation is directly inhibited. The Maf1-dependent and Rpc53-dependent processes are independently controlled by TORC1 signalling. However, they function together to quickly and efficiently inhibit RNA Pol III function, thereby reducing tRNA and 5S rRNA synthesis in response to unfavourable conditions (Moir and Willis 2013; Lee *et al.* 2015).

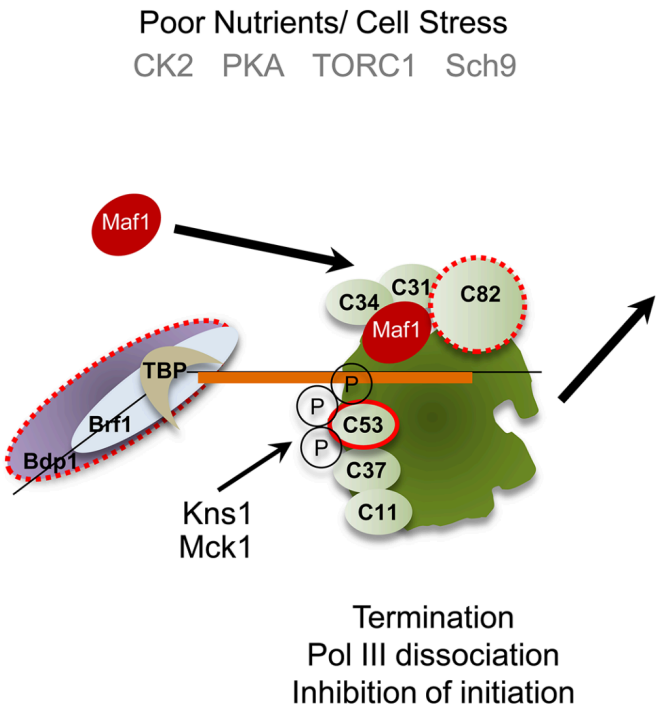

Figure 3.19 Regulatory network of RNA Pol III inhibition in *S. cerevisiae*.

RNA Pol III inhibition via Maf1 and Rpc53 is independently regulated; however, they function together for a quick and efficient response. Under nutrient stress, Maf1 enters the nucleus and binds to the polymerase to inactivate transcription initiation. Additionally, Kns1 and Mck1, the effector kinases of TORC1, are activated to phosphorylate Rpc53 (C53), a regulatory subunit of RNA Pol III. Kns1 acts as a priming kinase for phosphorylation via Mck1. Hyperphosphorylation of Rpc53 leads to a decreased affinity of RNA Pol III for TFIIIB which reduces the facilitated reinitiation process and terminates transcription. Together, these inhibitory processes lead to the termination of transcription and dissociation of RNA Pol III from the DNA template. Figure adapted from Lee *et al.* (2015).

3.3.2 Mechanisms and regulation of translation

After the transcription of specific DNA sequences into mRNA, its processing and export from the nucleus, translation follows (Hinnebusch 2011, 2014; Dever *et al.* 2016). Translation comprises a three-step pathway starting with initiation, progressing to elongation, and concluding with termination. Translation results in the synthesis of proteins by using mRNA as a template. Initiation is the most critical and intricate step, as it involves the coordination of 11 translational initiation factors and is a target for stress response (Hinnebusch 2014).

3.3.2.1 Assembly of the eukaryotic initiation factor 2 (eIF2)

The eukaryotic initiation factor 2 (eIF2) plays a crucial role in translation initiation as it brings the $tRNA_i^{Met}$ to the ribosome and enables recognition of the start codon, which is described in more detail in section 3.3.2.2 (Hinnebusch 2014). eIF2 is a heterotrimeric protein complex that consists of three subunits, α, β and γ, in *S. cerevisiae* encoded by the genes *SUI2*, *SUI3* and *GCD11*, respectively (Schmitt *et al.* 2010; Perzlmaier *et al.* 2013). The eukaryotic initiation factor is highly conserved in eukaryotes and archaea, too. Studies on the subunits of eIF2 highlighted its structural features. The α subunit comprises three domains: an N-terminal β-barrel (DI), a helical domain (DII) and a α-β domain (DIII). DI and DII form an immobile basis with a flexible DIII attached. The α subunit is also a target for phosphorylation and the conserved phospho-site, a serine residue (Ser51 in yeast), is located within a loop in the β-barrel. eIF2β is also composed of three domains: a lysine-rich N-terminal α-helix, which mediates binding to eIF2B and eIF5, a central α-β domain and a C-terminal zinc-binding domain (ZBD), which interacts with eIF2γ. The N-terminal domain is connected to the central core by a flexible linker and does not interact with the other domains. The γ subunit also consists of three domains. The N-terminal G-protein domain (DI) contains a guanine nucleotide binding pocket, which undergoes conformational changes to form an active, GTP-bound, and inactive GDP-bound state of the protein. Additionally, there are two β-barrels (DII and DIII) that form the subunit structure. eIF2γ also binds the $tRNA_i^{Met}$ and serves as the core of the complex by associating with the α and β subunits. However, eIF2α and eIF2β do not interact with each other. All three subunits are essential for cell viability, and correct assembly is required. The ATP-grasp protein Cdc123 was found to bring the three subunits of eIF2 together (Perzlmaier *et al.* 2013; Panvert *et al.* 2015). Cdc123 binds to DIII of eIF2γ which promotes an independent association with eIF2α and eIF2β (Figure 3.20). Thus, a heterotrimeric complex is formed and Cdc123 is released.

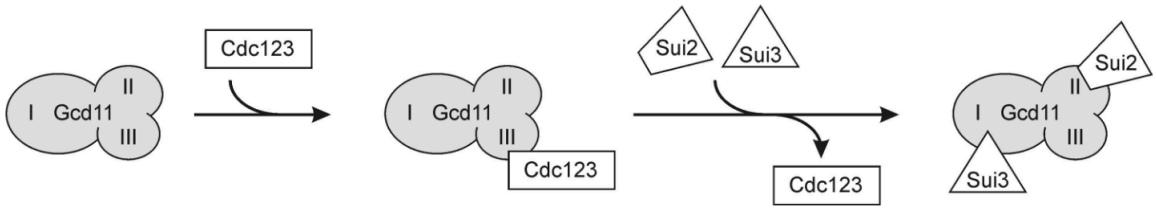

Figure 3.20 Assembly of the heterotrimeric complex of eIF2 in *S. cerevisiae*.

The assembly factor Cdc123 binds to domain 3 (III) of eIF2γ (Gcd11) and facilitates the independent recruitment of eIF2α (Sui2) and eIF2β (Sui3). After the subunits are joined, Cdc123 is released from the complex. Abbreviations: I – III: domains I – III of eIF2γ; Gcd11: eIF2γ; Sui2: eIF2α; Sui3: eIF2β. Figure adapted from Perzlmaier *et al.* (2013).

3.3.2.2 Insights into the mechanism of translation initiation

Translation initiation is the main regulatory step in the translation process (Gebauer and Hentze 2004; Hinnebusch 2011, 2014; Dever *et al.* 2016). It comprises multiple steps to assemble the ribosome correctly at the start codon. The first step in translation initiation is the formation of a ternary complex (TC) composed of eIF2, GTP, and $tRNA_i^{Met}$ (Figure 3.21). eIF2 is a heterotrimeric G-protein consisting of three subunits (α, β and γ, section 3.3.2.1). It is activated when GTP binds to the γ subunit. The affinity of $tRNA_i^{Met}$ is higher for eIF2-GTP than for eIF2-GDP. Once the TC is formed, it is recruited to the small 40S ribosomal subunit, and additional eukaryotic initiation factors, eIF1, eIF1A, eIF3, and eIF5, join to form the 43S pre-initiation complex (PIC) (Figure 3.21). Within the PIC, eIF1, eIF3, eIF5, and TC together form a multifactor complex (MFC) stabilised by the interaction of the N-terminal domains of eIF1A, eIF2, and eIF3 (Hinnebusch 2014; Dever *et al.* 2016). In parallel, the mRNA is activated by the binding of eIF4E, eIF4A, and eIF4B to the capped 5' end of the mRNA. Additionally, eIF4G, supported by the poly(A) binding protein Pab1 (PABP), binds to the poly(A) tail at the 3' end of the mRNA. This allows the formation of a stable circular mRNA complex facilitated by the interaction between eIFs and the ATP-dependent helicase activity of eIF4A (Figure 3.21). The 43S PIC is then bound to the circular mRNA complex at the 5' end (Figure 3.21). The complex starts scanning for the start codon, which usually consists of an AUG triplet supported by the optimal sequence context, the Kozak sequence (5'-GCC(A/G)CC AUG G-3'), along the mRNA (Figure 3.21) (Kozak 1986, 2005). Typically, a purine, A or G, is present at position -3, and a strong consensus G at position +4 supports the start codon context in *S. cerevisiae*. The scanning process involves the use of eIF2 and eIF5 to ensure that the start codon is recognised. Even though the Kozak sequence helps to recognize the start codon, an AUG codon in a weaker sequence context may be distinguished from non-AUG codons with the aid of eIF1 (Kozak 2005; Jackson *et al.* 2010; Hinnebusch 2011). When the start codon is identified within the peptidyl-tRNA (P) site of the 40S subunit, the 48S complex is formed, facilitated by bound eIFs (Figure 3.21). Additionally, irreversible hydrolysis of GTP bound to eIF2, catalysed by eIF5, is initiated. Thus, $tRNA_i^{Met}$ is correctly bound to the complementary start codon at the P site of the 40S ribosomal

subunit, and eIF2-GDP loses its affinity for $tRNA_i^{Met}$, which results in the release of eIF2-GDP, eIF1, and eIF5 from the complex (Figure 3.21). eIF5B-GTP enters the complex, and by hydrolysis of GTP, eIF5B catalyses the joining of the large 60S ribosomal subunit (Figure 3.21). In total, this results in the formation of the 80S ribosome with the $tRNA_i^{Met}$ correctly base-paired to the start codon AUG at the P site, followed by the transition to the elongation phase.

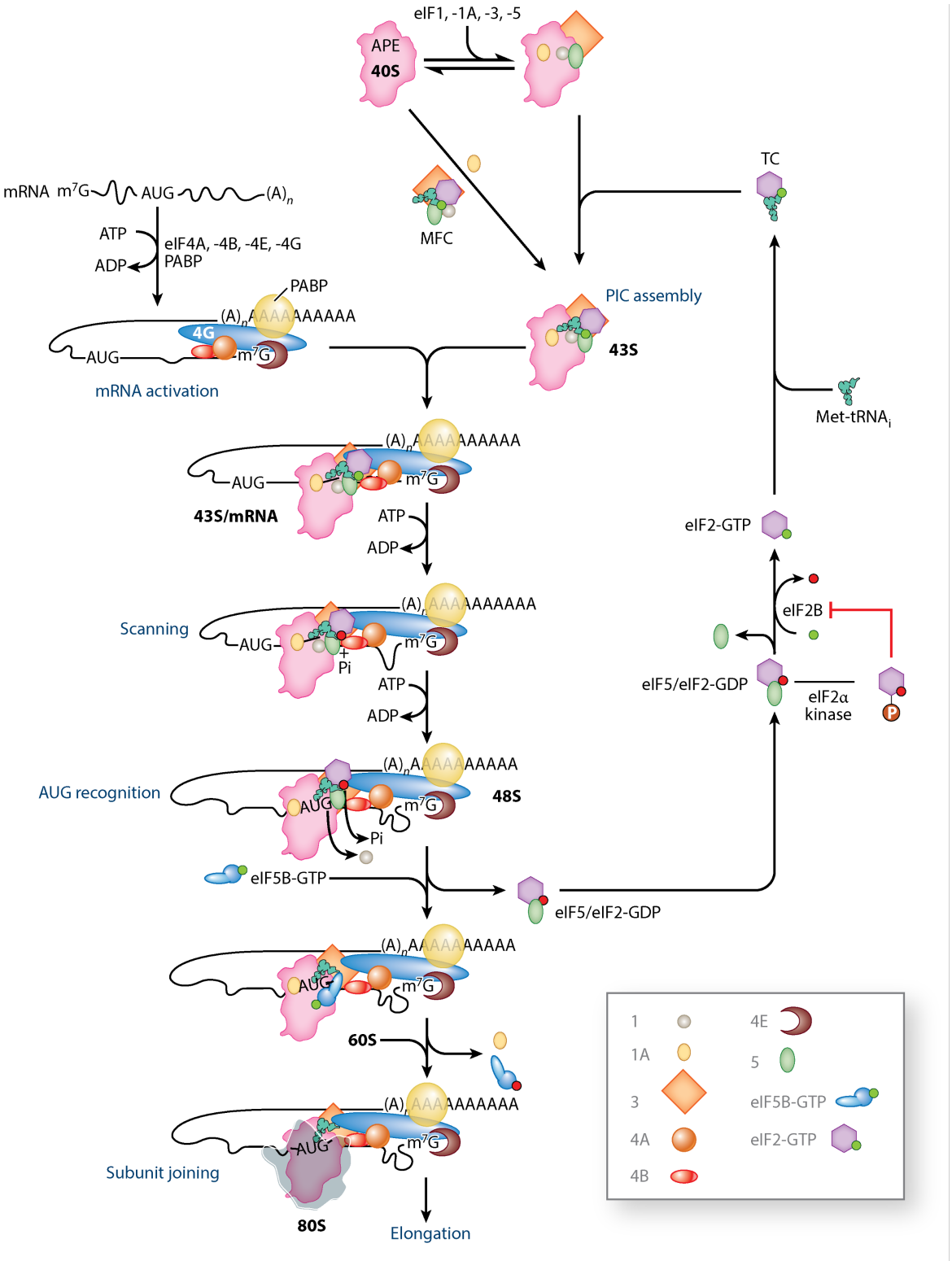

Figure 3.21 Translation initiation mechanism in *S. cerevisiae*. (Description on next page)

The first step in translation initiation is the formation of a ternary complex consisting of eIF2 (purple hexagon), GTP, and initiation methionyl tRNA ($tRNA_i^{Met}$). Together with the 40S ribosomal subunit, eIF1, eIF1A, eIF3, and eIF5, the 43S pre-initiation complex (PIC) is assembled. This complex is stabilised by a multifactor complex (MFC) that interacts with TC, eIF1, eIF3, and eIF5. The mRNA is activated by the binding of eIF4A, eIF4B, eIF4E, and eIF4G, supported by poly(A)-binding protein (PABP). This complex leads to the circularisation of the mRNA connecting the 5 'and 3' ends. Once this process is completed, the mRNA can join the 43S PIC and scanning along the mRNA begins. When the start codon is recognised by the TC, GTP of eIF2 is hydrolysed with the help of eIF5. This sets the $tRNA_i^{Met}$ at the correct position. eIF2-GDP and eIF5 are released from the complex and enter a recycling mechanism. eIF5B-GTP enters the complex and is hydrolysed to recruit the 60S ribosomal subunit. eIF5B-GDP and eIF1A are released once the large ribosomal subunit has joint and the 80S initiation complex (IC) is formed. Recycling of eIF2 is facilitated by eIF2B, a guanine exchange factor that replaces GDP with GTP, thereby activating eIF2. The recycling of eIF2 and circularised mRNA ensures fast reinitiation of the same mRNA once the first translation cycle is completed. Abbreviations: IC, initiation complex; Met-$tRNA_i$, methionyl initiator transfer RNA; MFC, multifactor complex; PABP, poly(A)-binding protein; PIC, pre-initiation- complex; TC, ternary complex. Figure from Hinnebusch (2014).

To ensure high turnover and fast reinitiation of translation, eIF2-GDP must be recycled (Gebauer and Hentze 2004; Hinnebusch 2011, 2014; Crawford and Pavitt 2019). Reactivation of eIF2 is possible by exchanging GDP with GTP, which is facilitated by the guanine nucleotide exchange factor (GEF) eIF2B (Figure 3.21). Active eIF2-GTP can then be integrated into a TC to ensure a high reinitiation rate. However, this process is also the main target of regulation (Gebauer and Hentze 2004; Crawford and Pavitt 2019). Under nutrient stress, for example amino acid starvation, Gcn2, an eIF2α kinase, is activated which phosphorylates Ser51 of the α subunit (Figure 3.22). This phosphorylation results in a higher affinity of eIF2B for eIF2-GDP. However, guanine exchange is inhibited (Figure 3.22). Through this mechanism, the eIF2-eIF2B complex is sequestered, the recycling of eIF2 is blocked, and the availability of active eIF2-GTP is drastically reduced (Figure 3.22). Hence, the formation of the ternary complex is decreased which leads to a global reduction in translation initiation.

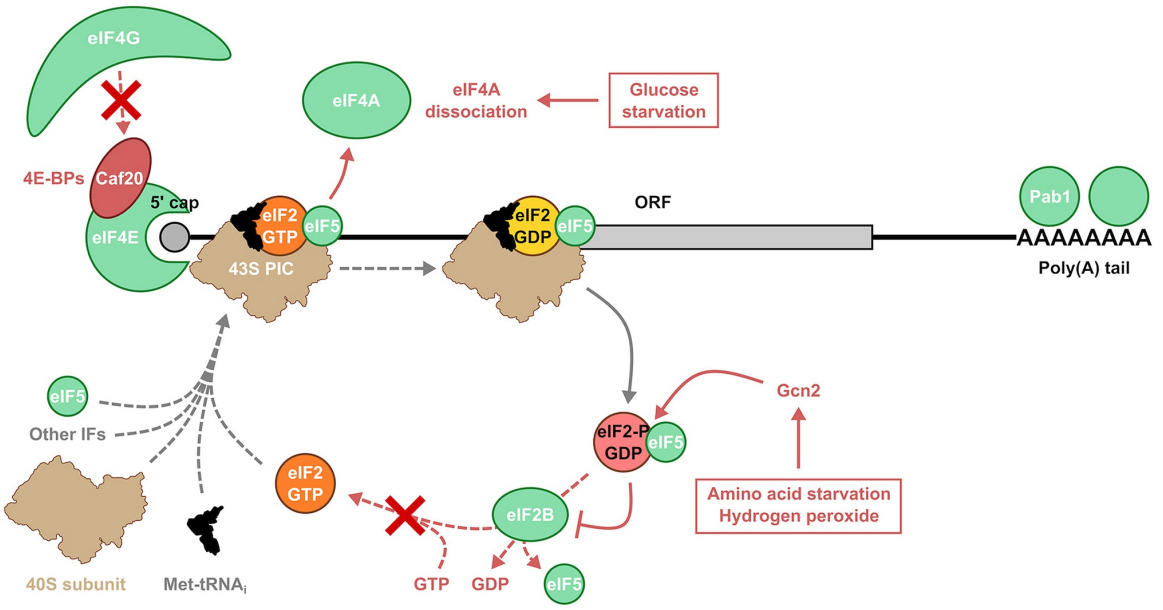

Figure 3.22 Regulatory mechanisms of stress response in *S. cerevisiae*.

Different stressors mediate the downregulation of translation. Glucose starvation leads to the dissociation of eIF4A and eIF4G can be inhibited from binding to eIF4E via 4E-binding proteins. Both processes lead to a reduction in translation initiation. A core regulatory factor, however, is eIF2. Under nutrient starvation (e.g. amino acid starvation) Gcn2 is activated. This kinase phosphorylates eIF2α. This phosphorylation increases the affinity of eIF2B for eIF2-GDP and blocks it from exchanging GDP with GTP. Therefore, eIF2 recycling decreases and the availability of eIF2-GTP is reduced. Hence, the formation of the ternary complex is diminished, and the global translation initiation rates are downregulated. Figure adapted from Crawford and Pavitt (2019).

3.3.2.3 Cap-independent mechanisms of translation initiation

In addition to the cap-dependent translation initiation mechanism explained in section 3.3.2.2, other cap-independent mechanisms have been identified in eukaryotes (Gebauer and Hentze 2004; Kozak 2005; Sonenberg and Hinnebusch 2009; Crawford and Pavitt 2019). The two major mechanisms are upstream open reading frame (uORF) and internal ribosome entry site (IRES)-dependent initiation.

Typically, the first start codon that is reached initiates translation in *S. cerevisiae*. However, the first AUG codon may not be recognised when it is in a weak sequence context, and ribosomes simply scan over it in the process of "leaky scanning" (Kozak 2005; Hinnebusch 2011; Hinnebusch *et al.* 2016; Crawford and Pavitt 2019). Translation initiation may occur at these sites if downstream AUGs are present. If the next start codon is in the reading frame of the first and there is no stop codon in between, translation can be initiated at both codons with a certain frequency to produce proteins of different lengths (Kozak 2005; Hinnebusch *et al.* 2016). If codons are not in frame with each other, different proteins may be translated. This process has already been described for *CPA1* in *S. cerevisiae* (Crawford and Pavitt 2019). Here, *CPA1* mRNA contains a uORF which encodes the arginine attenuator peptide (AAP). Under

conditions lacking arginine, only approximately 50 % of the ribosomes translate the AAP uORF. The remaining 40S ribosomes scan through this uORF and can be reinitiated at the *CPA1* ORF. When arginine is present, ribosomes only translate AAP and cannot scan further along the mRNA to reach the main ORF. This regulatory mechanism ensures the expression of Cpa1 only under arginine-sparse conditions, where it is necessary for arginine biosynthesis. An additional regulatory mechanism, ribosome reinitiation, occurs when the translation machinery does not dissociate after termination at a uORF and the following coding region can be reinitiated (Gebauer and Hentze 2004; Dever *et al.* 2016; Crawford and Pavitt 2019). The distance between the stop codon of the uORF and the coding region determines the reinitiation of the coding ORF. Here, a larger distance between uORF and ORF helps to assemble the 43S PIC in time, while the 40S ribosomal subunit remains bound to the mRNA and continues to the next start codon. When sufficient TC is available, reinitiation occurs. An intensely studied example of this mechanism is the translation of *GCN4*. The *GCN4* mRNA contains four uORFs that encode only small peptides. The translation of uORFs 1 and 2 promotes downstream scanning, as the surrounding sequences preserve the interaction of the 40S ribosomal subunit with the mRNA. Thus, 40S ribosomes can be reinitiated when sufficient $tRNA_i^{Met}$ for TC formation is present. Under optimal conditions, the recycling of eIF2 by eIF2B leads to the fast formation of TC and thus the translation of uORFs 3 and 4 (Figure 3.23). However, these uORFs terminate translation, and ribosomes dissociate from the mRNA before reaching the *GCN4* ORF. During stress, a reduced guanine exchange of eIF2-GDP leads to reduced availability of TC, which allows the 40S ribosomes to migrate past uORFs 3 and 4. Subsequently, the TC is re-acquired, and translation is reinitiated at the main *GCN4* ORF (Figure 3.23). This ensures a higher expression of Gcn4 under stress conditions, where it is needed for the stress response, as described in more detail in section 3.3.2.4.

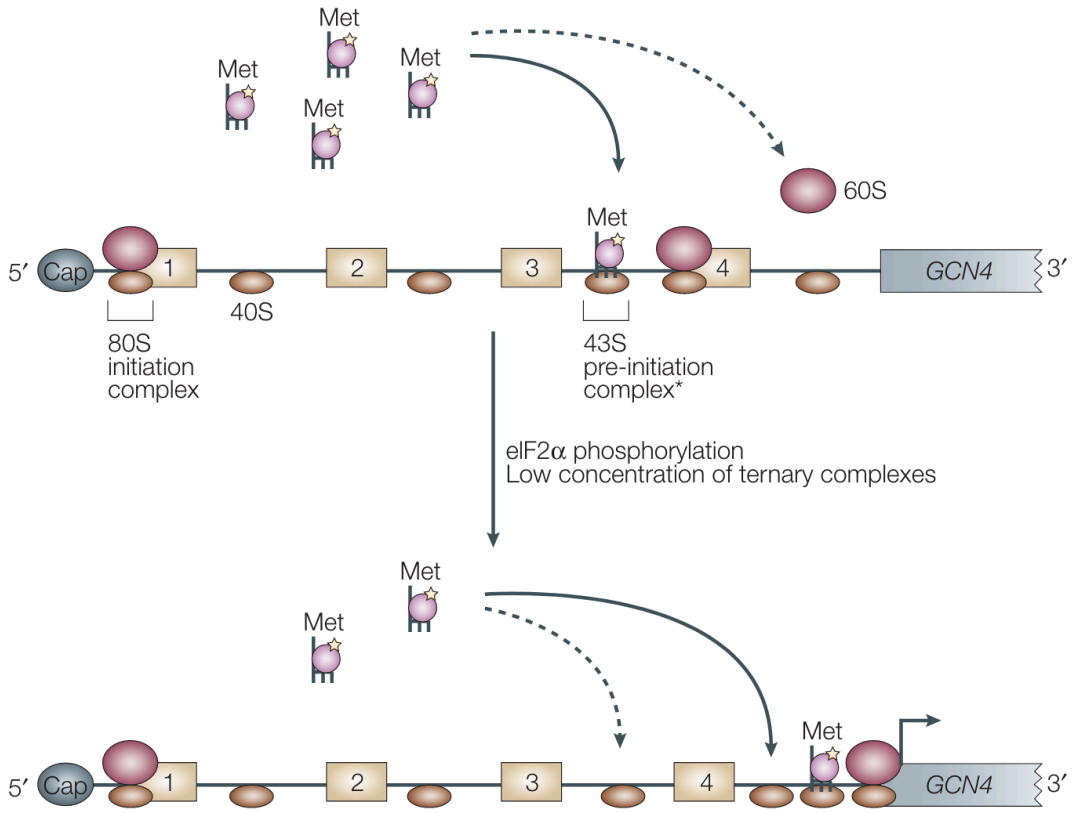

Figure 3.23 Translation initiation of the *GCN4* mRNA by ribosome reinitiation.

The mRNA of *GCN4* contains four uORFs in the 5' region. Under favourable conditions, translation initiation begins at the first start codon, which leads to the translation of small peptides from uORF 1 and 2. Specific sequences allow the 40S ribosomal subunit to remain bound to the mRNA and to further scan along it after termination of translation. With high TC levels, the ribosome is quickly reinitiated at uORFs 3 or 4. These uORFs, however, do not support further scanning of the ribosome after termination, the ribosome dissociates, and the *GCN4* ORF is only sparsely reached, expressing low levels of Gcn4. Under stress conditions, when Gcn4 is necessary to respond to changing nutrients, a phosphorylation of eIF2α leads to a decrease in TC. Reduction in available TC decreased the levels of translation initiation, mostly at uORF 1. After that, the 40S ribosomal subunit stays bound to the mRNA and scans along until eventually reinitiation takes place. Under stress conditions, this takes time, and ribosome reinitiation most likely takes place after uORF 4 has passed. This induces translation of the main *GCN4* ORF and an increase in protein expression compared to favourable conditions. Abbreviations: 1-4, uORF 1-4; 40S, 40S ribosomal subunit; 60S, 60S ribosomal subunit; Met, initiation methionyl tRNA; TC, ternary complex. Figure adapted from Gebauer and Hentze (2004).

Another cap-independent mechanism utilises internal ribosome entry sites (IRESs) (Hellen and Sarnow 2001; Gebauer and Hentze 2004; Jackson *et al.* 2010; Crawford and Pavitt 2019). IRESs are structures located in the 5' region or the open reading frame of mRNAs that directly recruit the ribosome to a position close to or at the initiation codon. IRES-mediated translation was first identified as a strategy for the regulation of viral mRNA expression. Through this cap-independent mechanism, viruses can translate their mRNAs, while the cap-dependent translation of the host mRNA is inhibited. Four subclasses were identified for viral IRESs, with eIF4E not being required for any of them, as the 5'-cap structure does not need to be recognised. IRESs are also present in cellular mRNAs, even though their distribution, for example, in yeast, and the exact mechanism of translation initiation remains unclear. Most likely, the binding of the eIF4G–eIF4A complex to IRESs is involved in translation initiation. mRNAs containing IRESs can also be translated by cap-dependent initiation, suggesting that IRESs are a possible mechanism for initiating translation under stress conditions when scanning is blocked.

3.3.2.4 Mechanisms of the integrated stress response

As described in section 3.3.2.2, eIF2 not only plays an important role in translation initiation but is also a key mediator of the stress response (Hinnebusch and Natarajan 2002; Crawford and Pavitt 2019; Costa-Mattioli and Walter 2020). A highly conserved signalling pathway, the integrated stress response (ISR), coordinates the adaptation to various stress conditions, such as nutrient deprivation, oxidative stress, or amino acid starvation. In yeast, ISR plays a crucial role in maintaining cellular homeostasis and in promoting cell survival by adapting gene expression to diverse stimuli. While there are multiple processes available for the stress response, such as the unfolded protein response (UPR), oxidative stress response, or heat shock response pathway, the main stress response in *S. cerevisiae* is the general control non-derepressible 2 (*GCN2*) pathway which is mediated by eIF2 (Dever 2002; Hinnebusch and Natarajan 2002; Morano *et al.* 2012; Pavitt 2018). The *GCN2* pathway coordinates cellular adaptation to amino acid starvation and other nutrient stress conditions. When nutrients are scarce, the serine/threonine kinase Gcn2 is activated by the binding of uncharged tRNAs to the histidyl-tRNA synthetase-like domain (HisRS) (Dever 2002; Hinnebusch and Natarajan 2002). This leads to a conformational change in the kinase domain of Gcn2, an increase in autophosphorylation, and activation of the kinase function. Gcn2 then phosphorylates the α subunit of eIF2, which results in a reduced recycling of eIF2-GDP by eIF2B, leading to a limitation of ternary complex and thus a global inhibition of translation initiation (section 3.3.2.2). However, this process also promotes the translation of specific mRNAs involved in amino acid biosynthesis, the general stress response, and metabolic adaptation, such as the transcription factor Gcn4 (Hinnebusch and Natarajan 2002; Sonenberg and Hinnebusch 2009; Pavitt 2018; Costa-Mattioli and Walter 2020). As previously described in section 3.3.2.3, *GCN4* is only translated under unfavourable conditions when ribosomes are reinitiated after inhibitory uORFs. This leads to a strong peak in Gcn4 protein expression. Gcn4 then induces the expression of many genes involved in amino acid biosynthesis, transport, and metabolism, which

allows cells to adapt to amino acid and nutrient starvation and maintain protein homeostasis. When stress is resolved, eIF2α is dephosphorylated by protein phosphatase 1 Glc7 (Pavitt 2018). ISR also interacts with other stress response pathways to coordinate cellular responses to various stress stimuli and to increase cellular survival.

3.3.3 The ubiquitin-proteasome system and protein degradation

Degradation plays a crucial role in maintaining protein homeostasis by reducing the availability of proteins for general turnover or eliminating defective proteins. *S. cerevisiae* utilises two main degradation pathways for protein quality control: autophagy and the ubiquitin-proteasome pathway (UPS) (Pilla *et al.* 2017; Pohl and Dikic 2019).

The conserved cellular process of autophagy is involved in the degradation and recycling of cytoplasmic components such as long-lived proteins, organelles, and aggregates (Mizushima 2007; Nakatogawa *et al.* 2009; Kraft *et al.* 2010; Pohl and Dikic 2019). It functions via the formation of autophagosomes, which are double-membrane vesicles that transport cargo for degradation. The pathway is also repressed by Tor1, a kinase subunit of the Target of Rapamycin Complex 1 (TORC1), and is induced by rapamycin, as TORC1 interacts with cargo targeted for degradation. The autophagy mechanism consists of four steps (Figure 3.24). First, a phagophore, a crescent-like membrane structure, is formed from the endoplasmic reticulum, which is regulated by the Atg1 kinase complex. The cargo is then selected through interactions with specific autophagy receptors and adapter proteins. When the cargo is selected, the phagophore expands and engulfs it, leading to the formation of a complete autophagosome. Finally, the autophagosome transports cargo to the lysosome in mammals or the vacuole in yeast, fuses with it, and targets the cargo for degradation by hydrolases. The resulting breakdown products are released into the cytoplasm for recycling.

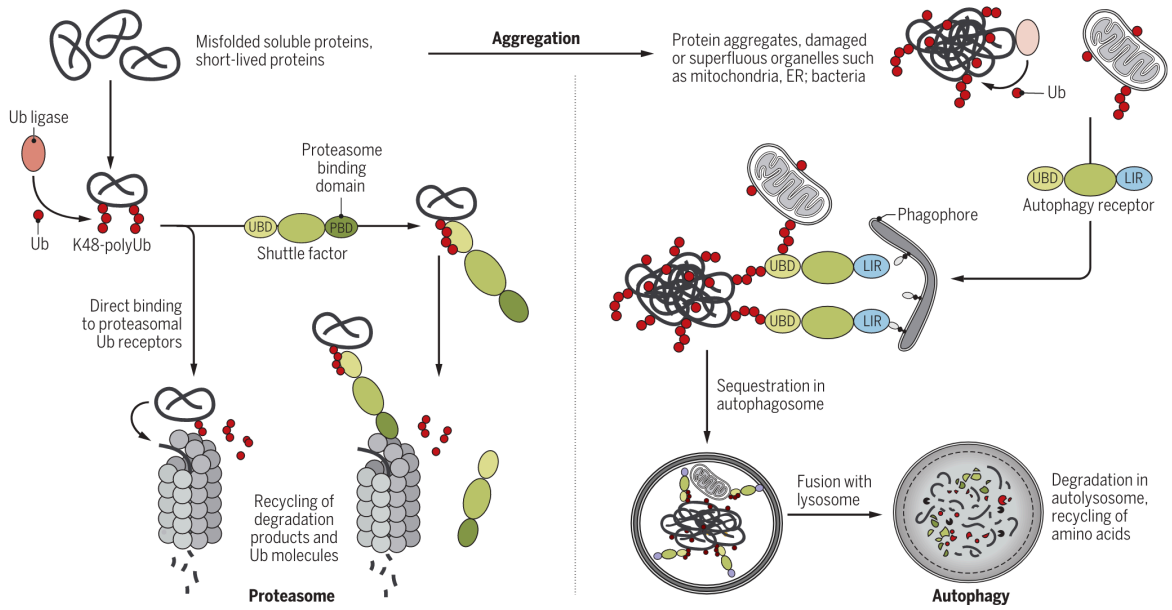

Figure 3.24 Mechanisms of protein quality control (PQC) in eukaryotic cells.

In the eukaryotic system, proteins may be degraded by two different mechanisms. First, misfolded soluble or short-lived proteins can be degraded by the proteasome. Target proteins are polyubiquitinated by ubiquitin ligases. The ubiquitin chain either targets the protein directly to the proteasome, or shuttle factors are bound to tether the substrate to the proteasome. Once attached to the proteasome, the target protein is degraded to small peptides that can be recycled. Ubiquitin molecules are also recycled. If proteins aggregate, are insoluble, or organelles shall be degraded, a second pathway, autophagy, comes into play. Here, a phagophore is formed. Autophagy receptors bind to organelles or protein aggregates, targeting them to the developing phagophores. The phagophore encloses the target and forms an autophagosome. These autophagosomes are then fused to lysosomes (or vacuoles in yeast), and the target protein aggregates or organelles are degraded. The process is non-specific, and amino acids are recycled. Abbreviations: LIR, LC3-interacting region motif, binding to autophagy receptors; PBD, proteasome binding domain; UBD, ubiquitin-binding domain. Figure from Pohl and Dikic (2019).

The ubiquitin-proteasome pathway is responsible for rapid and specific degradation of proteins by covalently attaching ubiquitin and targeting proteins to the proteasome (Kraft *et al.* 2010; Finley *et al.* 2012; Pilla *et al.* 2017; Pohl and Dikic 2019). While autophagy is mainly used as a bulk degradation pathway, the UPS is considered highly selective, with the covalent attachment of ubiquitin chains as a recognition motif for the 26S proteasome (Figure 3.24). Ubiquitin is a highly conserved, 76 amino acids small protein, which consists of seven lysine residues and serves as a molecular marker for proteins by forming ubiquitin chains (Hershko and Ciechanover 1998; Swatek and Komander 2016). Ubiquitination is catalysed by three enzymes: ubiquitin-activating enzyme (E1), ubiquitin-conjugating enzyme (E2), and ubiquitin ligase (E3) (Hershko and Ciechanover 1998; Finley *et al.* 2012; Pilla *et al.* 2017). E1 activates ubiquitin by forming a thioester bond between the C-terminal glycine of ubiquitin and a cysteine residue in the active site of E1 in an ATP-dependent manner. Activated ubiquitin is then transferred from E1 to a cysteine residue in the active site of E2. Finally, E3 ligase facilitates the transfer of ubiquitin from E2 to the target protein which is recognised by

the ligases. E3 ligases bring the substrate proteins in close proximity to the E2-ubiquitin conjugate for this conversion. This process mostly leads to the formation of polyubiquitin chains linked by different lysine residues of ubiquitin on the target protein (Hershko and Ciechanover 1998; Swatek and Komander 2016; Pilla *et al.* 2017). The most common ubiquitin chains are K48- and K63-linked chains, which target proteins for degradation by the 26S proteasome or are involved in signalling pathways, respectively. More than 50 % of all linkages are K48-linked chains, highlighting the importance of protein degradation signals. Once ubiquitinated proteins are recognised, they are targeted to the 26S proteasome (Figure 3.24), a large protease complex consisting of a 20S core particle (CP) capped by two 19S regulatory particles (RP) (Kraft *et al.* 2010; Budenholzer *et al.* 2017; Bard *et al.* 2018; Enenkel *et al.* 2022). The RPs consist of a lid and base subcomplex (Figure 3.25). While the base is crucial for the recognition of ubiquitin chains of more than four ubiquitin modifications by ubiquitin receptors, the lid cleaves the polyubiquitin chain from the substrate with the help of deubiquitinating enzymes (DUBs). Ubiquitin is also recycled in this process. Unfolding of the substrate protein is performed by the ATPase ring of the RP base, and the resulting unfolded protein is mechanically translocated into the 20S CP for proteolysis. The CP is cylindrical and consists of four hetero-heptameric rings which include seven α subunits on the two outer rings and seven β subunits on the two inner rings (Figure 3.25). The inner rings also contain catalytic sites responsible for protein degradation.

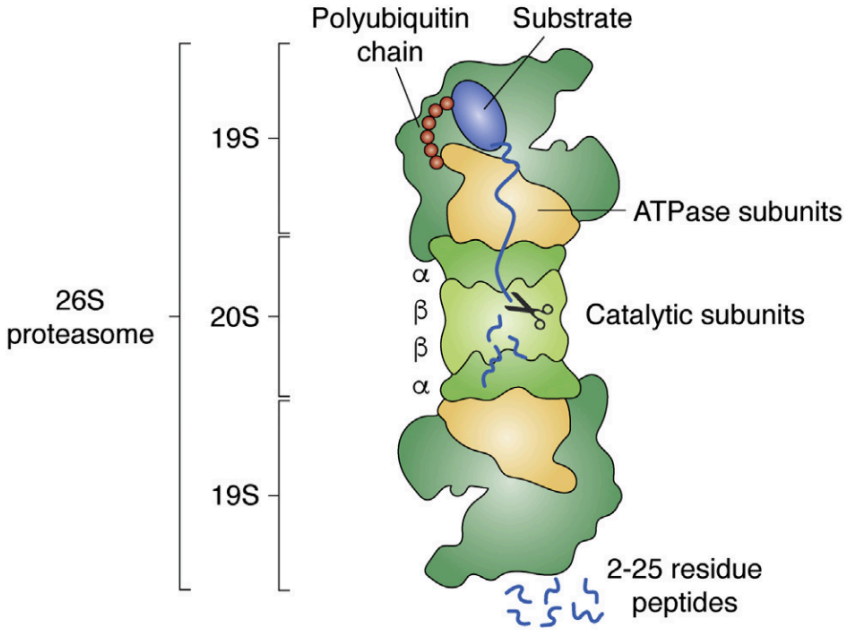

Figure 3.25 Composition of the 26S proteasome in *S. cerevisiae*.

The 26S proteasome consists of a 20S core particle (CP), flanked by two 19S regulatory particles (RP). The RPs comprise a base and lid subcomplex. The base is responsible for the recognition of ubiquitin chains on the target proteins, while the lid cleaves the polyubiquitin chain from the substrate. The ATPase subunits then unfold and target the substrate to the CP, which consists of four stacked rings. The outer rings consist of seven α subunits, and the inner rings are composed of seven β subunits. The catalytic sites are situated in the inner rings of the CP. The resulting small peptide residues are recycled, as well as cleaved ubiquitin molecules. Abbreviations: 19S, 19S regulatory particle; 20S, 20S core particle. Figure from Enenkel *et al.* (2022)

3.4 Target of Rapamycin Complex signalling network

The Target of Rapamycin Complex (TORC) is a highly conserved regulator of cell growth, metabolism, stress response, polarised organisation of the actin cytoskeleton, and endocytosis in eukaryotic cells from yeast to mammals to plants (Loewith and Hall 2011; Laplante and Sabatini 2012; Dobrenel *et al.* 2016; González and Hall 2017). Two independent TOR complexes were found to participate in different signalling pathways. TORC1 integrates signals from various environmental cues such as nutrient availability, energy status, and stress conditions to coordinate cellular responses and ensure optimal growth and survival. It may contain either Tor1 or Tor2 as the catalytic subunit and is rapamycin sensitive. Dysregulation of TORC1 signalling has been identified in various human diseases including cancer, metabolic disorders, and aging (Wullschleger *et al.* 2006; Guertin and Sabatini 2007; Laplante and Sabatini 2012; Howell *et al.* 2013) TORC2 specifically includes Tor2 as the catalytic subunit and is rapamycin insensitive (Loewith and Hall 2011; Laplante and Sabatini 2012). It controls the organisation of actin cytoskeleton, endocytosis, and sphingolipid synthesis.

However, this study focused only on TORC1 and its involvement in cell growth and metabolism.

3.4.1 Composition of the Target of Rapamycin Complex 1

The TOR complex was identified by analysing the mode of action of rapamycin, a lipophilic macrolide. Rapamycin, produced by the bacterium *Streptomyces hygroscopicus*, was first isolated in 1965 from soil samples collected from the Easter Island Rapa-Nui (Hall 1996; Dennis *et al.* 1999; Loewith and Hall 2011). Subsequent studies on this metabolite revealed that it inhibits the growth of tumour cells and leads to G_1 arrest. Later, it was found that rapamycin could block cell cycle progression in yeast and mammals, indicating a conserved target. More research has proposed the involvement of the cytosolic peptidyl-prolyl cis-trans isomerase FKBP12 (FK506-binding protein 12) in mammals and the corresponding Fpr1 in yeast in the activity of rapamycin. The conserved nature of FKBPs further supports the important mechanism of rapamycin. While studying rapamycin, FKBP was found to function only as a cofactor or receptor for targeting rapamycin to two proteins, Tor1 and Tor2. These two proteins are members of the PI kinase-related protein kinase (PIKK) family and are key components of TORC1.

The major regulator of cell growth, TORC1, is a large multiprotein complex that is likely dimeric (Dennis et al. 1999; Loewith and Hall 2011; González and Hall 2017). At its functional core, the serine/threonine kinase Target of Rapamycin (TOR) serves as the catalytic subunit of the complex. Additional regulatory subunits modulate TORC1 activity and substrate specificity (Loewith and Hall 2011; González and Hall 2017). In *S. cerevisiae*, the catalytic subunit consists of either Tor1 or Tor2, which are homologues of the mammalian TOR. The TOR proteins comprise five domains (Figure 3.26 A). The N-terminus includes HEAT repeats with 20 HEAT motifs of 40 amino acids that form two antiparallel α-helices as the binding region for TORC1 subunits. The FAT (FRAP-ATM-TRRAP) domain of 500 residues and the FRB (FKBP12-rapamycin-binding) domain of 100 residues are responsible for FKBP-rapamycin binding. At the C-terminus, the kinase domain and the FATC domain of 35 residues which are necessary for kinase function, follow. The FAT and FATC domains are found in all PIKK family members. The regulatory subunits of TORC1 are Kog1, a homologue of the mammalian Raptor, Lst8, and Tco89, all of which play essential roles in TORC1 assembly, localisation, and substrate recruitment (Figure 3.26 B). TORC1 is mainly bound to the vacuolar membrane, ensuring proximity to nutrient signals in the vacuole (Loewith and Hall 2011).

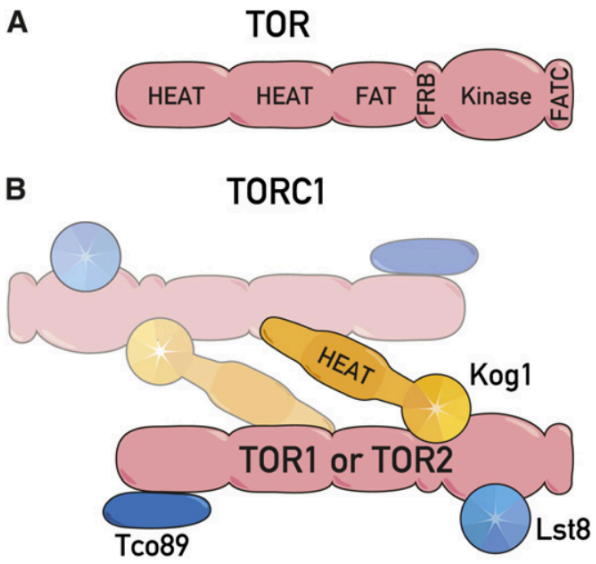

Figure 3.26 Composition of the Target of Rapamycin Complex 1 (TORC1) in *S. cerevisiae*.

A. TOR kinases consist of two HEAT domains at their N-terminal ends. HEAT domains contain approximately 20 HEAT repeats of 40 amino acids that form antiparallel α-helices. The following is a 500 aa FAT domain with modified HEAT repeats. The Ser/Thr kinase domain at the C-terminal end is framed by a 100 aa long FRB domain and a 35 aa FATC domain, which is essential for kinase function. B. TORC1 is likely a dimeric complex of 2 MDa. It contains the kinase subunits Tor1 or Tor2, and the regulatory subunits Kog1, Lst8, and Tco89. Kog1 contains HEAT repeats and a seven-bladed propeller with WD-40 repeats. Kog1 is important for complex formation. The binding of Kog1 to TOR is complicated because multiple domains of both proteins are involved in this process. Lst8 is composed of a seven-bladed propeller of WD-40 repeats and binds to the kinase domain of TOR. Tco89 binds to the HEAT domain of TOR. Abbreviations: FAT, FRAP-ATM-TRRAP; FRB, FKBP12-rapamycin-binding. Figure adapted from Loewith and Hall (2011).

3.4.2 Regulation of TORC1 activity

Nutrient availability, especially carbon and nitrogen signals, serves as a key regulator of TORC1 activity (Loewith and Hall 2011; González and Hall 2017; Deprez *et al.* 2018). Amino acids activate TORC1 via a mechanism involving Gtr1 and Gtr2, members of the RAG family of small GTPases, and Ego1, Ego2, and Ego3, which together form the EGO complex (EGOC) (Binda *et al.* 2009; Loewith and Hall 2011; González and Hall 2017; Morozumi and Shiozaki 2021). This promotes the activation and change in the distribution of vacuolar TORC1 in yeast and an additional translocation towards the vacuolar membrane in mammals. In *S. cerevisiae*, Gtr1 and Gtr2 form a heterodimeric complex that exists in inactive and active states. While Gtr1-GTP/Gtr2-GDP is the active state, Gtr1-GDP/Gtr2-GTP is the inactive state. Vam6 has been characterised as the most likely GEF for Gtr1 (Figure 3.27). The RAG family GTPases Gtr1/Gtr2 also interact with EGOC (Figure 3.27). Ego1 serves as a scaffold protein that interacts with Gtr1/Gtr2 and anchors TORC1 to the vacuolar membrane. The transmembrane protein, Ego3, serves as a tethering component to the vacuole. The active complex Gtr1-GTP/Gtr2-GDP interacts with EGOC, promoting TORC1 activation. TORC1 may

then phosphorylate downstream effectors, such as Sch9 and Tap42 protein phosphatase type 2A (PP2A), to promote cell growth and proliferation (Figure 3.27, and section 3.4.3). Under amino acid starvation, the GTPase complex Gtr1/Gtr2 is inactivated, leading to the inhibition of TORC1 activity. Multiple other factors, such as the Lst4/7 complex, SEACAT and SEACIT, LeuRS, and V-ATPase, integrate signals to the activity state of Gtr1/Gtr2, as depicted in Figure 3.27 (Loewith and Hall 2011; Deprez *et al.* 2018). This allows the cell to perform concerted regulation to conserve energy and adapt to nutrient stress. Furthermore, nutrient signals are integrated by only approximately 20 % by the RAG GTPase-dependent mechanism; thus, an additional pathway is required for the regulation of TORC1 (Hughes Hallett *et al.* 2014, 2015; Hindupur *et al.* 2015; Deprez *et al.* 2018). Glucose starvation signals are mediated by the AMP kinase (AMPK) Snf1 in *S. cerevisiae.* Under these conditions, TORC1 is downregulated by Kog1 phosphorylation (Figure 3.27). Snf1 phosphorylates or at least triggers the phosphorylation of Kog1 at positions Ser491 and Ser494 in a glutamine-rich prion-like motif. This leads to the dissociation of Kog1 from the TOR complex, and Kog1 relocates to reversible bodies on the vacuolar membrane, which, in turn, reduces TORC1 activity. Under favourable conditions, the vacuolar proton pump (V-ATPase) contrasts regulation via Snf1 and activates TORC1 through Gtr1 (Figure 3.27). However, its precise mechanism of action remains unclear.

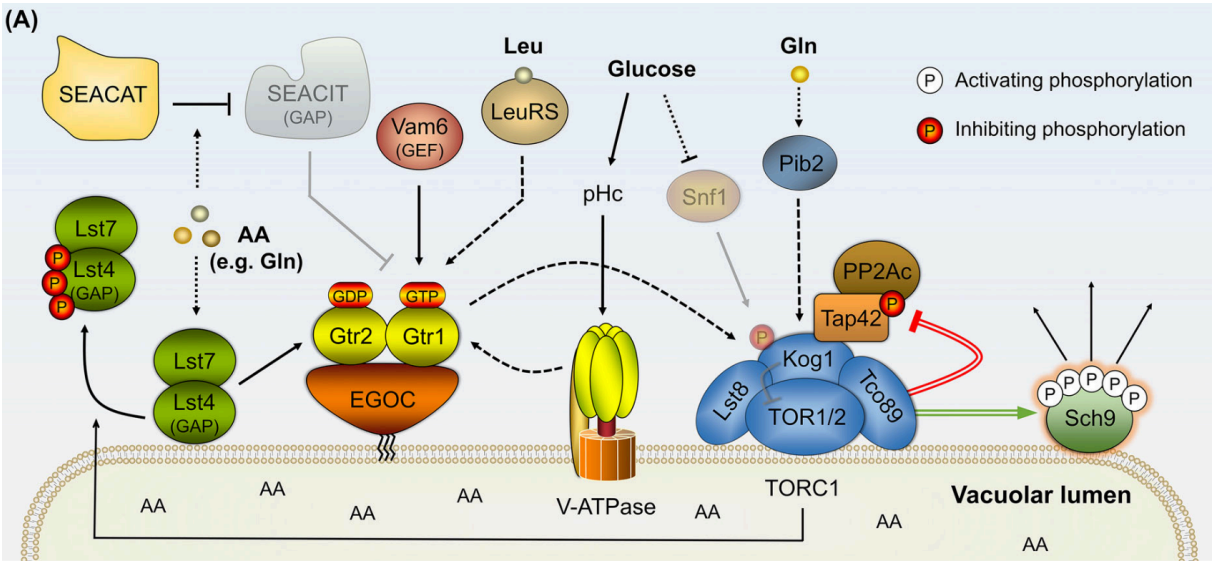

Figure 3.27 Upstream regulation of TORC1 in *S. cerevisiae*.

The activity of TORC1 (blue) is mediated by multiple mechanisms. Amino acid availability is integrated via the Gtr-EGO pathway. High amino acid concentrations lead to the formation of active Gtr1-GTP/Gtr2-GDP heterodimers. These RAG GTPases localise to the vacuolar membrane by binding to the EGO complex (EGOC). This tethering brings the complex into closer proximity to TORC1, increasing its activation. The RAG GTPase complex is positively regulated by many factors, such as leucyl-tRNA synthetase (LeuRS) and Vam6, which mediate Gtr1 activation; the Lst4/7 complex, which mediates Gtr2 activation; and SEACAT and SEACIT. Under favourable glucose conditions, the vacuolar ATPase pump (V-ATPase) acts upstream of Gtr1, which also activates TORC1. When glucose is limited, Snf1 downregulates TORC1 by directly phosphorylating Kog1. When TORC1 is active, it mediates a variety of downstream effectors that promote growth and inhibit stress response. Two major downstream effectors are direct phosphorylation of Sch9, which is activated by TORC1, and Tap42 PP2A, which is

inhibited by the direct phosphorylation of TORC1. Abbreviations: AA, amino acid; EGOC, EGO complex; LeuRS, leucyl-tRNA synthetase; PP2A, protein phosphatase 2 A; V-ATPase, vacuolar ATPase pump. Figure adapted from Deprez *et al.* (2018).

Another mechanism of TORC1 regulation has been found only in *S. cerevisiae*. Under glucose starvation conditions, TORC1 can oligomerize into large helical structures (Prouteau *et al.* 2017). These so-called TOROIDs (TORC1 organised in inhibited domains) are assumed to be an inactive state of TORC1. The assembly of this structure is reversible and involves a Gtr1/Gtr2 GTPase function; however, the exact mechanism remains to be elucidated. In mammals, an additional regulatory pathway, the TSC-RHEB-mediated regulation of mTORC1 activity, is present (Guertin and Sabatini 2007; Laplante and Sabatini 2012; Hindupur *et al.* 2015; Morozumi and Shiozaki 2021). The tuberous sclerosis complex (TSC), consisting of TSC1, TSC2, and TBC1D7, promotes the inactivation of Ras homologue enriched in brain (RHEB) GTPase by GTPase-activating protein (GAP) activity. This leads to a conversion from a GTP (active) to a GDP-bound (inactive) state of RHEB, which integrates multiple physiological stimuli. Active RHEB-GTP stimulates the kinase activity of mTORC1 on the lysosomal surface by direct interaction, which, together with the translocation of mTORC1 by EGOC, leads to activation of kinase function at the site of action. Under unfavourable conditions, TSC inactivate mTORC1 to save energy. Although this mechanism is essential for the control of mTORC1 function in mammals, it is not conserved in *S. cerevisiae*. The yeast RHEB-like GTPase Rhb1 is not a functional RHEB homologue and is, therefore, most likely not involved in TORC1 activation (González and Hall 2017; Morozumi and Shiozaki 2021). Altogether, these regulatory mechanisms ensure that TORC1 activity is properly mediated in response to the availability of amino acids and other nutrients or environmental cues, allowing efficient use of nutrients for growth and adaptation to changing conditions.

3.4.3 Effector kinases of TORC1 and downstream signaling

TORC1 regulates numerous downstream effectors to control cellular processes, such as protein synthesis, ribosome biogenesis, autophagy, and lipid metabolism (Loewith and Hall 2011; Hughes Hallett *et al.* 2014; González and Hall 2017; Deprez *et al.* 2018). Key effectors of TORC1 signalling in *S. cerevisiae* include the AGC kinase Sch9 and Tap42 PP2A. These effectors mediate TORC1-dependent responses to nutrient availability, stress conditions, and growth signals and even regulate changes within the diauxic shift (Galdieri *et al.* 2010; Loewith and Hall 2011).

3.4.3.1 Sch9 – the yeast AGC kinase family member

The yeast AGC kinase Sch9 is one of the best-characterised downstream targets of TORC1, and regulates cell growth, ribosome biogenesis, stress resistance, and lifespan (Loewith and Hall 2011; Hughes Hallett *et al.* 2014; González and Hall 2017; Caligaris *et al.* 2023). The AGC kinase family is named after the mammalian members, PKA, PKG, and PKC (Pearce *et al.* 2010). Phosphorylation of two conserved motifs leads to the activation of AGC family kinases (Urban *et al.* 2007; Loewith and Hall 2011;

Deprez *et al.* 2018; Caligaris *et al.* 2023). These conserved motifs include a "T" or "activation" loop that is located within the catalytic domain of the kinases (Thr570) as well as a hydrophobic motif (F-X-X-F/Y-S/T-F/Y) at the C-terminus. The phosphorylation of these sites, mediated by sphingolipid-activated kinases Pkh1/2 for the "activation loop" and TORC1 for multiple sites in the C-terminal domain, leads to stabilisation of the protein and an active conformation. Phosphorylation of Sch9 by TORC1 requires vacuolar localisation of Sch9 because it has a lower affinity for TORC1 than other TORC1 substrates (Takeda and Matsuura 2018). Additionally, Sch9 can be phosphorylated by Snf1 on Ser288, which leads to inactivation when carbon sources are limited (Deprez *et al.* 2018; Caligaris *et al.* 2023).

Under optimal conditions, TORC1 activates Sch9 through direct phosphorylation, which promotes the Sch9-mediated phosphorylation of various downstream targets involved in protein synthesis and proliferation (Urban *et al.* 2007; Loewith and Hall 2011; Hughes Hallett *et al.* 2014; Deprez *et al.* 2018). However, nutrient starvation leads to inhibition of Sch9 function. Sch9 promotes ribosome biogenesis by phosphorylating and activating ribosomal protein transcription factors (Loewith and Hall 2011; Hughes Hallett *et al.* 2014). Robust protein synthesis is crucial for cell survival, and the transcription and assembly of ribosomes containing 78 proteins and four rRNAs is a key step. To ensure correct processing, folding, assembly, and maturation, small RNA trans-acting factors or ribosome biogenesis (RiBi) factors, which are expressed in a TORC1-dependent manner, are required. The rDNA locus consists of the RNA Pol III-transcribed 5S rRNA gene, an intergenic spacer region, and the RNA Pol I-transcribed 35S rRNA gene, which encodes the 35S precursor of the mature 18S, 5.8S, and 25S rRNAs. This locus is located on chromosome XII and uses 150 tandem repeats for transcription. The co-transcriptional- processing of pre-rRNA is dependent on ribosomal proteins (RPs) (Tschochner and Hurt 2003), and the translation of these RPs is TORC1-dependent (Loewith and Hall 2011). The transcription of RiBi proteins and RPs requires a large amount of energy and is tightly regulated in multiple layers (Loewith and Hall 2011; Hughes Hallett *et al.* 2014). The transcription factor Sfp1, a split zinc-finger protein, is phosphorylated directly by TORC1, presumably leading to nuclear localisation and/or binding to the RP and RiBi promoters which enhances their expression (Figure 3.28). Additionally, Fhl1 and Rap1 bind constitutively to RP promoters, recruiting phosphorylated Ifh1 to Fhl1 when TORC1 is active (Figure 3.28). This stimulates the transcription of the RP genes, most likely by recruiting NuA4, a histone acetyltransferase, to the complex. When nutrients are scarce and TORC1 is inactive, Yak1 activates Crf1 phosphorylation (Figure 3.28). This subsequently binds to Fhl1 as a competitor of Ifh1 (Figure 3.28). Under optimal conditions, Sch9 inhibits phosphorylation of the transcription repressors Stb3 and Dot6/Tod6. However, when TORC1 is inactive, Sch9 no longer phosphorylates these proteins, and they can bind to the polymerase A and C (PAC) sites and ribosomal RNA processing elements (RRPE) in the RiBi promoters (Figure 3.28). Stb3 alone also binds to the RP promoters in T-rich sequences (Figure 3.28). With these repressors in place, RPD3L is recruited to promoter regions. The histone deacetylase complex completely

inhibits transcription. Additionally, transcription by RNA Pol III is regulated via TORC1-dependent mechanisms including Maf1 and Kns1 (section 3.3.1.2). While Sch9 regulates rRNA availability mainly via transcriptional mechanisms, it also regulates a variety of other catalytic steps of ribosome assembly, such as mRNA stability and post-transcriptional mechanisms (Loewith and Hall 2011).

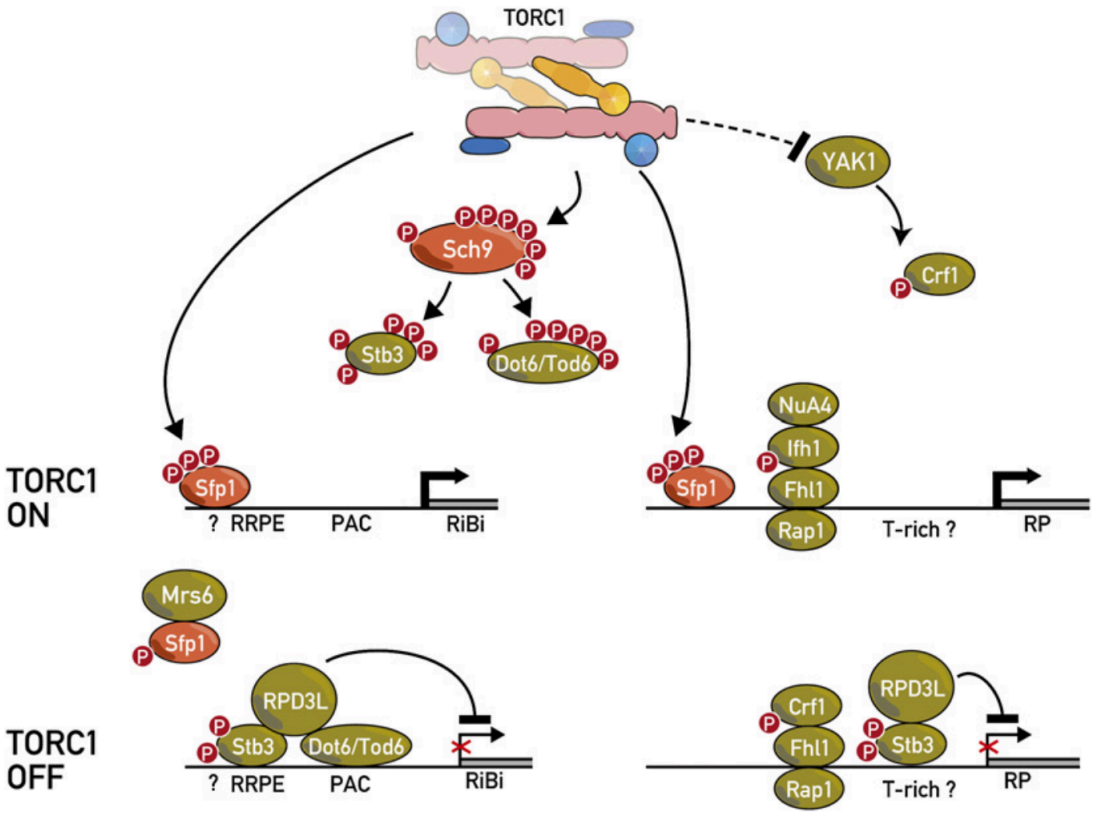

Figure 3.28 : Regulation of ribosome biogenesis mediated by TORC1 effector kinase Sch9.

Sch9 is phosphorylated by TORC1 and other kinases to activate its functions. When TORC1 is active (TORC1 ON), Sch9 directly phosphorylates Stb3 and Dot6/Tod6, thereby inactivating these repressors. TORC1 additionally phosphorylates Sfp1, a transcription factor that binds to the RiBi and RP genes. Additional transcription factors, Rap1, Fhl1, Ifh1, and NuA4, are recruited to RP genes to enhance transcription. When TORC1 is inactive (TORC1 OFF), Sfp1 is blocked from binding to the RiBi and RP genes by binding to Mrs6. Furthermore, Sch9 is inactive, leading to a decreased phosphorylation rate of Stb3. This may then bind to RiBi and RP genes and recruit additional factors. At RiBi, Dot6/Tod6 is bound to the PAC site when unphosphorylated, and together with Stb3, the RPD3L complex is recruited to block RiBi transcription. The transcription of RP genes is inhibited when Stb3 recruits RPD3L to the T-rich site of the promoter. Additionally, Crf1 blocks the binding of Ifh1 and NuA4 to Fhl1 and Rap1 in RP genes. These together lead to an inhibition of RP gene expression. Abbreviations: PAC, polymerase A and C site; RiBi, ribosome biogenesis factor; RP, ribosomal protein; RRPE, ribosomal RNA processing element. Figure from Loewith and Hall (2011).

During stress responses, for example, in diauxic shift, Sch9 modulates the activity of stress-responsive transcription factors, such as Msn2/4 and Gis1, as well as Hsf1, to initiate a quiescent state (Loewith and Hall 2011; Deprez *et al.* 2018). The activity of these stress-responsive factors is coordinated by Sch9's target Rim15 which directly phosphorylates Msn2 and Hsf1 when localised in the nucleus and indirectly phosphorylates Gis1 via endosulfines Igo1/2, which inhibits PP2A-Cdc55 phosphatase. In addition to transcriptional regulation, Sch9 directly phosphorylates and activates components of the translation machinery which enhances protein synthesis (Loewith and Hall 2011; Castilho *et al.* 2014; Yuan *et al.* 2017; González and Hall 2017). The activity of the conserved kinase Gcn2, responsible for eIF2α phosphorylation in response to stress, is not only regulated by uncharged tRNAs when cells lack amino acids, but also by its own phosphorylation (Cherkasova and Hinnebusch 2003; Loewith and Hall 2011; Castilho *et al.* 2014; Yuan *et al.* 2017). Under non-starvation conditions, Gcn2 is phosphorylated on Ser577, reducing its tRNA-binding affinity and thereby blocking kinase function (Figure 3.29). The kinase performing Gcn2 phosphorylation, however, has not yet been revealed. When TORC1 activity is inhibited, Gcn2 is dephosphorylated in a Tap42-PP2A-dependent manner (Figure 3.29) and autophosphorylated at Thr882/887. Consequently, this results in an increase in Gcn2 function and, thereby, phosphorylation of eIF2α. This activates the ISR and reduces overall Cap-dependent translation (section 3.3.2.4). In addition to the regulation of translation, TORC1 also targets additional translation factors, such as the 5' cap-binding protein eIF4E or the scaffold eIF4G, and is itself regulated by Gcn2 (Loewith and Hall 2011; Yuan *et al.* 2017). It is assumed that Gcn2 also directly phosphorylates Kog1 in response to amino acid starvation to downregulate TORC1 activity. This crosstalk between TORC1 and Gcn2 ensures a widespread response to changing nutrients. Sch9 functions as a major kinase hub for nutrient signals from multiple pathways that modulate growth adaptations to nutrient changes (Roosen *et al.* 2004; Urban *et al.* 2007; Loewith and Hall 2011; Yuan *et al.* 2017). Reduced Sch9 activity is associated with extended lifespan and increased stress resistance in yeast and other organisms.

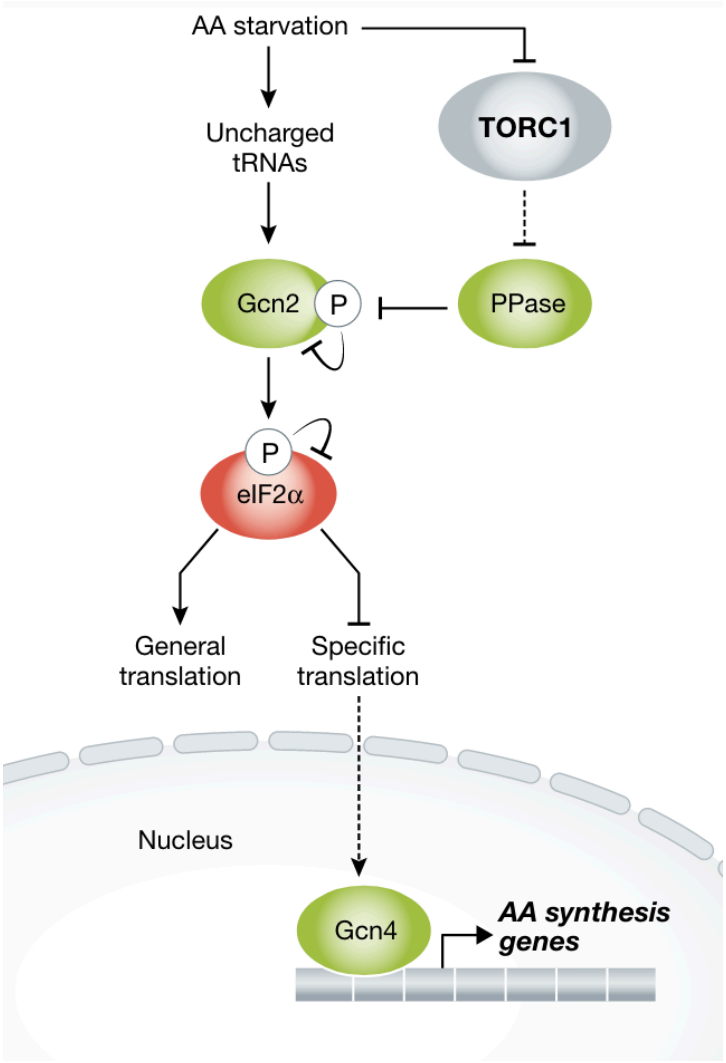

Figure 3.29 Crosstalk of the General Amino Acid Control (GAAC) and TORC1 regulation.

The activity of Gcn2, the only kinase that phosphorylates eIF2α in yeast, is mediated by amino acid availability and TORC1 activity. Under AA starvation, uncharged tRNAs bind to Gcn2 to activate the GAAC pathway, leading to the phosphorylation of eIF2α at Ser51 which inhibits eIF2 function. As part of the integrated stress response (ISR), this leads to a reduction in general translation and an upregulation of specific translation necessary for the stress response, for example, the transcription factor Gcn4. Gcn4 may then activate amino acid synthesis. However, Gcn2 is not only activated by uncharged tRNAs. Under favourable conditions, phosphorylation at Ser577 inhibits Gcn2 function as it reduces tRNA binding affinity. When nutrients are limited, TORC1 is inhibited which in turn activates Tap42 PP2A, among other factors. Tap42 PP2A then dephosphorylates Gcn2 activating its kinase function. An additional autophosphorylation fully enhances the activity and tRNA binding capacities. Abbreviations: AA, amino acid; GAAC, General Amino Acid Control; ISR, integrated stress response; PP2A, protein phosphatase type 2A. Figure adapted from González and Hall (2017).

3.4.3.2 Kns1 – a yeast kinase member of the LAMMER family

Another effector of TORC1 in *S. cerevisiae* is Kns1, a member of the LAMMER protein kinase family (Padmanabha *et al.* 1991; Lee *et al.* 2012; Lim and Park 2019). The family of LAMMER protein kinases is found in most eukaryotes, including Kns1 from *S. cerevisiae*, Lkh1/Kic1 from *Schizosaccharomyces pombe*, AFC1-3 from *Arabidopsis thaliana*, DOA from *Drosophila melanogaste*r, and hCLK1-4 from humans (Ben-David *et al.* 1991; Johnson and Smith 1991; Hanes *et al.* 1994; Yun *et al.* 1994; Bender and Fink 1994; Kim *et al.* 2001; Tang *et al.* 2003; Park *et al.* 2003). LAMMER kinases are essential in higher eukaryotes, but not in lower eukaryotes (Lim and Park 2019). These kinases comprise a unique and highly conserved amino acid sequence motif known as the EHLAMMERILG (or LAMMER) motif, which is located within subdomain X of their kinase domains, as depicted in Figure 3.30 (Hanes *et al.* 1994; Yun *et al.* 1994; Lee *et al.* 1996; Tang *et al.* 2003). The motif lies in an α-helix close to the substrate-binding cleft which most likely allows for contact with the substrates. The catalytic domain of LAMMER kinases is located at the C-terminus and is highly conserved. It contains subdomains responsible for phosphotransfer and substrate recognition. In contrast, the non-catalytic N-terminal domain is highly variable among species, and its function is still unknown. Thus, the precise mechanism of LAMMER kinase regulation and the possible influence of the N-terminal domain remain to be elucidated. However, it has been suggested that the NTD may include a regulatory and dimerization domain, as observed in studies of mammalian CLK1 (Menegay *et al.* 2000).

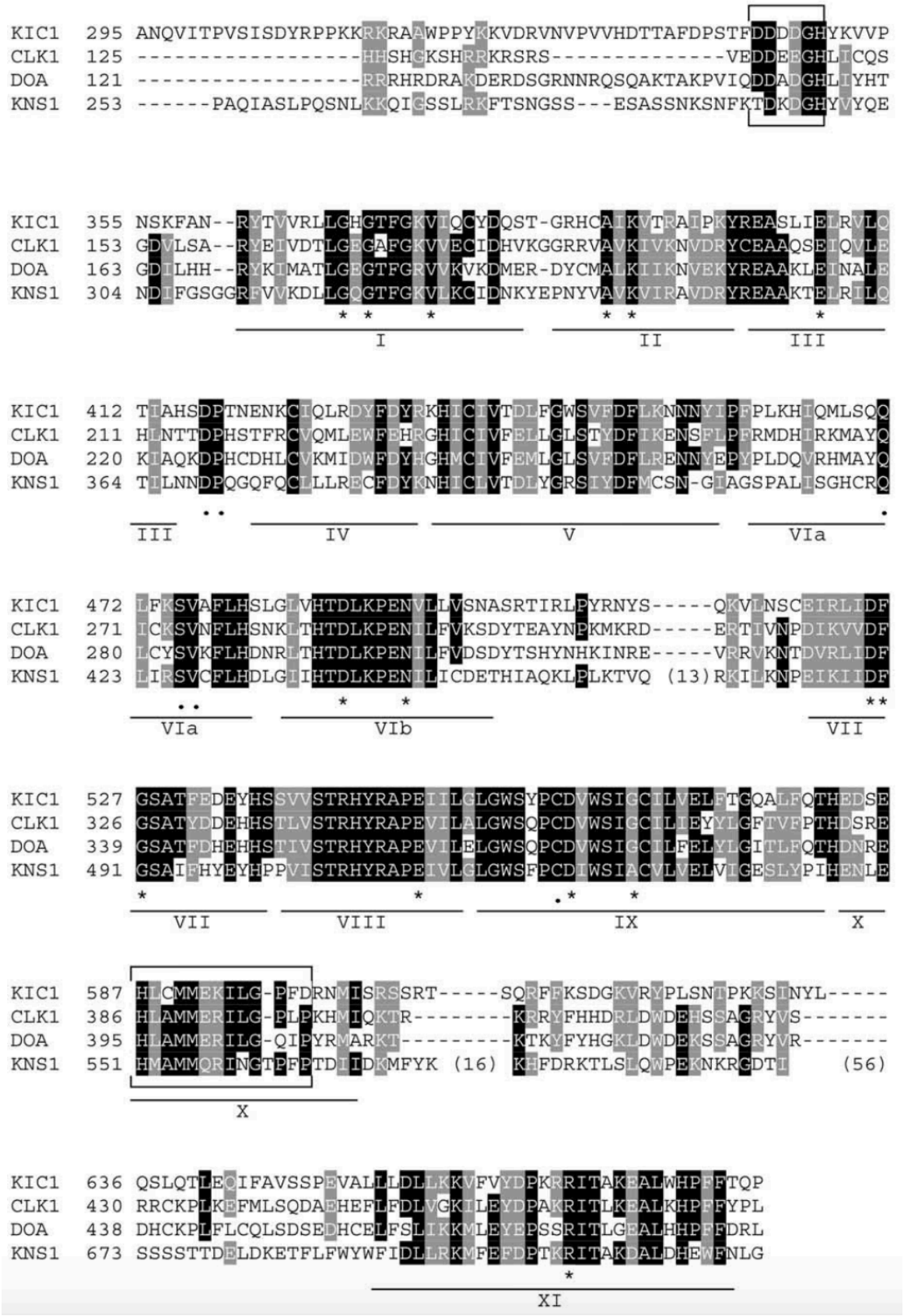

Figure 3.30 Sequence alignment of the catalytic domains of Kic1, CLK1, Doa and Kns1.

The sequences of Kic1 (*S. pombe*), CLK1 (*M. musculus*), Doa (*D. melanogaster*), and Kns1 (*S. cerevisiae*) were aligned using BLASTP, CLUSTALW and GCG. The introduced gaps are annotated with hyphens, and kinase subdomains are annotated with lines and Roman

numbers. Identical amino acids are indicated in black, while conserved substitutions are highlighted in grey. Asterisks indicate invariant residues in all the protein kinases. Additionally, dots mark the conserved amino acids in the LAMMER kinase family. Brackets indicate a DH-box (DDDNxDY)-like sequence and a LAMMER motif. Figure adapted from Tang *et al.* (2003).

Additionally, all LAMMER kinases tested thus far exhibit autophosphorylation activity on serine, threonine, and tyrosine residues *in vitro*, suggesting a new category of kinases (Ben-David *et al.* 1991; Lindberg *et al.* 1992; Yun *et al.* 1994; Lee *et al.* 1996; Moeslein *et al.* 1999). Dual specificity has not yet been discovered for exogenous substrates, as LAMMER kinases preferentially phosphorylate their targets on Ser and Thr residues. Mammalian CLK1-4 is localized mainly within the nucleus (Duncan *et al.* 1995; Menegay *et al.* 2000; Savaldi-Goldstein *et al.* 2003). However, CLK1 and CLK3 have also been reported to localise in the cytoplasm. Furthermore, nuclear localisation of CLK2 is dependent on the autophosphorylation of Ser141 (Nayler *et al.* 1998; Tang *et al.* 2003). It has also been shown that kinase-inactive CLKs localise to discrete speckles and are dephosphorylated (Duncan *et al.* 1995; Colwill *et al.* 1996; Nayler *et al.* 1998). Once autophosphorylation occurs, the activated CLKs diffuse throughout the nucleus. Many LAMMER kinases show presumed nuclear localisation signals in their N-terminus, which could indicate a conserved subcellular localisation and a shuttling mechanism could be involved (Menegay *et al.* 2000). Mammalian LAMMER kinases, particularly CLK1, regulate alternative splicing by interacting with and phosphorylating serine/arginine-rich splicing factors (Savaldi-Goldstein *et al.* 2003; García-Sacristán *et al.* 2005; Bullock *et al.* 2009). Additionally, it was found that the LAMMER kinases of *S. pombe*, *D. melanogaster*, and humans are required for the oxidative stress response, although the underlying mechanisms are not completely understood (Kim *et al.* 2001; Park *et al.* 2003). Furthermore, LAMMER kinases have been proposed to play an important role in signal transduction pathways. In humans, upregulation of CLK1 leads to the differentiation of neuronal cells and cell cycle arrest by activation of the MAP kinases ERK1 and ERK2 (Myers *et al.* 1994). CLK2 is phosphorylated by Akt in response to insulin signalling (Rodgers *et al.* 2010). This phosphorylation leads to an increase in autophosphorylation and stabilisation of the protein, which in turn phosphorylates transcriptional coactivators such as PGC-1 to repress gluconeogenic gene expression. LAMMER kinases are most likely involved in many cellular processes, making them key players in a wide range of functions, such as alternative splicing, pre-mRNA processing, oxidative stress response, cell growth, and cell wall biogenesis (Bender and Fink 1994; Sessa *et al.* 1996; Savaldi-Goldstein *et al.* 2003; García-Sacristán *et al.* 2005; James *et al.* 2009; Rodgers *et al.* 2010; Tang *et al.* 2011). Thus, appropriate kinase activity is crucial, as deregulation plays a central role in many human diseases (Suryadinata *et al.* 2010) and could impair key cellular functions in other organisms.

Despite a long history of research on LAMMER kinases, little is known about the yeast member Kns1. Kns1 is one of the largest members of this family because of its long,

unstructured N-terminal domain (Yun *et al.* 1994). The *KNS1* gene is not essential for yeast viability under favourable conditions (Padmanabha *et al.* 1991) which could be due to a possible unknown functional redundancy or specific unknown functions under unfavourable conditions, resulting in the evolution of many proteins (Gu *et al.* 2003; Deutscher *et al.* 2006; Lim and Park 2019). Surprisingly, 80 % of the yeast genome is non-essential under laboratory conditions, suggesting relevant functions in unfavourable environments (Papp *et al.* 2004). The assumption of functions under non-favourable conditions is supported by a genome-wide study that showed a growth defect of *Δkns1* in the presence of exogenous oleate (Lockshon *et al.* 2007), and a study that revealed filamentous growth defects in inducing conditions, such as nitrogen starvation, suggesting a cross-talk between PKA signalling and LAMMER kinase pathways (Lim and Park 2019).

Although the catalytic C-terminus is highly conserved within the family, Kns1 shows additional small inserts between subdomains (Yun *et al.* 1994). The LAMMER motif, EH**M**AMM**Q**RI**N**G in *S. cerevisiae* (Figure 3.30), differs slightly from the mammalian motif at three positions, as indicated in bold (Yun *et al.* 1994; Lee *et al.* 1996; Lim and Park 2019). The protein structure has not yet been resolved; however, new computational models have predicted a possible structure for Kns1 (Jumper *et al.* 2021; Varadi *et al.* 2022). The structure of the N-terminus is only predicted with low confidence (pLDDT < 50) using AlphaFold (Figure 3.31 A). The C-terminal domain (CTD) is predicted with high confidence (pLDDT > 70) using AlphaFold because of its highly conserved kinase structure (Figure 3.31 A). The low-abundance protein (approximately 160 molecules per cell in the exponential phase) localises to both the nucleus and cytoplasm and shifts towards a more nuclear fraction when cells are treated with rapamycin to inhibit TORC1 (Lee *et al.* 2012). Multiple nuclear localisation sequences are predicted in the NTD as well as the CTD (Figure 3.31 B), suggesting a modulation of localisation patterns in response to nutrient conditions (Yun *et al.* 1994; Kosugi *et al.* 2009). As shown in Figure 3.31 B, 20 phosphorylation sites were identified in multiple high-throughput attempts, nine of which have been associated with autophosphorylation sites (Albuquerque *et al.* 2008; Holt *et al.* 2009; Breitkreutz *et al.* 2010; Martinez Marshall 2011; Swaney *et al.* 2013; Schmitt *et al.* 2017; MacGilvray *et al.* 2020; Zhou *et al.* 2021; Lanz *et al.* 2021). While Lee *et al.* (2012) stated that the phosphorylation rate of Kns1 increases when TORC1 is inhibited by rapamycin treatment, interestingly, kinase-dead mutants did not show a rapamycin-dependent change, suggesting a largely auto-catalytic regulation of Kns1 under active conditions.

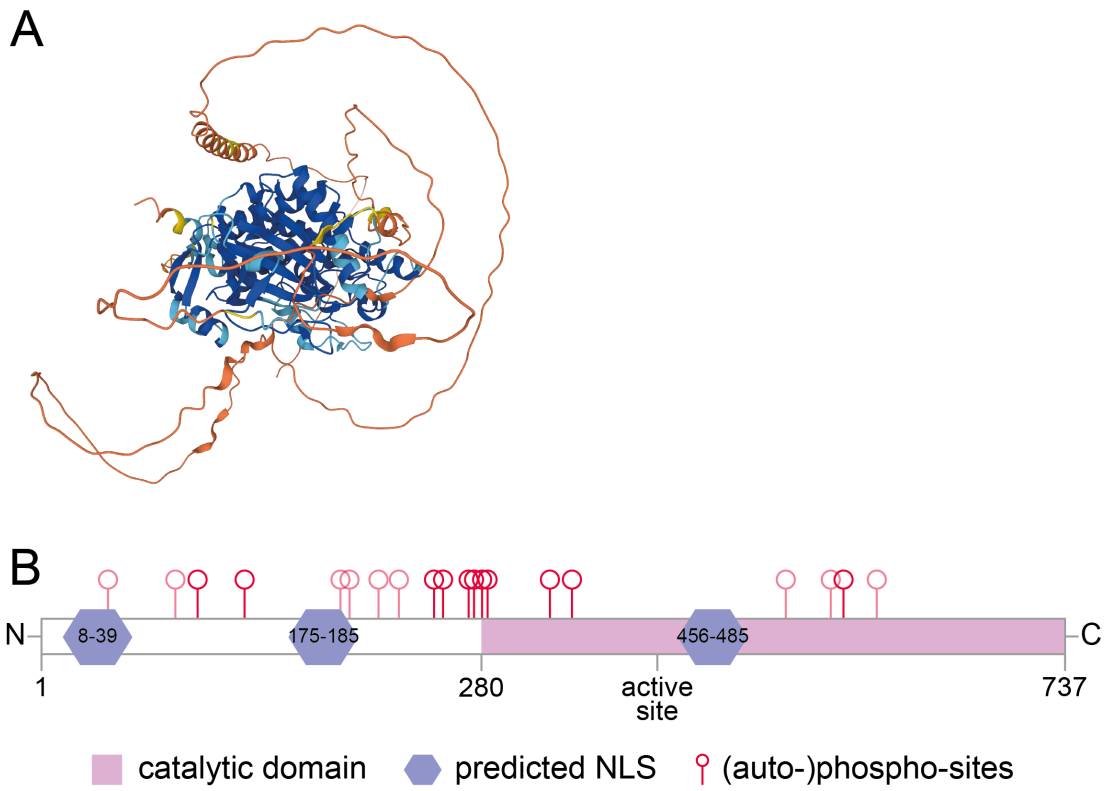

Figure 3.31 Kns1 protein characteristics.

A. AlphaFold prediction of Kns1 protein structure (Jumper *et al.* 2021; Varadi *et al.* 2022). The N-terminal domain (NTD) is predicted with a low confidence of pLDDT < 50 (orange). The catalytic C-terminal domain (CTD) is predicted with a high confidence of pLDDT > 70 (light and dark blue) because of its highly conserved kinase structure. Abbreviation: pLDDT, score prediction of local distance difference test. B. Scheme of Kns1 domain characteristics. The scheme depicts the catalytic domain, predicted nuclear localisation sequences, and (auto)phosphorylation sites that are not to scale. The catalytic domain begins at amino acid 280 and comprises the entire C-terminus (pink). Within this region, an active site is found at Asp440. Three nuclear localisation sequences (NLSs) were predicted using the cNLS Mapper (Kosugi *et al.* 2009). Two are found in the N-terminus, which has an unknown function and are located at positions 8 – 39 and 175 – 185 aa (blue). The third possible NLS was predicted to be close to the active site at positions 456 – 485 aa (blue). All 20 phospho-sites found in the high-throughput analyses are shown (red circles). Positions for autophosphorylation are indicated in light red. Abbreviations: aa, amino acid; NLS, nuclear localisation sequence.

Multiple *in vitro* kinase assays mapping the yeast phosphorylome and interactome have revealed potential Kns1 substrates (Ho *et al.* 2002; Ptacek *et al.* 2005; Krogan *et al.* 2006; Yu *et al.* 2008; Lee *et al.* 2008; Breitkreutz *et al.* 2010; Sanchez-Casalongue *et al.* 2015). A large variety of physical interactions were found in high-throughput- analyses, but only a small number of possible targets showed actual phosphorylation. Some of them include the Ca^{2+}/calmodulin-dependent kinase Cmk2; the serine/threonine kinase Atg1 required for vesicle formation during autophagy; a protein kinase of the Mitotic Exit Network, Cdc15; one of three pyruvate decarboxylase isozymes Pdc1; Laf1, a sterol-binding beta-propeller protein required for the transport of ergosterol from the plasma membrane to the endoplasmic reticulum; the trimeric heat shock transcription factor Hsf1, which activates genes in response to stress; and

Rpc53, the regulatory subunit of RNA Pol III. While many Kns1 targets have been identified over the years, very little *in vivo* work on its regulation has been done. Devare *et al.* (2020) elucidated the role of Kns1 in *PMA1* expression, a major regulator of cytoplasmic pH and plasma membrane potential, by directly phosphorylating Sir1 at Ser473, while Sanchez-Casalongue *et al.* (2015) highlighted the direct phosphorylation of Cbk1, a regulatory subunit of the kinase CK2, to regulate its substrate association and thereby mediate cell proliferation and survival. Additionally, the involvement of Kns1 on Rpc53 phosphorylation was thoroughly analysed by Lee *et al.* (2012), who stated that Rpc53 is hyperphosphorylated under unfavourable conditions, such as inhibition of TORC1 or stationary growth phase, when tRNA and ribosome synthesis are repressed. The hyperphosphorylation of Rpc53 is directly dependent on Kns1 together with Mck1, a member of the glycogen synthase kinase 3 (GSK3) family (Lee *et al.* 2012; Caligaris *et al.* 2023). Lee *et al.* (2012) revealed that Kns1 phosphorylates Rpc53 on Thr232, which enables further phosphorylation by Mck1 at positions Thr228 and Ser224. This pattern fits the general GSK3 phosphorylation mechanism using a "priming phosphate" at the +4 residue for efficient phosphorylation (Cohen and Frame 2001), suggesting that Kns1 is the priming kinase for Mck1 phosphorylation of Rpc53 (Lee *et al.* 2012). The increase in Rpc53 phosphorylation under unfavourable conditions, simulated by rapamycin treatment, is mediated by a 2- to 4-fold increase in Kns1 protein, its autophosphorylation, and nuclear accumulation of the protein (Lee *et al.* 2012; Gutiérrez-Santiago and Navarro 2023). This Rpc53 hyperphosphorylation then contributes to the repression of RNA Pol III activity and reduces the synthesis of tRNAs and 5S rRNAs, as described in section 3.3.1.2.

3.5 Summary of previous findings and research aims

LAMMER kinases have a large impact on many cellular processes and play key roles in the regulation of TORC1-dependent stress responses. This dual-specificity family of protein kinases is highly conserved and not well characterised. Characterisation of the members of higher eukaryotes has provided insights into the function and regulation of LAMMER kinases and their likely involvement in many diseases. Therefore, human paralogues have emerged as potential targets for the treatment of cancer and metabolic disorders (Muraki *et al.* 2004; García-Sacristán *et al.* 2005; Glatz *et al.* 2006; Bullock *et al.* 2009; Rodgers *et al.* 2010). To gain a mechanistic understanding of the role and regulation of Kns1 in *S. cerevisiae*, its effect on RNA Pol III activity is crucial as a first step for new therapeutic strategies targeting LAMMER kinases in the future.

Currently, knowledge of Kns1 is mainly derived from large-scale surveys and *in vitro* assays. The complexity of all Kns1 functions is yet to be determined. *KNS1* is a non-essential gene under standard conditions (Padmanabha *et al.* 1991). However, it is likely that this kinase possesses functions relevant under non-favourable conditions that are yet to be discovered. Work on the Kns1 domain structure revealed a conserved kinase domain at the C-terminus (Yun *et al.* 1994; Lee *et al.* 1996; Lim and Park 2019), but the function and role of the long N-terminus of the protein remains unclear. The dual specificity kinase function was evaluated *in vitro*, and Kns1 shows autophosphorylation at Ser, Thr, and Tyr residues, yet it was not unravelled if targets are also phosphorylated with dual specificity. Twenty phospho-sites have been detected by various large-scale analyses, nine of which have been assigned to autophosphorylation sites by Martinez Marshall (2011); however, their physiological function remains unclear. Localisation analyses have revealed no precise association with subcellular compartments thus far, and Kns1 was found in both the nucleus and cytoplasm (Lee *et al.* 2012). A tendency towards localisation in the nucleus is observed when TORC1 is inactive, which could be due to a shuttling mechanism. However, the molecular basis of Kns1 localisation has not been evaluated. A computational search for known nuclear localisation sequences revealed three potential NLSs within Kns1 (Table 1) that could be part of a regulatory shuttling system for the nuclear import of Kns1 (Kosugi *et al.* 2009). Their physiological relevance and the necessary post-translational modifications have not yet been defined.

Table 1 Predicted NLSs in *KNS1* calculated using the cNLS mapper.

Nuclear localisation sequences (NLSs) were predicted using cNLS Mapper with a score of 5 or higher. Given are the amino acid start positions (AA pos.), the respective nuclear localisation sequence, the mono- or bipartite sequence, and the corresponding score.

AA pos.	Sequence	Partite	Score
7	IGTRKRSRANMNNSTTTGPANNTSSNKTFLD	bipartite	5.3
8	GTRKRSRANMN	monopartite	6
175	PKKFKKQRTI	monopartite	7
456	QKLPLKTVQSLSKRRREASKGKRKILKNP	bipartite	6.8
463	VQSLSKRRREA	monopartite	6
465	SLSKRRREAS	monopartite	7

While a few potential Kns1 targets were found, only Rpc53 was thoroughly analysed (Lee *et al.* 2012). The RNA Pol III regulatory subunit Rpc53 is directly phosphorylated by Kns1 and, consequently, hyperphosphorylated by Mck1 under TORC1-inhibited conditions. Previous work has shown that Kns1 is an effector of TORC1 and directly inhibits RNA Pol III activity by Rpc53 phosphorylation. The phosphorylation patterns of Rpc53 have been studied extensively, but the regulatory mechanism and conditions that activate Kns1 remain unclear. Additionally, a previous study by Wojciech (2020) revealed that the mRNA levels of *KNS1* are low under favourable conditions and increase significantly in a mutant that reduces global translation rates (Table 2). However, mRNA levels of *RPC53* were slightly decreased under reduced translation compared to those under favourable conditions (Table 2). This supports the assumption that Kns1 might be involved in the regulation of stress response, together with the finding that *Δkns1* mutants show no phenotype under laboratory conditions.

Table 2 mRNA levels in WT and *Δ326* mutant and their corresponding changes.

Given are total mRNA reads from RNA sequencing of WT and *Δ326* mutant cells for the ORFs *KNS1* and *RPC53*. Additionally, the $\log_2$ fold change in each ORF was calculated. Abbreviation: FC, fold change. RNA sequencing data were obtained from Wojciech (2020).

ORF	WT	*Δ326*	$\log_2$ FC
KNS1	330	922	+1.45
RPC53	896	552	-0.68

The present study aimed to unravel the physiological roles and regulatory mechanisms of Kns1 in *S. cerevisiae*. To achieve this, the following objectives were established. First, eIF2-specific regulation should be evaluated to establish a connection between reduced global translation initiation rates and the corresponding stress response. Kns1 might be regulated via a reduction in eIF2 function and the adjacent integrated stress response, as suggested by the RNA sequencing data, which hinted at a crosstalk between the ISR and TORC1-mediated processes in regulating RNA Pol III activity. For this, the protein levels of Kns1 and Rpc53 phosphorylation patterns will be elucidated to compare different mutants that imitate the stress response in yeast. Additionally, a reporter system was established to analyse the promoter region of Kns1. Second, a possible connection between nutrient signal inputs and Kns1 regulation will be investigated. It is likely that Kns1 function is important for mediating TORC1 signals for a response under unfavourable conditions. As a major regulator of proliferation, TORC1 integrates a variety of nutrient signals; however, the regulation of Kns1 in response to these stimuli is not clear. The availability of carbon sources may play a crucial role in TORC1-/Kns1-dependent responses. Kns1 protein and Rpc53 phosphorylation levels were used to investigate the effects of different carbon sources, their timely adaptation to changes, and a variety of metabolic mutants to simulate reduced metabolic capacity. Furthermore, the regulation of TORC1 in response to carbon sources will be elucidated with a strong focus on its effector kinase, Kns1. The extent to which TORC1 is involved in the specific regulation of Kns1 under unfavourable conditions. For this, yet again, Kns1 protein levels and Rpc53 phosphorylation patterns are used to study different conditions of inhibited TORC1 activity. Moreover, we aimed to analyse the transcriptional regulation of Kns1, as the RNA sequencing data suggested a change in mRNA levels. Multiple regulatory layers can ensure a fast response under conditions of reduced cellular processes. To this end, the investigation of one or more transcription start sites under various conditions should be helpful, as well as the analysis of known transcription factors that could be involved in Kns1 transcriptional changes. Lastly, the characterisation of Kns1 properties regarding its localisation, autophosphorylation capacities, cellular growth, NTD function, and protein stability are the central focus of this work. Various molecular approaches have been used to study the protein in detail *in vivo*. In summary, the aim of this study was to investigate the regulation of Kns1 under different unfavourable conditions, in which its function could be necessary, as well as a thorough characterisation of the protein properties to explain its function.

4 RESULTS

Very little work, e.g. from Martinez Marshall 2011 and Lee *et al.* 2012, has been done to elucidate the potential role of Kns1. As an effector kinase of TORC1, and due to its involvement in the downregulation of RNA Pol III activity, it is likely that Kns1 plays an important role in anti-proliferative mechanisms within the cell. However, it remains unclear which signals lead to the regulation of Kns1 and how this response is mediated. Knowledge of the protein and its properties is also sparse. Therefore, it was a key focus of this work to unravel the possible regulatory pathways involved in Kns1 activation and to highlight some aspects of Kns1 protein characteristics.

4.1 Functional analysis of Kns1 in eIF2-specific processes

Translation is an essential part of protein synthesis. Translational initiation is the crucial step and central to many regulatory mechanisms. The eukaryotic translation initiation factor 2 (eIF2) is not only necessary for translation itself but also a regulator of stress response. Analyses of eIF2-dependent stress response provide insights into new factors involved in these processes. Previous RNA sequencing data suggested that the regulatory function of eIF2 could be linked to Kns1 expression (Wojciech 2020). These data revealed that the mRNA levels of *KNS1* were elevated in eIF2 deficient mutants compared to the WT levels. This suggests a potential function of Kns1 under stress conditions. An increase in mRNA levels would most likely lead to an increase in Kns1 protein levels, which is important for the regulation of processes. The eIF2-specificity of Kns1 regulation, the resulting effects on protein amount, and its connection to Rpc53 as a regulatory subunit of RNA Pol III were investigated.

4.1.1 General defects in growth deficient mutants

To study eIF2-dependent effects in *S. cerevisiae*, several stress mutants were utilised. In yeast, nutrient deficiencies lead to eIF2-specific activation of a stress response. This results in a decrease in eIF2 assembly or formation of the ternary complex, which reduces global translation initiation rates, but increases the specific stress response. To allow a detailed analysis of the effects of an activated stress response, models with reduced eIF2 availability were used and compared to models with overall reduced protein synthesis. To ensure that these yeast mutants were suitable for comparison, they were first characterised in terms of growth, cell cycle distribution as an indicator of proliferation rate, and phenotype in terms of cell volume and roundness. The mutants used in this study included a strain carrying a C-terminal truncation of Cdc123 at amino acid 326 (*Δ326*) which drastically reduces the availability of eIF2; a deletion of one of the paralogues of eIF4G (*Δtif4631*) which decreases efficient translation initiation; and a deletion of the high mobility group family member Hmo1 (*Δhmo1*) which reduces the overall transcription by RNA polymerase I (Figure 4.1 A).

To investigate the effects of genetic modifications on these mutants, a comparison with a wildtype (WT) yeast strain was performed. Phenotypic changes were visualized

using confocal microscopy. Figure 4.1 B shows an increase in the size and number of rounder cells of the *Δ326* and *Δtif4631* mutants compared to WT. Quantification of these strains showed that the cell volumes were not significantly different in all three backgrounds; however, roundness was increased to 100 % in *Δ326* and *Δtif4631* compared to WT (Figure 4.1 C, D). The DNA content was analysed by flow cytometry (Figure 4.1 E). The single DNA content (1C) indicating cells in G_1 phase showed a drastic increase in *Δ326, Δtif4631*, and *Δhmo1* (to approximately 30 – 40 % compared to 11 % in WT, Figure 4.1 F). This shift indicated a delay in the G_1/S transition in all mutants and suggested a reduced proliferation rate as a general response to stress. Furthermore, growth analysis revealed strong defects in all the three mutants tested. Growth on the glucose-containing medium was reduced (Figure 4.1 G).

The data revealed that the three selected mutants showed similar growth defects as a general cellular response to genetic manipulation and reduced protein synthesis. However, these effects do not account for specific regulatory mechanisms as the impairments of the mutants differ greatly. A comparison of the mutants for specific targets in the next chapter is suitable, as the general stress response was similar in all tested cellular processes.

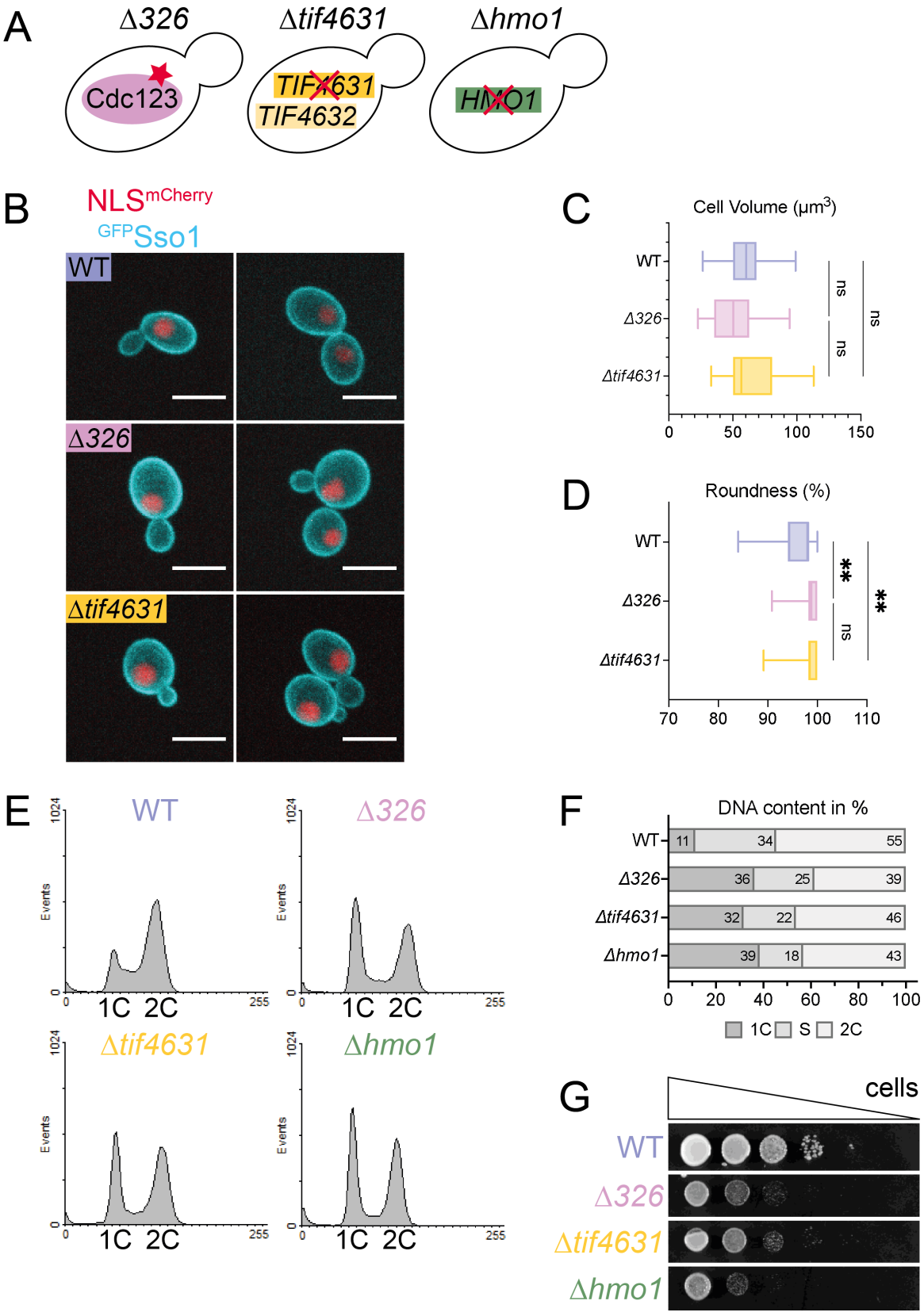

Figure 4.1 Growth defects in stress response mutants.

A. Three different mutants were used for the analyses. A C-terminal truncation (red star) of Cdc123 at amino acid 326 (*Δ326*), the deletion (red cross) of one paralogue of the eIF4G encoding genes (*Δtif4631*), and the deletion (red cross) of the high mobility group family

member Hmo1 (*Δhmo1*). B. Confocal analysis of the phenotypes of *Δ326* and *Δtif4631* compared to WT assessing cell volume and roundness. All strains used contained NLS-mCherry (red) as a nuclear marker and GFP-Sso1 (cyan) as a membrane marker. mCherry and GFP signals were detected at 5 % laser intensity and 200 ms exposure time. The Scale bar indicates 5 µm. C. The cell volumes were measured in μm^3. The length, width, and height of the cell, indicated by the layers in which the cell was documented, were used to calculate the volume (Equation 2). The distance between the layers within the measured z-stack was 0.6 µm. Number of quantified cells: n = 75 (except for *Δtif4631*: n = 50). Normal distribution was tested using the Shapiro-Wilk test, and statistics were calculated using the Kruskal-Wallis test (ns: $p \geq 0.05$). D. The roundness of cells was measured as a percentage (%). The area and perimeter of the cells were calculated from the measured length, width, and height of C. Roundness was then assessed from the area and perimeter of the cells (Equation 3). Number of quantified cells: n = 75 (except for *Δtif4631*: n = 50). Normal distribution was tested with Shapiro-Wilk and statistics were calculated with a one-way ANOVA (ns: $p \geq 0.05$, **: p = 0.001 - 0.01). E. Flow cytometric analysis of the used mutants to visualize cell proliferation rates. The DNA content was labelled and measured using SYTOX Green intercalations. 1C corresponds to single DNA content in G_1 phase and 2C corresponds to double DNA content after replication in G_2/M phase of the cell cycle. F. DNA content of the flow cytometric analysis in E was evaluated in FCS Express 6 and is depicted in %. G. Spot test of the used strains on glucose-containing plates incubated at 30 °C for 2 days to visualize growth defects.

4.1.2 eIF2-specific upregulation of Kns1 protein expression and activity

A previous study revealed that mRNA levels of *KNS1* were increased 3-fold in the *Δ326* mutant compared to WT (Wojciech 2020). Despite being at a low level, this could mean that Kns1 is necessary for eIF2-specific stress response. An increase in mRNA reads in an RNA-sequencing approach suggests higher transcription rates. However, it is not evident whether this is correlated with increased protein levels. If Kns1 is indeed involved in a response to diminished eIF2 availability and therefore reprogramming of RNA Pol III activity, then protein levels should also be increased under these conditions. Furthermore, Kns1 should be catalytically active to target Rpc53, a regulatory subunit of RNA Pol III, and reduce polymerase activity by phosphorylation. To verify the eIF2-specificity of this proposed effect, other growth-deficient mutants, described in section 4.1.1, were used as controls.

The levels of endogenous Kns1 were examined in the three stress mutants and compared to the WT (Figure 4.2 A). Kns1 expression was analysed by western blotting and Rpc53 phosphorylation levels were used as a readout for Kns1 kinase activity. Compared to the low levels of Kns1 in WT cells, an increase was observed in *Δ326* (Figure 4.2 B). Stress mutants independent of eIF2, but with similar general defects, such as *Δtif4631* and *Δhmo1*, showed WT-like Kns1 expression. Quantification of the signal intensities showed a significant 3-fold increase in mean protein in the *Δ326* mutant compared to the other mutants (Figure 4.2 C). Kns1 kinase function was visualized using the phosphorylation status of Rpc53 (Figure 4.2 D). In WT cells, the majority of Rpc53 (approximately 70 %, Figure 4.2 E) was unphosphorylated. This proportion shifted to 60 % phosphorylation in *Δ326* cells, indicating the involvement of eIF2. In *Δtif4631* and *Δhmo1*, the Rpc53 phosphorylation levels were at a minimum

of 15 – 20 %. These data confirmed that Kns1 is not only preferentially transcribed but also translated under eIF2-diminished conditions. The increase in protein levels was also correlated with specific activation of kinase function.

A growth test was performed to check for deficits resulting from the addition of a large epitope to endogenous Kns1. A comparison of WT and *Δ326* with and without 12xFLAG addition was performed and revealed only a minimal growth defect for the *Δ326* background with *KNS1-12xFLAG* (Figure 4.2 F). These minor effects most likely do not interfere with Kns1 expression. Thus, clear results were obtained.

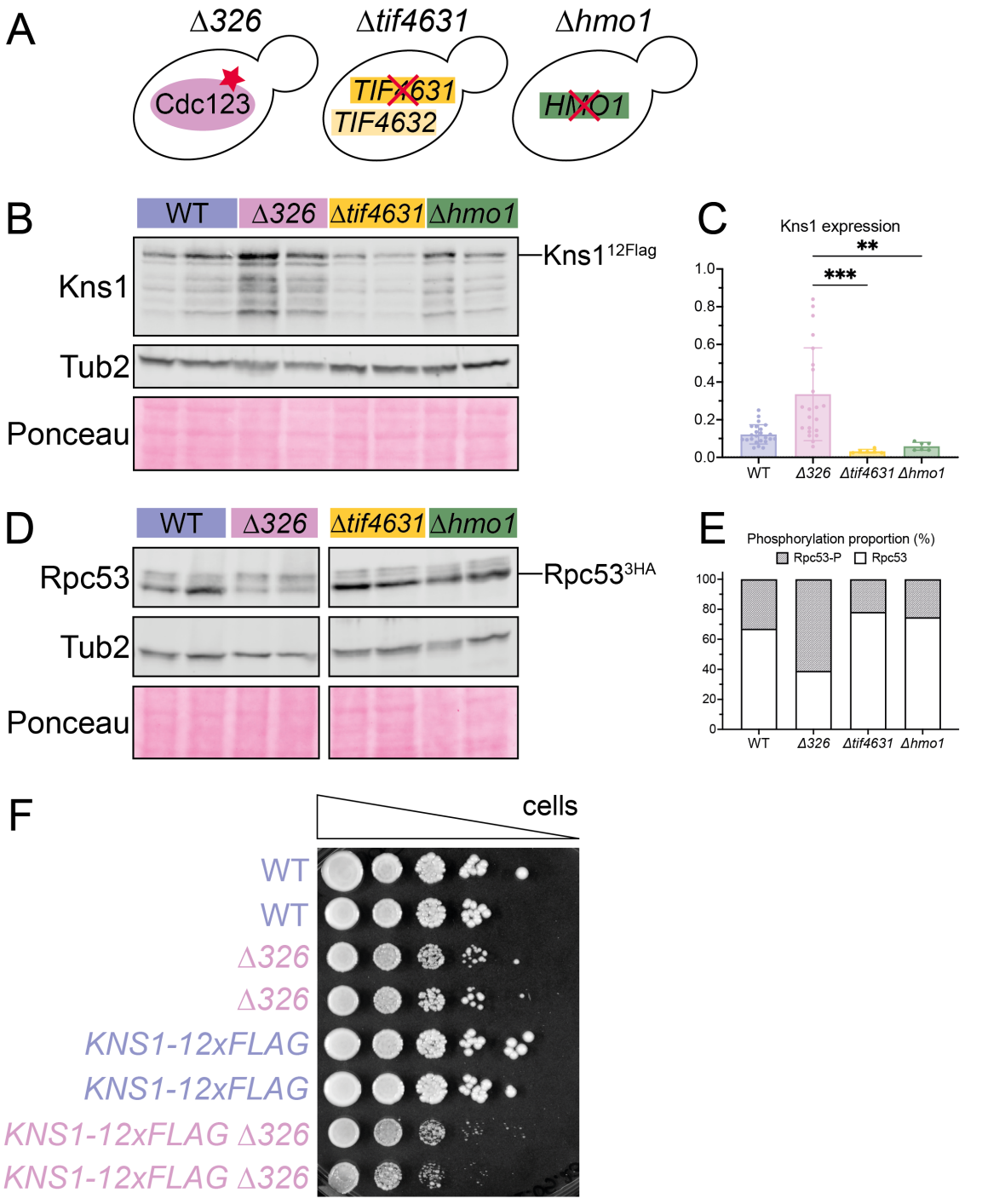

Figure 4.2 eIF2-specific increase in Kns1 expression and activity. (Description on next page)

A. Used mutants in this study include *Δ326*, a C-terminal truncation (red star) of Cdc123 at amino acid 326; *Δtif4631*, a deletion (red cross) of one paralog of eIF4G and *Δhmo1*, a deletion (red cross) of the high mobility group family member Hmo1. B. Western blot analysis of endogenous Kns1 protein expression in different mutants compared to WT. Kns1-12xFlag was detected with an α-Flag antibody. Tub2 was used as a reference and comparable protein loading was controlled via Ponceau staining. The loading was performed in two biological replicates for each strain. C. Quantification of the western blot signal intensities from B. Kns1 expression was normalised to Tub2 levels; individual values are indicated by dots ($n \geq 6$), and SD is given by bars. Normal distribution was tested with Shapiro-Wilk and statistics were calculated with Kruskal-Wallis test (ns: $p \geq 0.05$, *: $p = 0.01 - 0.05$). D. Western blot analysis of Rpc53 (phosphorylation) levels in different mutants. Rpc53-3HA was detected with an α-HA antibody. Slower migrating bands represent phosphorylated isoforms of Rpc53. Tub2 was used as a reference, and Ponceau staining was used to control equal protein loading. Two biological replicates were used for each strain background. E. Quantification of the western blot signals from D was performed. Phosphorylated and unphosphorylated signals were calculated in proportion to the total Rpc53 levels. The mean relative proportion of $n \geq 6$ was expressed as %. Grey portions indicate phosphorylated values and white boxes indicate unphosphorylated proportions. F. Growth analysis with spot test of the used Kns1-12xFlag containing strain in WT and *Δ326* background. The controls were WT and *Δ326* without epitope markers. Duplicates were spotted on XYD plates and incubated at 30 °C for two days.

4.1.3 Sufficiency and necessity of Kns1 for Rpc53 phosphorylation

Lee *et al.* 2012 have already proven that Rpc53 phosphorylation depends on Kns1 activity. According to this model, Kns1 serves as a priming kinase that phosphorylates Rpc53 at T232. Only after this initial phosphorylation can Mck1, another TORC1 effector kinase, further phosphorylate Rpc53, leading to its inactivation. However, this study did not analyse conditions where Kns1 is highly expressed and where its function is necessary to inhibit RNA Pol III activity in response to stress. As described in section 4.1.2, Rpc53 phosphorylation serves as a measure of Kns1 activity in this study. Therefore, it is important to verify the direct association between Kns1 and Rpc53 phosphorylation. It was assumed that Kns1 is not only necessary but also sufficient to trigger hyperphosphorylation of Rpc53 under varying conditions.

To test this hypothesis, *KNS1* was deleted in a Rpc53 background. Additionally, constitutive overexpression of Kns1 was used to verify the direct relationship between higher Rpc53 phosphorylation levels and increased Kns1 protein levels. As shown in Figure 4.3 A, only unphosphorylated Rpc53 was detected in all strains with a deletion of *KNS1*, independent of the WT or mutant background (> 90 % in Figure 4.3 B). However, with Kns1 overexpression, a significant shift towards the phosphorylated proportion (~ 90 %, Figure 4.3 B) was observed in WT and *Δ326*. These data strongly suggested that Kns1 is necessary for the phosphorylation of Rpc53 and is sufficient to increase the latter.

While changing the availability of Kns1 had drastic effects on the phosphorylation of Rpc53, the growth in the WT background was not affected (*Δkns1* and *pTEF-MYC-KNS1* in Figure 4.3 C and D, respectively). Interestingly, the growth of *Δ326* was more negatively affected when *KNS1* was deleted, indicating the strong importance of Kns1 function for growth under stress conditions (Figure 4.3 C). Correspondingly, the growth of the *Δ326* mutant was slightly improved when Kns1 was overexpressed (*pTEF-MYC-KNS1 Δ326*, Figure 4.3 D). This further hinted towards a positive effect of Kns1 on growth under stress conditions and the strong importance of Kns1 availability. Furthermore, the translational capacities of WT and strains overexpressing Kns1 were similar, as shown by polysome profiling in Figure 4.3 E, which indicated that the amount of Kns1 protein did not influence general protein synthesis.

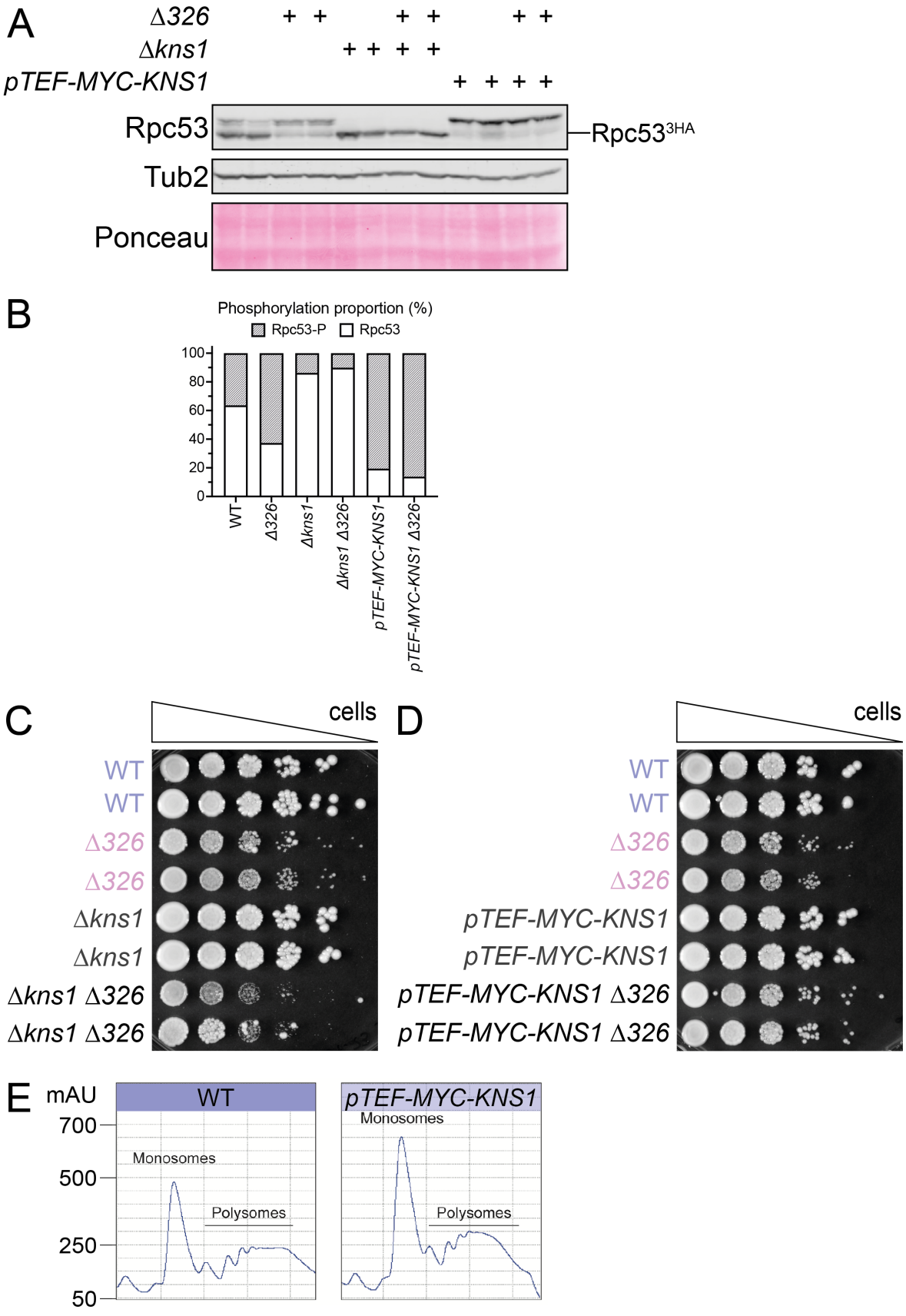

Figure 4.3 Kns1-dependent phosphorylation of Rpc53.

A. Western blot analysis of the phosphorylation of Rpc53. The strains used included WT, *Δ326*, *Δkns1*, a deletion of *KNS1*, *pTEF-MYC-KNS1*, a constitutive overexpression of *KNS1*, and double

mutants. Rpc53-3HA and its corresponding phosphorylation levels were detected using an α-HA antibody. Slower migrating bands represent the phosphorylated Rpc53 isoforms. Tub2 was used as a reference, and Ponceau staining was used to control for equal protein loading. Two biological replicates were used for each strain. + represents the background strain. B. Quantification of the signal intensities from A. Phosphorylated and unphosphorylated signals were calculated in proportion to the total Rpc53 levels. The mean relative proportion of n ≥ 4 was expressed as %. Grey portions indicate phosphorylated values and white boxes indicate unphosphorylated values. C. Spot tests of all deletion strains in biological duplicates containing WT, *Δ326*, *Δkns1*, and *Δkns1 Δ326*. Growth was analysed on XYD plates at 30 °C for two days. D. Spot test of the overexpression strains in biological duplicates containing WT, *Δ326*, *pTEF-MYC-KNS1*, and *pTEF-MYC-KNS1 Δ326*. Growth was analysed on XYD plates at 30 °C for two days. E. Polysome profiles of WT and *pTEF-MYC-KNS1*. RNA was separated on a sucrose gradient regarding its weight depending on ribosome loading and the fractions were then analysed in an Äkta. Monosomes and polysomes have also been annotated.

4.1.4 Increased Kns1 expression controlled by regulatory region

The increase in protein expression and activity of Kns1 in *Δ326* compared to WT, addressed in section 4.1.2, raised the question of the mechanisms responsible for this enhancement. RNA sequencing data from Wojciech 2020 already revealed a transcriptional fraction that leads to an increase in mRNA levels; however, it is not clear how this differential regulation is mediated. The relatively long 5' leader region of *KNS1* could be a potential target for transcriptional regulation via promoter regions or translational upregulation by the uORFs included in the transcript. An altered contribution of the 5' region on Kns1 expression could explain the increase in protein levels in *Δ326* as an eIF2-dependent response to stress.

To test this hypothesis, the entire 5' region, including the first three codons of *KNS1*, was cloned into a reporter construct (Figure 4.4 A). This reporter was then investigated under the WT and *Δ326* conditions (Figure 4.4 B). Western blot analysis of the reporter protein with different inputs, shown in Figure 4.4 C, showed strong expression in both the WT and *Δ326* strains. Quantitative analysis of the signals (Figure 4.4 D) revealed a slight increase in the reporter protein in *Δ326* compared to WT (approximately 1.5-fold), suggesting that the 5' region of *KNS1* may be involved in regulating its expression under stress conditions. However, this increase did not reflect the total change in Kns1 protein expression, as detected in section 4.1.2. Thus, the 5' region alone might not be sufficient for the regulation of Kns1 expression.

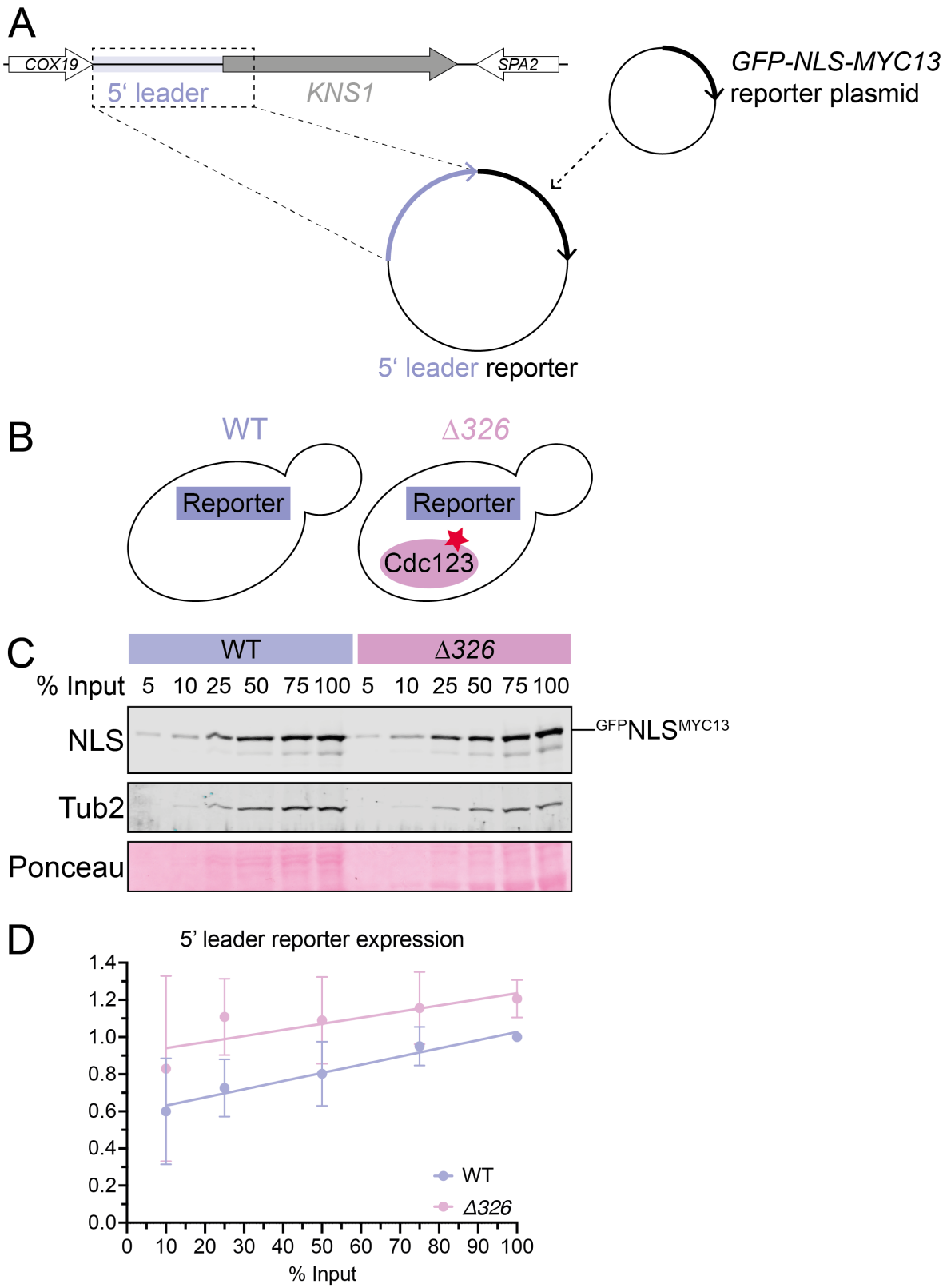

Figure 4.4 Increased reporter protein expression under control of Kns1 regulatory region.

A. Reporter construct consisting of the complete 5’ leader of *KNS1*, including the first three codons, and a GFP-NLS-MYC13 region. The plasmid was stably integrated into the marker site in the yeast genome. B. Used strain backgrounds for this study. A comparison of WT and *Δ326* was applied. C. Western blot analysis of the reporter in WT and *Δ326*. The reporter protein NLS

was detected using an α-MYC antibody and different levels of input were applied (annotated in %). Tub2 was used as a reference, and Ponceau staining was used to control protein levels. D. Quantification of the signals of C. The mean values of two technical replicates normalised to Tub2 are depicted as dots, and SD is shown by bars. The % inputs were visualized on the x-axis. The 5 % input was excluded because the signal intensity was too sparse for accurate quantification measurements. Linear regression was applied to both strain backgrounds (WT: blue, *Δ326*: pink).

4.1.5 ISR-dependent increase of Kns1 expression and activity

An increase in Kns1 expression in conditions with reduced eIF2 availability (*Δ326*) led to the assumption that Kns1 is a potential target of the integrated stress response (ISR). Especially under amino acid deficiency, Gcn2 is activated which phosphorylates the α subunit of eIF2 (Postnikoff *et al.* 2017). This leads to subsequent inactivation of eIF2 function, as the affinity of eIF2B to bind phosphorylated eIF2 is enhanced. This is followed by tight binding of eIF2B to eIF2, so that guanin exchange and recycling of eIF2 will not occur. Therefore, the total amount of available eIF2 to form active pre-initiation complexes was drastically reduced. Under these stress conditions, the overall rate of translation is reduced, and only specific mRNAs are translated (Pakos-Zebrucka *et al.* 2016; Postnikoff *et al.* 2017). One of these mRNAs that is specifically upregulated is *GCN4*, which encodes a transcription factor. When global translation is reduced, Gcn4 is synthesised, which in turn activates stress-responsive genes. Genetic reduction of eIF2 (*Δ326*) activates ISR in a Gcn2-independent manner. eIF2-specific reduction of translation initiation, either by eIF2α phosphorylation or by utilising the *Δ326* mutant, activates Gcn4 via ISR. Thus, Gcn4 could potentially increase Kns1 protein levels by either directly promoting its transcription or by indirectly influencing factors that are necessary for increased Kns1 levels. If Kns1 protein amounts are indeed dependent on ISR and Gcn4 in particular, then a deletion of *GCN4* should prevent the Kns1 protein increase under stress conditions.

To address the potential link between ISR and Kns1 activation (Figure 4.5 A), ISR mutants were used to study expression and activity. The mutants used for this approach included a deletion of the kinase Gcn2 (*Δgcn2*), a deletion of the transcription factor Gcn4 (*Δgcn4*) and a combination of both with the aforementioned *Δ326*. As a control in this western blot analysis, both WT and *Δ326* were used and showed the expected increase in endogenous Kns1 expression in *Δ326* compared to WT, as depicted in Figure 4.5 B. The deletion of either one of the ISR components under normal conditions (*Δgcn2 or Δgcn4*) resulted in WT expression, as the ISR was not active either way. Deletion of *GCN2* in a *Δ326* background could neither enhance Kns1 expression nor decrease its protein levels to WT levels (Figure 4.5 B). Kns1 expression is likely to increase due to the low availability of eIF2. Activation of the ISR by phosphorylating eIF2 in a Gcn2-dependent manner is not necessary. However, deletion of *GCN4* in the *Δ326* background led to a drastic decrease in Kns1 expression to almost the WT level (Figure 4.5 B, C). This indicates that the upregulation of Kns1 expression via an eIF2-dependent mechanism is mediated by Gcn4. Reduced eIF2 availability alone does

not seem sufficient to activate the regulatory pathway that increases Kns1 levels. Therefore, Kns1 expression was Gcn4-dependent. However, it has not been completely evaluated whether this connection is direct or indirect. Correspondingly, Rpc53 phosphorylation levels were examined to determine Kns1 activity in ISR mutants. The phosphorylation levels of Rpc53 increased from approximately 20 – 30 % in WT, *Δgcn2*, and *Δgcn4* to 50 – 60 % in *Δ326* background, except for *Δgcn4 Δ326* (Figure 4.5 D, E). Deletion of *GCN4* in a *Δ326* background led to a WT phosphorylation pattern of Rpc53, as shown in Figure 4.5 D and E. This matches the Gcn4-dependent upregulation of Kns1 expression, indicating that an increase in Kns1 protein levels is potentially linked to its activity.

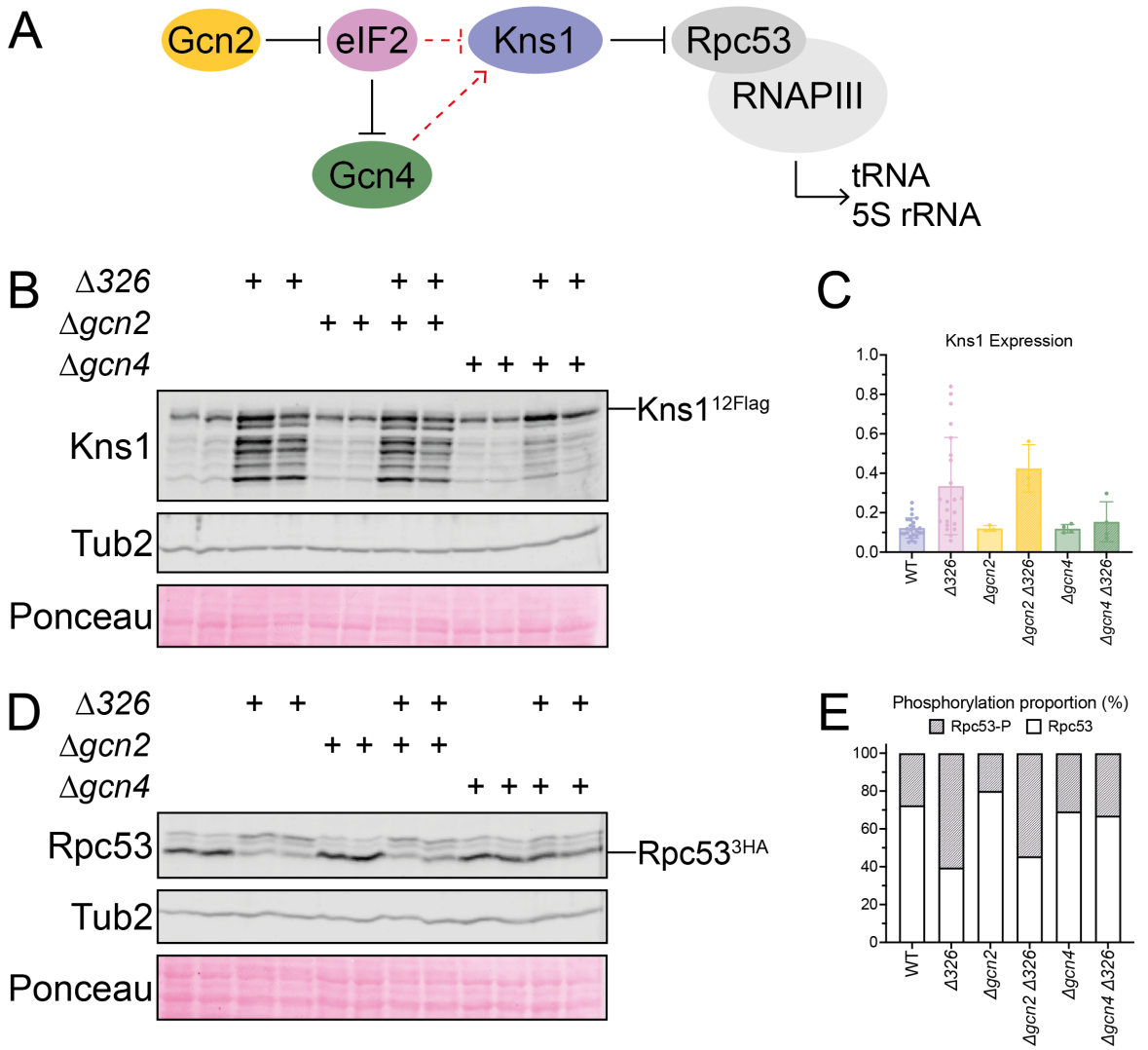

Figure 4.5 Gcn4-dependent expression of Kns1.

A. Schematic overview of the connections between integrated stress response (ISR), eIF2, and Kns1. Black arrows indicate known relationships and red dashed arrows indicate unknown connections. Bars show inhibitory regulation and arrows indicate activating connections. B. Western blot analysis of endogenous Kns1 protein levels in different ISR deletion mutants. strains used were WT, *Δ326*, *Δgcn2*, *Δgcn4*, and double mutants (the corresponding genotypes are indicated by +). Biological duplicates of each background were applied, and Kns1-12xFlag was detected using an α-Flag antibody. Tub2 was used as a reference, and proper loading was controlled using Ponceau staining. C. The signal intensities from B were quantified and

normalized to Tub2. Single values (n ≥ 4) are depicted as dots, and standard deviation (SD) is given with bars. Normal distribution was tested with Shapiro-Wilk, and statistics were calculated using the Kruskal-Wallis test (all comparisons ns: p ≥ 0.05, not depicted). D. Western blot analysis of Rpc53 and its phosphorylation in different deletion mutants. The same strain backgrounds as in B were applied (genotype combinations are indicated by +). Slower migrating bands represent phosphorylated Rpc53 isoforms. Rpc53-3HA was detected using the α-HA antibody. Tub2 was used as a reference and protein loading was controlled using Ponceau staining. E. Phosphorylated and unphosphorylated signals from D were calculated in proportion to total Rpc53 levels. The mean relative proportion of n ≥ 4 is given in %. Grey portions indicate phosphorylated values and white boxes indicate unphosphorylated values.

4.2 Increased Kns1 expression and activity in response to metabolic activity reduction

The ISR is activated by a variety of environmental conditions, including amino acid deficiency, glucose starvation or oxidative stress (Pakos-Zebrucka et al. 2016; Costa-Mattioli and Walter 2020). While the ISR is an important pathway to adapt to changing conditions, it is crucial for cells to return to high proliferation states with preferred nutrient availability as fast as possible. Therefore, metabolic pathways, especially glucose sensing, are indispensable to keep energy production high and protein synthesis running (Broach 2012). In *S. cerevisiae*, nutrients not only serve as the substrates for growth but also as a signal molecule. As the connection of ISR activation, especially Gcn4 availability, and Kns1 expression hinted to a possible function of Kns1 in response to changing nutrient conditions, an approach on checking metabolic influences was pursued. Physiological conditions with altered metabolic activity, different carbon sources and various pathways involved in glucose metabolism were analysed in the following.

4.2.1 Increased Kns1 expression and activity during diauxic shift

The ISR is especially important when nutrient availability changes and metabolic reprogramming should take place to ensure proper survival of the cells. Under physiological conditions, the diauxic shift is one such situation. When the glucose supply is exhausted, *S. cerevisiae* undergoes a metabolic shift and switches from energetically less efficient fermentation to respiration (Busti et al. 2010; Galdieri et al. 2010). This change in energy consumption is called the diauxic shift. During this time, cells alter their global expression and protein synthesis to quickly adapt to and metabolise ethanol and other non-fermentable sources. ISR thereby helps in metabolic reprogramming, mostly at the transcriptional level. Kns1 is eIF2- and Gcn4-dependent, as described in section 4.1.5, and its expression seems to increase under stress conditions when transcription and translation capacities need to be reduced. As metabolic reprogramming takes place during the diauxic shift, it is possible that Kns1 expression and activity are regulated by a change in metabolism under physiological conditions and is required for reprogramming in the diauxic shift.

Growth curve analyses were performed to visualize potential changes in Kns1 expression and activity during the diauxic shift. Such a curve displays growth starting with exponential cells, subsequently going through a diauxic shift, and ending in a lag phase (post-diauxic). Measurements were conducted every 90 min approximately after one cell cycle (Figure 4.6 A). Optical density (OD_{600}) was used as an indicator of actual growth. Endogenous Kns1 expression gradually increased as the cells grew longer (Figure 4.6 B) with increasing technical degradation. While the OD_{600} reached a maximum level of 4.5, Kns1 protein was lagging and still increased (Figure 4.6 C). To verify the activity of Kns1, Rpc53 phosphorylation levels were evaluated. After two rounds of the cell cycle, at 180 min, the first increase in phosphorylated protein was detected (Figure 4.6 D). After another cell cycle, a clear shift towards phosphorylation was observed (Figure 4.6 D, 270 min). The phosphorylation of Rpc53 increased gradually over time, starting at approximately 30 % and reaching a maximum of 80 % after 450 min, as shown in Figure 4.6 E. The OD_{600} indicated a lag-phase at 4.5 after this time (Figure 4.6 E). Controls that were maintained in the exponential phase during the entire growth curve analysis showed constant expression. Phosphorylation of Rpc53 was directly dependent on Kns1 activity, as shown in Figure S 1. These results suggest specific regulation of Kns1 expression within the diauxic shift and a potential role in genetic reprogramming during metabolic stress.

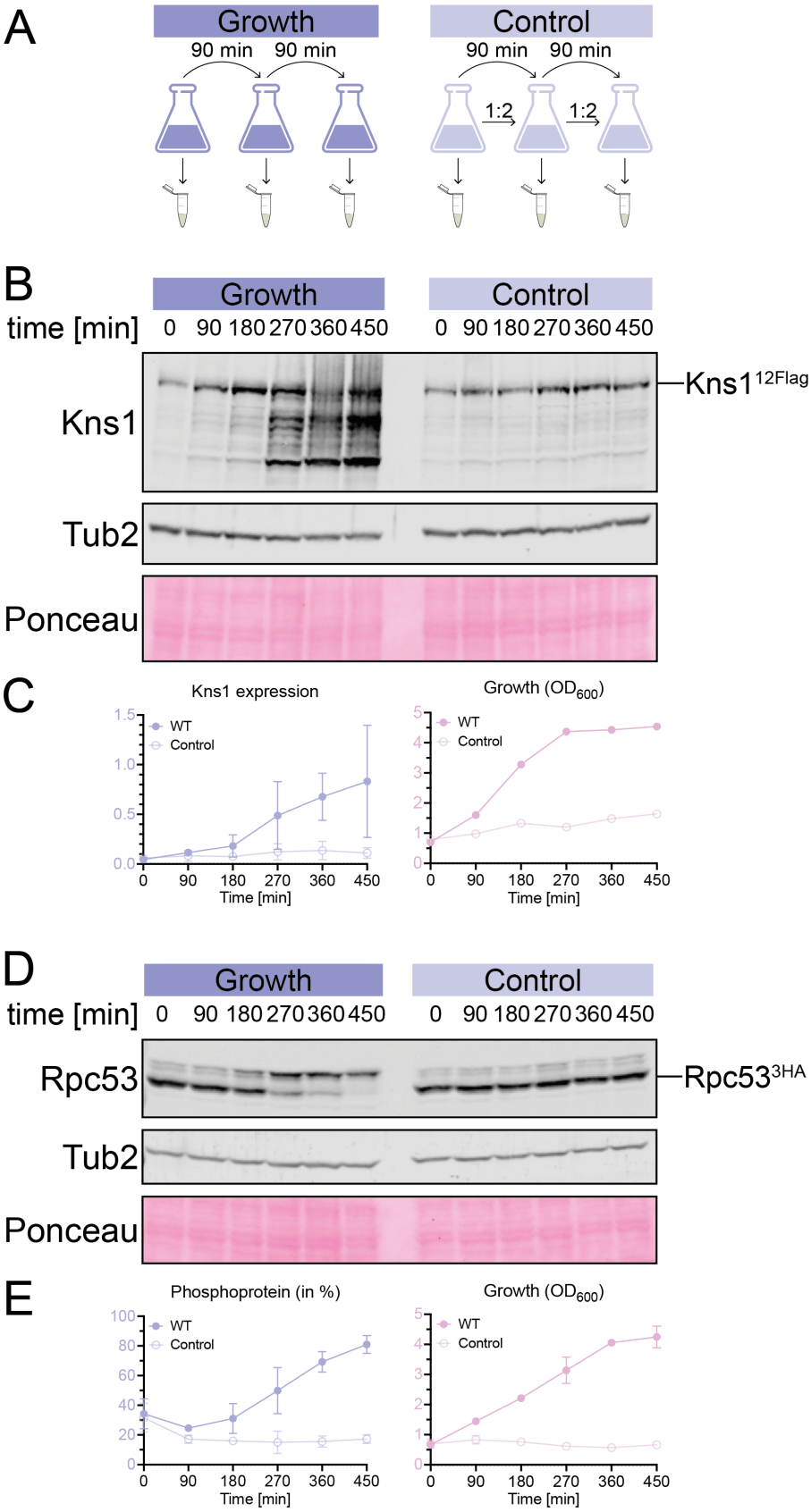

Figure 4.6 Kns1 expression and activity increases during diauxic shift.

A. Schematic overview of the experimental setup. Growth was measured every 90 min and a control was maintained in the exponential growth phase by diluting it at a ratio of 1:2 every 90 min. B. Western blot analysis of endogenous Kns1 in a growth curve. The samples were

collected every 90 min. Kns1-12xFlag was detected using an α-Flag antibody. Tub2 was used as a reference, and proper loading was controlled using Ponceau staining. C. Graphical visualisation of Kns1 expression normalised to Tub2 (growth: blue filled circles; control: blue open circles). Degradation bands were included in the Kns1 expression measurements. OD_{600} was used to determine the growth phases (growth: pink filled circles; control: pink open circles). Mean values (n = 2) are depicted as circles, and standard deviation (SD) is given with bars. D. Western blot analysis of Rpc53 expression and phosphorylation in a growth curve. Samples were taken every 90 min. Slower migrating bands represent phosphorylated isoforms of Rpc53. Rpc53-3HA was detected using α-HA antibody. Tub2 was used as a reference, and proper loading was controlled with Ponceau staining. E. Graphical visualisation of Rpc53 phosphorylation in relation to total protein (%) (growth: blue filled circles; control: blue open circles). OD_{600} was used to check the growth phases (growth: pink filled circles; control: pink open circles). Mean values (n = 2) depicted as circles and SD is given with bars.

To further validate the role of ISR in the regulation of Kns1 expression and activity in the diauxic shift, the ISR mutants from section 4.1.5 were analysed in a growth curve as well. The experimental approach was the same as before and is schematically displayed in Figure 4.7 A. Rpc53 phosphorylation in a *Δgcn2* background was measured (Figure 4.7 B). Compared with exponential growth, only minor changes in phosphorylation levels were detected with increasing growth. Using a deletion of *GCN2* only led to an increase of up to 50 % in phosphorylated Rpc53 (Figure 4.7 B, C), which was less than that in WT cells (Figure 4.6 E). Similar patterns were verified with *Δgcn4* background, blocking the reprogramming effects of ISR (Figure 4.7 D). The Rpc53 phosphoprotein level in *Δgcn4* cells increased only slightly to approximately 40 % after 450 min, while the OD_{600} increased to 4.5, as depicted in Figure 4.7 E. However, phosphorylation of Rpc53 during the diauxic shift was independent of Gcn3, a subunit of eIF2B (Figure S 2). These data suggest that the increased Rpc53 phosphorylation rates during the diauxic shift are ISR-dependent. Kns1 expression levels were assumed to be ISR-dependent in the diauxic shift, which in turn led to an increased proportion of Rpc53 phosphorylation. The metabolic switch leads to reprogramming via ISR, which most likely influences protein synthesis of KNS1 to regulate RNA Pol III activity under these conditions.

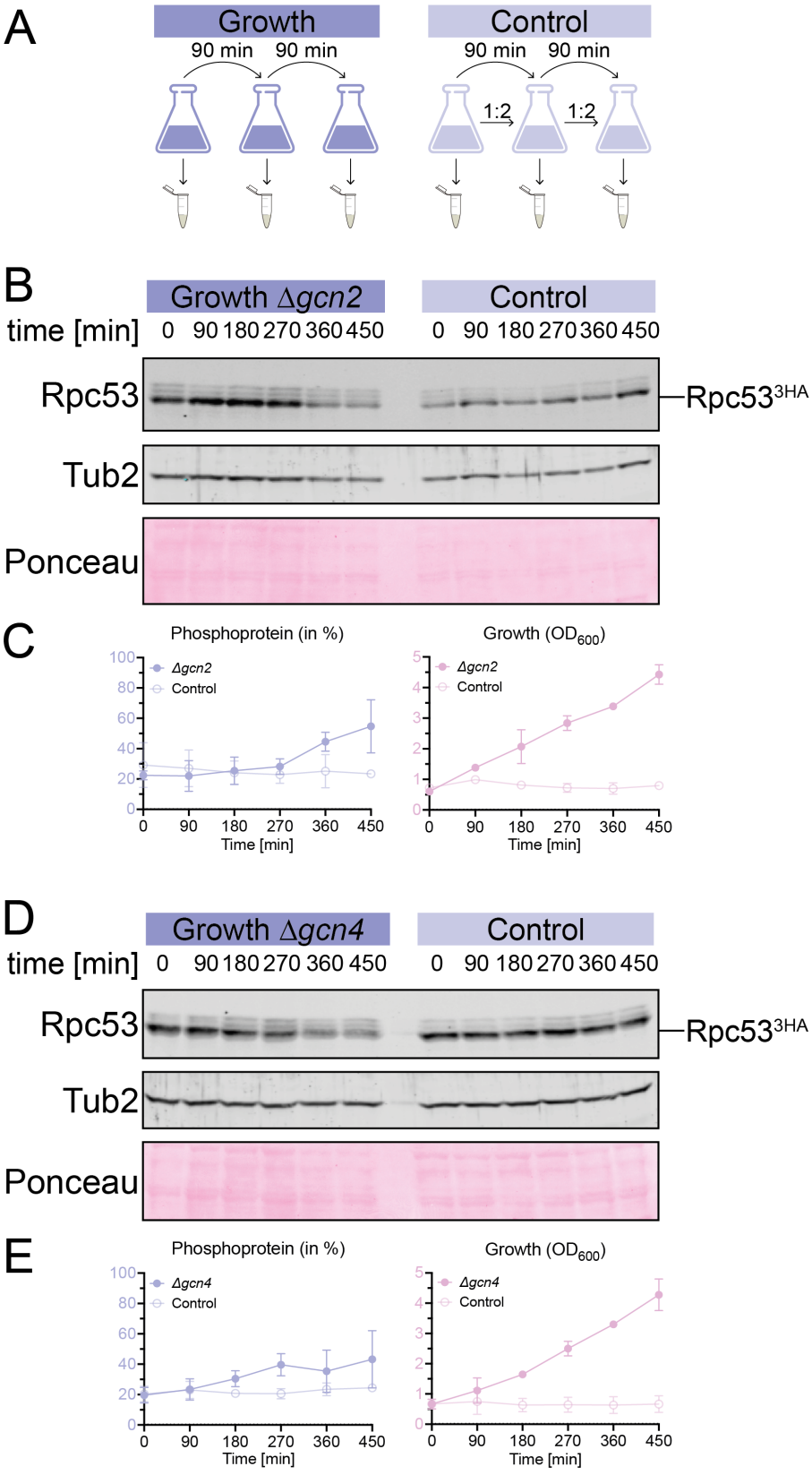

Figure 4.7 Change of Rpc53 phosphorylation during diauxic shift dependent on ISR.

A. Schematic overview of the experimental setup. Growth was measured every 90 min, and a control was maintained in the exponential growth phase by diluting it 1:2 every 90 min. B. Western blot analysis of Rpc53 expression and phosphorylation levels in *Δgcn2* background during growth. Samples were taken every 90 min. Slower migrating bands represent phosphorylated isoforms of Rpc53. Rpc53-3HA was detected using α-HA antibody. Tub2 was

used as a reference and with Ponceau staining a proper loading was controlled. C. Graphical visualisation of Rpc53 phosphorylation in relation to total protein (%) (growth: blue filled circles; control: blue open circles). OD_{600} was used to determine the growth phases (growth: pink filled circles; control: pink open circles). Mean values (n = 2) depicted as circles and standard deviation (SD) is given with bars. D. Western blot analysis of Rpc53 expression and phosphorylation levels in *Δgcn4* background during growth. Samples were taken every 90 min. Slower migrating bands represent phosphorylated isoforms of Rpc53. Rpc53-3HA was detected using α-HA antibody. Tub2 was used as a reference, and proper loading was controlled using Ponceau staining. E. Graphical visualisation of Rpc53 phosphorylation in relation to total protein (%) (growth: blue filled circles; control: blue open circles). OD_{600} was used to check the growth phases (growth: pink filled circles; control: pink open circles). Mean values (n = 2) depicted as circles and SD is given with bars.

4.2.2 Induction of Kns1 expression in non-preferred carbon sources

The ISR and changes during the diauxic shift are mainly regulated by nutrient availability (Busti *et al.* 2010; Galdieri *et al.* 2010; Pakos-Zebrucka *et al.* 2016; Costa-Mattioli and Walter 2020). A proper adaptation to changing conditions is crucial to ensure high proliferation rates under optimal conditions and to maintain a suitable energy consumption under unfavourable conditions. Physiological demands are diverse in a dynamic background, such as the diauxic shift. A precise assessment can only be performed in a stable environment. To investigate the possible carbon source-dependent mechanism of Kns1 regulation, three conditions were chosen. Optimal growth and normal protein synthesis were analysed using glucose (D) as the preferred carbon source for *S. cerevisiae* (Atiyeh and Duvnjak 2003; Broach 2012). Glucose serves not only as an energy source in glycolysis but also as a signal molecule in many pathways. Raffinose (Raf), a tri-saccharide, was used to mimic the intermediate conditions. Raffinose is a poorly fermentable carbon source that can be hydrolysed to glucose, galactose, and fructose (Atiyeh and Duvnjak 2003; Zhou *et al.* 2017). Metabolising raffinose requires glycosidases and multiple steps until glucose enters glycolysis. Non-fermentable carbon sources, such as glycerol (Gly), can only be catabolised by oxidative respiration (Zimmermann *et al.* 2011; Klein *et al.* 2017) and therefore imitates post-diauxic conditions when glucose is completely depleted. Kns1 expression and activity were upregulated in diauxic and post-diauxic conditions as well as in correlation with an activated ISR. It was assumed that Kns1 is regulated under unfavourable nutrient conditions, such as in raffinose or glycerol utilisation.

To elucidate which signals are integrated in Kns1 regulation and the underlying mechanism, steady-state levels of the three different carbon sources were assessed (Figure 4.8 A). The expression of Kns1 was then analysed by western blot analysis, which showed a significant increase in protein levels under raffinose and glycerol conditions compared to glucose (Figure 4.8 B). Kns1 levels in raffinose showed an approximately 12-fold increase, glycerol even 15-fold, compared to those in glucose (Figure 4.8 C). The phosphorylation levels of Rpc53 in different carbon sources showed a fitting response, as depicted in Figure 4.8 D. The proportion of phosphorylated to unphosphorylated Rpc53 shifted from 30 % in D to approximately

80 – 90 % phosphoprotein under unfavourable conditions (Figure 4.8 E). The shift in Rpc53 phosphorylation was directly dependent on Kns1 activity, as shown in Figure S 3. Furthermore, regulation by the 5' leader region was tested. The reporter, described in section 4.1.4, was applied to three different carbon sources. However, the change in NLS protein expression was minimal (Figure 4.8 F). The increase in reporter protein in raffinose was about 2-fold, in glycerol it was significantly about 3-fold, compared to glucose levels (Figure 4.8 G). This suggests that the 5' leader region alone is not sufficient to increase Kns1 expression levels to a significant extent in non-preferred carbon sources and opens questions on how Kns1 is additionally regulated.

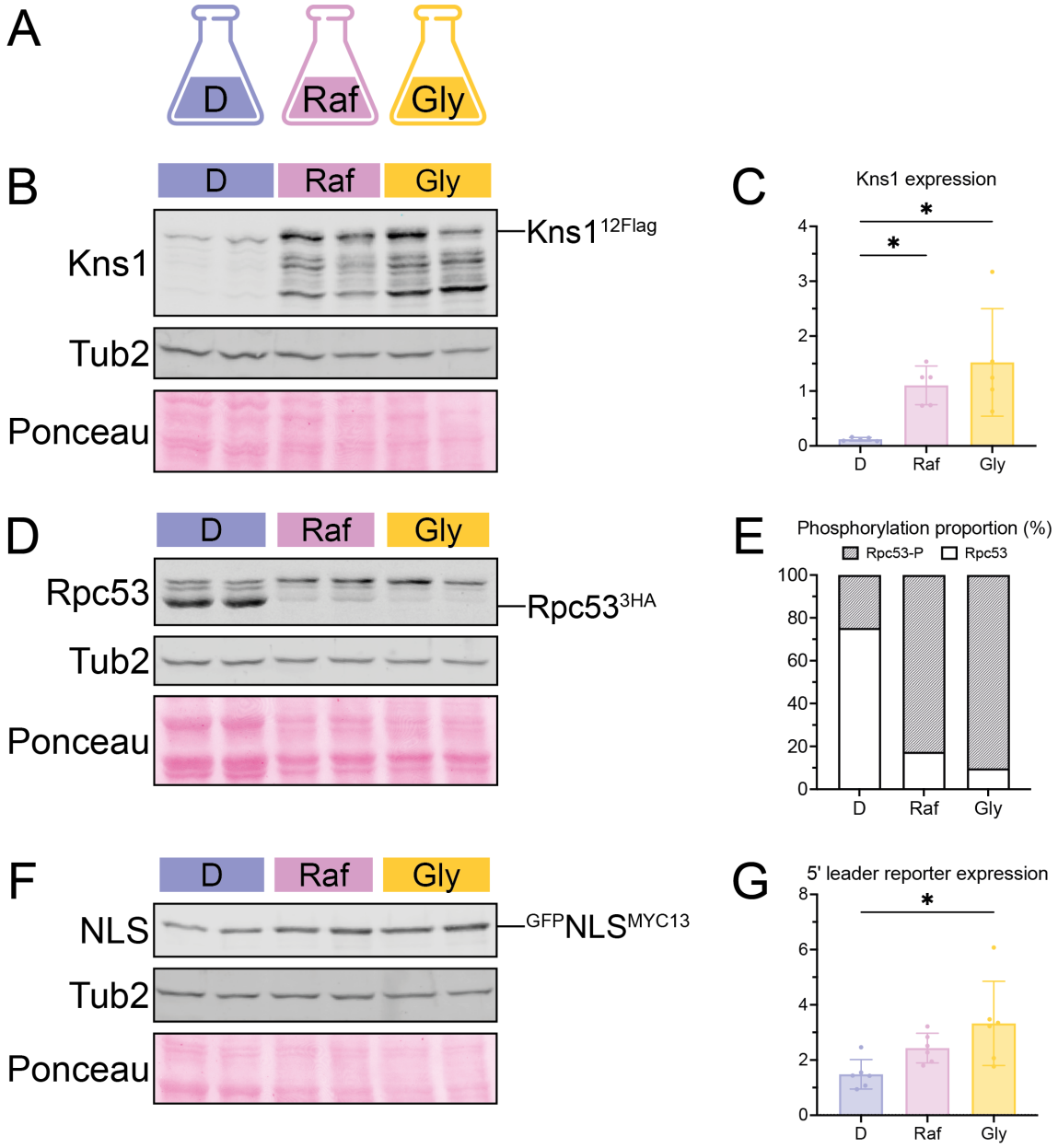

Figure 4.8 Kns1 expression and activity dependent on carbon source availability.

A. Used carbon sources for this experiment were glucose (D), raffinose (Raf) and glycerol (Gly). B. Western blot analysis of endogenous levels of Kns1 in different carbon sources. Biological duplicates were applied, and Kns1-12xFlag was detected using an α -Flag antibody. Tub2 was used as a reference and with the help of Ponceau staining proper loading was controlled.

C. Signal intensities from B were quantified and normalized to Tub2. Single values (n = 5) are depicted as dots, and the standard deviation (SD) is given by the bars. Normal distribution was tested with Shapiro-Wilk and statistics were calculated with Kruskal-Wallis test (ns: $p \geq 0.05$, not depicted; *: $p = 0.01 - 0.05$). D. Western blot analysis of Rpc53 expression and phosphorylation levels in different carbon sources. Slower migrating bands are phosphorylated isoforms of Rpc53. Rcp53-3HA was detected by using an α-HA antibody. Tub2 was used as a reference, and proper loading was controlled with Ponceau staining. E. Phosphorylated and unphosphorylated signals from D were calculated in proportion to total Rpc53 levels. The mean relative proportion was expressed as a percentage (n = 5). Grey portions indicate phosphorylated values and white boxes indicate unphosphorylated values. F. Western blot analysis of 5' leader reporter in different carbon sources. The reporter peptide NLS was detected using an α-MYC antibody in two biological replicates for each condition. Tub2 was used as a reference, and Ponceau staining was used to control protein levels. G. Quantification of the signals of F. Single values (n = 6) normalized to Tub2 are depicted as dots and SD is shown by bars. Normal distribution was tested with Shapiro-Wilk and statistics were calculated with an ordinary one-way ANOVA (ns: $p \geq 0.05$, not depicted; *: $p = 0.01 - 0.05$).

One possible mechanism is carbon source-specific localisation of the protein, which could lead to a strong increase in Kns1 within the nucleus under unfavourable conditions. To visualize endogenous Kns1, GFP fusions were carried out and live-cell confocal microscopy was performed. The cells were incubated in the aforementioned carbon sources and kept under optimal growth conditions, while microscopy was performed. The strains used for this approach contained an additional fluorescent protein that served as a co-localisation marker to visualize the nucleus. In this case, NLS-mCherry was used as a nuclear co-marker. Kns1 localisation in glucose was barely detectable, as the signal was very weak and dispersed throughout the cells (Figure 4.9 B). Calculation of nuclear enrichment revealed a coefficient of 1.1, which suggested dispersed localisation in the cytoplasm and nucleus (Figure 4.9 C). Cells grown in Raf showed an increase in signal intensity (Figure 4.9 B), as expected from the enhanced protein levels already analysed in Figure 4.8 B. Kns1 is localized throughout the whole cells, but with an enrichment of nuclear signal, as indicated by the rise in the mean enrichment factor to 1.7 (Figure 4.9 C). Stronger signals were detected in cells grown in Gly. Kns1 was detected in the cytoplasm but was significantly enriched in the nucleus (mean nuclear enrichment of 2.8), and co-localised with the NLS-mCherry marker (Figure 4.9 B, C). These data suggest that a significant increase in carbon source-specific nuclear proteins could play an additional role in the upregulation of Kns1 under unfavourable conditions.

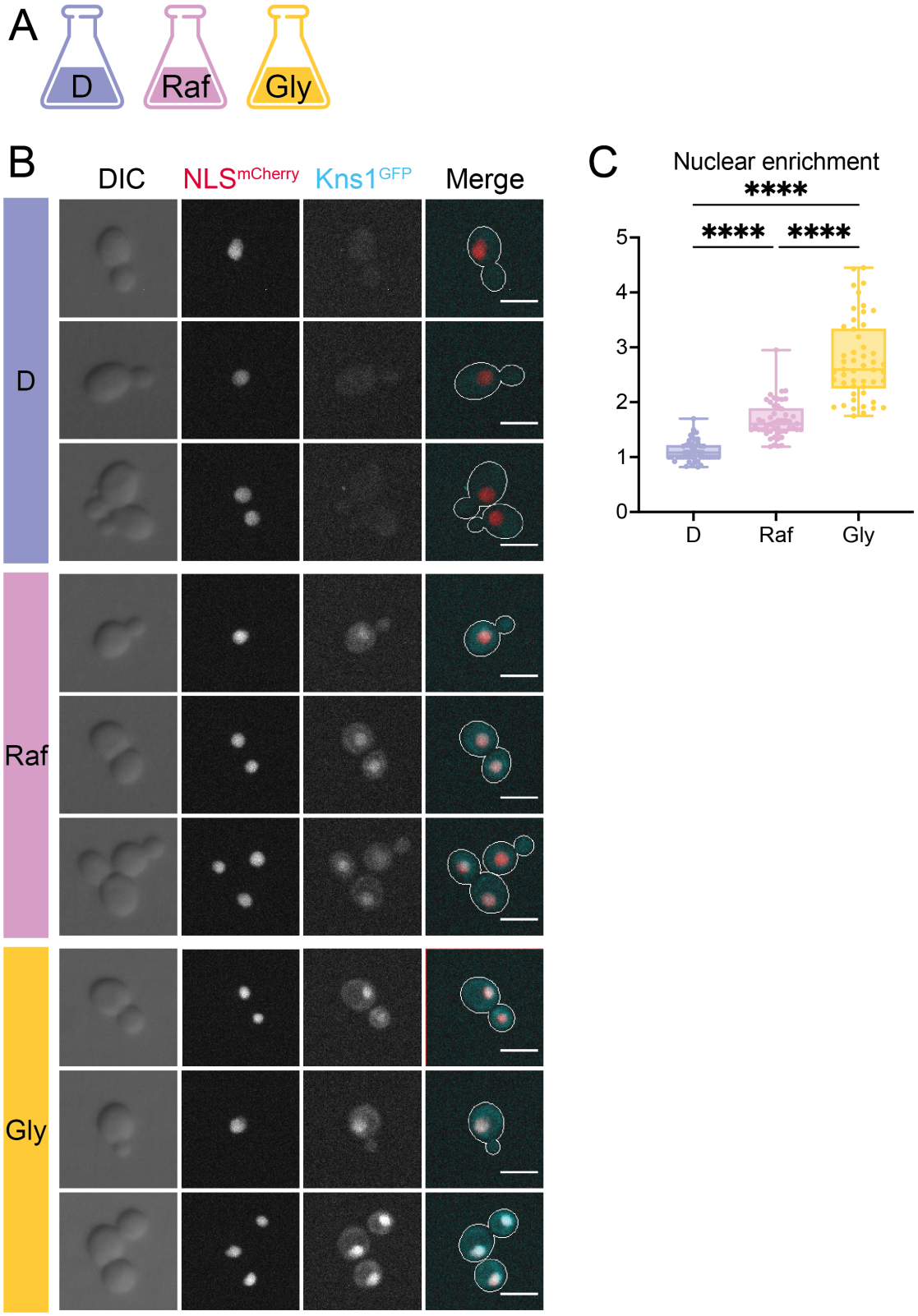

Figure 4.9 Carbon source dependent nuclear enrichment of endogenous Kns1.

A. Used carbon sources for this experiment were glucose (D), raffinose (Raf) and glycerol (Gly). B. Confocal analysis of endogenous Kns1 in different carbon sources. All strains used contained NLS-mCherry (red) as a nuclear co-marker and Kns1-GFP (cyan). The mCherry signal was detected at a 5 % laser intensity and 200 ms exposure time. The GFP signal was detected at 40 % laser intensity and a 200 ms exposure time. Three representative single cells are presented for each condition. Scale bar indicates 5 µm. C. Quantification of the nuclear signal

intensities. The mean pixel density was measured in a 7 × 7 px square located within the cytoplasm and nucleus in 50 cells. The proportion of enrichment of nuclear signals to cytoplasmic signals was calculated for each cell type. All values are depicted as dots. The box indicates the minimum-to-maximum value, and the mean nuclear enrichment is given as a line within the box. Normal distribution was tested using the Shapiro-Wilk test, and statistics were calculated using the Kruskal-Wallis test (****: $p < 0.0001$).

Further analyses were performed to address the question of how Kns1 expression is precisely regulated under unfavourable conditions. A previous study showed that the global reduction in translational efficiency in an eIF2-specific manner (*Δ326*) led to a change in metabolism and genetic reprogramming, even under glucose conditions (Wojciech 2020). As the *Δ326* mutant showed less pronounced effects on Kns1 expression in this study than different carbon sources and physiological conditions, it was of great interest to assess the connection between metabolic effects mediated via eIF2. The three carbon sources were tested in the WT and *Δ326* backgrounds (Figure 4.10 A). Kns1 protein expression was analysed in a western blot approach. A slight increase in protein levels in the *Δ326* cells under glucose conditions was detected, as expected (Figure 4.10 B). The already demonstrated significant increase in raffinose and glycerol could be reproduced in the WT background (Figure 4.10 C). The *Δ326* mutant, however, showed no significant increase in these conditions compared to the WT, as depicted in Figure 4.10 B and C. Correspondingly, the phosphorylation levels of Rpc53 increased from 30 % in WT to 70 % in *Δ326* (Figure 4.10 E). Additionally, a strong increase in unfavourable carbon sources compared with glucose was observed in the WT. The percentage of phosphoprotein increased to 80 – 90 % (Figure 4.10 E). Again, the eIF2 mutant did not show significant differences in the Rpc53 phosphorylation proportion in Raf and Gly compared to the WT background, as displayed in Figure 4.10 D and E. In summary, these data suggest a strong influence of nutrient availability on the expression and activity of Kns1, which can also be simulated by reducing global translation initiation, leading to metabolic reprogramming.

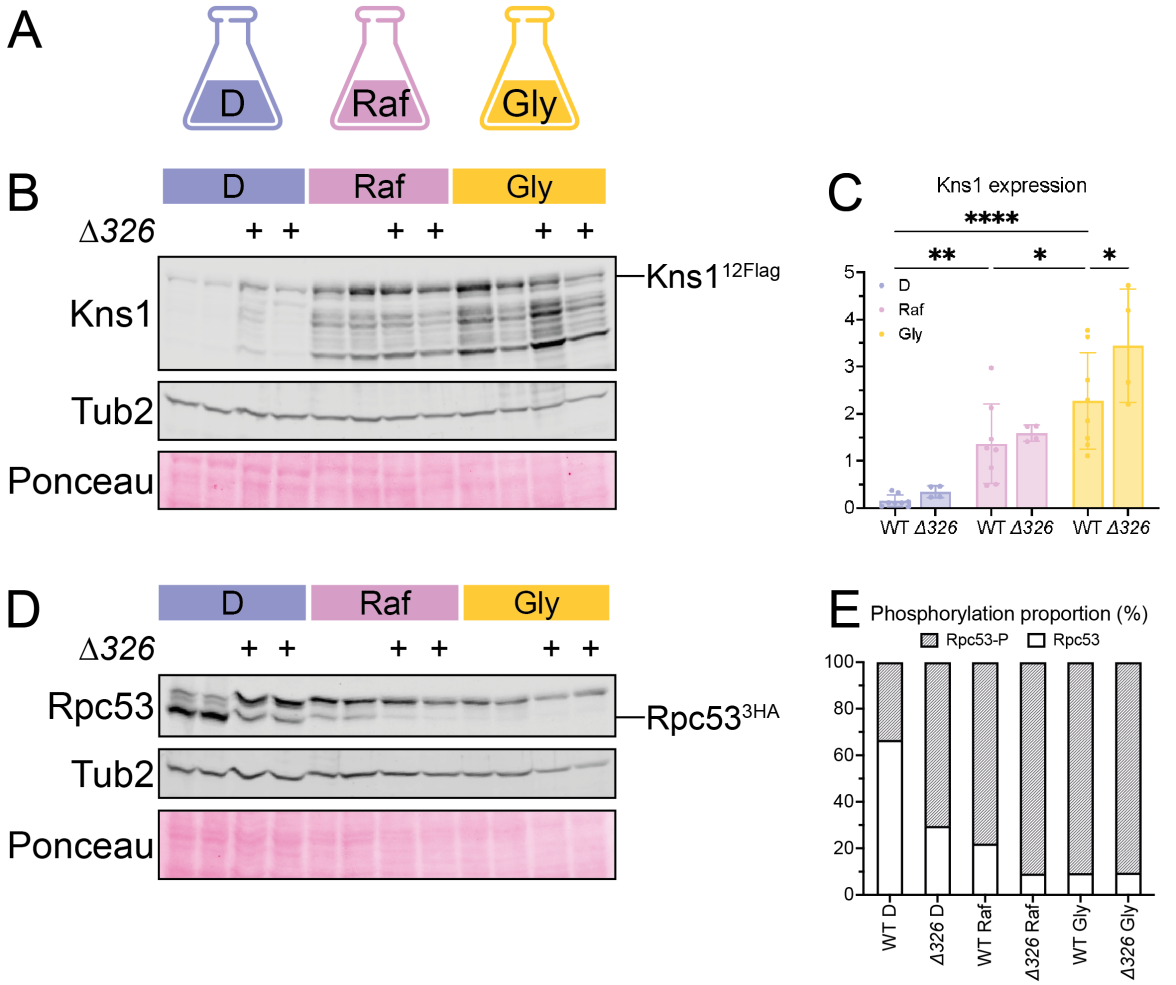

Figure 4.10 Carbon source dependency of Kns1 in WT and *Δ326* mutant.

A. Used carbon sources for this experiment were glucose (D), raffinose (Raf) and glycerol (Gly). B. Western blot analysis of endogenous Kns1 levels in WT and *Δ326* background in different carbon sources. Biological duplicates of Kns1-12xFlag were detected using an α-Flag antibody. Tub2 was used as a reference and with the help of Ponceau staining proper loading was controlled. The genetic background is indicated with +. C. Signal intensities from B were quantified and normalized to Tub2. Single values (n = 4) are depicted as dots and the standard deviation (SD) is represented by bars. Statistics were calculated with a two-way ANOVA (ns: $p \geq 0.05$, not depicted, *: $p = 0.01 - 0.05$, ***: $p = 0.0001 - 0.001$; ****: $p < 0.0001$). D. Western blot analysis of Rpc53 expression and phosphorylation levels in WT and *Δ326* background in different carbon sources. Rpc53 was detected using an α-HA antibody. Slower migrating bands represent phosphorylated Rpc53 isoforms. Tub2 was used as a reference, and overall protein loading was controlled using Ponceau staining. Genetic background is indicated with +. E. Phosphorylated and unphosphorylated signals from D were calculated in proportion to total Rpc53 levels. The mean relative proportion is expressed as a percentage (n = 4). Grey portions indicate phosphorylated values and white boxes indicate unphosphorylated values.

As the reduced availability of active eIF2 complex leads to activation of the ISR by a strong translation of Gcn4 and Kns1 protein levels are Gcn4-dependent (section 4.1.5), a possible ISR-dependency under unfavourable carbon sources was investigated. For this, the ISR mutants from section 4.1.5 were used. The analysis was performed under three different carbon source conditions as described previously (Figure 4.11 A).

Rpc53 phosphorylation was detected by western blotting, which showed an expected increase in phosphorylation levels in unfavourable media in the WT background (Figure 4.11 B). The same high proportion of phosphorylated Rpc53 was visible in the *Δgcn2* and *Δgcn4* backgrounds in raffinose and glycerol, as depicted in Figure 4.11 B. The proportion of phosphorylated Rpc53 increased from 30 – 40 % in glucose to 80 – 90 % in raffinose or glycerol in all backgrounds (Figure 4.11 C). This strongly indicates that the change in phosphorylation of Rpc53 under non-glucose conditions is independent of ISR, and metabolic reprogramming can take place without Gcn4.

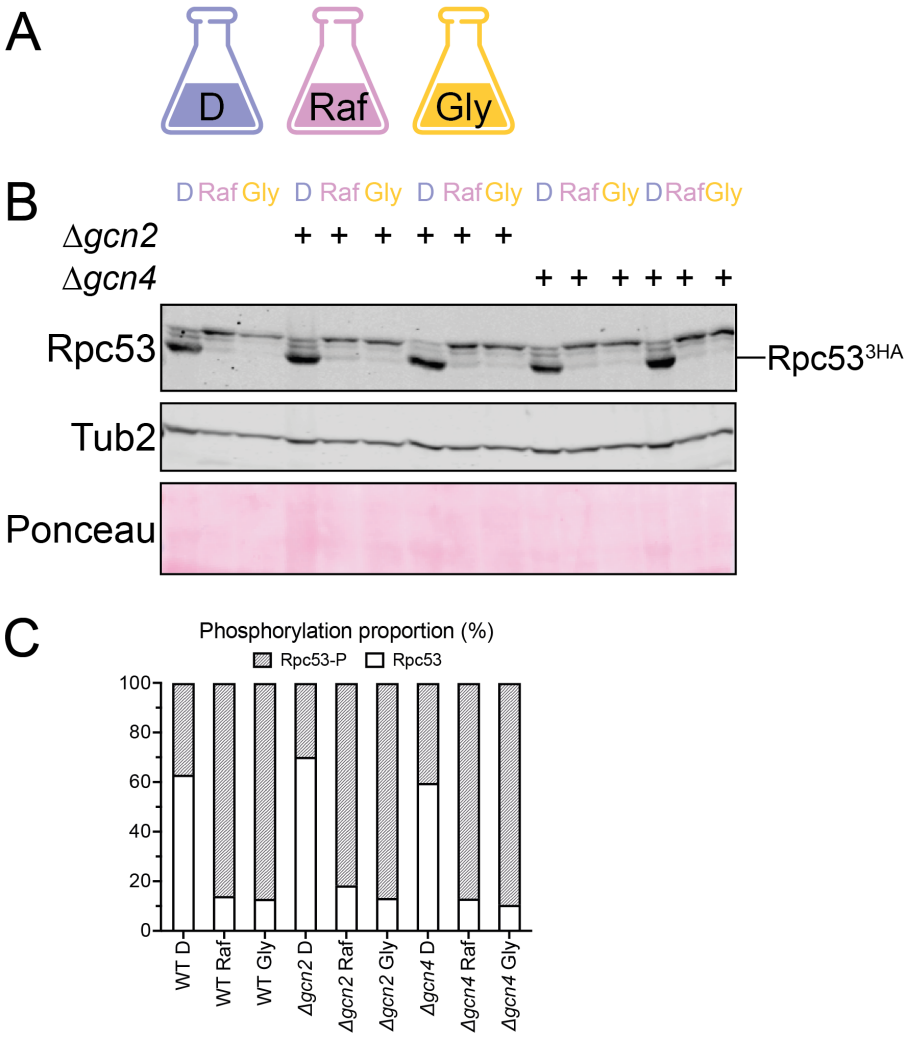

Figure 4.11 Change in Kns1 activity in altered carbon sources independent of ISR.

A. Used carbon sources for this experiment were glucose (D), raffinose (Raf) and glycerol (Gly). B. Western blot analysis of Rpc53 expression and phosphorylation levels in WT, *Δgcn2* and *Δgcn4* background in different carbon sources. Rpc53 was detected using an α-HA antibody. Slower migrating bands are phosphorylated isoforms of Rpc53. Tub2 was used as a reference and overall protein loading was controlled using Ponceau staining. Genetic background is indicated with +. The experiment was conducted by Kathrin Preußel Danger for this work. C. Phosphorylated and unphosphorylated signals from B were calculated in proportion to total Rpc53 levels. The mean relative proportion is expressed as a percentage (n = 2). Grey portions indicate phosphorylated proportions and white boxes indicate unphosphorylated proportions.

4.2.3 Dynamic modulation of Kns1 expression and activity in response to carbon source changes

The strong influence of steady-state levels of different carbon sources (section 4.2.2) indicated that the regulation of Kns1 expression and activity is regulated when carbon source conditions are changing. To verify the dynamics of this altered expression, a nutrient switch mimicking progression through a diauxic shift was utilised. A defined picture was elucidated with controlled shifts in the carbon sources.

The carbon source switch from glucose to unfavourable conditions was performed using both Kns1 expression and Rpc53 phosphorylation levels. The experimental setup included a change from glucose to raffinose or glycerol as well as a control treatment that switched from glucose to glucose (Figure 4.12 A). Before the shifts started, a reference value was obtained. The carbon source shift was documented at intervals of 30 min. Kns1 expression gradually increased over the analysed time of two hours in both switches when compared to the constant glucose conditions (Figure 4.12 B, C). Quantification of the signals normalised to Tub2 levels also showed a significant but gradual increase over time, while control expression remained constant (Figure 4.12 D). Rpc53 phosphorylation levels gradually increased in both shifts (Figure 4.12 E, F). However, the increase in phosphorylation was faster than that in Kns1 expression, and after 90 min, a maximum of 80 – 90 % phosphorylated proportion was reached (Figure 4.12 G).

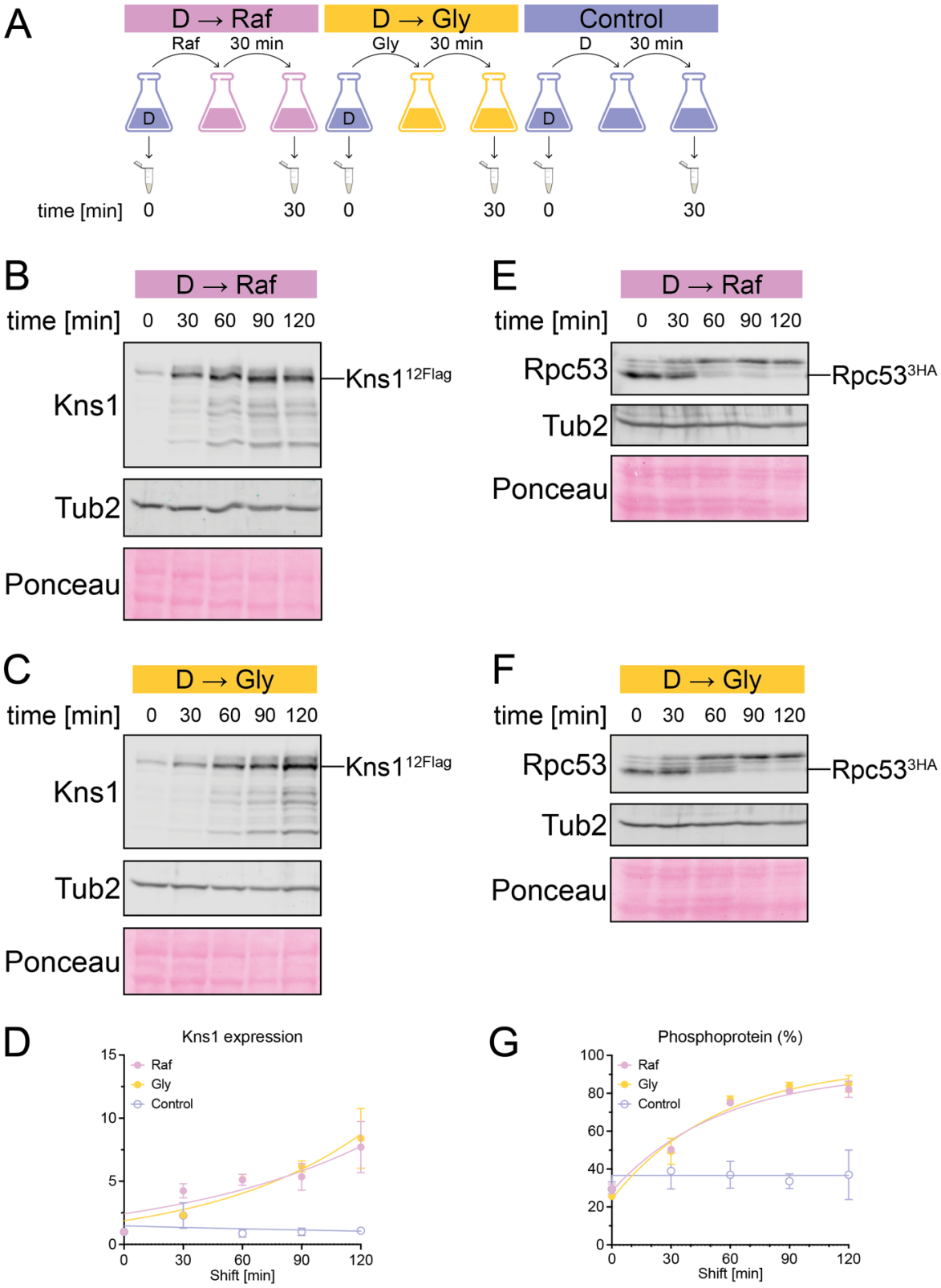

Figure 4.12 Kns1 expression and activity dynamics switching from preferred to non-preferred carbon source conditions.

A. Experimental setup of the carbon source shift. The starting cultures included glucose (D) and served as a time point of 0. The medium was then replaced with either raffinose (Raf)- or glycerol (Gly)-containing media and incubated for 30 min. Samples were then taken every 30 min for 2 h. The medium was changed from glucose- to glucose-containing medium as a control and treated in the same manner as the shifts. B. Western blot analysis of endogenous

Kns1 levels in a carbon source shift from D to Raf. Kns1-12xFlag was detected using an α-Flag antibody. Tub2 was used as a reference and with the help of Ponceau staining proper loading was controlled. The sampling intervals are indicated in minutes. Control data can be found in Figure S 4. C. Western blot analysis of endogenous Kns1 levels in a carbon source shift from D to Gly. Kns1-12xFlag was detected using an α-Flag antibody. Tub2 was used as a reference, and Ponceau staining controlled the proper protein loading. The sample intervals are given in min. The control data can be found in Figure S 4. D. Signals from B and C were quantified. Kns1 levels were normalised to those of Tub2. Mean values from two biological replicates (control n = 4) are indicated by circles, and standard deviations (SD) are given in bars. A nonlinear regression curve was fitted to each condition indicated by the lines (D → Raf: pink; D → Gly: yellow; control: blue). E. Western blot analysis of Rpc53 expression and phosphorylation levels in a carbon source shift from D to Raf. Rpc53-3HA was detected using an α-HA antibody. Slower migrating bands represent phosphorylated Rpc53 isoforms. Tub2 was used as a reference, and proper loading was controlled using Ponceau staining. Sample intervals are given in min. Control data can be found in Figure S 5. F. Western blot analysis of Rpc53 expression and phosphorylation levels in a carbon source shift from D to Gly. Rpc53-3HA was detected using an α-HA antibody. Slower migrating bands reveal phosphorylated Rpc53 isoforms. Tub2 was used as a reference and Ponceau staining controlled a proper protein loading. Sampling intervals are indicated in min. The control data can be found in Figure S 5. G. Signals from E and F were quantified. The proportion of phosphorylated Rpc53 to total protein was calculated as a percentage. Mean values from two biological replicates (control n = 4) are indicated by circles and SD is given in bars. A nonlinear regression curve was fitted to each condition indicated by the lines (D → Raf: pink; D → Gly: yellow; control: blue).

Investigating the kinetics of Kns1 expression and Rpc53 phosphorylation levels as a means to measure Kns1 activity when conditions change from unfavourable (Raf or Gly) to fermentative conditions. The experiment began with media containing either raffinose or glycerol. The available carbon source was exchanged for glucose, and samples were taken at 30 min intervals for two hours in total (Figure 4.13 A, D). Kns1 expression was detected by western blotting in both experiments (Figure 4.13 B, E). The protein levels dropped to a minimum close to zero within the first 30 min, as depicted in Figure 4.13 C and F. A control switch from either raffinose to raffinose or glycerol to glycerol showed consistently high levels of Kns1 expression, indicating a significant change in expression under the aforementioned conditions and a fast adaptation of Kns1 to switching situations.

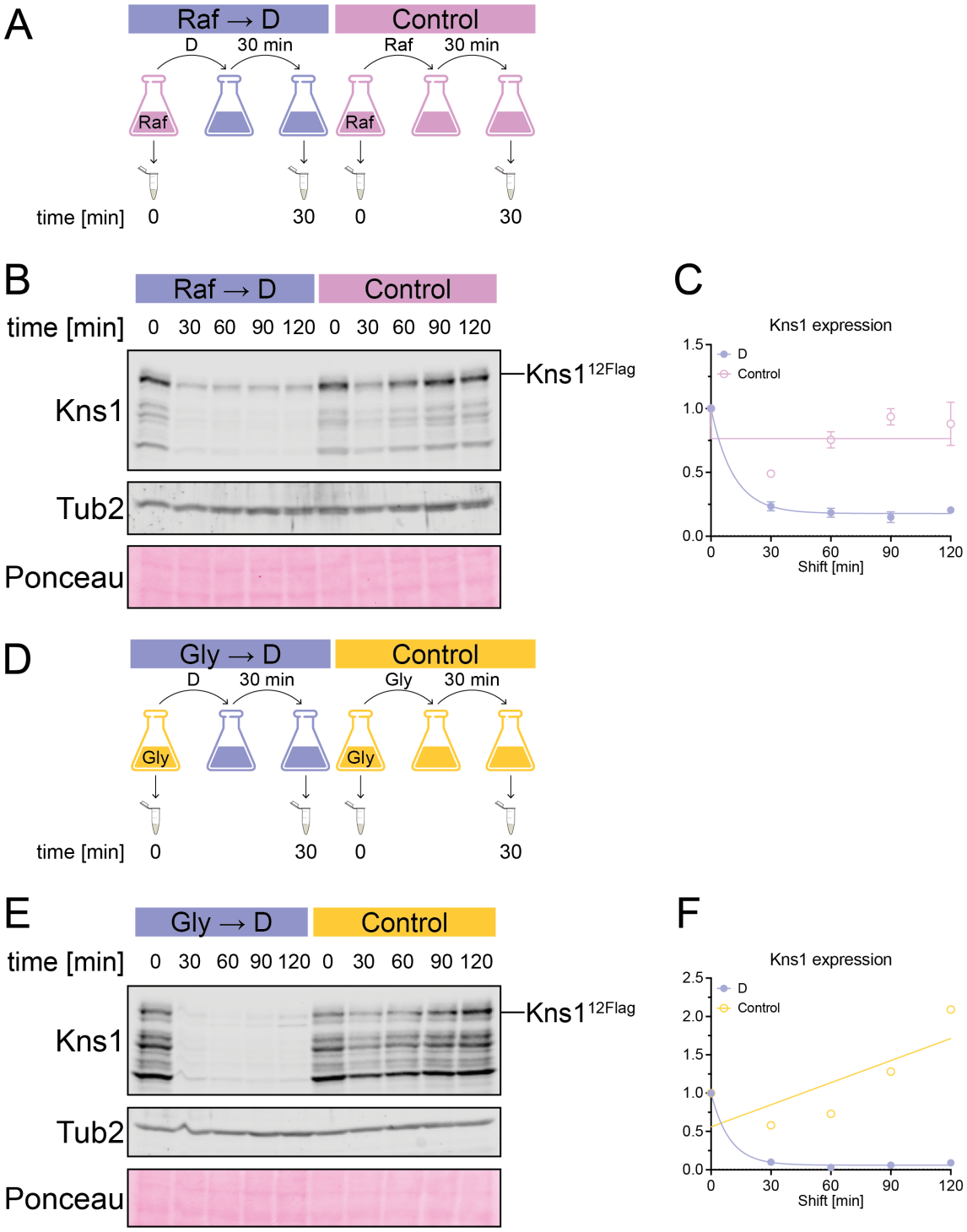

Figure 4.13 Kns1 expression kinetics switching from unfavourable to favourable conditions.

A. Experimental setup of the carbon source shift. The starting cultures included raffinose (Raf) and served as a time point of 0. Afterwards, the medium was replaced with a glucose (D)-containing medium and incubated for 30 min. Samples were then taken every 30 min for 2 h in total. Changing the medium from raffinose- to raffinose-containing medium was used as a control and treated in the same manner as the shifts. B. Western blot analysis of endogenous Kns1 levels in a carbon source shift from Raf to D. Kns1-12xFlag was detected using an α-Flag antibody. Tub2 was used as a reference and with the help of Ponceau staining proper loading was controlled. The sample intervals are indicated in minutes. C. The signals from B were then quantified. Kns1 levels were normalized to Tub2. Mean values from two biological replicates are indicated by circles, and standard deviations (SD) are given in bars. A

nonlinear regression curve was fitted to the experiment and control indicated by the lines (Raf → D: blue; control: pink). D. Experimental setup of the shift. The starting cultures included glycerol (Gly) and served as a time point of 0. Afterwards the medium was exchanged to glucose (D)-containing medium and incubated for 30 min. Samples were then taken every 30 min for 2 h in total. Changing the medium from glycerol- to glycerol-containing medium was used as a control and treated in the same manner as the shifts. E. Western blot analysis of endogenous Kns1 levels in a carbon source shift from Gly to D. Kns1-12xFlag was detected using an α-Flag antibody. Tub2 was used as a reference and Ponceau staining controlled a proper protein loading. The sampling intervals were given in minutes. F. Signals from E were quantified. Kns1 levels were normalized to Tub2. A nonlinear regression curve was fitted to each condition indicated by the lines (Gly → D: blue; control: yellow).

Rpc53 phosphorylation, however, showed a more stable effect when conditions were altered to a favourable carbon source. When shifting from raffinose to glucose, the phosphorylated proportion reduced from 90 % to 70 %, after the analysed two hours (Figure 4.14 B, C). When switching from non-fermentable glycerol to glucose, phosphorylation of Rpc53 dropped from 90 % to 30 % in two hours (Figure 4.14 E, F). This indicates a faster dephosphorylation of Rpc53 when conditions are changed drastically; however, it also shows more persistent phosphorylation in comparison to Kns1 expression levels in total. Possibly, this process involves active dephosphorylation, which is slower than repression of Kns1 expression.

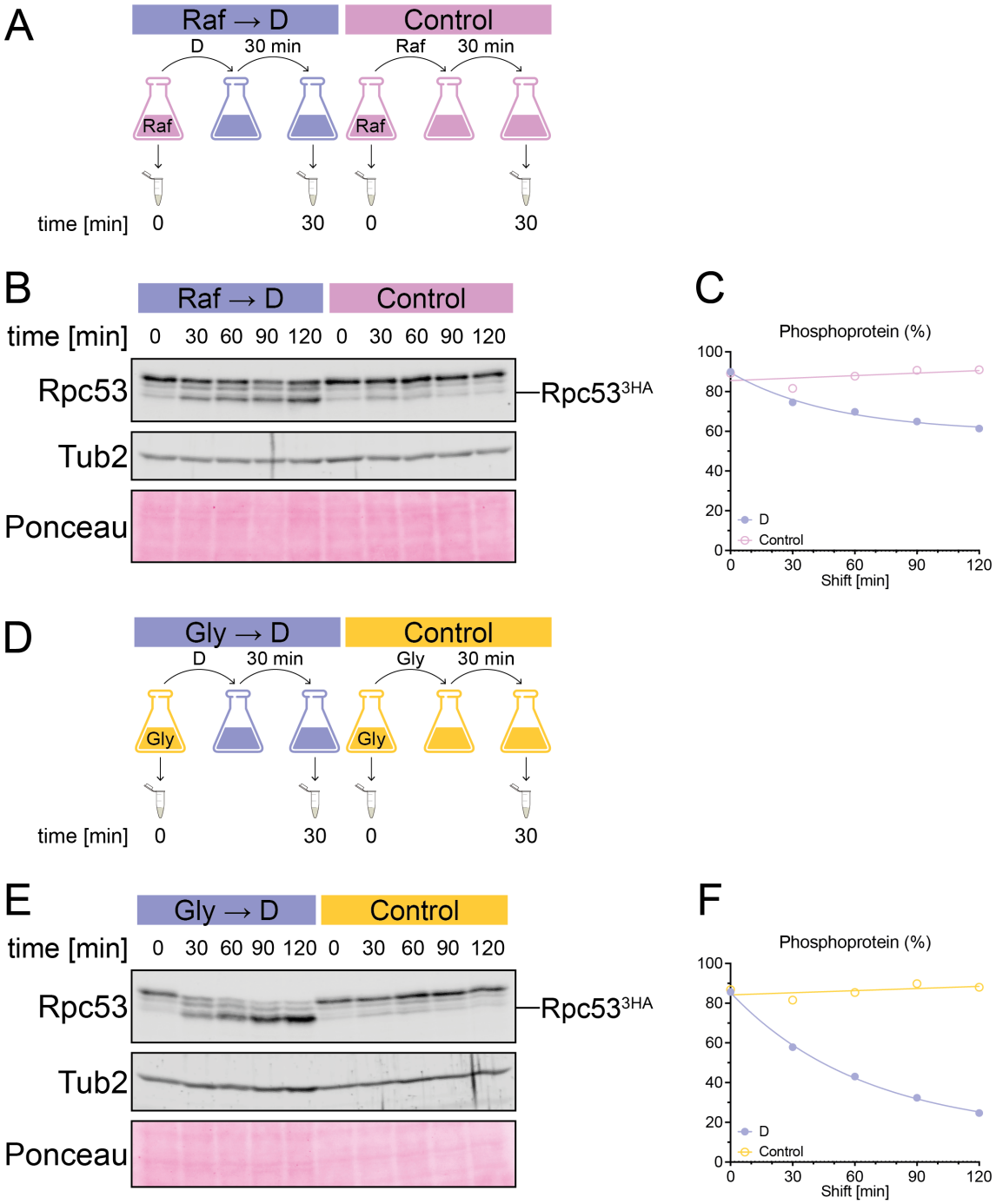

Figure 4.14 Rpc53 phosphorylation kinetics switching from unfavourable to favourable conditions.

A. Experimental procedure of the carbon source shift. Starting cultures included raffinose (Raf) and served as a time point 0. Afterwards the medium was exchanged to glucose (D)-containing medium and incubated for 30 min. Samples were then collected every 30 min for 2 h. Changing the medium from raffinose- to raffinose-containing medium served as a control and was treated the same as the shift. B. Western blot analysis of Rpc53 expression and phosphorylation levels in a carbon source shift from Raf to D. Rpc53-3HA was detected using an α-HA antibody. Slower migrating bands indicate the phosphorylated Rpc53 isoforms. Tub2 was used as a reference and with the help of Ponceau staining proper loading was controlled. Sample intervals are indicated in min. C. Signals from B were quantified. The single values are indicated by circles. A nonlinear regression curve was fitted to each condition indicated by the lines (Raf → D: blue; control: pink). D. Experimental procedure of the carbon source shift. Starting

cultures included glycerol (Gly) and served as a time point 0. Afterwards the medium was exchanged to glucose (D)-containing medium and incubated for 30 min. Samples were then taken every 30 min for 2 h in total. Changing the medium from glycerol- to glycerol-containing medium was used as a control and treated in the same manner as the shift. E. Western blot analysis of Rpc53 expression and phosphorylation levels in a carbon source shift from Gly to D. Rpc53-3HA was detected using an α-HA antibody and slower migrating bands are phosphorylated isoforms of Rpc53. Tub2 was used as a reference and Ponceau staining controlled a proper protein loading. Sampling intervals are given in min. F. Quantification of the signals from E. Single values are indicated by circles. A nonlinear regression curve was fitted to the conditions indicated by the lines (Gly → D: blue; control: yellow).

4.2.4 Enhanced Kns1 expression and activity in metabolic processes

Previous results of this study revealed that Kns1 regulation is affected by unfavourable carbon sources and the metabolic switch from fermentation to respiration. Glucose not only serves as a nutrient supplier but also as a signal molecule (Broach 2012; Conrad *et al.* 2014). Key enzymes that regulate glucose utilisation are found in glycolysis and connect glucose levels to fast cell proliferation (Peeters *et al.* 2017). Kns1 activity is linked to anti-proliferative mechanisms, in contrast to high glycolytic flux. If Kns1 expression and activity are not only linked to carbon sources but are also negatively influenced by glycolytic flux, blocking glycolysis should increase Kns1, similar to non-fermentable carbon sources. The two key enzymes that efficiently mediate glycolytic flux are Hxk2 and Pfk2. The hexokinase Hxk2 phosphorylates imported glucose to glucose-6-phosphate in the first step of glycolysis (Peeters *et al.* 2017). The Phosphofructokinase Pfk2 is responsible for the conversion of fructose-6-phosphate to fructose-1,6-bisphosphate, which connects glycolysis to the Ras/cAMP/PKA pathway, regulating cell proliferation (Peeters *et al.* 2017).

To verify whether low glycolytic flux also influences Kns1 expression and activity to ensure its anti-proliferative function, glycolytic mutants were studied. The mutants *Δhxk2*, a deletion of hexokinase 2, and *Δpfk2*, a deletion of one subunit of phosphofructokinase 2, were analysed and compared to *Δ326* and WT (Figure 4.15 A). Kns1 protein levels were analysed on a western blot and showed increased expression in all three mutants compared to WT (Figure 4.15 B). The increase was similar in all mutants, approximately 2-fold compared to WT levels (Figure 4.15 C). Corresponding results were obtained for Rpc53 phosphorylation levels, as shown in Figure 4.15 D. The proportion of phosphorylated protein increased to 60 – 70 % in all three mutants compared to 30 % in WT cells (Figure 4.15 E). The *KNS1* 5' leader reporter, first described in section 4.1.4, was utilised once more to check for regulatory influences of the 5' region in the three different mutants. Reporter protein levels, however, were similar, with no significant increase in all three tested mutants (Figure 4.15 F, G), indicating regulation of Kns1 expression at the post-translational level when glycolytic flux was reduced.

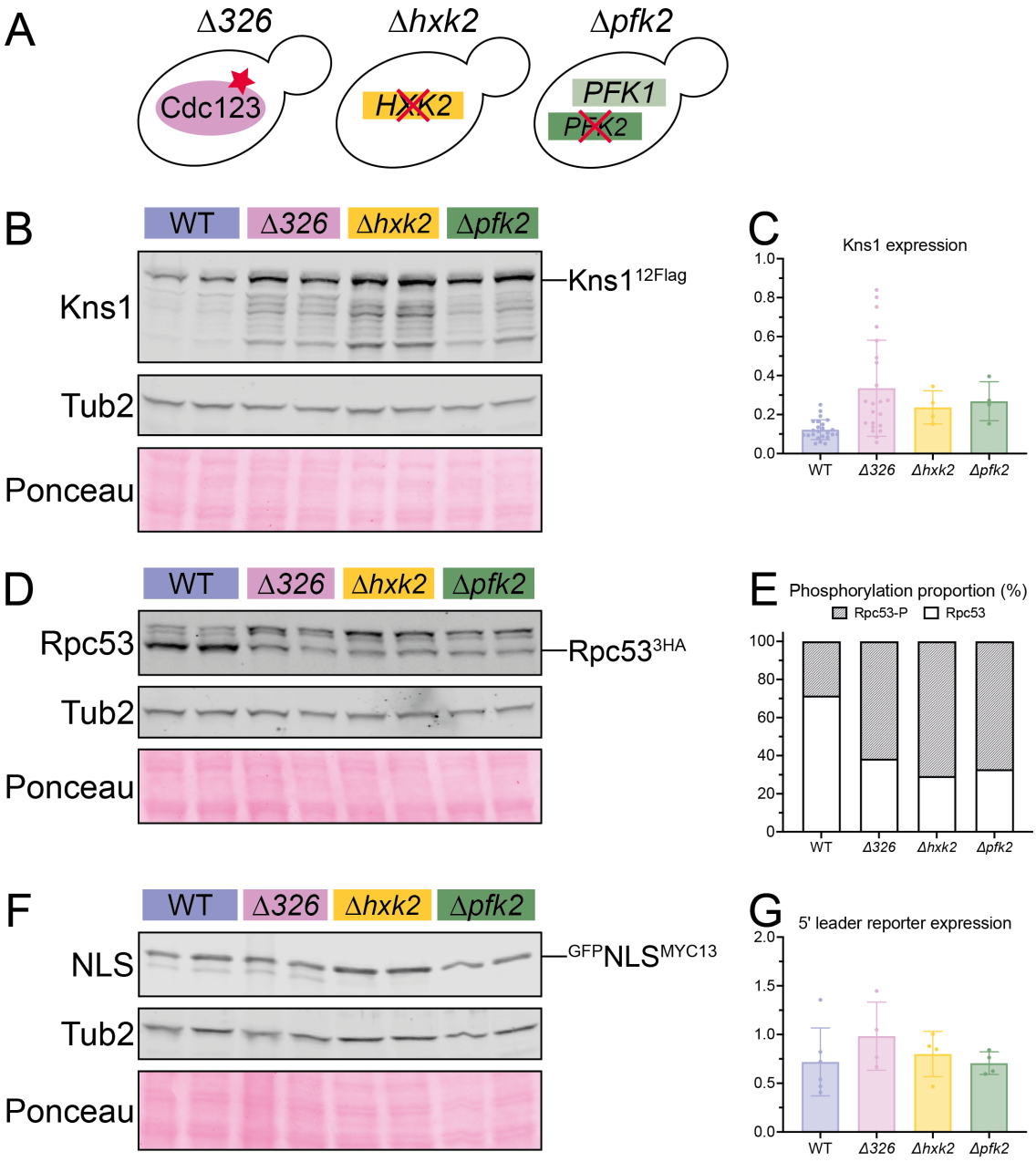

Figure 4.15 Increased Kns1 expression and activity in glycolytic mutants.

A. Used mutants in this study include *Δ326*, a C-terminal truncation (red star) of Cdc123 at amino acid 326; *Δhxk2*, a deletion (red cross) of the hexokinase *HXK2* and *Δpfk2*, a deletion (red cross) of one subunit of the phosphofructokinase *PFK2*. B. Western blot analysis of endogenous Kns1 protein expression in different mutants compared to WT. Kns1-12xFlag was detected with an α-Flag antibody. Tub2 was used as a reference and comparable protein loading was controlled via Ponceau staining. Loading was performed in two biological replicates for each background strain. C. Quantification of western blot signal intensities from B. Kns1 expression was normalised to Tub2 levels; individual values are indicated by dots (n ≥ 4), and standard deviation (SD) is given by bars. Normal distribution was tested with Shapiro-Wilk and statistics were calculated with Kruskal-Wallis test (all comparisons ns: p ≥ 0.05, not depicted). D. Western blot analysis of Rpc53 (phosphorylation) levels in different mutants. Rpc53-3HA was detected with an α-HA antibody. Slower migrating bands represent phosphorylated isoforms of Rpc53. Tub2 was used as a reference, and Ponceau staining was used to control equal protein loading. Two biological replicates were used for each strain background. E. Phosphorylated and unphosphorylated signals from D were calculated in proportion to total

Rpc53 levels. The mean relative proportion was expressed as % (n ≥ 4). Grey portions indicate phosphorylated proportions and white boxes indicate unphosphorylated proportions. F. Western blot analysis of the 5' leader reporter in different mutants. The reporter protein, NLS, was detected using an α-MYC antibody. Tub2 was used as a reference and the Ponceau staining was utilised to control protein levels. G. Quantification of the signals from F. Mean values of two technical replicates normalized to Tub2. Individual values are indicated by dots (n ≥ 4) and SD is indicated by bars. Normal distribution was checked using the Shapiro-Wilk test, and statistics were tested with one-way ANOVA (all comparisons ns: p ≥ 0.05, not depicted).

Another well-characterised pathway that regulates gene expression in response to glucose availability is the AMP-kinase (AMPK) pathway (Carlson 1999; Broach 2012). In *S. cerevisiae*, *SNF1* encodes an AMP kinase. Under glucose conditions, Snf1 is inactivated by the phosphatase Reg1-Glc7 (Gancedo 1998; Broach 2012). Unphosphorylated Snf1 cannot enter the nucleus. Additionally, Reg1-Glc7 dephosphorylates Mig1 which is imported into the nucleus where it represses glucose-repressed genes. By this mechanism, the stress response is blocked, and the transcription of genes is inhibited (Figure 4.16 A). When glucose levels are exhausted, Reg1-Glc7 becomes inactive. The phosphorylation of Snf1, that is now present, allows Snf1 to be imported to the nucleus. Together with the cofactor Gal83, Snf1 is activated and targets various proteins for phosphorylation. One target is Mig1, which is exported from the nucleus in its phosphorylated form and is thereby inhibited. This in turn derepresses the glucose-repressed genes which are necessary for the stress response (Figure 4.16 A). Snf1 might also have different targets including Kns1, which could be either activated directly by Snf1 or could be a glucose repressed gene activated by removing the repressor Mig1. Activation of Snf1 under glucose conditions might simulate non-glucose conditions, and Kns1 expression should consequently be increased.

Different AMPK mutants were used to study the relationship between this pathway and Kns1 expression and activity. The mutants included *Δ326*, as a comparative value; *Δsnf1*, a deletion of the kinase; *Δreg1*, a deletion of the phosphatase; and the double mutants *Δsnf1 Δreg1* and *Δsnf1 Δ326*. Kns1 expression was investigated in these mutants and showed high protein levels in *Δreg1*, even stronger than those in *Δ326* (Figure 4.16 B). The increase in *Δreg1*, which activates Snf1 under glucose conditions, was significant compared to the WT levels (Figure 4.16 C). All the other mutants showed WT-like Kns1 expression. A different situation was observed for Rpc53 phosphorylation levels. *Δsnf1*, *Δsnf1 Δreg1*, *Δ326* and *Δsnf1 Δ326* showed a slight increase in phosphorylation compared to WT. Rpc53 phosphorylation in *Δreg1* background was enhanced even more than in the other mutants (Figure 4.16 D). The proportion of phosphorylated protein shifted from 30 % in WT to approximately 50 % in *Δsnf1* and *Δsnf1 Δreg1*, and to 60 – 70 % in *Δreg1*, *Δ326*, and *Δsnf1 Δ326*, as depicted in Figure 4.16 E. This indicates that only slight changes in the Kns1 protein level may lead to stronger phosphorylation of Rpc53 when a certain threshold is reached. Furthermore, this experiment strongly suggested that Snf1 is involved in the regulation

of Kns1, either by direct phosphorylation or indirectly by activating glucose-repressed genes, as the activity of Snf1 under glucose conditions leads to a significant increase in Kns1 expression and activity.

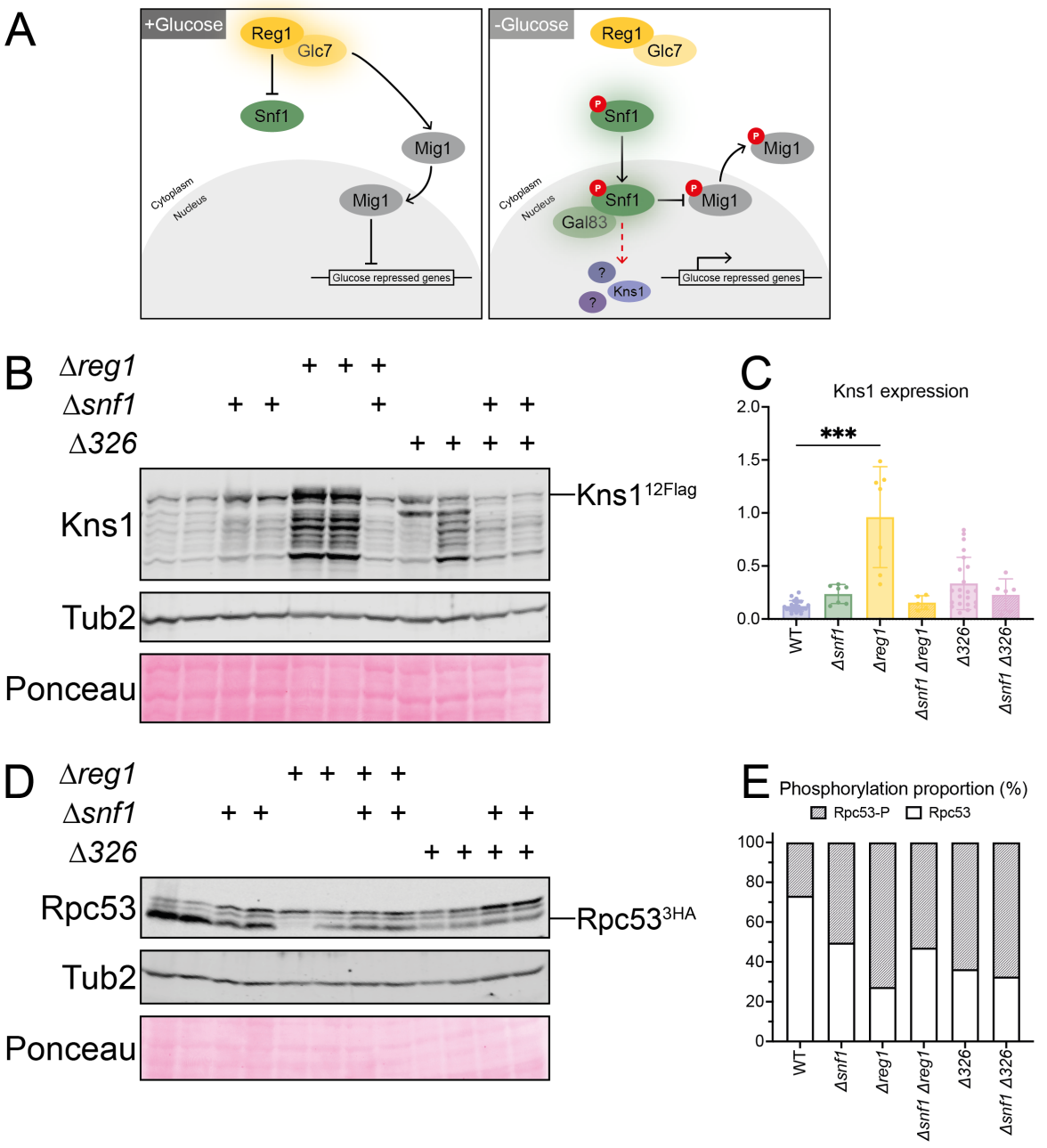

Figure 4.16 Increased Kns1 expression and activity in AMPK mutants.

A. Schematic overview of AMPK pathway under glucose conditions and glucose starvation. Reg1-Glc7 dephosphorylates Snf1, thereby inactivating it under glucose conditions. Glc7 also acts as an activator of Mig1, which is imported into the nucleus and thereby blocks glucose-repressed genes. Under starvation conditions, Reg1-Glc7 is inactive, phosphorylated Snf1 is imported to the nucleus, and further activated by Gal83. Nuclear Mig1 is phosphorylated by Snf1 and exported to the cytoplasm. Thus, glucose-repressed genes were activated. Kns1 is a potential target of Snf1. Bars show inhibitory regulation and arrows indicate activating connections. Red circles are phosphorylation. B. Western blot analysis of endogenous Kns1 in AMPK mutants. Kns1-12xFlag was detected with an α-Flag antibody. Tub2 was used as a

reference and a comparable protein loading was controlled via Ponceau staining. Loading was carried out in two biological replicates of each strain background. The genotypes are indicated by +. C. Quantification of western blot signal intensities from B. Kns1 expression was normalised to Tub2 levels; individual values are indicated by dots ($n \geq 6$), and standard deviation (SD) is given by bars. Normal distribution was tested with Shapiro-Wilk and statistics were calculated with Kruskal-Wallis test (ns: $p \geq 0.05$, not depicted; ***: $p = 0.0001 - 0.001$). D. Western blot analysis of Rpc53 (phosphorylation) levels in different AMPK mutants. Rpc53-3HA was detected with an α-HA antibody. Slower migrating bands represent phosphorylated isoforms of Rpc53. Tub2 was used as a reference and Ponceau staining controlled equal protein loading. Two biological replicates were loaded for each strain background. Genotypes are indicated with +. E. Phosphorylated and unphosphorylated signals from D were calculated in proportion to total Rpc53 levels. The mean relative proportion of $n \geq 4$ is given in %. Grey portions indicate phosphorylated proportions and white boxes indicate unphosphorylated proportions.

4.3 TORC1-mediated regulation of Kns1 expression and activity

The target of rapamycin complex 1 (TORC1) is known to be a major controller of cell growth and proliferation and integrates a variety of signals, including nutrient availability (Broach 2012; Dobrenel et al. 2016; González and Hall 2017). TORC1, consisting of TOR1 or TOR2, Kog1, Tco89, and Lst8, promotes anabolic processes, such as protein synthesis, and represses catabolic processes, such as autophagy (Loewith and Hall 2011; González and Hall 2017). Overall, it stimulates cell growth by phosphorylating several proteins that regulate metabolic pathways (Loewith and Hall 2011; Hughes Hallett et al. 2014). One downstream target of TORC1 is the rather unknown LAMMER family kinase Kns1, that is known to phosphorylate Rpc53 and thereby contributes to the inactivation of RNA Pol III (Lee et al. 2012). As this study has already shown a potentially important role of Kns1 under unfavourable and translational stress conditions, it was crucial to elucidate the contribution of TORC1 on the upregulation of Kns1 expression and activity.

4.3.1 Upregulation of Kns1 expression and activity upon TORC1 downregulation

TORC1 activity can effectively be inhibited with the antibiotic rapamycin. Rapamycin was first found in a soil sample containing *Streptomyces hygroscopicus* and was later used as an antifungal agent (Loewith and Hall 2011; Dobrenel *et al.* 2016). In *S. cerevisiae*, rapamycin exposure leads to a nutrient starvation phenotype including translational inhibition, increase in autophagy and upregulation of pathways to utilise unfavourable nutrient sources, which are all processes that are mediated by the central controller of cell growth, TORC1. As Kns1 is negatively regulated by TORC1 (Lee *et al.* 2012), an artificial inhibition of TORC1 by rapamycin should lead to increased Kns1 protein levels and activity. Furthermore, elucidating the connection between reduced translation initiation and TORC1 activity may shed light on the regulatory mechanism of Kns1. If a global decrease in translation blocks TORC1 activity, Kns1 expression may not change further when TORC1 is inhibited by rapamycin.

The first link between TORC1 activity and Kns1 protein levels was established in different backgrounds. Rapamycin was used to block TORC1 activity. The experiment included a reference time point of 0, and 30 min time intervals after the treatment for two hours, as described in Figure 4.17 A. A comparison between the WT and *Δ326* was performed. First, Kns1 protein levels were analysed in WT and *Δ326* cells and showed a gradual increase over the measured two hours (Figure 4.17 B). As expected, the time point 0 of *Δ326* showed a higher signal than that of the WT. Quantification of the intensity values showed that WT and *Δ326* reached a similar maximum expression after 2 h of rapamycin treatment, although the initial level of *Δ326* was higher (Figure 4.17 C). These data suggest that Kns1 expression is indeed increased when TORC1 is inhibited and that a global translational reduction might not be sufficient to completely block TORC1 activity. Figure 4.17 D shows that inhibition of TORC1 also led to an increase in Rpc53 phosphorylation in both the WT and *Δ326*. 60 min after treatment, both backgrounds showed strong phosphorylation levels on western blotting. The proportion of phosphorylation quickly increased 30 min after treatment to 50 % in WT (from 30 % before treatment) and 70 % in *Δ326* (from 50 % at 0 min) and reached a maximum of approximately 80 % phosphorylation after 60 min in both backgrounds (Figure 4.17 E). This indicated that the maximum phosphorylation level of Rpc53 was reached independently of the proportion at the start. Although Kns1 expression and activity were drastically increased after TORC1 inhibition, a correlation between this effect and Kns1 promoter activity could not be verified (Figure S 6). Blocking TORC1 with rapamycin influences both WT and *Δ326* cells and leads to a stronger increase in Kns1 expression and activity. The effect of TORC1 inhibition on cell proliferation was also investigated. DNA content was detected by flow cytometry in WT and *Δ326* cells before and after rapamycin treatment (60 min). Both WT and *Δ326* showed increased 1C content after rapamycin treatment, indicating a shift towards G_1 phase, as depicted in Figure 4.17 F. WT cells showed 13 % 1C DNA content (indicating cells in G_1 phase), which increased to 52 % after rapamycin treatment (Figure 4.17 G). The *Δ326* mutant already showed an increased 1C DNA content in the flow cytometry, as expected (40 % 1C content), which was even more elevated to 60 % after inhibiting TORC1 (Figure 4.17 G). Hence, blocking TORC1 activity leads to a decreased G_1/S transition rate and reduced cell proliferation, as can be expected from the central controller of cell growth.

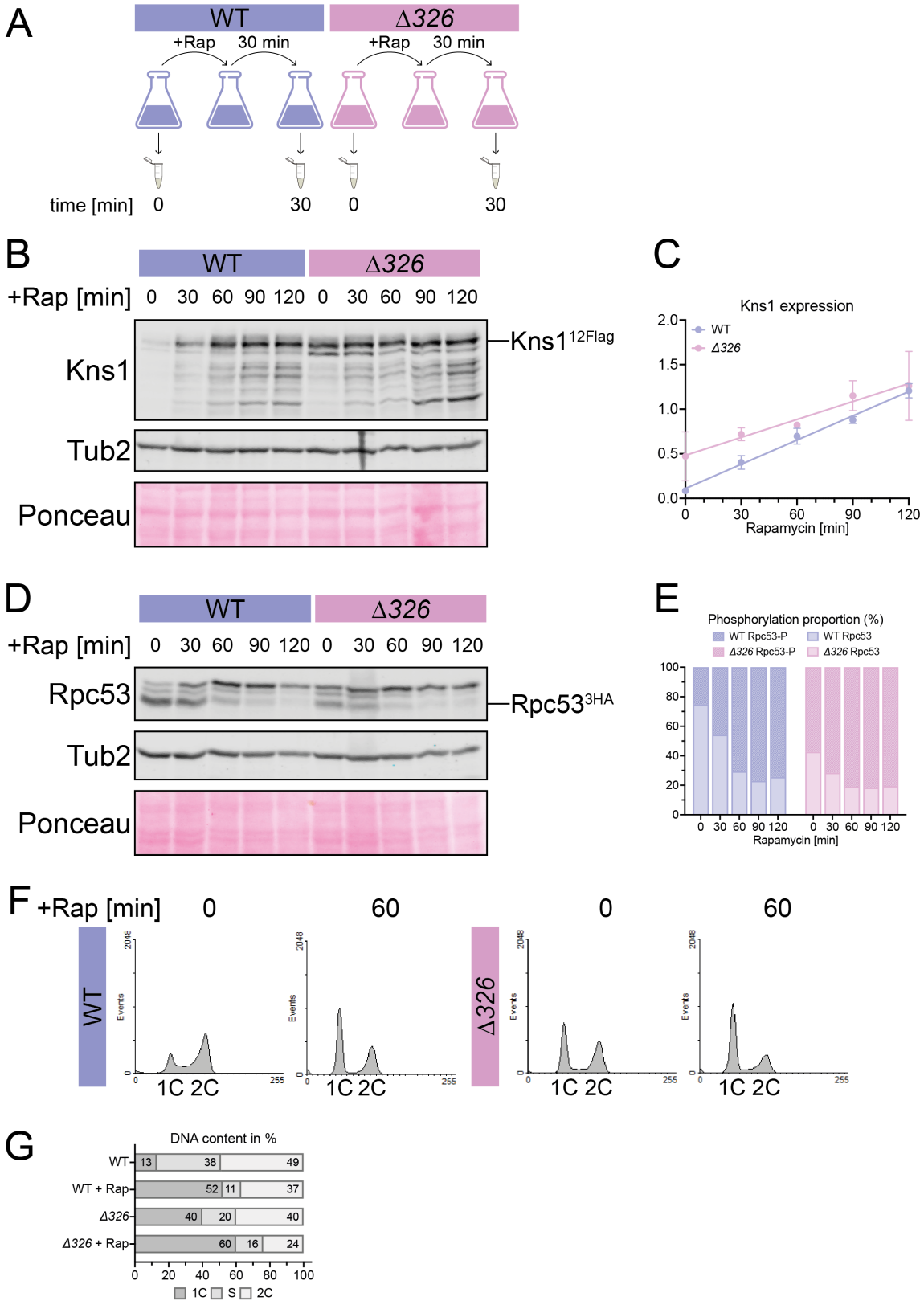

Figure 4.17 Increased Kns1 expression and activity upon downregulation of TORC1.

A. Experimental procedure for rapamycin inhibition. Exponentially growing cells served as the time point of 0. Rapamycin was added and the mixture was incubated for 30 min. Samples were collected every 30 min. B. Western blot analysis of endogenous Kns1 protein levels in WT and *Δ326* in rapamycin treatment for two hours in total. Kns1-12xFlag was detected using an α-Flag antibody. Tub2 was used as a reference and with the help of Ponceau staining proper

loading was controlled. Sampling intervals are given in min. C. Signal intensities from B were quantified and normalized to Tub2. The mean value (n = 2) is depicted as dots, and the standard deviation (SD) is given with bars. A linear regression line was then fitted to the data. WT is indicated in blue and *Δ326* in pink. D. Western blot analysis of Rpc53 and its phosphorylation in a rapamycin treatment comparing WT and *Δ326*. This treatment was conducted for two hours in total. Slower migrating bands are phosphorylated isoforms of Rpc53. Rpc53-3HA was detected using the α-HA antibody. Tub2 was used as a reference and protein loading was controlled using Ponceau staining. Sample intervals are indicated in min. E. Phosphorylated and unphosphorylated signals from D were calculated in proportion to total Rpc53 levels. The mean relative proportion is expressed as a percentage. Grey portions indicate phosphorylated proportions and white boxes indicate unphosphorylated proportions. F. Flow cytometric analysis of WT and *Δ326* cells with and without rapamycin treatment. Rapamycin treatment was performed for 60 min. Profiles of WT (blue) and *Δ326* (pink) cells are shown, including single DNA content (1C) referring to G_1 phase and double DNA content (2C) referring to G_2/M phase. G. DNA content of the flow cytometric analysis in F was evaluated in FCS Express 6 and is depicted in %. The DNA content was assigned to different cell cycle phases. 1C DNA content (dark grey) and 2C DNA content (white) were calculated. DNA content that could not be clearly assigned to either portion was annotated as S-phase cells (light grey).

4.3.2 TORC1-dependent regulation of Kns1 under different carbon sources

TORC1 is regulated by several nutrient inputs (Broach 2012; Dobrenel *et al.* 2016; González and Hall 2017). Changes in nutrient availability led to a reduction in TORC1 activity and, therefore, upregulation of pathways important for yielding energy from non-glucose carbon sources. Kns1 expression showed a significant upregulation under non-fermentable carbon source conditions (section 4.2.2). A possible involvement of TORC1 in the increase in Kns1 expression and activity under nutrient-starved conditions is likely.

To further investigate the influence of nutrients on the regulation of Kns1 via TORC1, rapamycin treatment was performed using different carbon sources. The treatment was conducted for 1 h, as a longer treatment did not drastically change the effect, as described in section 0. A sample harvested before treatment was used as a reference. The three conditions were glucose (D), raffinose (Raf), and glycerol (Gly) (Figure 4.18 A). Kns1 expression levels before treatment were significantly increased by approximately 5-fold in Raf and Gly compared to glucose, as expected from the previous results (Figure 4.18 B, C). Protein levels were slightly enhanced after rapamycin treatment compared to non-treated cells in glucose, but remained constant in raffinose and glycerol (Figure 4.18 B, C). Correspondingly, the phosphorylation of Rpc53 increased to 70 % in treated cells in glucose compared to 30 % in untreated cultures (Figure 4.18 D, E). The shift towards phosphorylated proportion was even stronger in raffinose and glycerol before treatment than in glucose. Here, phosphorylation levels increased to over 90 %, as depicted in Figure 4.18 E. However, a TORC1 block in raffinose and glycerol did not lead to further increases in this proportion. Overall, these data suggest that altered carbon sources influence TORC1 activity and, therefore, mediate Kns1 expression and activity. TORC1 is most likely

already inhibited by non-glucose carbon sources and therefore unable to activate the pathways necessary for the utilisation of non-fermentable nutrients.

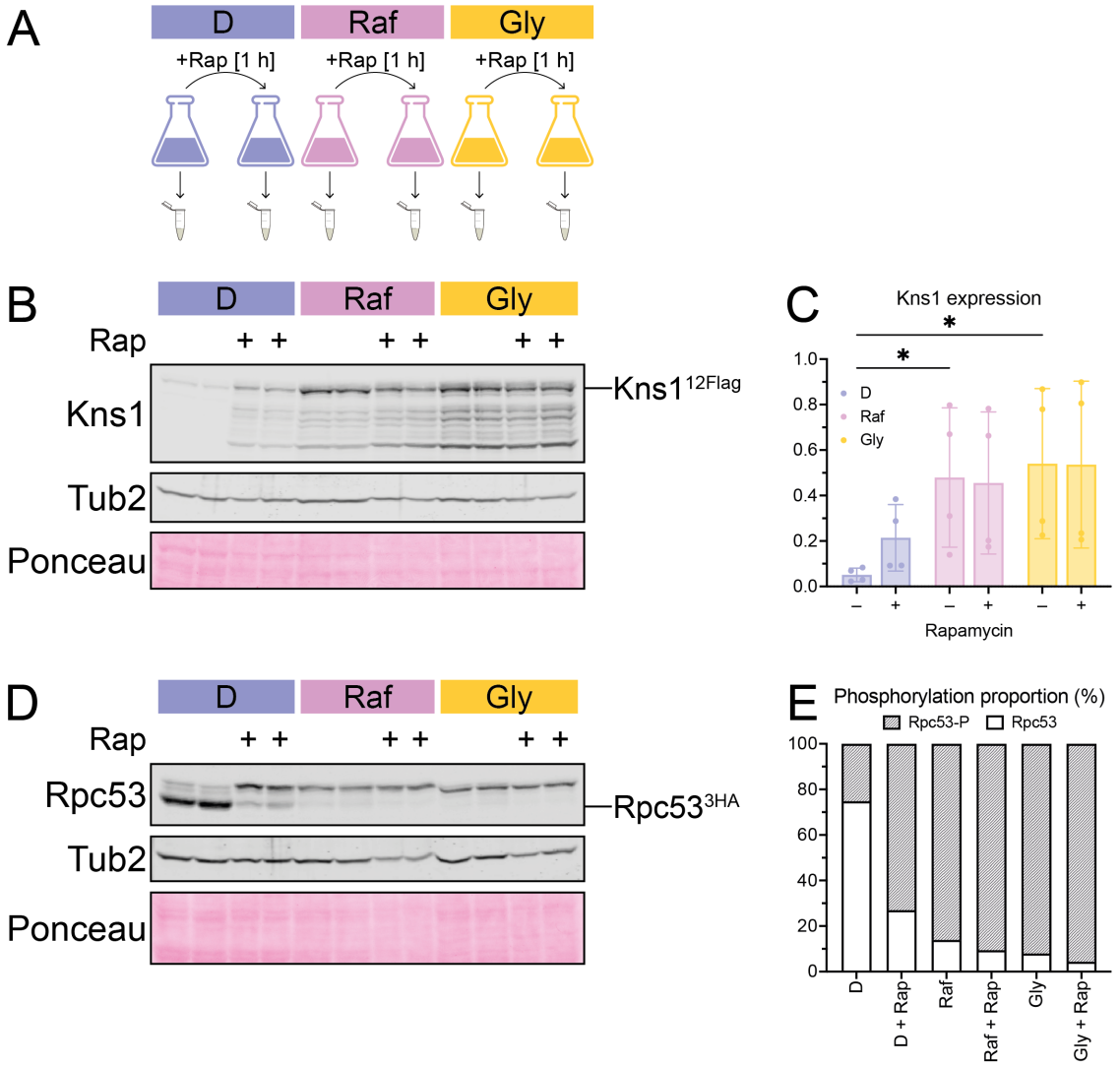

Figure 4.18 Carbon source response affects Kns1 expression and activity under TORC1 downregulation.

A. Used carbon sources for this experiment were glucose (D), raffinose (Raf) and glycerol (Gly). Rapamycin (Rap) was added to each growing culture for 1 h before sampling. B. Western blot analysis of endogenous levels of Kns1 in different carbon sources with (indicated by +) and without TORC1 block via rapamycin. Biological duplicates of Kns1-12xFlag were detected using an α-Flag antibody. Tub2 was used as a reference and with the help of Ponceau staining proper loading was controlled. C. Signal intensities from B were quantified and normalized to Tub2. Single values (n = 4) are depicted as dots and standard deviation (SD) is given with bars. Normal distribution was tested with Shapiro-Wilk and statistics were calculated with a two-way ANOVA (ns: $p \geq 0.05$, not depicted; *: $p = 0.01 - 0.05$). D. Western blot analysis of Rpc53 expression and phosphorylation levels in different carbon sources during rapamycin treatment. TORC1 block via rapamycin was conducted for 1 h (indicated by +). Slower migrating bands are phosphorylated isoforms of Rpc53. Rcp53-3HA was detected with an α-HA antibody. Tub2 was used as a reference and with Ponceau staining proper loading was controlled. E. Phosphorylated and unphosphorylated signals from D were calculated in proportion to total Rpc53 levels. The mean relative proportion is given in % (n = 4). Grey portions indicate phosphorylated proportions and white boxes indicate unphosphorylated values.

These results were confirmed using the TORC1 mutant instead of rapamycin treatment. The gene encoding the non-essential kinase subunit TOR1 was deleted (*Δtor1*), reducing the overall activity of TORC1, and the mutant was investigated in different carbon sources compared to the WT background (Figure 4.19 A). As expected, a significant increase in Kns1 expression was detected under raffinose and glycerol conditions compared to that in the WT background (Figure 4.19 B, C). The *Δtor1* mutant showed only a tendency towards Kns1 increase in glucose and glycerol compared to the WT under the same conditions (Figure 4.19 C). However, Kns1 levels in raffinose were similar in both WT and *Δtor1*. These data indicated that Kns1 protein levels are likely independent of Tor1 expression. Analysis of Rpc53 phosphorylation showed increased levels of raffinose (to 80 %) and glycerol (to 90 %) compared to glucose (approximately 30 %) in the WT background (Figure 4.19 D, E). An increase in phosphorylation was also observed in the *Δtor1* background in glucose. Here, the phosphorylated proportion shifted from 30 % in WT to approximately 60 % in *Δtor1* (Figure 4.19 E). The differences in unfavourable conditions between WT and *Δtor1* were minimal. This further suggests a Tor1-independent regulation of Kns1 expression and activity under non-glucose conditions, whereas the activity of Kns1 is Tor1-dependent under favourable conditions when TORC1 regulates major processes.

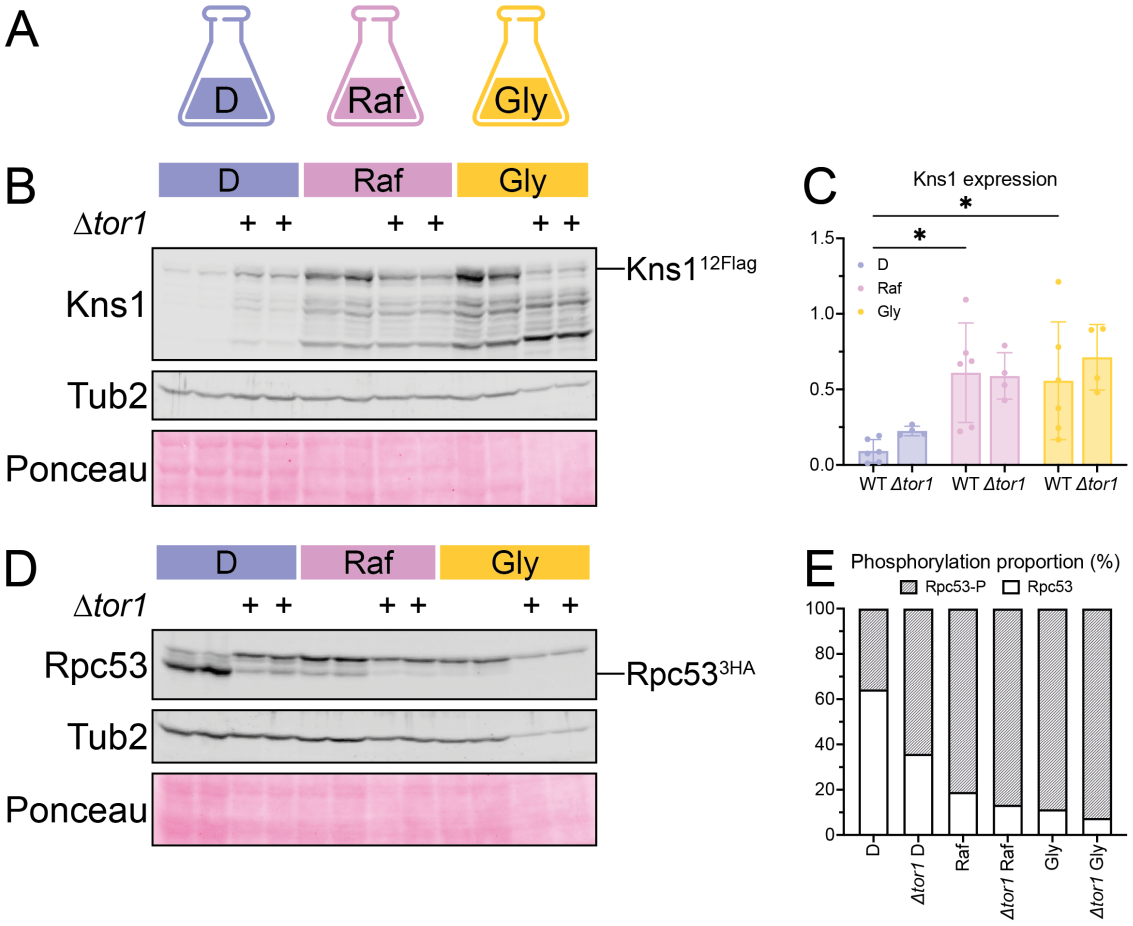

Figure 4.19 Tor1-independent increase of Kns1 expression and Tor1-dependent increase of activity. (Description on next page)

A. Carbon sources used for this experiment were glucose (D), raffinose (Raf) and glycerol (Gly). B. Western blot analysis of endogenous levels of Kns1 comparing WT with *Δtor1* (+) in different carbon sources. Biological duplicates of Kns1-12xFlag were detected using an α-Flag antibody. Tub2 was used as a reference and with the help of Ponceau staining proper loading was controlled. C. Signal intensities from B were quantified and normalized to Tub2. Single values ($n \geq 4$) are depicted as dots and standard deviation (SD) is given with bars. Normal distribution was tested with Shapiro-Wilk and statistics were calculated with a two-way ANOVA (ns: $p \geq 0.05$, not depicted; *: $p = 0.01 - 0.05$). D. Western blot analysis of Rpc53 expression and phosphorylation levels comparing WT and *Δtor1* (+) in different carbon sources. Slower migrating bands are phosphorylated isoforms of Rpc53. Rcp53-3HA was detected with an α-HA antibody. Tub2 was used as a reference and with Ponceau staining proper loading was controlled. E. Phosphorylated and unphosphorylated signals from D were calculated in proportion to total Rpc53 levels. The mean relative proportion of $n \geq 4$ is given in %. Grey portions indicate phosphorylated proportions and white boxes indicate unphosphorylated proportions.

4.4 Mechanisms of Kns1 expression

Proteins are the most abundant macromolecules in various cell types. A substantial portion of these cells (over 20 %) is dedicated to producing ribosomes and translation factors, which in turn facilitate further protein synthesis (Polymenis and Aramayo 2015). *S. cerevisiae* synthesises approximately 13,000 proteins per second (Dever *et al.* 2016). Protein synthesis itself consists of multiple processes that are tightly regulated: transcription, mRNA transport and stability, translation, and post-translational modifications which lead to an increase in protein production. In contrast to protein synthesis, protein destruction also occurs (Belle *et al.* 2006). All these processes contribute to the heterogeneity of protein abundance within cells, and an increase in protein levels may have multiple reasons. Having analysed various conditions with increased Kns1 expression in this study, the question of how these regulations arise remains. The RNA sequencing data from Wojciech (2020) clearly showed an increase in mRNA levels under stress conditions which could indicate differentiated transcription of *KNS1*. Therefore, transcriptional regulation was evaluated in this study.

4.4.1 Increased *KNS1* transcription

A possible mechanism for differentially expressed genes under varying conditions is the use of multiple transcription start sites (TSS). As described by Rojas-Duran and Gilbert (2012) four 5' ends of the *KNS1* transcript were detected at positions -86 bp, -94 bp, -240 bp and -276 bp (Figure 4.20 A). Additionally, Nagalakshmi *et al.* (2008) reported that *KNS1* has a long 5' region of 457 bp and has the potential for upstream open reading frames (uORFs). Both hint towards the synthesis of different transcripts depending on the conditions.

To analyse potential transcript lengths, transcription start site mapping using primer extension was used. The complete 5' region was evaluated at different positions (schematic overview, Figure 4.20 A), including a control within the *KNS1* ORF (+3 bp). The reverse-transcribed cDNA (from position +1950 bp) and a control without reverse

transcriptase (-RT) were analysed using different primers. The resulting PCR products are depicted in Figure 4.20 B. Four different conditions were tested in total: glucose (D), raffinose (Raf), glycerol (Gly), and diauxic cells (diaux), as these four conditions showed significant increases in Kns1 protein levels in sections 4.2.1 and 4.2.2. All approaches yielded PCR products at all sites. In particular, +3 bp, -86 bp, -276 bp, -400 bp, and -500 bp showed strong bands, whereas -749 bp showed a lower intensity. As bands were obtained for all positions tested, no clear limitation to the transcription start site could be concluded. Furthermore, all conditions showed similar results, indicating the same TSS for *KNS1* independent of the nutrient background. Additionally, different transcription rates can influence the protein levels under different conditions. Therefore, mRNA levels under glucose (D), raffinose (Raf), glycerol (Gly), and diauxic conditions (diaux) were tested using qPCR. The $\Delta\Delta C_T$ values of *KNS1* mRNA levels normalised to *CDC10* levels were calculated from eight independent replicates (Figure 4.20 C). The mRNA levels were not significantly different among the tested conditions. The log2 fold changes (log_2 FC, Figure 4.20 D) of the qPCR data showed a slight increase of approximately 2-fold in glycerol and diauxic cells compared to glucose conditions. This minimal difference, however, does not display the strong protein changes of Kns1 under non-glucose conditions, as explained in section 4.2.2.

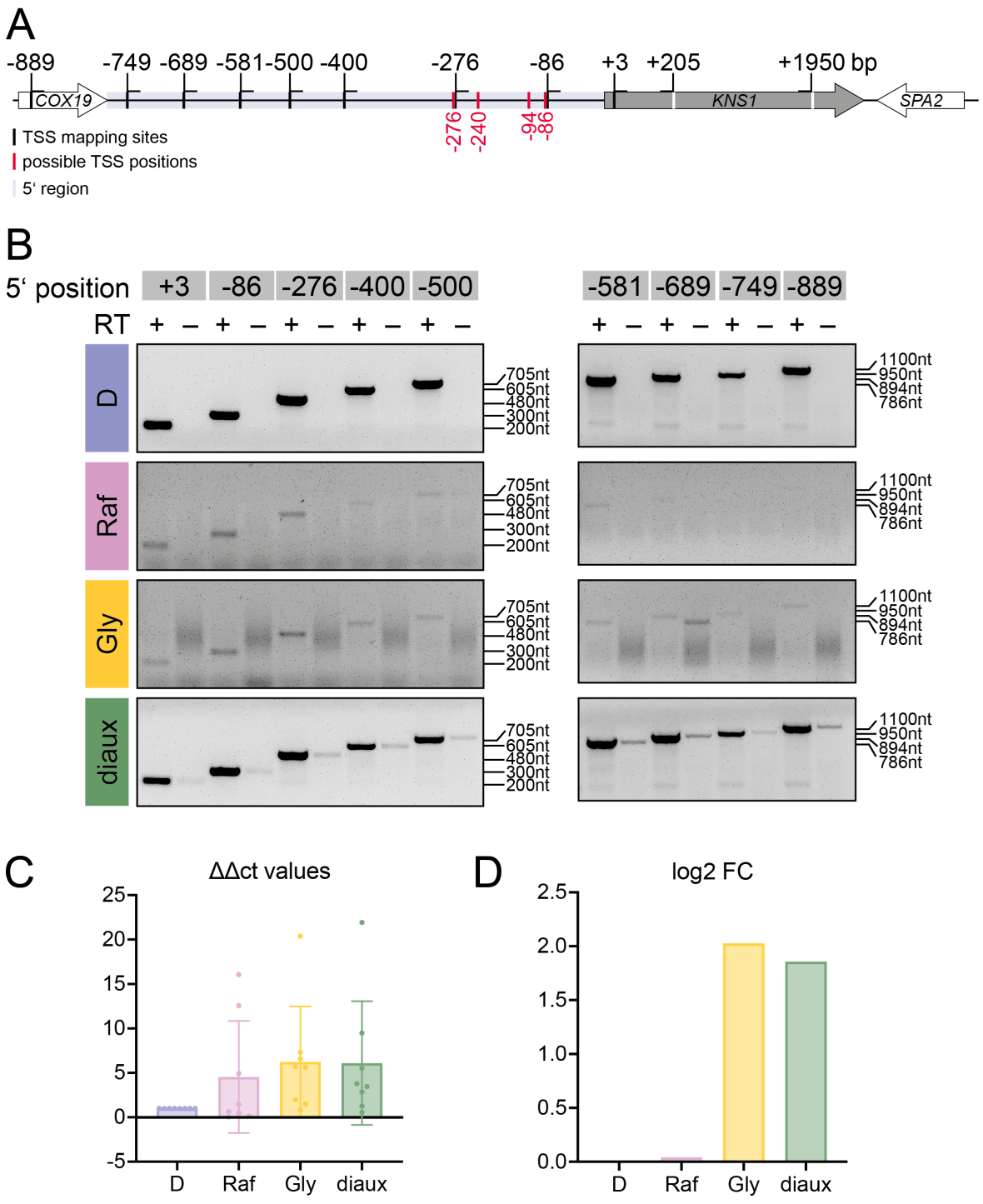

Figure 4.20 Increased transcription levels in unfavourable conditions.

A. All positions used for transcription start site (TSS) mapping of *KNS1*. The scheme shows *COX19*, the upstream ORF next to *KNS1*, the complete 5' region of *KNS1* highlighted in blue, *KNS1* ORF in grey and *SPA2*, the downstream ORF of *KNS1*. Reverse transcription started from +1950 bp in *KNS1*. The primer extension PCR used the position +205 bp as reverse primer and different forward primers of the same length as mapping sites. All mapping sites (black bars) are given with their respective position. In red possible TSS positions are shown (Rojas-Duran and Gilbert 2012). B. Transcription start site mapping of *KNS1* in glucose (D), raffinose (Raf), glycerol (Gly) and diauxic (diaux) conditions. A control for DNA contamination was conducted for every TSS position using an input with no reverse transcriptase (RT). RT inputs are depicted with + (TSS mapping) or - (control). TSS mapping sites (5' position) are given in grey

boxes. C. *KNS1* mRNA levels analysed by qPCR in different conditions (D: glucose, Raf: raffinose, Gly: glycerol, diaux: diauxic cells). Eight independent replicates were used for qPCR. The *KNS1* C_T values were normalized to *CDC10*. Glucose conditions were used as reference for the calculation of $\Delta\Delta C_T$ values. All eight single values are depicted as dots and SD is given with bars. D. Mean log2 fold changes (FC) calculated from the eight individual $\Delta\Delta C_T$ values from C. An increase of mRNA levels in comparison to glucose conditions indicated by the fold changes in different conditions.

4.4.2 Transcriptional regulation of *KNS1* via transcription factors

As data from section 4.4.1 suggested that partial regulation of Kns1 occurs at the transcriptional level, the analysis of the involvement of transcription factors was of interest. A list of 39 potential transcription factor-binding sites for *KNS1* was obtained from the YeasTRACT database (Monteiro *et al.* 2020; Teixeira *et al.* 2023). Of these sites, two promising candidates, Cat8 and Ume6, which are involved in metabolic regulation, were selected for analysis.

Cat8 is a transcription factor that binds to carbon source response elements (CSREs) in the absence of glucose (Hedges *et al.* 1995; Hiesinger *et al.* 2001; Broach 2012; Deng *et al.* 2023). When glucose levels are low, Cat8 is activated by increased transcription and additional phosphorylation by Snf1 (Randez-Gil *et al.* 1997). This activation leads to the binding of CSREs in the promoter region of target genes, which are involved in gluconeogenesis and the glyoxylate cycle. Therefore, Cat8 is essential for the utilisation of non-fermentable carbon sources. In the presence of glucose, Mig1 represses *CAT8* transcription. Given the increased transcription and protein levels of Kns1 under unfavourable conditions (section 4.4.1 and 0), Kns1 could be a potential target gene for derepression by Cat8 under non-fermentable carbon sources.

A deletion of *CAT8* (*Δcat8*) was studied to analyse the involvement of Cat8 in the increase in Kns1 expression under non-glucose conditions. Different carbon sources, as depicted in Figure 4.21 A, were used under steady-state conditions. Kns1 protein levels were compared in WT and *Δcat8* cells in a western blot approach. Figure 4.21 B shows a significant increase in Kns1 expression in Raf and Gly compared to glucose. However, deletion of *CAT8* did not change this increase. The significant 7- to 10-fold increase in WT cells in Raf and Gly was similar in *Δcat8* (Figure 4.21 C). It must be noted that the quantification of *Δcat8* in glycerol was incomplete due to technical difficulties. Corresponding Rpc53 phosphorylation levels were investigated (Figure 4.21 D). As expected, western blot analysis showed a high proportion of unphosphorylated Rpc53 in glucose and increased phosphorylation signals in Raf and Gly in the WT background. The *Δcat8* background showed similar values under both glucose and non-glucose conditions (Figure 4.21 D). The levels of Rpc53 phosphorylation in WT and *Δcat8* under glucose conditions were approximately 20 – 30 % and increased to 80 – 90 % in raffinose and glycerol (Figure 4.21 E). This analysis suggests that Cat8 is not involved in the increased Kns1 expression under unfavourable conditions.

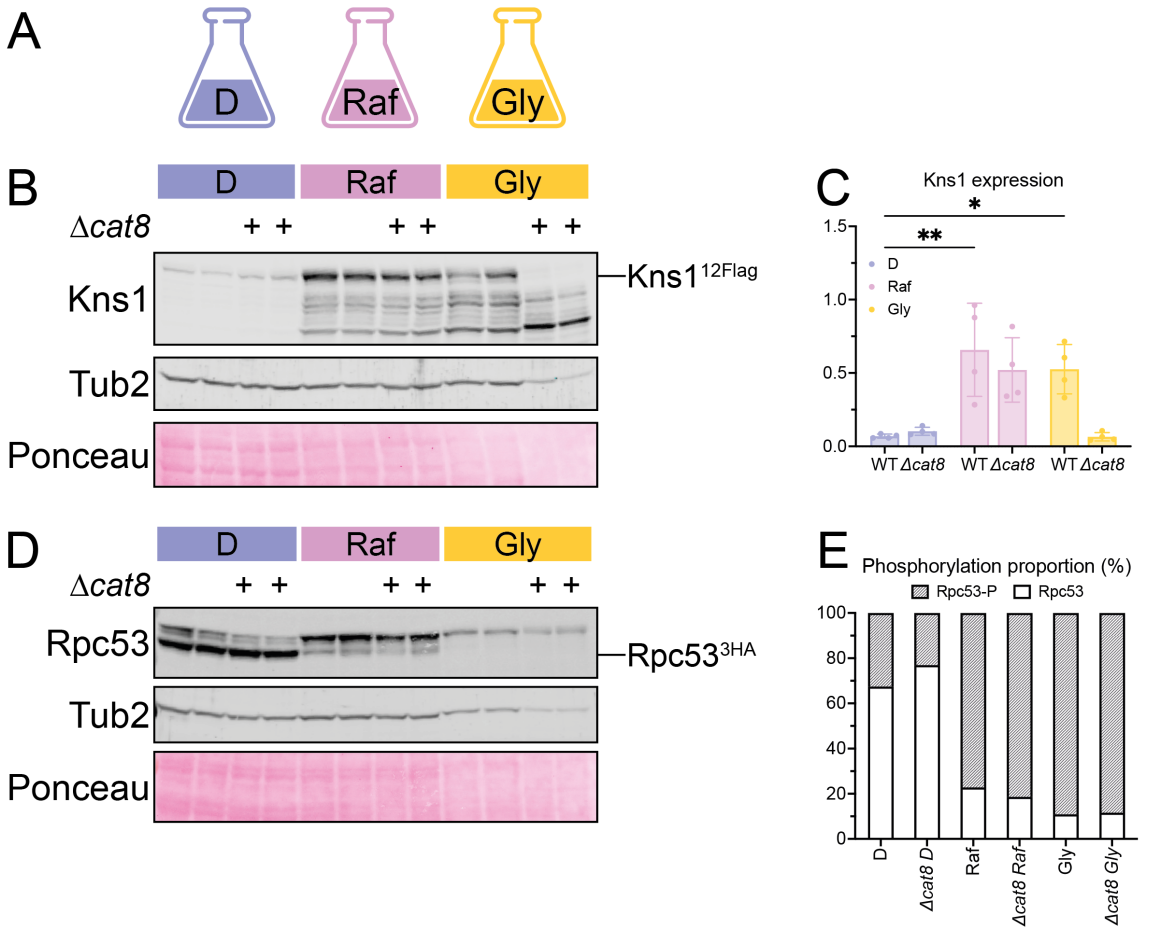

Figure 4.21 Cat8-indepentend increase of Kns1 expression and activity in non-fermentable conditions.

A. Used carbon sources for this experiment were glucose (D), raffinose (Raf) and glycerol (Gly). B. Western blot analysis of endogenous levels of Kns1 in different carbon sources comparing WT and *Δcat8* (+). Biological duplicates were applied and Kns1-12xFlag was detected using an α-Flag antibody. Tub2 was used as a reference and with the help of Ponceau staining proper loading was controlled. C. Signal intensities from B were quantified and normalized to Tub2. Single values (n = 4) are depicted as dots and SD is given with bars. Normal distribution was tested with Shapiro-Wilk and statistics were calculated with a two-way ANOVA (ns: $p \geq 0.05$, not depicted; *: p = 0.01 - 0.05; **: p = 0.001 - 0.01). D. Western blot analysis of Rpc53 expression and phosphorylation levels in different carbon sources comparing WT and *Δcat8* (+). Slower migrating bands are phosphorylated isoforms of Rpc53. Rcp53-3HA was detected with an α-HA antibody. Tub2 was used as a reference and with Ponceau staining proper loading was controlled. E. Phosphorylated and unphosphorylated signals from D were calculated in proportion to total Rpc53 levels. The mean relative proportion of n = 4 is given as a percentage. Grey portions indicate phosphorylated proportions and white boxes indicate unphosphorylated proportions.

Ume6 plays a crucial role in regulating gene expression, both negatively and positively (Strich *et al.* 1994; Jackson and Lopes 1996). Additionally, it controls carbon and nitrogen metabolism, and aligns metabolic activity with meiosis (Williams *et al.* 2002). Ume6 recruits the Sin3-Rpd3 complex for transcriptional repression (Kadosh and Struhl 1997, 1998). The Rpd3 complex acts as a histone deacetylase, which helps to regulate gene expression by limiting the accessibility for binding of transcription

factors (Kadosh and Struhl 1998; Yang and Seto 2008). Under glucose starvation conditions, Rpd3 is necessary for changes in the histone acetylome and transcriptome (Hsieh *et al.* 2022). It directly represses growth-promoting genes by deacetylation but indirectly promotes the expression of genes related to gluconeogenesis and fat metabolism by releasing acetate. Acetate can be recycled for subsequent histone acetylation by the SAGA complex. Recently, it was demonstrated that TORC1 inhibition leads to inactivation of Rpd3, resulting in the induction of autophagy (Li *et al.* 2023). The potential binding site of Ume6 suggests a regulation of Kns1 expression via Sin3-Rpd3. Ume6 could be responsible for the recruitment of histone deacetylase and, therefore, the repression of *KNS1* transcription under favourable conditions, as well as the induction of *KNS1* transcription by Rpd3 relocation under non-glucose conditions.

To investigate this connection, a yeast strain containing a deletion of *RPD3* (*Δrpd3*) was studied using different carbon sources. The carbon sources used included glucose, raffinose, and glycerol, as shown in Figure 4.22 A. Kns1 protein levels in the WT and *Δrpd3* backgrounds were analysed. Western blotting revealed that Kns1 levels were similar in WT and *Δrpd3* in the presence of glucose (Figure 4.22 B, C). However, Kns1 expression varied between the WT and *Δrpd3* in the presence of raffinose and glycerol. As expected, WT cells showed high levels of Kns1 in the presence of Raf and Gly (Figure 4.22 B). However, in *Δrpd3* background, Kns1 expression was lower, as shown in Figure 4.22 B. WT cells showed an approximately 7-fold increase in Kns1 protein expression under unfavourable conditions compared to glucose (Figure 4.22 C). The expression of Kns1 in Raf and Gly in *Δrpd3* background was decreased compared to WT and hinted towards an involvement of Rpd3 in the increase of Kns1 expression under non-preferred conditions. A slight effect on Kns1 expression was reflected by Rpc53 phosphorylation. As shown in Figure 4.22 D, Rpc53 levels were analysed using western blotting. WT and *Δrpd3* backgrounds were compared for the different carbon sources. Under glucose conditions, both backgrounds showed a high proportion of unphosphorylated Rpc53, as expected (Figure 4.22 D). Similar to other experiments, for example in section 4.2.2, WT cells showed a phosphorylation rate of approximately 30 % in glucose, which increased to 80 – 90 % in raffinose and glycerol (Figure 4.22 E). In *Δrpd3* background, the phosphorylation levels were WT-like in glucose (approx. 30 %, Figure 4.22 E), and the phosphorylation proportion only increased to 60 % in Raf and 80 % in Gly (Figure 4.22 D, E). These data suggest that the strong expression of Kns1 under unfavourable conditions is Rpd3-dependent, and that transcriptional regulation of *KNS1* during metabolic reprogramming might occur. Furthermore, this indicated that at least a smaller portion of the phosphorylation of Rpc53 is independent of Rpd3, and that another kinase might be involved in phosphorylating Rpc53 under non-glucose conditions.

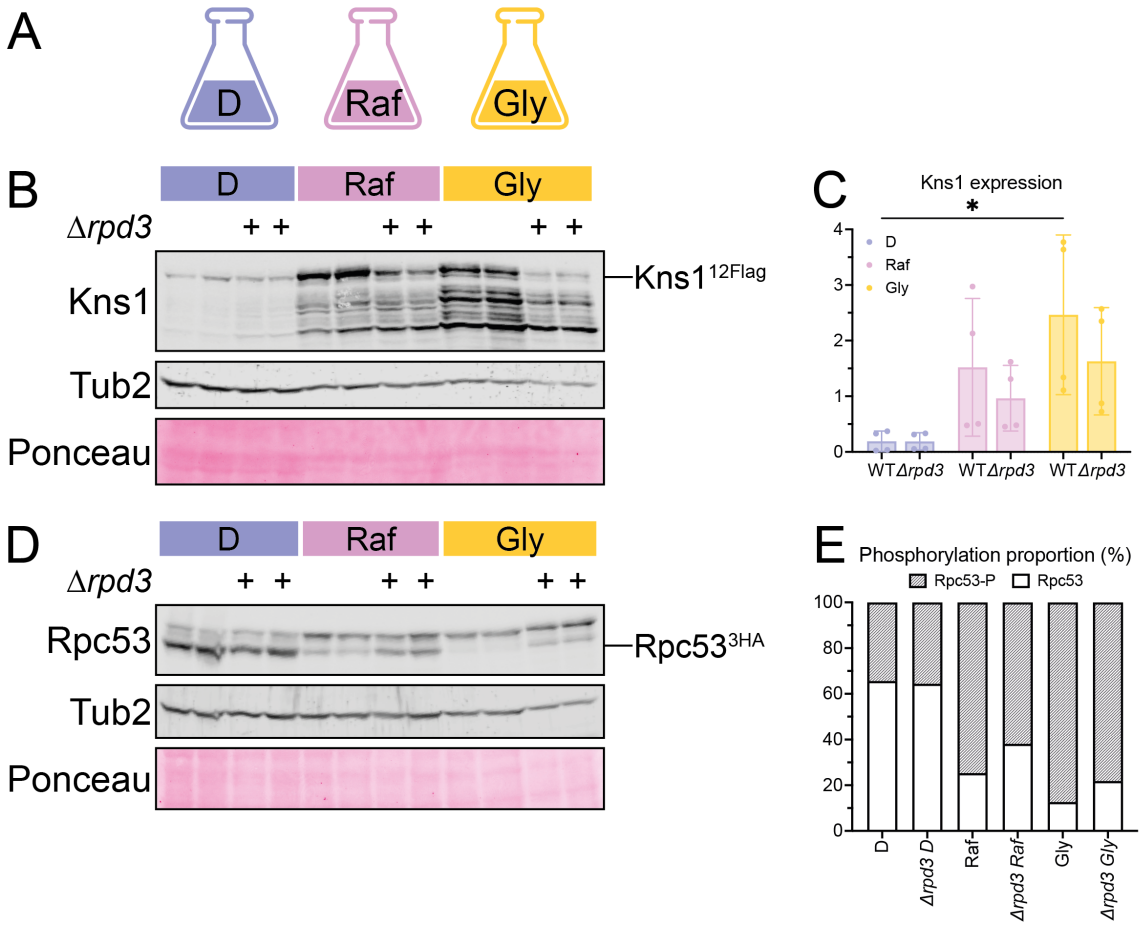

Figure 4.22 Rpd3-dependent increase of Kns1 expression and activity in non-preferred carbon source conditions.

A. Used carbon sources for this experiment were glucose (D), raffinose (Raf) and glycerol (Gly). B. Western blot analysis of endogenous levels of Kns1 in different carbon sources comparing WT and *Δrpd3* (+). Biological duplicates were applied and Kns1-12xFlag was detected using an α-Flag antibody. Tub2 was used as a reference and with the help of Ponceau staining proper loading was controlled. C. Signal intensities from B were quantified and normalized to Tub2. Single values (n = 4) are depicted as dots and SD is given with bars. Normal distribution was tested with Shapiro-Wilk and statistics were calculated with a two-way ANOVA (ns: $p \geq 0.05$, not depicted; *: $p = 0.01 - 0.05$). D. Western blot analysis of Rpc53 expression and phosphorylation levels in different carbon sources comparing WT and *Δrpd3* (+). Slower migrating bands are phosphorylated isoforms of Rpc53. Rcp53-3HA was detected with an α-HA antibody. Tub2 was used as a reference and with Ponceau staining proper loading was controlled. E. Phosphorylated and unphosphorylated signals from D were calculated in proportion to total Rpc53 levels. The mean relative proportion is given in % (n = 4). Grey portions indicate phosphorylated proportions and white boxes indicate unphosphorylated proportions.

4.5 Characterization of Kns1 protein properties

As a rather unexplored kinase, little is known about Kns1 regulation and its properties. To better understand the underlying mechanisms, characterisation of Kns1 function, domains, and protein properties is of great interest and will be highlighted in the following chapter.

4.5.1 Nuclear localisation of Kns1

The precise localisation of proteins within cells is essential for directing them to an appropriate environment in which they can effectively perform their functions (Nightingale *et al.* 2019). Many proteins are dynamically localised and move between subcellular compartments. Others specifically localise to targeted areas within the cell. Furthermore, many proteins are regulated by a variety of signals that determine their localisation. Additionally, post-translational modifications such as phosphorylation may influence protein localisation. However, specific localisation can induce interactions with binding partners, such as other proteins or metabolic substrates, and is therefore highly important for cell survival.

Kns1 is known to phosphorylate Rpc53, a subunit of RNA Pol III, and its function is likely to be conducted within the nucleus. Lee *et al.* (2012) found Kns1 in the cytoplasm and nucleus, indicating the possibility of protein shuttling. Kns1 could be targeted to the nucleus when its kinase function is needed. Specific relocation of Kns1 can be mediated by nuclear localisation sequences, post-translational modifications, or interactions with transporters. However, the properties of Kns1 are unknown; only the C-terminal domain, including the LAMMER motif, was proposed via an alignment by Tang *et al.* (2003). Characterising the different domains of Kns1 is central to unravel the mechanisms behind its localisation. To this end, different fragments of Kns1 were analysed for their localisation under optimal and stress conditions.

A nuclear localisation mapper predicted three different nuclear localisation sequences (NLS) for Kns1 (Kosugi *et al.* 2009). Two potential NLSs are located in the N-terminal domain, 8 – 39 aa and 175 – 185 aa, and one is close to the active site D440 in the C-terminus, 456 – 485 aa. Further predictions with NLStradamus supported amino acid positions 467 – 482 (Nguyen Ba *et al.* 2009). To analyse their function and overall localisation patterns, different Kns1 fragments were used (Figure 4.23). A WT full-length construct (WT), a full-length but kinase dead construct with a mutation at D440A (KD, mutation described by Martinez Marshall (2011)), the N-terminal portion of Kns1 from 1 – 289 aa (NTD), a short fragment of the NTD including the first predicted NLS from 1 – 174 aa (NTD(1-174)), a second short fragment of the NTD including the second predicted NLS from 166 – 289 aa (NTD(166-289)), the catalytic C-terminus with the potential third NLS from 280 – 737 aa (CTD) and an elongated CTD to additionally include a predicted NLS from the NTD, ranging from 166 – 737 aa (CTD(166-737)). All fragments were overexpressed to increase the signal intensity for confocal microscopy. The fragments were fused to GFP to visualize localisation, and all strains contained an NLS-mCherry co-marker to visualize the nucleus. The different

fragments were analysed using confocal microscopy. The detection of the co-marker was stable throughout the experiment, and the laser intensities of the GFP-fused constructs were adapted to their signal intensity. Varying signals from cell to cell indicated the mobility of the protein, even under overexpressed conditions. The overall expression levels and differences between the fragments were checked by western blotting before the analysis (Figure S 7 and Figure S 8).

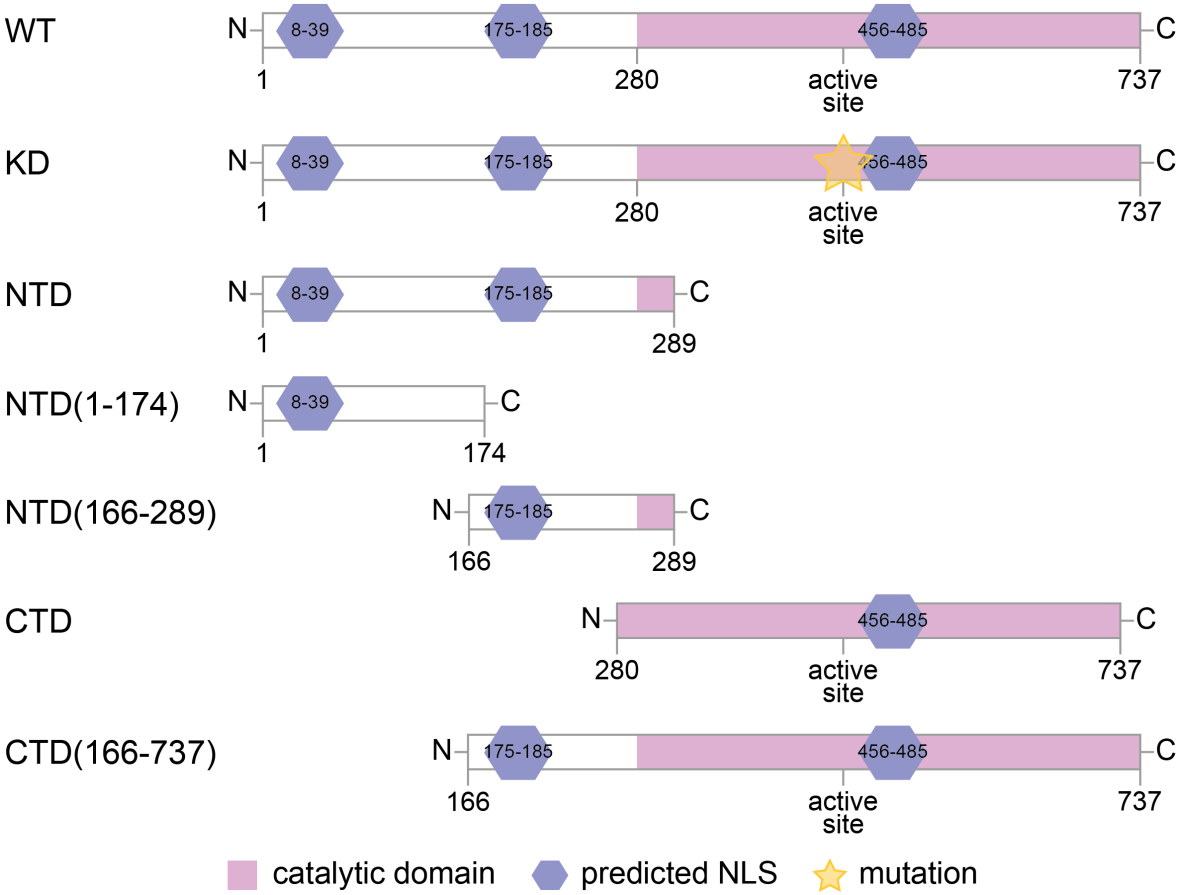

Figure 4.23 Overexpression constructs used in this study.

The protein fragments used for this study included a full-length WT version of Kns1, a kinase dead (KD) version with point-mutated D440A (Martinez Marshall 2011), the long, unstructured N-terminal domain (NTD) from 1 to 289 aa, a short version of the NTD including one predicted NLS from 1 to 174 aa (NTD(1-174)), a second short version of the NTD including a second predicted NLS from 166 to 289 aa (NTD(166-289)), the C-terminal catalytic domain (CTD) including a third predicted NLS from 280 to 737 aa, and a longer version of the CTD including an NLS from the NTD from 166 to 737 aa (CTD(166-737)). Depending on the experiment, the fragments were either overexpressed by the constitutive promoter *pTEF* or by inducible *pGAL*. All three NLSs predicted from the NLS mapper are indicated in blue (Kosugi et al. 2009). Mutations are indicated by a yellow star, and the catalytic domain is highlighted in pink.

The constructs described in Figure 4.23 showed differentiated localisation. Representative single-cell images are shown in Figure 4.24 A. The nuclear enrichment coefficient was calculated for all fragments (Equation 1). The coefficient utilises the concentration of pixels (mean pixels) in an assigned area within the cytoplasm and nucleus. The coefficients of both compartments indicate a portion of the nuclear signal. An enrichment coefficient of ≤ 1 indicated a stronger signal intensity in the cytoplasm, whereas a nuclear enrichment of > 1 suggested a stronger signal in the nucleus compared to the cytoplasmic portion of the protein. Using these coefficients, an evaluation of protein localisation can be made. WT full-length Kns1 was strongly localised in the nucleus with a mean nuclear enrichment of 2.8 (Figure 4.24 B). The catalytically inactive version, KD, was also localised in the nucleus, indicating localisation independent of kinase function (Figure 4.24 A). However, the nuclear enrichment coefficient increased significantly to 4.0 (Figure 4.24 B). The CTD revealed that the predicted NLS close to the active site was not functional, as this construct was solely located in the cytoplasm (nuclear enrichment of 1.2; Figure 4.24 B). The long unstructured N-terminus was of great interest and revealed a function in localisation, as the NTD was mainly located within the nucleus and showed a significant nuclear enrichment of 3.8 (Figure 4.24 A, B). With two predicted NLSs within the NTD, investigation of shortened versions is a promising approach. The NTD(1-174) showed nuclear localisation, but to a lesser extent and not exclusively compared to the NTD (Figure 4.24 A). The nuclear enrichment was significantly decreased to 1.8 compared to NTD (Figure 4.24 B). NTD(166-289) showed similar localisation as the NTD(1-174). It showed mostly nuclear localisation, but lower levels as NTD, and a slight increase in cytoplasmic levels (Figure 4.24 A). The mean nuclear enrichment of 1.9 was similar to NTD(1-174) (Figure 4.24 B). This suggests that each of the predicted NLSs in the NTD is sufficient for nuclear localisation; however, both NLSs are required for the significant nuclear enrichment of Kns1. As a high level of Kns1 in the nucleus most likely has severe effects on cell proliferation and viability by downregulating RNA Pol III transcription, a growth test of these strains was conducted. Growth on glucose medium revealed WT-like growth for all tested fragments (Figure 4.24 C). The overexpression of different fragments did not interfere with growth.

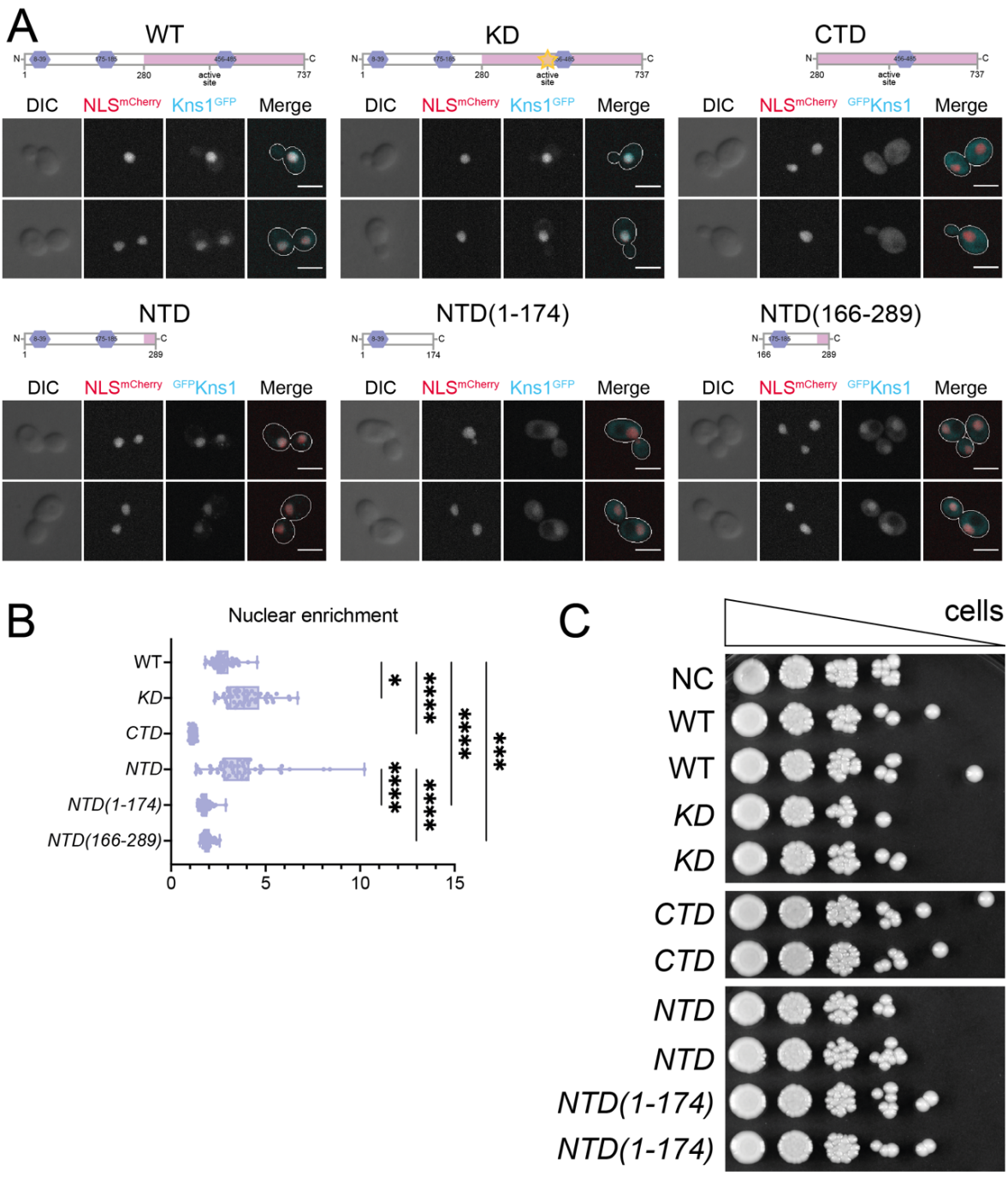

Figure 4.24 Nuclear localisation of Kns1 dependent on N-terminal domain.

A. Six different *pTEF*-overexpression constructs of Kns1 were used. WT: Kns1 overexpressed; KD: Kns1 with mutated active site D440A; CTD: C-terminal domain including 280 – 737 aa; NTD: N-terminal domain including 1 – 289 aa; NTD(1-174): first 174 aa of the NTD; NTD(166-289): second fragment of the NTD including 166 – 289 aa. All overexpression constructs were fused to green fluorescent protein (GFP; cyan). The strains contain NLS-mCherry as a nuclear marker (red). Confocal analysis was performed by visualising 14 slices from each channel. mCherry signals were detected with 5 % laser intensity and 200 ms exposure time. GFP signals were detected using the following laser intensities. WT: 20 %, 200 ms; KD: 20 %, 200 ms; CTD: 5 %, 100 ms; NTD: 3 %, 100 ms; NTD(1-174): 5 %, 100 ms; NTD(166-289): 7 %, 200 ms . The scale bar indicates 5 µm. B. Nuclear enrichment of the signals from A was quantified. The mean pixel density was measured in a 7 × 7 px square located within the cytoplasm and the nucleus in n = 50 cells. The enrichment proportion of the

mean nuclear signal/cytoplasmic signal was calculated for each cell. All single values are depicted as dots. The box indicates the minimum to maximum value and the mean nuclear enrichment is given as a line within the box. Normal distribution was tested with Shapiro-Wilk and statistics were calculated with a Kruskal-Wallis test (*: p = 0.01 - 0.05, ***: p = 0.0001 - 0.001, ****: p < 0.0001). C. Spot test of the strains used from A, including a WT negative control without an additional overexpression construct (NC). XYD plates were incubated at 30 °C for 2 days to visualize growth.

As previous data from this work suggested, Kns1 is activated and elevated in expression under non-glucose conditions (section 4.2.2). Therefore, the localisation patterns were studied in different carbon sources by examining the altered localisation in glucose, raffinose, and glycerol (Figure 4.25 A). The fragments described above were used for confocal analysis, with NLS-mCherry as the co-marker. Representative single cells are displayed with constant detection conditions for glucose (D), raffinose (Raf), and glycerol (Gly) for each respective fragment. The nuclear enrichment was calculated for all fragments and conditions (Equation 1). As described above, coefficients ≤ 1 indicated cytoplasmic localisation, while a value > 1 showed an increase in nuclear signal in relation to the cytoplasmic signal. WT Kns1 showed similar localisation for all three conditions, with slightly decreasing protein levels in glycerol (Figure 4.25 B). The corresponding nuclear enrichment decreased from 2.8 in glucose and 2.9 in raffinose to 2.3 in glycerol (Figure 4.25 C, left panel). Localisation patterns were not different for the kinase dead version in all three carbon source backgrounds (KD, Figure 4.25 B). The strong nuclear enrichment values of 4.0 for glucose, 3.4 for raffinose and 3.6 for glycerol conditions (Figure 4.25 C, middle panel) supported a kinase function-independent nuclear localisation, even under stress conditions. Analysis of the CTD revealed cytoplasmic localisation in all conditions and similar low enrichment coefficients of 1.2 in glucose and raffinose and 1.4 in glycerol (Figure 4.25 B and C, right panel). Additionally, evaluation of the different N-terminal fragments showed an interesting function of the NTD in Kns1 protein localisation. All fragments showed nuclear localisation in all carbon sources (Figure 4.25 D). Interestingly, NTD showed significant increases in the mean nuclear enrichment in raffinose and glycerol compared to glucose. The coefficient rose from 3.8 in glucose to 8.8 in Raf and even 10.8 in Gly (Figure 4.25 E, left panel). Therefore, the NTD plays a crucial role in increasing nuclear Kns1 protein levels under unfavourable conditions. NTD fragment 1-174 including one of the two predicted NLSs, also showed significant differences in nuclear enrichment under altered conditions, but to a minor extent. The mean value of 1.8 (D) and 1.9 (Raf) only rose to 2.2 in glycerol (Figure 4.25 E, middle panel). NTD(166-289) contributed greatly to the carbon source-dependent nuclear localisation of Kns1, as shown by the enrichment values. In glucose, NTD(166-289) showed a mean nuclear enrichment of 1.9, while raffinose conditions significantly increased this value to 2.5 and glycerol to 2.6 (Figure 4.25 E, right panel). In summary, these data suggest that the nuclear localisation of Kns1 depends on the NTD, with both active NLSs being important for proper localisation. Surprisingly, the activity of the second NLS (from amino acids 175 – 185) seemed to be highly important for the carbon

source-dependent localisation of Kns1, which was even stronger in the full NTD fragment. However, this effect was not observed for the full-length protein, indicating that other regulatory mechanisms might be present as well.

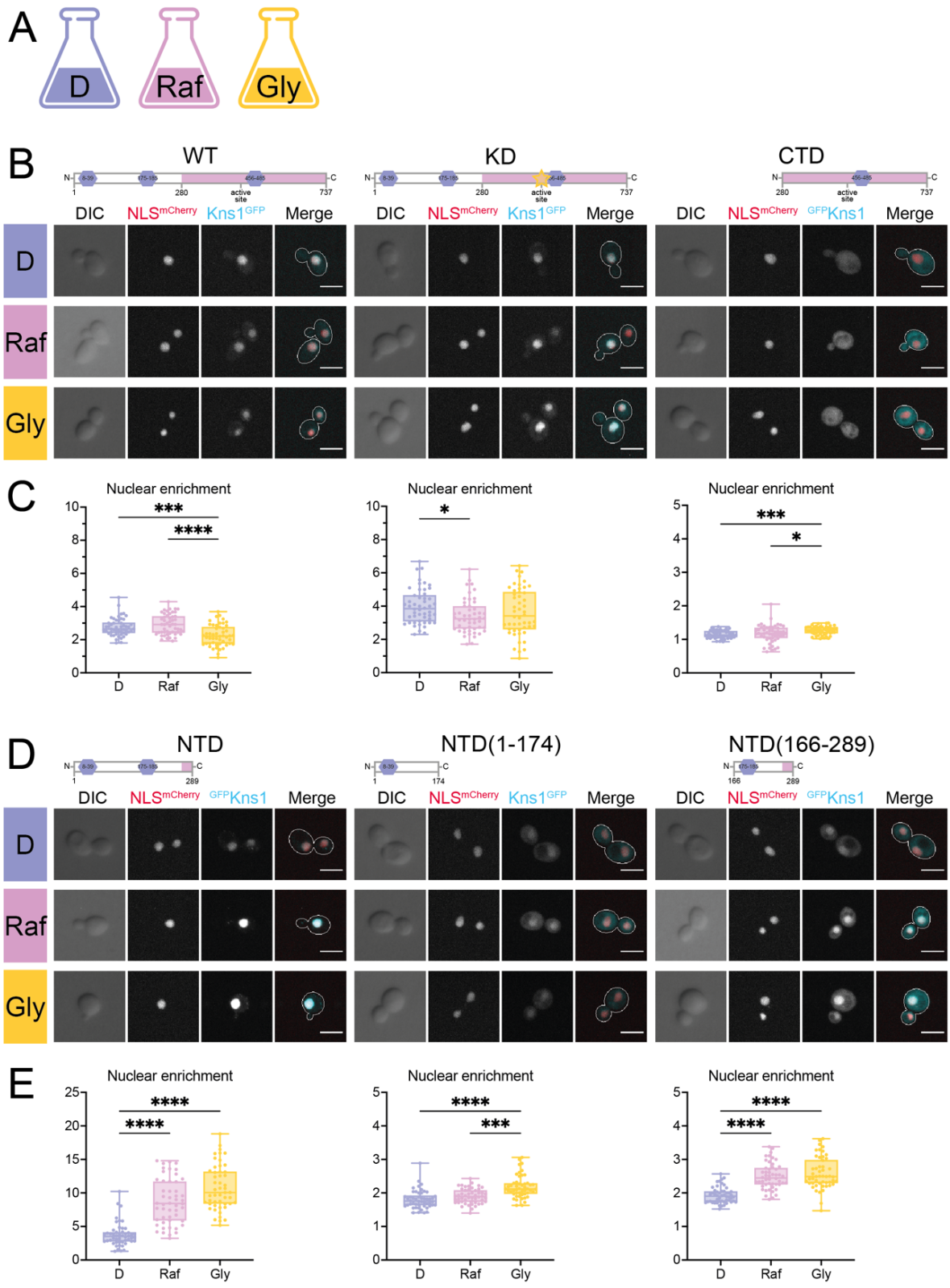

Figure 4.25 Nuclear localisation of Kns1 under different carbon sources.

A. The carbon sources used for confocal microscopy are glucose (D), raffinose (Raf), and glycerol (Gly). B. The same overexpression constructs and microscopy approach from Figure

4.24 A were used. The WT, KD, and CTD constructs were fused to GFP (cyan). The strains contain NLS-mCherry as a nuclear marker (red). mCherry signals were detected with 5 % laser intensity and 200 ms exposure time. The GFP signals varied and were detected with the following laser intensities. WT: 20 %, 200 ms; KD: 20 %, 200 ms; CTD: 5 %, 100 ms. All visualisation conditions were kept constant for the comparison of the carbon sources. The scale bar indicates 5 µm. C. Nuclear signal intensities in relation to cytoplasmic signals were calculated for all fragments from panel B (WT, left panel; KD, middle panel; CTD, right panel). Mean pixel density was measured in a 7 × 7 px square located within the cytoplasm and nucleus (n = 50). The enrichment proportion of mean nuclear signal/mean cytoplasmic signal was calculated for each cell. All single values are depicted as dots. The box indicates the minimum to maximum value and the mean nuclear enrichment is given as a line within the box. Normal distribution was tested with Shapiro-Wilk and statistics were calculated with a Kruskal-Wallis test (*: p = 0.01 - 0.05, ***: p = 0.0001 - 0.001, ****: p < 0.0001). D. Overexpression constructs from Figure 4.24 A (NTD, NTD(1-174), NTD(166-289) were fused to GFP (cyan). The strains contain NLS-mCherry as a nuclear marker (red). mCherry signals were detected with 5 % laser intensity and 200 ms exposure time. The GFP signals varied and were detected with the following laser intensities. NTD: 3 %, 100 ms; NTD(1-174): 5 %, 100 ms; NTD(166-289): 7 %, 200 ms. All visualization conditions were kept constant for the comparison of carbon sources. The scale bar indicates 5 µm. E. Nuclear signal intensities in relation to cytoplasmic signals were calculated for all fragments from D (NTD, left panel; NTD(1-174), middle panel; NTD(166-289), right panel). The mean pixel density was measured in a 7 × 7 px square located within the cytoplasm and the nucleus (n = 50). The enrichment proportion of mean nuclear signal/mean cytoplasmic signal was calculated for each cell. All single values are depicted as dots. The box indicates the minimum to maximum value and the mean nuclear enrichment is given as a line within the box. Normal distribution was tested using the Shapiro-Wilk test, and statistics were calculated using the Kruskal-Wallis test (***: p = 0.0001 - 0.001, ****: p < 0.0001).

To study even stronger levels of Kns1 in an inducible system, WT, KD, CTD, and CTD(166-737) fragments were overexpressed using *pGAL*. A strain background with NLS-mCherry as the co-marker was used. Localisation was analysed by confocal microscopy under varying detection conditions for all fragments to determine different signal intensities. As expected, the full-length fragment (WT) showed nuclear localisation, similar to the KD (Figure 4.26 A). However, nuclear enrichment slightly decreased to 5.2 in the KD compared to 7.7 in the WT (Figure 4.26 B). The CTD showed cytoplasmic localisation, and the coefficient confirmed this with a value of 1.2 (Figure 4.26 A, B). By overexpressing a longer fragment, such as CTD(166-737), the kinase domain could be shuttled into the nucleus (Figure 4.26 A), verifying the necessity of the second NLS in the NTD for nuclear localisation. The nuclear enrichment of 4.1 confirmed a significant increase in specific localisation (Figure 4.26 B). The growth of these strains was analysed in a spot test on RafGal plates (inducing the *GAL* promoter) and Raf conditions as a control (Figure 4.26 C). The analysis revealed that strong expression of a full-length catalytically active construct within the nucleus (WT) leads to severe growth defects. Similar defects were detected for a catalytically active CTD that was shuttled to the nucleus by extending to the NLS at positions 175 – 185 aa (CTD(166-737)). Cytoplasmic CTD or kinase-inactive fragments (KD) showed WT-like growth. This suggested a connection between the nuclear localisation of catalytically active fragments and lethality, which was only visible in strong overexpression under *pGAL*.

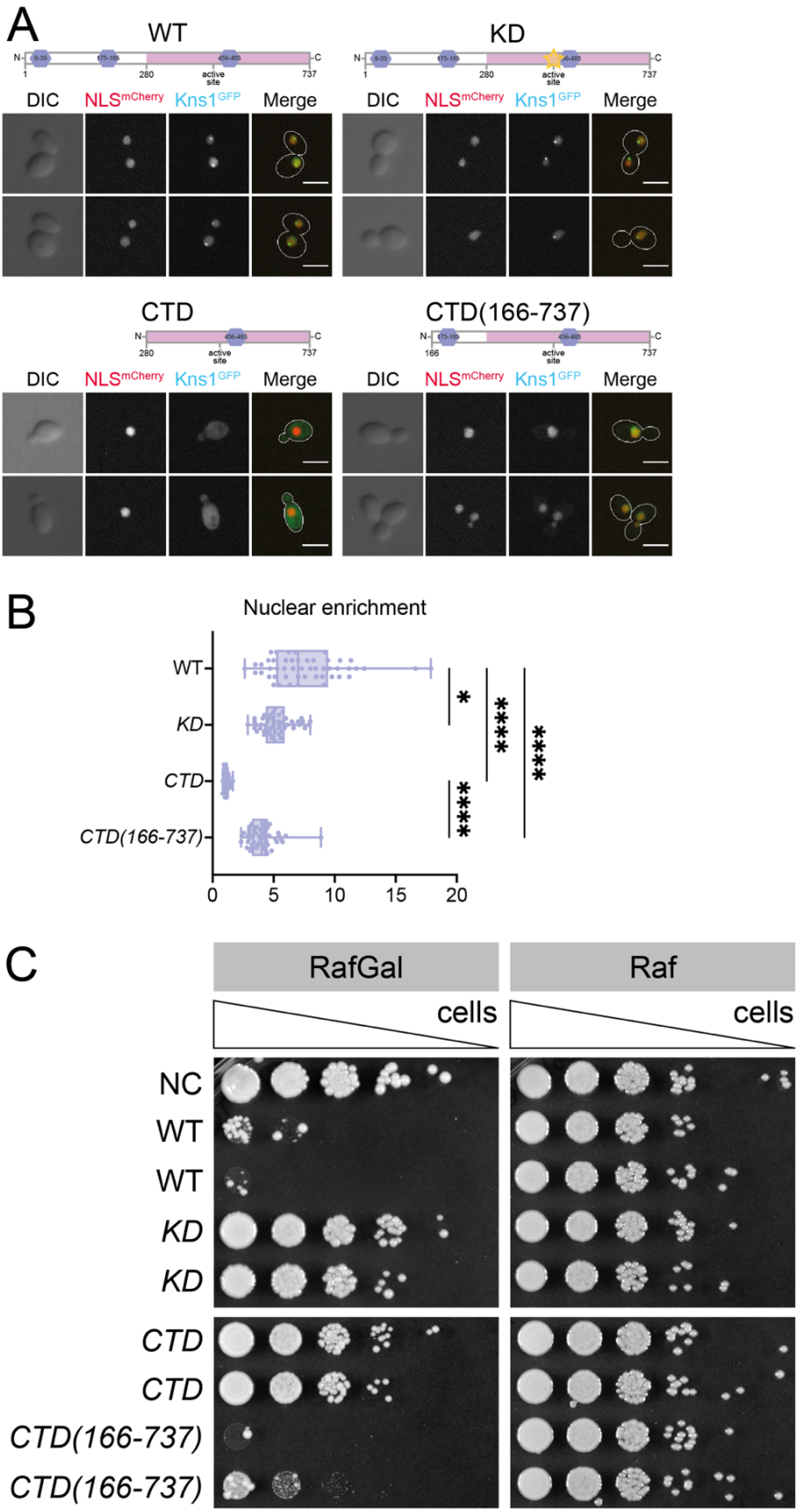

Figure 4.26 Strong overexpression of nuclear, uninhibited Kns1 leads to toxic growth defect.

A. Four different *pGAL*-overexpressing constructs of Kns1 were used. WT: Kns1 overexpressed; KD: Kns1 with mutated active site D440A; CTD: C-terminal domain including 280 – 737 aa;

CTD(166-737): fragment of Kns1 including 166 – 737 aa. All overexpression constructs were fused to GFP (cyan), and NLS-mCherry was used as the nuclear marker (red). Confocal analysis was performed after two hours after induction of *pGAL* with 2 % galactose and visualizing 14 slices of each channel. mCherry signals were detected with 5 % laser intensity and 200 ms exposure time. The GFP signals varied and were detected with the following laser intensities. WT: 3 %, 20 ms; KD: 3 %, 20 ms; CTD: 3 %, 50 ms; CTD(166-737): 3 %, 10 ms. The scale bar indicates 5 µm. B. Nuclear signal intensities of each fragment from A were calculated in relation to the cytoplasmic signal levels. Enrichment was measured using the mean pixel density of a 7 × 7 px square located within the cytoplasm and nucleus (n = 50). The proportion of the mean nuclear signal/mean cytoplasmic signal was calculated as nuclear enrichment for each cell. All single values are depicted as dots. The box indicates the minimum to maximum value and the mean nuclear enrichment is given as a line within the box. Normal distribution was tested with Shapiro-Wilk and statistics were calculated with a Kruskal-Wallis test (*: p = 0.01 - 0.05, ***: p = 0.0001 - 0.001, ****: p < 0.0001). C. Spot test of the strains used from A. Analysis of RafGal (induced *pGAL*) and Raf (control) plates incubated at 30 °C for two days to visualize growth.

4.5.2 *In vivo* autophosphorylation capability of Kns1

Kns1 contains 20 annotated phospho-sites (Albuquerque *et al.* 2008; Holt *et al.* 2009; Breitkreutz *et al.* 2010; Martinez Marshall 2011; Swaney *et al.* 2013; Schmitt *et al.* 2017; MacGilvray *et al.* 2020; Zhou *et al.* 2021; Lanz *et al.* 2021), nine of which are autophosphorylation sites (Martinez Marshall 2011). However, the (auto)phosphorylation capacities of Kns1 were only detected by in vitro analyses. These phosphorylation sites can be differentially phosphorylated under different conditions and can be targets of a multitude of kinases and autophosphorylation. Differentiated phosphorylation can regulate Kns1 activity in response to changing environmental conditions. Nuclear localisation and shuttling of the protein, as described in section 0, could also be regulated in a phosphorylation-dependent manner. To evaluate the possible influence of autophosphorylation on Kns1 activity, the phosphorylation levels were investigated *in vivo*.

As the phosphorylation shift of Kns1 was barely visible in the western blot, a phos-tag approach was used. Adding higher concentrations of phos-tag to the SDS gel helped resolve the phosphorylation isoforms. Overexpression of Kns1 using the constitutive promoter *TEF2* ensures proper protein levels for detection. A kinase-dead variant of Kns1, as described in section 0, was used to study the autophosphorylation capacities in comparison to WT Kns1. A background with (WT) and without endogenous Kns1 (*Δkns1*) was used to validate the influence of low levels of active Kns1. The phos-tag western blot analysis is shown in Figure 4.27 A Catalytically active Kns1 in both WT and *Δkns1* showed the expected band at approximately 100 kDa and another slower migrating band. This phosphorylated isoform disappeared when a kinase-dead version of Kns1 was used, independent of the endogenous background (Figure 4.27 A). The high phosphorylated proportion of Kns1 (approximately 70 %) in the catalytically active WT background was slightly minimised to 60 % when endogenous Kns1 was deleted in *Δkns1* background (Figure 4.27 B). 10 – 20 % of phosphorylated Kns1 was still present when a kinase-dead variant was overexpressed, in both WT and *Δkns1*

background (Figure 4.27 B). This strongly suggests that the major portion of Kns1 phosphorylation is indeed autophosphorylation, but another kinase may be involved to a small extent. The characteristics of the overexpressed constructs were analysed in growth and proliferation assays to confirm the WT behaviour of Kns1 in these strains. Growth was tested in a spot test (Figure 4.27 C) under three different conditions: glucose (D) as the preferred carbon source and raffinose (Raf) and glycerol (Gly) as non-preferred carbon sources. The growth of all strains in the WT and *Δkns1* background was tested and showed only little variance but no severe phenotypes. All strains overexpressing Kns1 showed growth similar to that of the WT (Figure 4.27 C). Flow cytometry revealed that the proliferation rates of Kns1 overexpression (catalytically active and kinase dead) were WT-like (Figure 4.27 D, WT not depicted), with approximately 20 % of the cells with 1C DNA content indicating G_1 phase (Figure 4.27 E, WT not depicted). Similar to the GFP fusions described in section 4.5.1, constitutive overexpression via *pTEF2* does not influence the growth and proliferation phenotypes of Kns1.

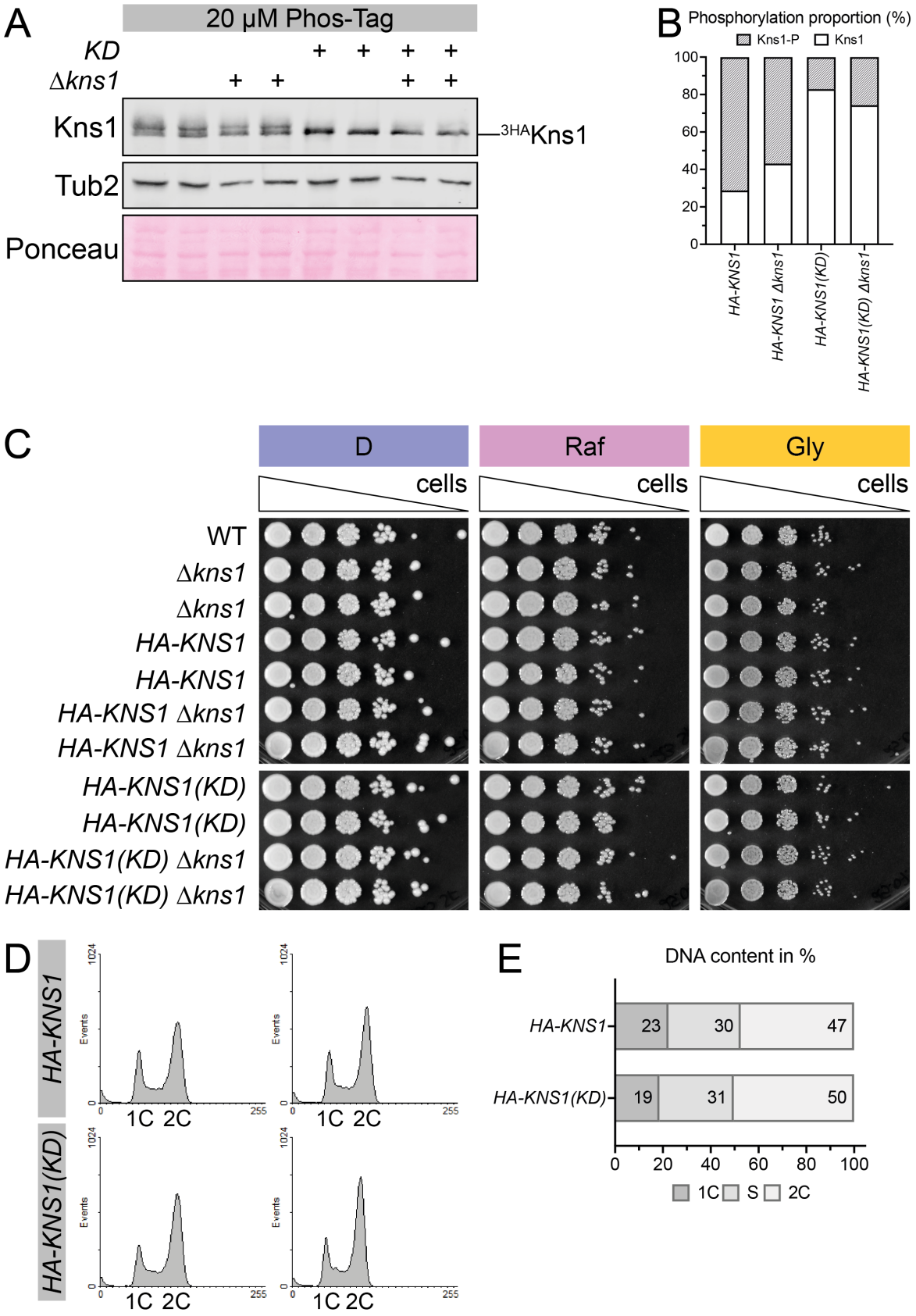

Figure 4.27 Strong autophosphorylation capacities of Kns1 *in vivo*.

A. Phos-Tag western blot analysis of constitutively overexpressed Kns1 in WT, KD (kinase dead, D440A mutation) and *Δkns1* backgrounds. All genotypes are indicated by +. The phos-tag was added at a concentration of 20 µM. Biological duplicates were applied, and 3HA-Kns1 was detected using an α-HA antibody. Slower migrating bands are phosphorylated Kns1 isoforms.

Tub2 was used as a reference and with Ponceau staining proper loading was controlled. B. Phosphorylated and unphosphorylated signals from A were calculated in proportion to total Kns1 levels. The mean relative proportion is given in %. Grey portions indicate phosphorylated proportions and white boxes indicate unphosphorylated proportions. C. Spot test analysis of all used strains from A in different carbon sources (D: glucose; Raf: raffinose; Gly: glycerol). Incubation was performed at 30 °C for two days. D. Flow cytometric analysis of Kns1 overexpression. The experiment was performed by Kathrin Preußel Danger. Two biological replicates are depicted; the WT control is not shown. DNA profiles show single DNA content (1C), and double DNA content (2C). E. DNA content of four biological replicates of each genotype from D was quantified using FCS Express 6 and is depicted in %. The DNA content was assigned to the different cell cycle phases. 1C DNA content (dark grey) visualized cells in G_1 phase, 2C DNA content (white) cells in G_2/M phase. DNA content that couldn't be clearly assigned to either portion was annotated as S phase cells (light grey).

4.5.3 Kns1 growth defect in response to non-preferred carbon sources

Papp *et al.* (2004) suggested that Kns1 is required for growth under specific conditions. This was also observed in a genome-wide phenotypic study (Lockshon *et al.* 2007) which revealed that *Δkns1* cell growth is inhibited in the presence of exogenous oleate. These studies suggest that Kns1 is necessary for growth under stressful conditions. Considering that Kns1 expression showed drastic changes under different carbon sources in the present study (section 4.2.2), which suggests a function in nutrient stress response, the analysis of growth properties in different carbon source backgrounds was imminent.

Growth analysis was performed in the form of a spot test (Figure 4.28 A). The deletion and constitutive overexpression of Kns1 (*Δkns1* and *MYC-KNS1*, respectively) in WT and *Δ326* background was studied in three different carbon sources, glucose (D), raffinose (Raf), and glycerol (Gly), as previously described. Deletion or overexpression of Kns1 led to WT-like growth in the tested duplicates (Figure 4.28 A). *Δ326* showed decreased growth in glucose compared to WT (Figure 4.28 A). The double mutant *MYC-KNS1 Δ326* showed similarly reduced growth rates, whereas *Δkns1 Δ326* showed slightly decreased growth compared to *Δ326* (Figure 4.28 A). These data suggest that the deletion of Kns1 in unfavourable conditions, such as *Δ326*, where increased activity of Kns1 is necessary, leads to reduced growth of these cells. This effect was more visible under non-glucose conditions in the *Δ326* background. In Raf and Gly, the double mutant *Δkns1 Δ326* showed stronger growth defects than *Δ326* (Figure 4.28 A). The effects on cell proliferation were evaluated using flow cytometry. Neither the deletion of Kns1 (*Δkns1*) nor the overexpression of Kns1 (*MYC-KNS1*) influenced cell cycle profiles, as described in Figure 4.28 B. The 1C DNA content, indicating the G_1 phase, in the WT background ranged from 10 to 20 %, similar to the WT levels in glucose (Figure 4.28 C). The flow cytometry profiles shifted towards 1C content in *Δ326* background for all strains, independent of Kns1 availability (Figure 4.28 B). The DNA content shifted to approximately 40 – 50 % for the G_1 phase (Figure 4.28 C), indicating a reduced G_1/S transition in strains with a *Δ326* background. Kns1, however, did not influence the cell proliferation rates in this study.

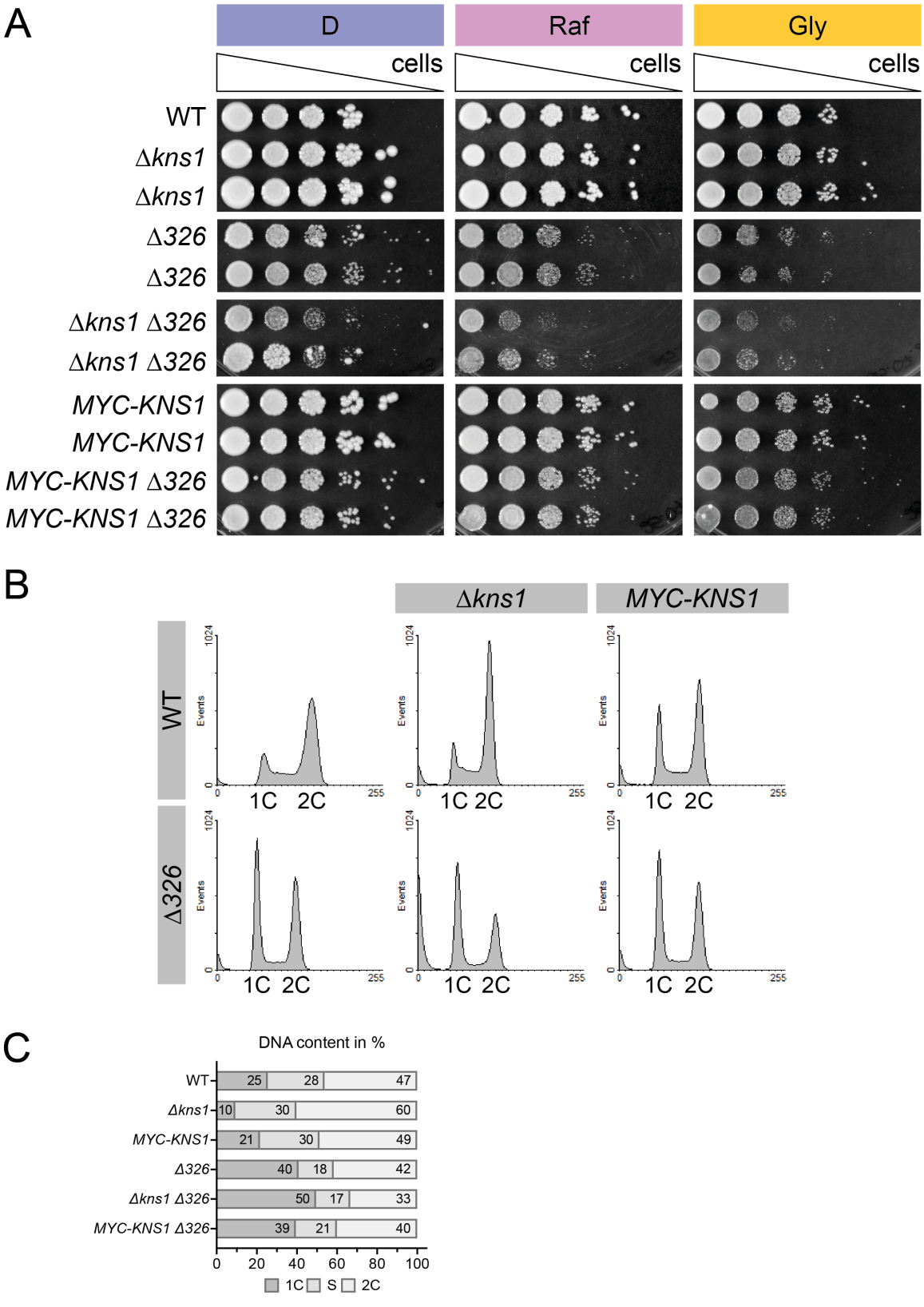

Figure 4.28 Minimal growth phenotype in glycerol conditions.

A. Spot test comparing the growth of WT, *Δkns1*, *Δ326*, *Δkns1 Δ326*, *pTEF-MYC-KNS1*, and *pTEF-MYC-KNS1 Δ326* on different carbon sources. The strains were tested on glucose (D), raffinose (Raf), and glycerol (Gly) plates and inoculated at 30 °C for two days. B. Flow cytometric analysis of the strains tested in A. Different genotypes are indicated with grey boxes.

DNA profiles show signal DNA content (1C), indicating G_1 phase, and double DNA content (2C), indicating G_2/M phase. C. The DNA contents of two biological replicates of each genotype from B were quantified in FCS Express 6 and depicted in %. The DNA content was assigned to the different cell cycle phases. 1C DNA content (dark grey) visualized cells in G_1 phase, 2C DNA content (white) cells in G_2/M phase. DNA content that couldn't be clearly assigned to either portion was annotated as S phase cells (light grey).

4.5.4 The regulatory role of the N-terminal domain of Kns1

The N-terminal domain of proteins is often responsible for their regulation and stability (Jadhav and Wooten 2009). Because Kns1 has a long, unstructured N-terminal domain with no described function yet (Figure 3.31 A), the question of the potential involvement of this region in the (self-)regulation of Kns1 arose. A possible regulatory function, in addition to its importance in localisation described in section 4.5.1, could be the inactivation of the catalytic C-terminal domain as a mechanism to express Kns1, but to keep it inactive under favourable conditions and release the inhibitory effect to boost Kns1 activity under stressful conditions. To test this hypothesis a yeast-2-hybrid (Y2H) assay should reveal the necessary interaction between Kns1's N-terminal domain (NTD) and the C-terminal domain (CTD). Y2H is based on the activation of a reporter gene, in this case *lacZ*, via a *lexA* operator (Figure 4.29 A). The operator is activated only when a transcription factor is bound. This transcription factor is composed of a DNA-binding domain (LexA-BD) and activation domain (B42-AD). The fusion of each of the domains to proteins helps study interactions. When both tested proteins interact, they bring the split domains of the transcription factor in close proximity to ultimately activate the reporter gene (Figure 4.29 A).

In this study, the tested proteins were the NTD and CTD of Kns1, first introduced in section 4.5.1, to analyse self-interactions. The substrate X-Gal, overlaid on the plates, is used as an indicator of *lacZ* activity, as the expressed β-galactosidase can enzymatically convert X-Gal into a blue dye. Blue colonies, therefore, show *lacZ* expression and interaction of Kns1 subunits. CTD was fused to the DNA-binding domain, whereas NTD was fused to B42-AD (Figure 4.29 A). Y2H revealed that this interaction took place, as the colonies of CTD-LexA-BD and NTD-B42-AD were blue (Figure 4.29 B). The corresponding controls with only one of the two fusion proteins showed no change in colour, as depicted in Figure 4.29 B. This experiment suggests that an interaction between the C-terminal and N-terminal domains of Kns1 is likely. The potential inhibiting function of Kns1(NTD), especially under optimal conditions, is released under unfavourable conditions. If the N-terminal domain regulates Kns1 under altering conditions, Kns1 activity is inhibited when the NTD is active. Therefore, overexpression of NTD under conditions of high Kns1 activity could lead to a decrease in kinase function and, hence, reduced Rpc53 phosphorylation levels. Three different carbon sources, glucose (D), raffinose (Raf), and glycerol (Gly), were analysed (Figure 4.29 C). Phosphorylation of Rpc53 served as a readout for Kns1 activity. Under conditions of high Kns1 activity and therefore strong Rpc53 phosphorylation, like Raf or Gly (described in section 4.2.2), an additional high level of Kns1(NTD) was not

sufficient to reduce phosphorylation (Figure 4.29 D). In glucose, Rpc53 phosphorylation with and without additional NTD was approximately 50 % (Figure 4.29 E). In the presence of raffinose and glycerol, the phosphorylated proportion increased to 80 – 90 %, as expected (Figure 4.29 E). NTD overexpression minimally decreased this value. Overexpression with *pTEF2* was either not strong enough to achieve the desired effects, or the inhibition was not directly regulated by high levels of the N-terminal domain.

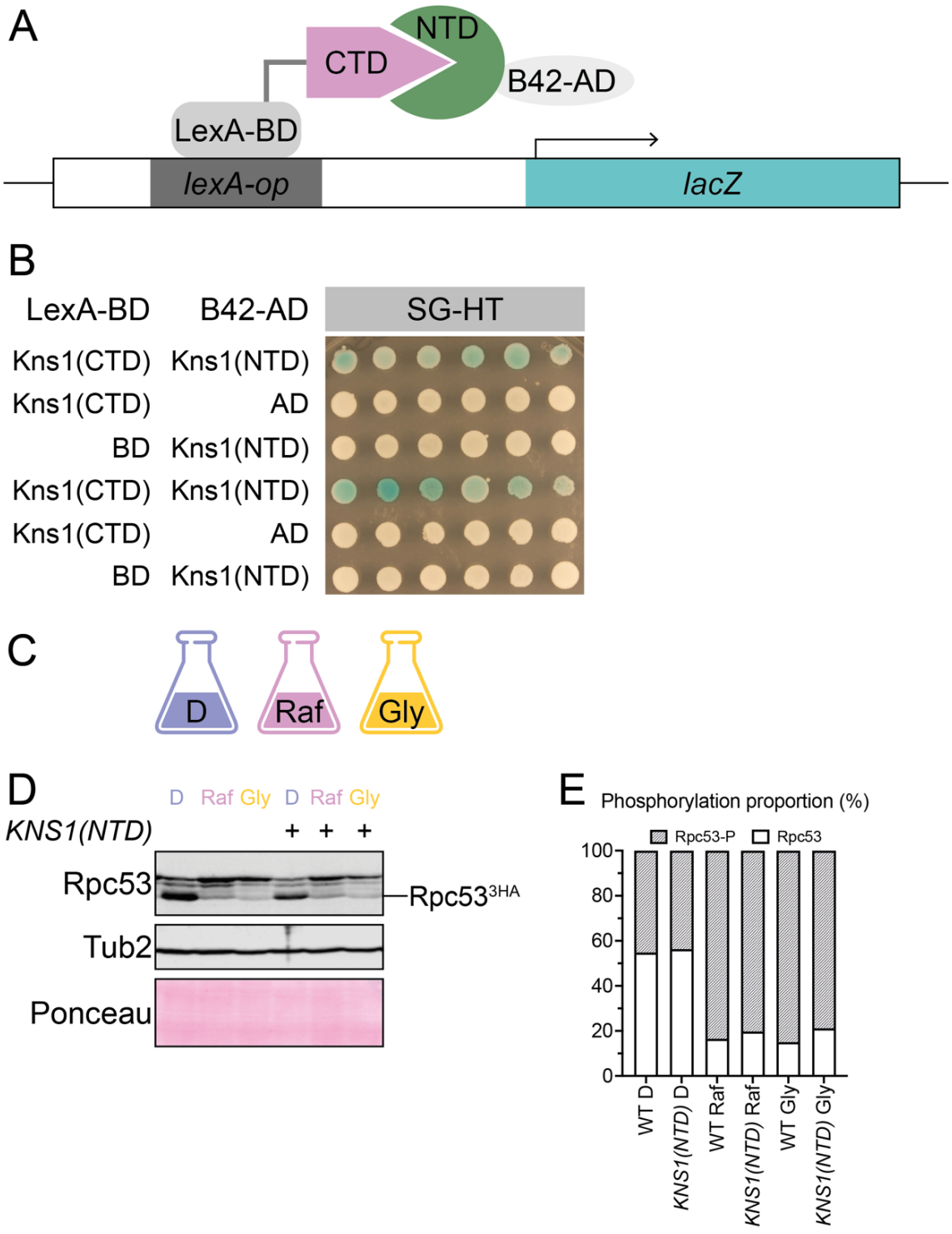

Figure 4.29 Regulatory function of the N-terminal domain of Kns1. (Description on next page)

A. Yeast-2-hybrid (Y2H) assay to check interaction of the Kns1 N-terminal domain (NTD) with the C-terminal domain (CTD). A transcription factor is split into its DNA-binding domain (BD), LexA, and its activating domain (AD), B42. When the fused interaction partners bring both transcription factors in proximity, the reporter gene *lacZ* is activated. The activation of *lacZ* could then be detected by the colour change of X-Gal on the plates. B. Y2H performed by Antje Machetanz-Morokane. Kns1(CTD) was fused to LexA-BD and Kns1(NTD) was fused to B42-AD. Controls for the self-interaction of the domains, including only one part of the transcription factor, were also conducted. Six independent transformants with the fusion constructs were plated on SGal-His-Trp (SG-HT) plates and X-Gal was added. Colour change was detected after two days of incubation at 30 °C. C. The carbon sources used for western blot analysis are glucose (D), raffinose (Raf), and glycerol (Gly). D. Western blot analysis of phosphorylation levels of Rpc53 in response to increased Kns1(NTD) levels in different carbon sources. The analysis was performed by Kathrin Preußel Danger. The strain background with the additional *pTEF-GFP-KNS1(NTD)* is indicated by +. Slower migrating bands are phosphorylated isoforms of Rpc53. Rcp53-3HA was detected with an α-HA antibody. Tub2 was used as a reference and with Ponceau staining proper loading was controlled. Only one of two biological replicates for each condition is depicted E. Quantification of signal intensities from D. Phosphorylated and unphosphorylated signals were calculated in proportion to total Rpc53 levels. The mean relative proportion of n = 2 is given as a percentage. Grey portions indicate phosphorylated proportions and white boxes indicate unphosphorylated proportions.

4.5.5 High instability and rapid degradation of Kns1

The half-life of proteins is largely dynamic and protein abundance within cells shows strong heterogeneity (Belle *et al.* 2006). A correlation between mRNA levels and protein abundance can be observed, yet genes with similar mRNA levels may produce proteins with significantly different abundances. One possible explanation for this effect is the protein half-life. Belle *et al.* (2006) measured the half-life of over 3500 proteins and found a mean half-life of 43 min and over 150 unstable proteins (half-life < 4 min). As evaluated previously, Kns1 protein levels are low under pro-proliferative conditions and increase under stress. In addition to increased transcription, an increase in protein stability may be the reason for this. To investigate this, the stability and turnover of Kns1 were analysed.

To analyse protein stability, re-synthesis was inhibited. Cycloheximide was used to block translation, and different time points were analysed afterwards (Figure 4.30 A). A comparison between WT and *Δ326* was used to differentiate the effects under normal and stress conditions. In steady state conditions, *Δ326* cells showed an increased level of Kns1 which could be due to increased stability (section 4.1.2). Kns1 protein levels were evaluated before and after cycloheximide treatment in 30 min intervals (Figure 4.30 B). In both WT and *Δ326* background, Kns1 levels were drastically decreased after the first 30 min, as depicted in Figure 4.30 B. Although *Δ326* showed stronger Kns1 levels before the treatment, both backgrounds only retained approximately 30 % of the protein after 30 min of blocking re-synthesis (Figure 4.30 C). This clearly suggests a high instability of Kns1 in both WT and *Δ326* conditions.

A possible degradation pathway involved in the high instability of Kns1 is the APC/C-dependent degradation. The anaphase-promoting complex APC/C is an E3 ubiquitin

ligase involved in cell cycle-dependent degradation of substrates (Davey and Morgan 2016). Cdc20 and Cdh1 act as activator subunits and are required for substrate interactions. Cdh1 was activated during early anaphase throughout the G_1 phase. As analyses in unfavourable conditions, where Kns1 protein levels were increased, showed a shift towards the G_1 phase (section 4.1.2 and 4.3.1), a potential regulation of Kns1 degradation by the APC/C-Cdh1 complex was evaluated. APC/C-Cdh1 may be responsible for the degradation of Kns1 in the G_1 phase, which ensures a fast G_1/S transition under favourable conditions. The reduction in APC/C activity under unfavourable conditions could in turn be attributed to an increase in Kns1 protein levels. To test whether APC/C-Cdh1 is involved in the high turnover of Kns1, overactivation of the APC/C complex was used. This could increase the degradation of specific targets, one of which could be Kns1. An inducible version of Cdh1 was used under the control of *pGAL*. The addition of galactose (Gal) activated the APC/C-Cdh1 complex in the experimental setup (Figure 4.30 D). Kns1 stability was measured 60 and 120 min after the activation of Cdh1. Constitutive overexpression of Kns1 was used in this experiment (*pTEF2-MYC-KNS1*). Despite the high amount of Cdh1 expressed after Gal-induction, Kns1 protein levels remained similar to normal conditions (Figure 4.30 E). After two hours of strong induction of the APC/C complex, Kns1 expression decreased minimally. The high instability analysed in Figure 4.30 B could not be achieved by the high activity of the APC/C-dependent degradation.

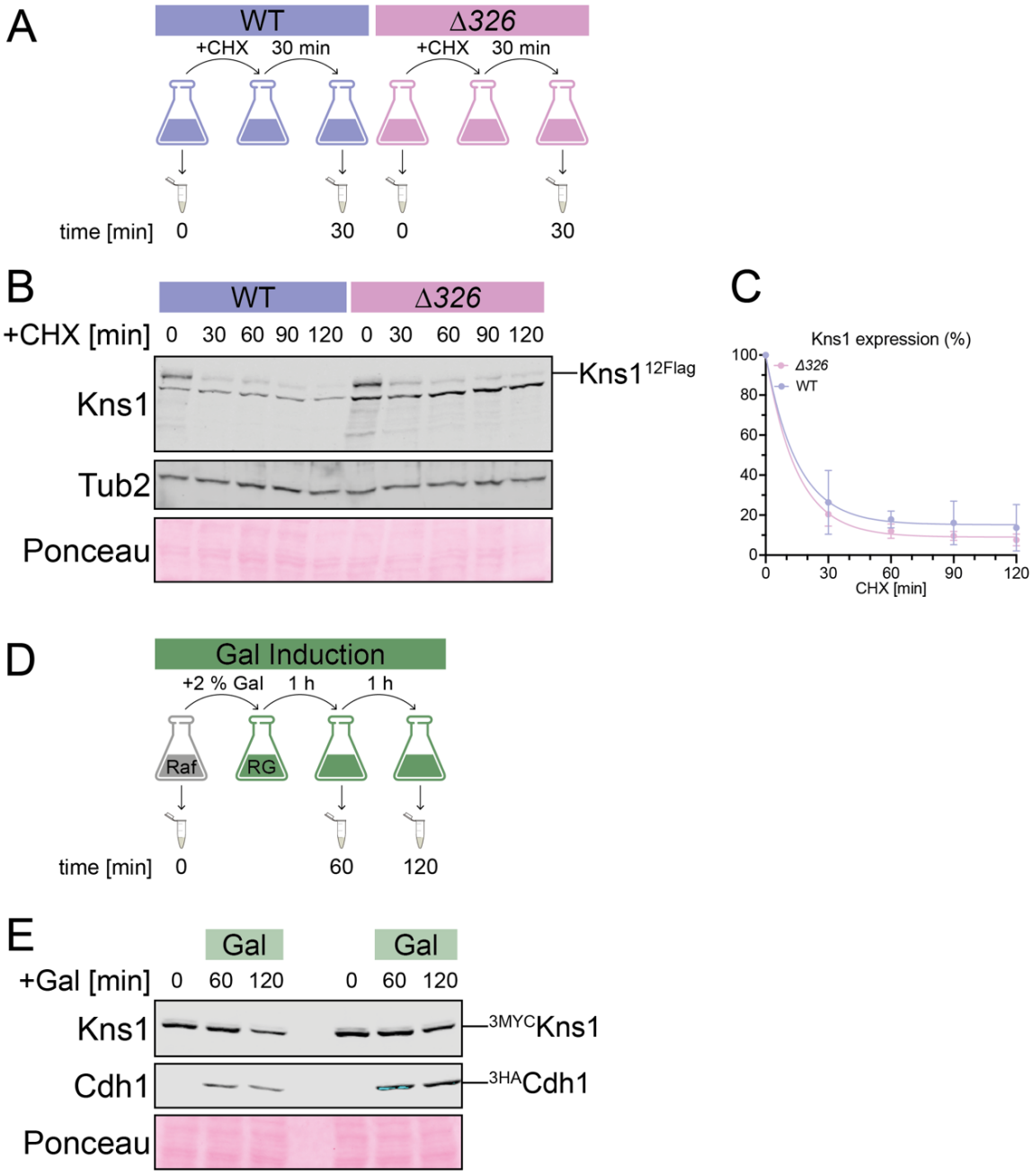

Figure 4.30 Kns1 shows high instability independent of APC/C degradation.

A. Experimental procedure of cycloheximide (CHX) inactivation of translation. Exponentially growing cultures were used as timepoint 0. Subsequently, cycloheximide was added, and the mixture was incubated for 30 min. Samples were taken at 30 min time intervals for two hours in total. WT and *Δ326* were compared. B. Western blot analysis of endogenous Kns1 comparing WT and *Δ326* after cycloheximide treatment. Kns1-12xFlag was detected using an α-Flag antibody. Tub2 was used as a reference and with the help of Ponceau staining proper loading was controlled. After CHX addition, samples were taken at 30 min intervals (+CHX (min)). C. Signals from B were quantified. Kns1 levels were normalized to Tub2. The proportions in relation to each time point 0 are given in %. Mean values from two biological replicates are indicated by circles and standard deviation (SD) is given in bars. A nonlinear regression curve was fitted to every condition indicated by the lines (WT: blue, *Δ326*: pink). D. Experimental setup for galactose induction of Cdh1. The starting culture was in raffinose-containing medium and served as the time point 0. Then, 2 % galactose was added, and induction took place for one hour. Samples were taken after one and two hours of induction. E. Western blot analysis of constitutively overexpressed Kns1 and inducible Cdh1. 3MYC-Kns1 was detected using an

α-Myc antibody and 3HA-Cdh1 was detected using an α-HA antibody. Ponceau staining was used to control proper loading. Samples were taken 60 and 120 min after Gal induction (+Gal (min)).

As the instability of Kns1 was similar in WT and *Δ326* (Figure 4.30 B) even though protein levels were increased under steady-state conditions for *Δ326* (Figure 4.2 B), the analysis of protein stability in non-glucose conditions was of central interest. Under unfavourable conditions such as raffinose or glycerol, Kns1 expression also increased significantly (Figure 4.8 B). Furthermore, the switch from respirating to fermenting conditions, described in section 4.2.3, showed a fast reduction of Kns1 levels, indicating a quick turnover depending on different carbon sources. Hence, the stability and turnover rates were elucidated in glucose, raffinose, and glycerol, with inhibition of re-synthesis by adding cycloheximide (Figure 4.31 A). Western blot analysis revealed the expected increase in Kns1 expression in Raf and Gly compared to that in glucose (Figure 4.31 B). After 30 min of cycloheximide treatment, Kns1 levels dropped drastically in glucose, as described in Figure 4.31 B. Kns1 expression in Raf and Gly also decreased; however, at a slower rate compared to glucose conditions (Figure 4.31 B). Quantification of these signals in relation to the untreated state of each condition revealed that raffinose-grown cells showed a similar decrease in Kns1 protein levels as glucose-grown cells and a high instability with only 20 % of the initial protein level remaining after 60 min (Figure 4.31 C). Kns1 expression in glycerol, however, decreased at a lower rate, maintaining approximately 50 % after 30 min, and only dropping to 20 % of the original protein amount after two hours (Figure 4.31 C). This indicated that the stability of Kns1 slightly increased under respiratory conditions, such as glycerol.

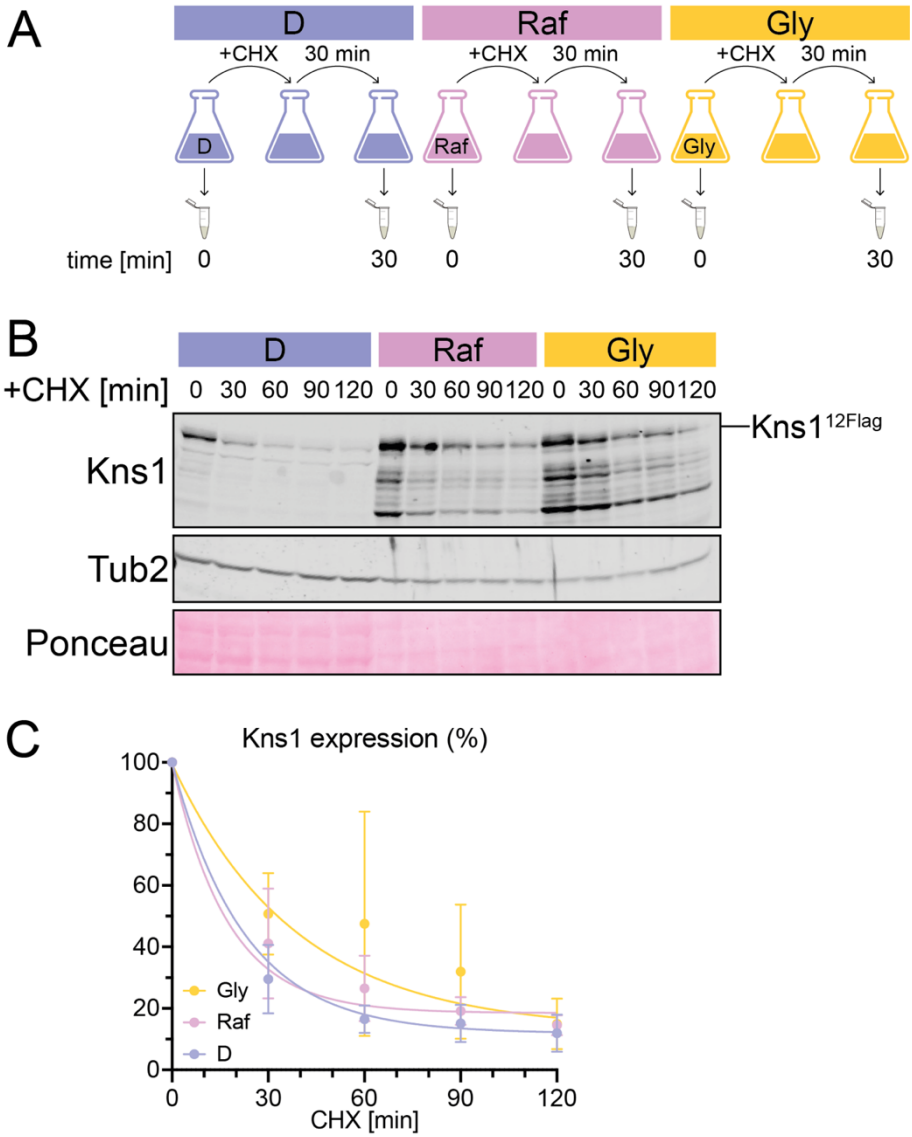

Figure 4.31 Kns1 shows high instability in various conditions.

A. Experimental procedure of cycloheximide (CHX) inactivation of translation. Exponentially growing cultures of different carbon sources were used as timepoint 0. Afterwards cycloheximide was added and incubated for 30 min. Samples were taken in 30 min time intervals for two hours in total. Glucose (D), raffinose (Raf), and glycerol (Gly) were compared. B. Western blot analysis of endogenous Kns1 in varying carbon sources after cycloheximide treatment. Kns1-12xFlag was detected using an α-Flag antibody. Tub2 was used as a reference and with the help of Ponceau staining proper loading was controlled. Sampling after CHX addition was done at 30 min intervals (+CHX (min)). C. Signals from B were quantified. Kns1 levels were normalized to Tub2. The proportion in relation to each time point 0 was calculated as a percentage. Mean values from two biological replicates are indicated by circles and standard deviation (SD) is given in bars. A nonlinear regression curve was fitted to every condition indicated by the lines (D, blue; Raf, pink; Gly, yellow).

To gain a deeper understanding of the degradation of Kns1, which appears to vary based on the conditions and is unlikely to involve APC/C-Cdh1, the 26S proteasome was examined in detail. The 26S proteasome is responsible for a major part of the regulated proteolysis and mediates a variety of cellular processes (Liu et al. 2007;

Budenholzer et al. 2017; Bard et al. 2018). It specifically recognises ubiquitinated proteins in the cytoplasm and nucleus and degrades these targets into small peptides via an ATP-dependent mechanism. Proteasomes can be inhibited experimentally by adding an inhibitor, such as MG132, which blocks the active sites efficiently (Liu et al. 2007). When the 26S proteasome is specifically blocked, this could lead to a distinct stabilisation of Kns1 if it is usually targeted by the ubiquitin proteasome pathway.

To test this hypothesis, we used MG132 to inhibit proteasomal degradation. Further inhibition of new protein synthesis helped to detect a stabilising effect on Kns1 under different conditions (Figure 4.32 A and B). A control with DMSO instead of MG132 was used to verify the possible stabilising effects of the 26S proteasome. Western blot analysis of Kns1 levels in glucose revealed a fast degradation independent of the 26S proteasome, as protein levels dropped to a minimum of < 20 % after 60 min in both proteasomal inhibition and control groups (Figure 4.32 C and D). Zooming in for the first 30 min, where most of the protein degradation already takes place, 10 min intervals were used for the same experiment in Figure 4.32 E. Inhibition of the 26S proteasome led to a slower decrease in Kns1 levels compared with the control. After 10 min, approximately 80 % of Kns1 was present with proteasomal inhibition, whereas only 20 % was present in the control (Figure 4.32 F). However, after 30 min, Kns1 was degraded in a 26S proteasome-independent manner, as shown in this experiment. The control also revealed that after 10 min, Kns1 levels decreased to their minimum, suggesting a high turnover rate of less than 10 min (Figure 4.32 F). Cells grown in raffinose showed 26S proteasome-dependent delay in degradation after 30 min (Figure 4.32 G). The rapid degradation to lower than 40 % protein level after 30 min in raffinose was slightly stabilised to 60 % when the proteasome was blocked (Figure 4.32 H). An even stronger effect was detected in glycerol-grown cells, as depicted in Figure 4.32 I. Inhibiting the 26S proteasome led to almost stable Kns1 expression throughout the 90 min of the analysis. Compared to the degradation of less than 30 % protein in the control, the treated cells remained at 90 % Kns1 levels (Figure 4.32 J). The same was true after 90 min. Inhibition of the proteasome led to a 60 % decrease in protein, while Kns1 was degraded to 20 % in the control (Figure 4.32 J). In total, this suggests that carbon source-dependent degradation of Kns1 is dependent on the 26S proteasome. Kns1 might be stabilised by inhibiting the proteasome under all conditions; however, the strongest effect was observed in glycerol which also showed the strongest increase in protein levels under steady-state conditions, as described in section 4.2.2. The significant increase under varying conditions might be regulated by a reduction in the proteasomal degradation of Kns1 as a response to stress. The high turnover of Kns1, therefore, seems to be a regulatory mechanism that keeps Kns1 levels low but facilitates a quick increase in Kns1 when necessary.

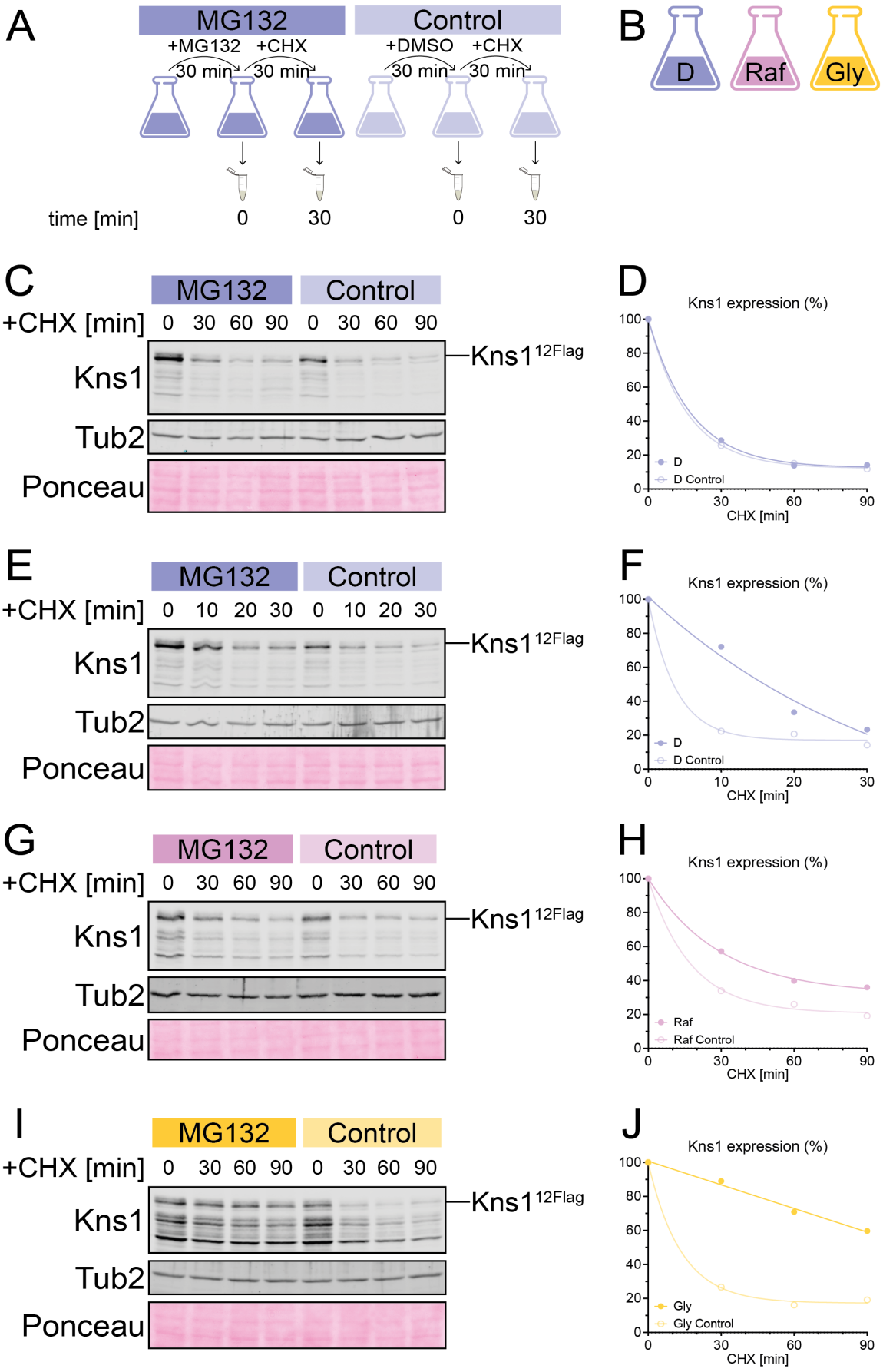

Figure 4.32 High degradation rates of Kns1 dependent on 26S proteasome. (Description on next page)

A. Experimental procedure for the MG132 shutoff. Exponentially growing cells from the background strain *Δise1* were treated with MG132 to completely block proteasomal degradation. After 30 min, a sample was taken at time point 0. Subsequently, cycloheximide (CHX) was added to inhibit protein re-synthesis. Additional samples were taken at 30 min intervals for 1.5 h a total. As a control, DMSO was added instead of MG132 and incubated similarly. CHX was subsequently added to block protein synthesis. The experiment was conducted at 30 °C to overcome the growth defects of *Δise1* (Figure S 9). B. The experiment was performed using different carbon sources including glucose (D), raffinose (Raf), and glycerol (Gly). C. Western blotting of MG132 shutoff in glucose analysing endogenous Kns1. Kns1-12xFlag was detected using an α-Flag antibody. Tub2 was used as a reference and with the help of Ponceau staining proper loading was controlled. The time after CHX addition is given in min. D. Signals from C were quantified. Kns1 levels were normalized to Tub2. The proportion of Kns1 protein in relation to each time point 0 was calculated and is given as a percentage. Single values are indicated by circles. A nonlinear regression curve was fitted to the experiment and the corresponding control. E. Western blot of the MG132 shutoff in glucose analysing endogenous Kns1 in shorter time intervals. MG132 block was performed for 30 min; however, samples after CHX addition were taken every 10 min. Kns1-12xFlag was detected using an α-Flag antibody. Tub2 was used as a reference and with the help of Ponceau staining proper loading was controlled. Time after CHX addition is given in min. F. Signals from E were quantified. Kns1 levels were normalized to Tub2. The proportion of Kns1 protein in relation to each time point 0 was calculated as %. Single values are indicated by circles. A nonlinear regression curve was fitted to experiment and corresponding control. G. Western blot of the MG132 shutoff in raffinose analysing endogenous Kns1. Kns1-12xFlag was detected using an α-Flag antibody. Tub2 was used as a reference and with the help of Ponceau staining proper loading was controlled. Time after CHX addition is given in min. H. The signals from G were quantified. Kns1 levels were normalized to Tub2. The proportion of Kns1 protein in relation to each time point 0 was calculated in %. Single values are indicated by circles. A nonlinear regression curve was fitted to experiment and corresponding control. I. Western blot of the MG132 shutoff in glycerol analysing endogenous Kns1. Kns1-12xFlag was detected using an α-Flag antibody. Tub2 was used as a reference and with the help of Ponceau staining proper loading was controlled. Time after CHX addition is given in min. J. The signals from I were quantified. Kns1 levels were normalized to Tub2. The proportion of Kns1 protein in relation to each time point 0 was calculated and given in %. Single values are indicated by circles. A nonlinear regression curve was fitted to experiment and corresponding control.

5 DISCUSSION

S. cerevisiae adjusts its behaviour and growth rates by integrating many different nutrients, such as carbon sources, nitrogen availability, or amino acids (Busti *et al.* 2010; Broach 2012). This precise fine-tuning involves a variety of processes such as fast mitotic growth in rich media and quiescent states in response to starvation. To regulate these processes, nutrients have a dual function. Nutrients serve as a source of energy for growth and simultaneously as a signal molecule. Both functions are interdependent and equally important. Adaptation to changing conditions is highly dependent on protein homeostasis (i.e. proteostasis). As all cellular pathways are controlled by a multitude of proteins, regulation of proteostasis is crucial, and complex processes are involved (Sonenberg and Hinnebusch 2009; Grandi and Bantscheff 2019). The process of regulating protein availability involves complex interplay between various mechanisms, including transcriptional and translational regulation, protein degradation, and protein trafficking. Additionally, alterations in protein availability can have significant effects on cellular processes such as cell growth, differentiation, and metabolism, making it a critical process that must be tightly controlled (Grandi and Bantscheff 2019; Chen *et al.* 2023). Defects in protein synthesis can also lead to various diseases and disorders, strengthening the importance of understanding the complex mechanisms involved in protein availability to develop effective strategies for the prevention and treatment of these diseases and disorders (Balch *et al.* 2008; Chen *et al.* 2023).

The focus of this study was the LAMMER kinase Kns1, an effector kinase of TORC1, the master regulator of proliferation, in yeast. Although many processes are important for adapting proteostasis to changing conditions, TORC1 plays an essential role. TORC1 integrates many nutrients and intracellular signals and distributes them via many regulatory pathways (Hall 1996; González and Hall 2017; Battaglioni *et al.* 2022). Kns1 is negatively regulated by TORC1 and could be an antagonist of the pro-proliferative regulation of TORC1 (Lee *et al.* 2012). Kns1 directly phosphorylates Rpc53, a regulatory subunit of RNA Pol III, thereby contributing to transcriptional inactivation. This study aimed to address the regulation of Kns1 and identify its potential connections to external signals. This study revealed that the expression of Kns1 is regulated in multiple layers. It shows differentiated transcriptional and translational levels as well as increased protein stability and protein activation under unfavourable conditions. The activation of Kns1 occurs fast and is independent of a high level of global protein synthesis, as it is required under non-preferred conditions with low expression capacities. Additionally, this study presents evidence for its regulation under a variety of stress conditions. Kns1 protein levels and activity are increased under non-favourable carbon source conditions, as well as low translational activity. Regulation mediated by inactivation of TORC1 also suggests a response to other nutrient signals. Kns1 directly promotes inactivation of RNA Pol III via Rpc53 phosphorylation under these conditions to repress tRNA and rRNA synthesis when proliferation is paused.

5.1 Multifaceted layers of the regulation of Kns1 expression

Kns1 showed increased protein levels and activity under various stress conditions. A gradual shift upon changing conditions hints at the regulation on multiple layers. The regulation of transcription and translation seems likely. Therefore, Kns1 expression was analysed to evaluate the layers of regulation.

5.1.1 Influence of transcriptional regulation on Kns1 expression

As the first step in protein synthesis, transcription plays a crucial role in the regulation of protein availability (Turowski and Boguta 2021). The expression of many proteins is mainly regulated by the transcription of their corresponding genes. Transcriptional reprogramming, for example, plays a crucial role in changing carbon sources (Busti *et al.* 2010). During the diauxic shift, when yeast switches from fermentation to respiration owing to the lack of glucose as an energy source, transcriptional reprogramming is activated. Genes necessary for the metabolism of non-fermentable carbon sources and respiration are activated and glucose-dependent transcription is repressed. These changes in gene expression allow the cell to utilise alternative carbon sources and generate energy through respiration, which is crucial for survival during periods of limited glucose availability.

Kns1 showed significantly increased protein levels under steady-state non-preferred conditions (section 4.2.2). Additionally, Rpc53 phosphorylation, an indicator of Kns1 activity, was increased. However, the analysis of the reporter, which includes the complete 5' regulatory region of *KNS1*, did not show similar increases, which indicates that transcription is likely not involved in this increase upon carbon source change. However, integrating the reporter into the endogenous genetic environment resulted in a different outcome (Hartmann 2024). The correct genetic surroundings led to a significant increase in reporter protein levels under unfavourable conditions. This suggests a regulation of Kns1 expression via the regulatory region and additional other sequences in the adjacent environment, which are not depicted in the reporter system used in this study. The involvement of structures or sequences outside the 5' regulatory region also suggested that the expression of Kns1 is highly regulated at the transcriptional level. RNA sequencing data by Wojciech (2020) showed a 3-fold increase in *KNS1* mRNA levels in the *Δ326* mutant compared with the WT. This further supports regulation at the transcriptional level. However, Kns1 protein levels were enhanced even more in non-glucose conditions and in cells in the diauxic shift. Elucidation of transcriptional regulation that leads to strong protein expression under nutrient-dependent conditions was performed by qPCR. This data, even though preliminary, suggested a 2-fold change in mRNA levels in glycerol and diauxic conditions (section 4.4.1). Technical difficulties, such as a high variance of single experiments and a slightly variable housekeeping gene for normalisation, reduced the power of these results, and further examination is required. The data still hinted at transcriptional regulation upon altering conditions, similar to the RNA sequencing data from Wojciech (2020). Additionally, Kns1 protein levels were eIF2- and Gcn4-dependent (section 4.1.5). This strengthens the theory of transcriptional

regulation, as eIF2- and Gcn4-dependent protein increases are most likely part of the integrated stress response involved in reprogramming. In particular, Gcn4 is a major regulator of genetic reprogramming, because it directly activates genes under stress conditions. *KNS1* could be a Gcn4 target that is usually repressed under optimal conditions and is only expressed to a high extent when activated by Gcn4. The strong expression under non-favourable carbon sources and the Gcn4-dependency strongly suggest *that KNS1* is a glucose-repressed gene that is only activated under non-preferred conditions and in the integrated stress response, where its function in downregulating RNA Pol III is required.

While Gcn4 could be the only transcription factor regulating Kns1 expression, it is likely that other factors are also involved. Carbon source-dependent transcription factors can help activate Kns1 expression under non-fermentable conditions. Utilising multiple transcription factors could help regulate transcription in response to a multitude of stress signals and quickly adapt to the conditions present. The YEASTRACT+ database revealed consensus sequences for a variety of well-known transcription factors in *KNS1*, including Cat8 and Ume6 (Monteiro *et al.* 2020; Teixeira *et al.* 2023). Cat8 is known to be involved in the derepression of many genes when conditions shift from fermentative to non-fermentative, for example, during diauxic shift (Hedges *et al.* 1995). Its expression is repressed by Mig1, a repressor that inhibits non-fermentative genes under glucose conditions (Roth *et al.* 2004). Under non-glucose conditions, Mig1 is phosphorylated and exported from the nucleus, so that glucose-repressed genes can be transcribed. Cat8, when transcribed, then binds to carbon source-responsive elements (CSREs) at other sites to derepress genes necessary for the non-glucose response (Randez-Gil *et al.* 1997; Roth *et al.* 2004). Glucose not only regulates *CAT8* transcription but also Cat8 activity. Cat8 is phosphorylated under non-fermentative- conditions. However, when glucose is present, Cat8 is dephosphorylated and inhibited. In addition, Cat8 is a target of Snf1 (Busti *et al.* 2010). The activity of Snf1 is regulated by carbon source availability, and Snf1 is required for derepression of targets used in respiration and metabolism of non-fermentable sources. Given its important role in the derepression of glucose-repressed genes, Cat8 might play a crucial role in regulating Kns1 in non-fermentative conditions. The possible connection was investigated in this study, which revealed no significant influence of Cat8 on Kns1 protein levels under different carbon sources (section 4.4.2). The activity of Kns1 was further not altered by Cat8 availability. The significant increase in Kns1 expression under non-glucose conditions could not be explained by the enhanced transcription mediated by Cat8. Under these conditions, *KNS1* is likely not a target gene of Cat8.

Ume6, a DNA-binding protein, is a key transcriptional regulator of early meiotic genes; however, it is also known to regulate genes involved in carbon and nitrogen metabolism (Strich *et al.* 1994; Vershon and Pierce 2000). Ume6 is required for the recruitment of Sin3 and Rpd3 subunits of the histone deacetylase complex (HDAC) (Kadosh and Struhl 1997, 1998). This complex then positively and negatively regulates the transcription of target genes by the deacetylation of histone

H3 and histone H4 (Rundlett *et al.* 1996). Furthermore, Rpd3 is necessary for transcriptome changes under glucose starvation conditions (Hsieh *et al.* 2022). It directly inhibits the expression of genes that stimulate growth by deacetylating them, but indirectly promotes the transcription of genes involved in gluconeogenesis by releasing acetate, which can be recycled by the SAGA complex for subsequent histone acetylation. As mentioned above, *KNS1* comprises a binding sequence for Ume6, which could potentially recruit Rpd3 and Sin3 to form an HDAC on *KNS1*, thereby repressing its transcription under favourable conditions. Transcriptional regulation under changing carbon source conditions via this complex can lead to alterations in gene expression and protein levels. A deletion of *RPD3*, however, could only contribute to the change in protein levels of Kns1 under non-fermentative conditions to a minor extent (section 4.4.2). However, the repressing function of Rpd3 by deacetylating *KNS1* under glucose conditions could not be verified. The recruitment of Rpd3 to Ume6 on its *KNS1* site does not seem to be essential for blocking Kns1 expression in glucose, which is then released by Rpd3 relocation in raffinose and glycerol. Interestingly, Kns1 protein levels slightly decreased under non-fermentable conditions when Rpd3 was missing. Kns1 expression appeared to be Rpd3-dependent under these conditions, suggesting the recycling of acetate released by Rpd3 from other histone sites. The SAGA complex may use free acetate to acetylate histones at *KNS1*, thereby activating its transcription under unfavourable conditions. This indirect effect of Rpd3 was also observed for Kns1 activity. Kns1 activity was slightly reduced under non-fermentable conditions in the *Δrpd3* background, as indicated by the shifted proportion of Rpc53 phosphorylation. It is further possible that Rpd3 is necessary to repress or activate other targets involved in the activation of Kns1. Another kinase may be required to phosphorylate and thereby increase the kinase activity of Kns1. A phosphatase may also be involved in dephosphorylation of the kinase domain of Kns1. Therefore, Rpd3 would regulate Kns1 activity indirectly by activating other targets, and direct recruitment to *KNS1* sites mediated by Ume6 would not be required.

A transcriptomic reaction to altering conditions is key for a fast response to adapted gene expression. Many genes contain different transcription start sites (TSS) depending on the environmental conditions to quickly change their expression (Rojas-Duran and Gilbert 2012). TSS heterogeneity then leads to different lengths of mRNAs which may also regulate translational efficiency. On the one hand, this may include the efficiency of AUG scanning along longer or shorter versions of the mRNA which changes the pace of translation initiation. However, regulatory mechanisms that depend on uORFs may vary with mRNA length. The more uORFs are integrated into the RNA, the more likely regulation is via ribosome skipping. Furthermore, different mRNA lengths may alter their structure and regulation through these mechanisms. Although knowledge of TSS heterogeneity is common, its effect on translational regulation is still not fully characterised. As *KNS1* has a longer 5' region than many other genes, its regulation by different transcription start sites is possible. Nagalakshmi *et al.* (2008) and Rojas-Duran and Gilbert (2012) have stated different uORF sites for Kns1 which would further hint to alternative TSS depending on the conditions. In this study,

possible differences in TSS under varying carbon source conditions were elucidated. A map of transcript lengths was constructed by analysing different positions within the 5' region. Conditions, where Kns1 protein levels were increased, showed, however, no significant difference in transcript length (section 4.4.1). It remains unclear whether transcript mapping by a primer extension approach is efficient in revealing differences, as the analysis also showed a positive result for the negative control which must include a transcript starting from within the upstream ORF *COX19*. This suggests a technical issue in reverse transcription of the mRNA, so that upstream ORFs are included in the cDNA as well, or it suggests a natural transcript consisting of two ORFs that are simultaneously transcribed. Usually, *S. cerevisiae* contains only monocistronic genes, with one ORF per transcript (Hecht *et al.* 2002). Polycistronic genes are characteristic of the prokaryotic system. While the eukaryotic translation mechanism by scanning the mRNA does not include the possibility of reinitiation on another ORF after termination, several exceptions have been stated in the literature. Small uORFs positioned in the 5' leaders of genes modulate translation, as described for *GCN4* or *YAP1* (Hinnebusch 1997; Vilela 1998; Dever *et al.* 2016). Cap-independent translation using IRESs has been reported in *S. cerevisiae* which suggests the possibility of polycistronic gene expression (Hellen and Sarnow 2001; Jackson *et al.* 2010; Crawford and Pavitt 2019). Additionally, cap-independent translation has mainly been found in nutrient-starved conditions and in genes that have a long 5' untranslated region (5'UTR) (Hecht *et al.* 2002). The mitochondrial genomes of many yeast species also include multiple examples of polycistronic transcripts encoding several proteins from one mtRNA molecule (Manthey and McEwen 1995; Toffaletti *et al.* 2003). One example is *COX1*, which encodes subunit I of cytochrome c oxidase, which is part of a longer mtRNA co-transcribing tRNAs and the ORFs *AAP1*, *OLI2*, and *ENS2* (Manthey and McEwen 1995; Timón-Gómez *et al.* 2018). With its long 5' region, *KNS1* could potentially be part of a rare polycistronic mRNA, including its upstream open reading frame (ORF) *COX19*, which is required for cytochrome c oxidase assembly. If this is the case, the regulatory region, including the transcription start site of *KNS1*, is even upstream of *COX19*. This further suggests that the experiment conducted in this study did not include an actual transcription start site. The long 5' leader region of *KNS1* could be important for cap-independent translation under nutrient-starved conditions that differentially express the gene. If *COX19* is not included in a polycistronic transcript, the TSS data of this study indicates that there are no differences in *KNS1* transcript length under starved conditions when protein expression changes drastically. Additionally, all potential uORF sites, as reported by Nagalakshmi *et al.* (2008) and Rojas-Duran and Gilbert (2012), were included in the transcript under all conditions. This might hint at a translational regulation of *KNS1*, similar to that of *GCN4*. The uORFs appear to be included in the mRNA and could lead to differentiated translational initiation of the *KNS1* ORF. Under pro-proliferative conditions, translation may be initiated at the uORFs, thereby keeping the translation of *KNS1* low. When conditions change, reducing the availability of translation factors and tRNAs might lead to ribosome skipping and potential initiation at the *KNS1* ORF. This, in turn,

increases the protein level and further reduces the availability of tRNAs and rRNAs to downregulate translation.

5.1.2 Importance of differentiated translation initiation on Kns1 expression

S. cerevisiae must quickly adapt to environmental changes to ensure proper growth and division. Both transcriptional and translational rates can influence the proteome in a steady state and in response to stress (Crawford and Pavitt 2019). Blocking protein synthesis globally by repressing translation is a rapid way to adapt to limited nutrient and energy availability. The most important step in the regulation of translation is the initiation process, which is complex and rate-limiting for most mRNAs. Global translational regulation is mediated by eIF2 (Gebauer and Hentze 2004; Crawford and Pavitt 2019). Recycling of eIF-GDP to eIF2-GTP, performed by the guanine exchange factor eIF2B, is a crucial step for high levels of reinitiation and, therefore, a strong target for regulation. Stress activates the phosphorylation of eIF2α by Gcn2, which increases the affinity of eIF2 for eIF2B. This in turn changes eIF2 to a competitive inhibitor and blocks the guanine exchange function of eIF2B. This leads to a global reduction in active eIF2-GTP, which can be integrated into ternary complexes. In response, translation initiation levels are diminished, and translation is globally repressed.

Previous RNA sequencing data from Wojciech (2020) showed an increase in *KNS1* mRNA levels in *Δ326* cells compared with WT. The corresponding protein response to eIF2 stress was evaluated. This study revealed that a reduction in global translation via eIF2 results in increased mRNA and protein levels of Kns1. This change was significantly enhanced compared to other growth-deficient mutants, indicating a specific eIF2-dependent stress response for Kns1 regulation. Kns1 does not seem to be activated in response to slow growth but specifically induces a response when cellular reprogramming occurs. This correlates well with the activity of Kns1, measured by Rpc53 phosphorylation in this study, which showed an increase in the phosphorylated proportion only in low eIF2 conditions. It is stated by Lee *et al.* (2012) that Kns1 serves as a priming kinase for Rpc53 phosphorylation and Mck1 subsequently phosphorylates two more sites. In addition, our data showed a strong dependence of Rpc53 phosphorylation on Kns1. Kns1 is both necessary and sufficient for a strong change in phosphorylation. Furthermore, the change in Kns1 expression at the mRNA and protein levels in a translationally repressed background again raised the question of a possible association with promoter regulation. To solve this mystery, a reporter including the complete 5' region and the first three codons of *KNS1* was used. Under conditions of high Kns1 protein levels (*Δ326*), the reporter was insufficient to reproduce this finding. This suggests only a minor role of the 5' region in the regulation of Kns1 and a more prominent role of translational and post-translational mechanisms. However, it must be noted that the reporter does not display full Kns1 regulation, as the construct was not in an endogenous environment, and other structural surroundings are likely missing in this analysis. As described in section 5.1.1, Hartmann (2024) found that the integration site of the reporter plays a crucial role in

its function. Using the reporter at its endogenous site, protein expression was drastically increased compared to integration at a marker site. It is likely that the reporter in the *Δ326* mutant used in this study would also exhibit higher protein levels when used in an endogenous environment. Additionally, as already mentioned in section 5.1.1, a polycistronic transcript including the small open reading frame *COX19* upstream of *KNS1* would enhance the opportunity for differentiated regulation of translation. It is possible that the translation of *KNS1* is regulated by sequences or structures upstream of *COX19*, which may be included in a long mRNA. Furthermore, uORFs may play a substantial role in regulating translation under nutrient-deficient conditions. The increase in Kns1 protein levels under these stress conditions could also be explained by a higher translational rate in a mechanism similar to that of *GCN4*, in addition to the increase in transcription, as suggested by RNA sequencing data.

5.1.3 Impact of the integrated stress response on Kns1 regulation

While global translation is reduced when eIF2-GTP availability is decreased, specific mRNAs are better translated under these conditions (Gebauer and Hentze 2004). One example is *GCN4*, which has four upstream ORFs that usually maintain translation at a minimum level (Hinnebusch and Natarajan 2002). When the availability of the ternary complex is reduced upon stress, leaky scanning of the uORFs occurs (Hinnebusch *et al.* 2016), and the *GCN4* ORF may be translated. This enhances the amount of Gcn4 under stress conditions, where it activates the transcription of stress-responsive genes. This process is known as integrated stress response. Regulation mediated by eIF2 availability gave rise to Kns1 being a target of Gcn4 within the integrated stress response. Gcn4 could directly or indirectly regulate Kns1 expression and activity in response to stress via eIF2. The data presented in this study showed that Kns1 protein levels in *Δ326* background were dependent on Gcn4. The *Δ326* mutant, which included activated ISR, showed high levels of Kns1, as previously described. Under these conditions, Gcn4 expression increased. When *GCN4* is deleted from this background, the Kns1 response is reduced. This suggested that Gcn4 is involved in the stress-dependent increase in Kns1 protein levels. This was also true for Kns1 activity. Under conditions where the ISR was active and global translation initiation rates decreased, phosphorylation of Rpc53 increased. However, this effect was lost when Gcn4 was deleted, indicating a direct correlation between Kns1 expression and activity under these conditions. In contrast, previous data from Wojciech (2020) revealed that *KNS1* mRNA levels were Gcn4-independent. It must be noted that the RNA sequencing data were obtained from the S288C background, whereas this study was performed in W303. However, considering that *KNS1* mRNA reads are independent of Gcn4, precluding direct transcriptional regulation, Gcn4 may play an indirect role in Kns1 regulation. Presumably, one or multiple targets of the Gcn4 response are directed to modify Kns1 post-translationally to alter its expression and activity. Phosphorylation of Kns1, for example, could increase its stability and activate kinase function, leading to an increase in Kns1 protein levels and an increase in Rpc53 phosphorylation level. If this activation mechanism is mediated by the targets of Gcn4, deletion of Gcn4 may have broader effects.

In summary, regulation of *KNS1* gene expression is likely to occur in multiple layers. *KNS1* transcription is increased under non-favourable conditions, most likely regulated by transcription factors. A carbon source-responsive element could be included in the 5' region of *KNS1* and target transcription factors to the gene in response to nutrient stress. The detected Gcn4-dependency and Kns1 protein increase under ISR conditions, however, seem to be an indirect effect, as *KNS1* mRNA levels are independent of Gcn4 in the S288C background. Gcn4 could, therefore, be relevant for activating Kns1 protein under stress conditions. Additionally, the transcription factor Cat8 was not required for nutrient-dependent transcription of *KNS1*. However, the expression of Kns1 under unfavourable conditions was indirectly Rpd3-dependent. It is likely that Rpd3 mediates increased Kns1 expression under glucose-starved conditions by releasing acetate from other histones. This free acetate can then be recycled by the SAGA complex to acetylate histones on *KNS1*, thereby activating it, even when nutrients are sparse. In addition to the transcriptional layer, the regulation of Kns1 expression at the translational level is likely. A slight increase in mRNA levels may not be sufficient for a significant increase in protein levels under stress conditions. An increase in translation mediated by uORFs in a mechanism similar to *GCN4* is possible, albeit not yet unveiled.

5.2 The regulatory role of the N-terminal domain in protein localisation and activity

The regulation of proteins at the post-translational level is of similar importance as transcriptional and translational regulation. Protein abundance and activity should be tightly controlled to maintain proper proliferation rates and to adapt quickly to changing environments. It is striking that Kns1 contains a long N-terminal domain, but with no function yet annotated and no predicted structure (Jumper *et al.* 2021; Varadi *et al.* 2022). The most likely unstructured, disordered region could play an essential role in regulating Kns1 function, as the C-terminal domain includes a catalytic function. Even more persuading is the fact that two of the three annotated NLSs are located in the N-terminal domain (NTD), contributing to the localisation of Kns1 (Kosugi *et al.* 2009). Most LAMMER kinases analysed to date have also shown NLSs in the N-terminal domain (Martinez Marshall 2011). This could further hint towards the evolutionary conservation of nuclear localisation. To evaluate the localisation patterns, different fragments of Kns1 protein were analysed in this study and revealed a mostly nuclear localisation for the whole protein regardless of its catalytic activity (section 4.5.1). The catalytic domain alone was not able to localise to the nucleus and showed a uniform distribution of proteins in the cytoplasm. Both NLSs within the NTD were able to shift a large amount of Kns1 into the nucleus, but its localisation was not exclusive. The proportion of nuclear proteins for both NTD fragments was lower than that for full-length Kns1. This strongly suggests a combined function of both NLSs for substantial and fast nuclear localisation, while both sequences alone are sufficient for nuclear localisation. A similar mechanism was present for Maf1 localisation. Maf1, also a target of TORC1 and a negative regulator of RNA Pol III, inhabits two distinct nuclear localisation sequences, both of which are necessary for proper localisation (Moir *et al.*

2006; Wei *et al.* 2009; Wei and Zheng 2010; Moir and Willis 2013). Under optimal conditions, the phosphorylation of two amino acids close to the N-terminal NLS leads to cytoplasmic translocation. This phosphorylation switches the NLSs off and Maf1 is exported from the nucleus, thereby losing its targets. A process similar to that of Maf1 regulation may be plausible for Kns1. The two distinct NLSs in Kns1 work together for fast and precise localisation to the nucleus. Post-translational- modifications can regulate the activity of these NLSs in response to varying conditions. Kns1 localisation was evaluated in different carbon sources to address potential localisation changes under varying conditions. While the protein levels increased under non-glucose conditions (section 4.2.2), the localisation pattern did not change (section 4.5.1). Both NLSs are necessary under non-fermentative conditions. Interestingly, the fragment of Kns1 containing NLS(175-185 aa) showed a more drastic increase in expression under non-fermentative growth conditions compared to the fragment with NLS(8-39 aa). This suggests a more prominent role of the second NLS under non-glucose conditions, although both NLSs are still required for their full potential. The negative effect of Kns1 on RNA Pol III activity and, therefore, cell proliferation, was confirmed when studying toxicity. Strong overexpression of the catalytic domain of Kns1 was correctly localised within the nucleus using the NLS(175-185 aa), which led to highly toxic effects similar to those of full-length Kns1. With these almost inviable effects, it was assumed that regulation of localisation is required to inactivate the high anti-proliferative potential of Kns1 under favourable conditions.

Similar to Maf1, Kns1 contains many phosphorylation sites, some of which are close to the two NLSs. As described above, phosphorylation close to the NLSs of Maf1 leads to inactivation of these sequences, translocating Maf1 from the nucleus to the cytoplasm (Sidorova *et al.* 1995; O´Conalláin *et al.* 1999; Sidorova and Breeden 2003). Hence, regulation through the phosphorylation of Kns1, depending on nutrient availability, is likely. Several LAMMER kinases are regulated by autophosphorylation (Lee *et al.* 1996). In a study by Martinez Marshall (2011), nine specific autophosphorylation sites were characterised, which further suggested a regulatory function of autophosphorylation. In this study, autophosphorylation was tested in the overexpression context. Kns1 phosphorylation is dependent on its catalytic activity *in vivo* (section 4.5.2). While little phosphorylation was also detected with the kinase dead variant of Kns1, the main proportion was only measured with catalytically active Kns1. This finding suggests the importance of autophosphorylation in Kns1 regulation. The localisation of Kns1 might be dependent on autophosphorylation close to NLSs to inactivate them.

It is also possible that autophosphorylation serves as priming phosphorylation for TORC1-dependent phosphorylation at other sites or that TORC1-dependent phosphorylation acts as a priming phosphorylation for autophosphorylation, which together inactivates Kns1 activity, not only by blocking its translocation to the nucleus but also inactivating catalytic function or target recognition. A possible shuttle mechanism with the option to switch NLSs on and off could include the help of importins or exportins. An important mediator of the translocation of many proteins is

Msn5 (Kaffman *et al.* 1998; Schüller 2003). The exportin Msn5 is known to regulate the localisation of Mig1 in response to carbon sources. It interacts with the phosphorylated transport domain of Mig1, thereby exporting the protein from the nucleus. Msn5 also functions as an importin for other proteins. Preliminary data from the group, not depicted in this study, however, revealed that deletion of *MSN5* does not change Kns1 localisation. A nutrient-dependent shuttling mechanism for Kns1 localisation is most likely Msn5-independent.

Additionally, a possible regulatory effect of (auto)phosphorylation on Kns1 is its catalytic inactivation. With an unknown function of the long N-terminal domain, it was hypothesised that the NTD might play an inhibitory role by interacting with the catalytic domain. A possible physical contact can inhibit or block the catalytic centre for the substrates. This interaction might also be regulated by Kns1 phosphorylation. To validate this hypothesis, a yeast-2-hybrid was conducted to visualize the physical contact between the NTD and CTD of Kns1 (section 4.5.4). The data presented in this work revealed an interaction between these two Kns1 sub fragments. It is still unclear whether this interaction is *in cis* or *in trans*; however, physical contact is likely. A potential negative regulatory role of the NTD was also supported by a study on human CLK1 kinase (Menegay *et al.* 2000). The NTD of CLK1 was found to be responsible for the inhibition of catalytic activity, as a truncation of said domain led to a significant increase in CLK1 activity. Furthermore, a destabilising effect of the NTD of Kns1 was established, as all fragments of this study containing the NTD were significantly lower in protein abundance than fragments without the NTD, even when overexpressed by the constitutive promoter *TEF2* (Figure S 7). Inactivation of Kns1 by self-interaction mediated by (auto-)phosphorylation can lead to destabilisation of the protein. By this mechanism, protein levels and activity would be downregulated simultaneously, ensuring a high proliferation rate under growth conditions. When Kns1 is required under non-glucose conditions, fast activation of the protein is possible by inhibiting the destabilising function of the N-terminal domain via dephosphorylation, without extra effort to synthesise new proteins when nutrients are sparse. This activates the catalytic function, and a fast response is possible.

5.3 Protein turnover and instability of Kns1

Proteins are essential for several cellular processes and functions. Unsurprisingly, cells have developed multiple mechanisms to adapt to changing conditions (Pilla *et al.* 2017). Maintenance of a healthy proteome is crucial, and many pathways are involved. These are commonly known as protein quality control (PQC). Although protein synthesis is a tightly regulated multi-step process, it is also slow and not perfectly suited for the adaptation of the proteome to fast-changing conditions. Protein degradation is a quicker way to regulate protein availability which simultaneously ensures correct folding at the same time. Additionally, the interdependence of protein synthesis and degradation regulates the concentration of proteins within each cell (Grandi and Bantscheff 2019). Hence, protein degradation systems are as important as protein synthesis. PQC consists of two processes: the ubiquitin-proteasome

system (UPS) and autophagy. Both processes require polyubiquitin chains to recognise degradation targets (Lu *et al.* 2017; Pilla *et al.* 2017). The UPS then utilises the 26S proteasome, consisting of the regulatory particle and the core particle (Hershko and Ciechanover 1998; Budenholzer *et al.* 2017). This process is essential for the degradation of many soluble proteins in the cell, most of which are short-lived (high turnover rate), allowing a rapid change in abundance when necessary. Autophagy is a non-essential- process, mostly utilised under nutrient starvation, where the autophagosome fuses with the vacuole and degrades large protein complexes or aggregates (Nakatogawa *et al.* 2009).

The low protein abundance of Kns1 under glucose conditions suggests that it is a rather unstable protein. Furthermore, the analyses of the regulatory function of the NTD indicated a destabilising function (section 5.2). To unravel the underlying mechanisms, Kns1 turnover and possible degradation pathways were analysed in this study. To study protein stability, a translational block was used to inhibit protein synthesis. Cycloheximide, first isolated from *Streptomyces griseus*, is commonly used to inhibit eukaryotic translation (Cooper and Bossinger 1976; Schneider-Poetsch *et al.* 2010). Even though it is still not completely clear how the substance works, it strongly blocks translational elongation by binding to the ribosome and inhibiting translocation. Blocking protein synthesis and analysis of Kns1 levels in a time series revealed a rapid loss of Kns1 (section 4.5.5). Both tested backgrounds, WT and *Δ326*, showed a drastic drop in protein abundance 30 min after the inhibition of protein synthesis. This strongly suggests that the half-life of Kns1 is below 30 min. This indicates that Kns1 is a very unstable protein, and that the basal level of Kns1 should be kept low. As Kns1 has an anti-proliferative function by reducing overall transcription by RNA Pol III, this instability could help maintain pro-growth conditions within the cells. Other regulators of cell proliferation, such as cyclins and transcription factors, are often short-lived proteins that ensure a fast response to changing stimuli. While Kns1 protein abundance increased significantly in non-glucose carbon sources, stability was not significantly increased. The cycloheximide shutoff only showed a slight trend towards a longer half-life of Kns1 in glycerol, but the effect was highly dependent on an accurate CHX block and varied with experiments. Nevertheless, the slight tendency suggested that an increase in stability under glycerol conditions might influence the protein abundance in parts. With an overall assumed short half-life of Kns1 of less than 30 min, a fast degradation pathway must be responsible for this, which could also be a part of the upregulation under different stress conditions.

Specific degradation of Kns1 via the UPS was more likely, assuming that Kns1 remained soluble and was exported to the cytoplasm when not needed. Autophagy, although mediated by TORC1, only degrades larger aggregates, and there is no evidence that Kns1 can form such aggregates. As stated above, the UPS requires targeting by polyubiquitin chains. The protein sequence of Kns1 was analysed to identify consensus sequences for ubiquitination. A ubiquitinated D-box or KEN box can be recognised by the anaphase promoting complex/cyclosome (APC/C) and can serve as a motif necessary for substrates of the proteasome (Jadhav and Wooten 2009). The minimal

consensus sequence for a D-box is R-A/T-A-L-G-X-I/V-G/T-N, whereas the KEN box comprises the amino acid stretch, K-E-N-X-X-X-N. Both motifs can be recognised by Cdh1 or Cdc20 to recruit the APC/C complex for ubiquitination. However, no motifs were present in Kns1. Nevertheless, the involvement of the APC/C-Cdh1 complex was tested in this study and it was revealed that an overactive APC/C-Cdh1 complex was not sufficient to facilitate the degradation of Kns1 (section 4.5.5). Another possible mechanism for predicting protein stability is the N-end rule, which suggests that the half-life of proteins correlates with their N-terminal amino acid residues (Jadhav and Wooten 2009). Stabilising amino acids include methionine, serine, alanine, threonine, valine, and glycine, and are usually enriched in the N-terminal domains of proteins with a half-life of over 20 h. Destabilising amino acids include phenylalanine, leucine, aspartic acid, lysine, and arginine in the N-terminus, and are most often enriched in proteins with half-lives of 3 min or less. Calculating the destabilising residues in the NTD of Kns1 and comparing the amino acid frequencies in the NTD with those of the full-length protein led to enrichment ratios of < 1 for all destabilising amino acids (Table 45). This suggests that the residues are not enriched in the N-terminus of Kns1, and therefore, the NTD might not be able to destabilise the protein via the N-end rule. However, it is unclear what contribution the NTD plays in destabilising the Kns1 protein, and this part of the puzzle remains to be solved.

The contribution of the APC/C complex could not be detected in this study, whereas the involvement of the 26S proteasome in Kns1 degradation is highly likely. Analyses using the proteasome inhibitor MG132, while simultaneously blocking new protein synthesis with cycloheximide, revealed carbon source-dependent degradation via the UPS (section 4.5.5). Blocking proteasomal degradation helped to stabilise Kns1 under glucose conditions for approximately 10 min, until degradation resumed, most likely via an alternative pathway. Surprisingly, the high turnover of Kns1 was stabilised under non-fermentative conditions to a large degree for over 90 min. This clearly shows that the 26S proteasome is involved in the degradation of Kns1, probably in a carbon source-dependent manner, as previously described for other proteins (Gancedo 2008). For example, FbPase and Mdh1 are degraded in a glucose dependent manner. It has been proposed that vacuolar proteases and UPS are involved in the degradation of these two proteins. This furthermore gives rise to the possibility that other degradation mechanisms, e.g. vacuolar proteases, could still play a minor role in reducing Kns1 protein abundance under favourable conditions. Vacuolar-dependent degradation is supported by components of TORC1, Tco89, and Tor1, which are located at the membrane of the vacuole (Loewith and Hall 2011). The system is mostly active in starved cells after glucose repletion and can support the fast degradation of Kns1 after its function is required under starvation conditions. It is conceivable that a combination of vacuolar degradation and degradation via the UPS is required to maintain low Kns1 protein levels under all different stress conditions, such as non-fermentable carbon sources and starvation.

5.4 Metabolic regulation of Kns1 protein expression

Metabolic regulation in response to different nutrients is a key aspect of growth control (Broach 2012). As metabolic flow generates energy to create macromolecules for synthesis and helps to create molecules for cell division, it is of great importance for cells to adapt their activity in response to the available nutrients. Carbon source availability is a major aspect of this process. The yeast cells exhibited a hierarchical pattern of carbon source consumption. Glucose and fructose are favoured and used whenever possible. Other mono-, di-, and trisaccharides, such as sucrose, raffinose, and trehalose, are utilised less favourably. All carbon sources that must be catabolised by oxidative phosphorylation, such as glycerol, ethanol, or acetate, will only be used if not otherwise possible. This hierarchy is maintained by the inhibition of oxidative phosphorylation in the presence of glucose. Key enzymes of glycolysis and gluconeogenesis are blocked, and a transcriptional network of glucose repression is used. Even though energetically unfavourable, yeast keep up with the fermentation of glucose to ethanol under aerobic conditions, also known as the Crabtree effect. Multiple hypotheses have been proposed to explain why yeast uses fermentation; the reason behind this remains unsolved. However, it has been reported that protein phosphorylation patterns and transcription levels are rapidly altered when carbon sources are changed from non-fermentable to glucose. Metabolic reprogramming also occurs after glucose depletion. Regulation of these signalling networks in *S. cerevisiae* is a key advantage for fast metabolic, proliferative, and transcriptional reprogramming.

Using the diauxic shift, the most natural shift from fermentation to oxidative phosphorylation was analysed. Growing cells through the diauxic shift when the stress response is activated, and cells undergo metabolic reprogramming, show that Kns1 protein levels are increased in late diauxic phases (section 4.2.1). A gradual increase in the protein level over time indicated that the expression of Kns1 only slowly adapted to changing conditions. It is not a quick burst of Kns1 protein but rather an adaption with time. The longer the cells grew, the more Kns1 accumulated in them. Regulation of multiple layers, most likely at the transcriptional and translational level, is possible, as described in section 5.1. Under these physiological conditions, a simple increase of protein by stabilisation seemed not to be the only regulation, as a block of degradation would not take four hours to be present. Metabolic reprogramming that occurs during a diauxic shift could also affect *KNS1* transcription. An increase in transcription rates and thereby higher mRNA levels could in total lead to a stronger protein expression in the end (section 5.1.1). It is also conceivable that cells do not increase protein levels too drastically, even with a slight shift in carbon source availability, to ensure a high rate of transcription by RNA polymerase III as long as possible. When glucose levels are depleted completely, a change in Kns1 expression, and thereby inactivation of RNA Pol III function, seems to be sufficient to retain energy. This was also correlated with the Rpc53 phosphorylation patterns. The dynamics of Rpc53 phosphorylation, in contrast to Kns1 protein, are different (section 4.2.1). Phosphorylation levels remained low, with a WT-like level for over two hours until a certain threshold of Kns1 protein was reached. Only when sufficient Kns1 is present and activated, Rpc53

phosphorylation increases. The levels rise quickly, taking only one proper cell cycle until the maximum proportion of phosphorylation is reached. This process is likely supported by Mck1, as Kns1 was proposed the priming kinase by Lee *et al.* (2012). A further increase in Kns1 level after the maximum phosphorylation of Rpc53 is reached does not alter the proportions, as only priming phosphorylation is dependent on Kns1 and later hyperphosphorylation to the maximum level is Mck1-dependent. It has also been suggested that there is an excess of Kns1 due to a delay in its activation process and due to a fast turnover rate of the protein (section 5.3). While it is clear that a stress response takes place during the diauxic shift (Hinnebusch and Natarajan 2002; Crawford and Pavitt 2019), it is not straightforward to detect the influence of ISR components on Rpc53 phosphorylation and RNA Pol III activity. Phosphorylation levels were especially dependent on the presence of Gcn2 and Gcn4. A block of ISR directly led to a reduction in the proportion of phosphorylated proteins in the late diauxic phases. This indicates that the function of Kns1 is dependent on ISR in the diauxic shift. Without the activation of Kns1, most likely by Gcn4, Rpc53 cannot be inhibited. Interestingly, glucose starvation leads to translational inhibition, independent of eIF2α phosphorylation, and this process occurs in less than 1 min, as reported by Ashe *et al.* (2000). eIF2α phosphorylation increases only at a later stage. A similar pattern was also observed in the diauxic shift in this study. Rpc53 phosphorylation, mediated by an increase in Kns1 expression, most likely in response to reduced translation initiation, increased before eIF2α was phosphorylated (Figure S 10). Inhibition of translation independent of eIF2α phosphorylation could still activate the ISR and thereby regulate Kns1 expression and activity during the diauxic shift. One possible explanation for Gcn4-dependent regulation during diauxic shift is that *KNS1* is a direct target of Gcn4, like many other stress-responsive genes. Furthermore, it is possible that Gcn4 is involved indirectly, for example, in the activation of phosphatases that dephosphorylate and thereby activate Kns1 in a late diauxic shift.

Furthermore, in this study, the influence of different carbon sources on Kns1 expression and activity was tested in a steady state as an indicator of changes in metabolic reprogramming, similar to diauxic shift conditions (section 4.2.2). Glucose was used as the preferential carbon source, raffinose as a less favoured carbon source, and glycerol was utilised only in oxidative phosphorylation. These three conditions yielded interesting results. Despite being catabolised differently, raffinose and glycerol showed similar effects on Kns1 protein levels and phosphorylation of Rpc53. In both unfavourable conditions, the protein level of Kns1 increased significantly and phosphorylated proportions of Rpc53 shifted to a maximum. The effects were strong and resembled those observed during the diauxic shift. This suggests that the input coordinated during the diauxic shift is most likely also carbon source. Other nutrients, such as nitrogen availability, were not analysed in this study and could influence the regulation, too. However, carbon source availability is one of the major nutrient limitations a cell can encounter. Localisation studies revealed that activation of Kns1 may play an important role in its regulation, as the localisation was not changed in

different carbon source backgrounds (section 4.2.2). Kns1 is mainly localised in the nucleus, and its nuclear proportion is stable under different conditions. The potential integration of the carbon source is a stress response via eIF2. Translational capacity is reduced in response to nutrient deficiencies, leading to an increase in specific stress response factors (Pakos-Zebrucka *et al.* 2016; Costa-Mattioli and Walter 2020). As described previously, this study used the *Δ326* mutant to simulate eIF2-specific responses. The reduction of translational rates under non-favourable conditions, however, did not influence the expression of Kns1 (section 4.2.2). The carbon source regulated Kns1 expression and activity; however, a reduction in translation did not add to this effect. This indicates that the carbon source, as a nutrient stimulus, is an upstream regulator. Translation initiation is reduced under unfavourable conditions, and an additional eIF2-dependent reduction is not necessary. As mentioned above, Ashe *et al.* (2000) suggested a reversible inhibition of translation by glucose depletion which is independent of eIF2 phosphorylation, which could potentially also play a role in Kns1 regulation under non-glucose conditions. Furthermore, analysis of ISR mutants lacking Gcn2 or Gcn4 underlined a regulation of Kns1 expression, independent of eIF2α phosphorylation, but Gcn4-dependent. The carbon source adaptation of Kns1 in this study appears to involve a fast translational change that can be mediated by eIF2α phosphorylation or other influences on translation initiation which finally leads to Gcn4 activation. To narrow down the pathway activated by different carbon sources and that regulates Kns1 expression and activity, different mutants were used to simulate a block in glycolysis. Glycolysis, as the major process of metabolic flux, could play an important role in integrating non-glucose signals to regulate processes throughout the cell. PKA is mainly influenced by glycolytic flux, mediated by Ras, and a change in cAMP levels. A possible connection between the metabolic flux and transcription by RNA Pol III is plausible. Blocking glycolytic flux at two key steps (*Δhxk2* and *Δpfk2*) resulted in a similar increase in Kns1 expression as inhibiting the translation rates via eIF2 (section 4.2.4). The rise in Kns1 levels and activity is not as strong as in non-favourable conditions, yet it shows an influence of metabolic flux on the regulation of Kns1. An analysis with a promoter construct of *KNS1* revealed that only a small amount of the significant change under non-glucose conditions was accounted for by the promoter region. A regulation that takes place beyond the promoter is thereby proven (section 5.1). Post-translational modifications that stabilise or activate Kns1 under conditions other than glucose may be important mechanisms for increasing the response.

Additionally, a response at the transcriptional level indicates a slower accumulation of proteins (Grandi and Bantscheff 2019). To verify the kinetics of Kns1 expression, the subsequent activation of the Rpc53 phosphorylation time series was analysed. The data shifting from glucose to non-favourable carbon source revealed a gradual increase in Kns1 over time (section 4.2.3). This is similar to the graduality during the diauxic shift, as previously described. This slower increase in protein levels showed that the response acts over time and not instantly. This finding supports the idea that transcriptional reprogramming leads to an increase in protein levels. Similar to the

diauxic shift, Rpc53 phosphorylation shifts after a certain threshold for carbon source exchange. When sufficient Kns1 is expressed and activated, the phosphorylated proportion increases and reaches a maximum shortly thereafter. The catalytic activity of Kns1 as a priming kinase for Rpc53 was supposedly high. A drastic contrast is the switch from unfavourable conditions to glucose. The inactivation of Kns1 is quick. The protein could barely be detected after 30 min which suggested a very high turnover of Kns1, as described in section 5.3. The protein is rapidly degraded and has high turnover rates. This is in line with the assumption that Kns1 must be kept at a very low level under pro-proliferative conditions to maintain transcription by RNA Pol III. When the stabilising effect, most likely consisting of an increase in transcription and a reduction in post-translational modifications, is removed, Kns1 levels decrease to a minimum to restore the normal synthesis rates. In contrast, the phosphorylation of Rpc53 persists longer when glucose is returned as the sole carbon source. This is because the modifications must be specifically removed. Therefore, it is likely that a phosphatase must first be expressed to dephosphorylate Rpc53 after the switch is completed. It is not described in the literature before which phosphatase targets Rpc53 and this remains to be solved.

Another well-known signal transductor for nutrient inputs, especially glucose, is the AMP kinase Snf1 (Broach 2012). Snf1 inactivates the repressor of glucose-repressed genes under glucose-deficient conditions, thereby activating the response to change from fermentation to oxidative phosphorylation. Kns1 is also a part of a regulatory process that changes from fermentation to respiration. It is also known that Snf1 is influenced by TORC1 activity, linking the AMPK pathway to Kns1 regulation. Snf1 might play a role in phosphorylating targets that are necessary to activate Kns1 under unfavourable conditions. In contrast, *KNS1* could also be a glucose-repressed gene repressed by Mig1 under normal conditions and is preferentially expressed under non-glucose conditions. The analysis in this study revealed that activation of Snf1 under glucose conditions led to a significant increase in Kns1 expression and activity (section 4.2.4). It is not yet explained if this is due to a direct catalytic function of Snf1 on Kns1 or if it's an indirect regulation via derepression of glucose repressed genes, but it can be stated that Kns1 is regulated via Snf1. An alternative regulatory pathway could be that active Snf1 directly phosphorylates Kog1, the regulatory subunit of TORC1 (González and Hall 2017). This would lead to the dissociation of Kog1 from the complex and inactivation of TORC1. This, in turn, increases Kns1 protein levels and leads to an increase in Kns1 activity.

5.5 Regulation of Kns1 via TORC1

TORC1 is a major regulator of cell growth and is conserved among eukaryotes (Broach 2012). In *S. cerevisiae*, TORC1 responds mainly to environmental stimuli and nitrogen quality. TORC1 activity is diminished upon nitrogen starvation. An increase in nitrogen or intracellular amino acid levels leads to an increase in TORC1 activity. The nitrogen levels are mostly linked to TORC1 by the EGO complex. The downstream response of TORC1 is mediated by two distinct pathways: protein kinase Sch9 and protein phosphatase 2 A (PP2A). Sch9 directly connects TORC1 activity to growth. PP2A is regulated by Tap42, which is phosphorylated and bound by TORC1. Upon starvation and inactivation of TORC1, Tap42 is released along with PP2A complexes. Tap42 may act as a positive regulator and direct PP2A to specific targets. It also regulates itself by dephosphorylating Tap42, thereby inactivating PP2A targeting. Both effector pathways are necessary for the modulation of phosphorylation patterns and growth adaptation in response to nitrogen levels.

Another effector kinase of TORC1 is Kns1, with only little known about its regulation (Martinez Marshall 2011; Lee *et al.* 2012; Padmanabha *et al.*). However, the mechanisms by which TORC1 regulates Kns1 remain unclear. This study addressed changes in Kns1 expression and activity in response to altered TORC1 activity. Rapamycin treatment, which inhibits TORC1 function, resulted in a gradual increase in Kns1 protein levels over time. After one hour already a large increase was detected, which was sufficient to shift the proportion of Rpc53 phosphorylation to a maximum level. While the *Δ326* mutant started with a higher Kns1 expression level compared to the WT, as described in section 4.3, the steady increase after inhibition of TORC1 was similar. After two hours of treatment, Kns1 levels increased in a similar manner. This was also true for Kns1 activity, as Rpc53 phosphorylation was increased to a maximum in both WT and *Δ326* cells in the same manner. Therefore, regulation by TORC1 seems to be independent of regulatory mechanisms via eIF2, and supports the idea that TORC1 is the major regulator of cell growth (Hall 1996; Loewith and Hall 2011; González and Hall 2017; Battaglioni *et al.* 2022).

Additionally, this study aimed to unravel the effects of nutrient input on TORC1 and its regulatory effects on Kns1. TORC1 integrates many different nutrients and environmental signals through various signalling pathways. However, the integration of glucose as a signal has not yet been completely solved, and Kns1 may be a potential target for this. As described in section 4.3, Kns1 is strongly regulated by changing the availability of carbon sources. Additionally, the inhibition of TORC1 function under different carbon source conditions revealed interesting findings. While changing carbon sources expectedly increased Kns1 expression and activity drastically, inactive TORC1 could not further enhance this effect under non-glucose conditions. Under unfavourable conditions, TORC1 is already shut off, so further inhibition cannot change its expression. These findings strongly suggest the integration of carbon source signals by the TORC1 pathway with Kns1 as the negative effector kinase to regulate anti-proliferative conditions to save energy and resources. Similar results were detected for

the inactivation of TORC1 partially by deleting the catalytic subunit Tor1 (section 4.3.2). Tor2, which has a homologous function as the catalytic subunit, cannot resolve TORC1 function under non-preferred conditions. This further suggests that the downregulation of TORC1 by unfavourable carbon sources is a major regulatory signal.

It is conceivable that the full potential of Kns1 regulation lies in a combination of protein increase via eIF2 and TORC1; both pathways are likely influenced by nutrient availability as the main stimulus, leading to a gradual increase in Kns1 expression. A global reduction in translational capacity via eIF2 regulates Kns1 protein expression, for example, by an increase in transcription mediated by Gcn4 or other nutrient-specific transcription factors. TORC1 most likely integrates nutrient signals into post-translational modifications of Kns1, which regulate its activity, stability, and localisation. All processes display a critical interplay between fast and slow options to adapt Kns1 expression to changing conditions. Rapid changes in post-translational modifications, such as phosphorylation, could display the first response to nutrient changes, followed by a lasting effect at the transcriptional and translational levels.

5.6 Proposed model for Kns1 regulation

In summary, it can be stated that Kns1 is a novel regulator that integrates nutrient signals via multiple pathways (Figure 5.1). Kns1 is regulated by transcription, translation, protein activity, localisation, and degradation. Multiple layers of regulation are integrated via different pathways. Under glucose conditions, the carbon source acts as a signal molecule. This leads to high availability of eIF2 for translation initiation induced by high glycolytic flux and optimal nutrient conditions. These high initiation rates block Gcn4 translation, thereby inhibiting the ISR. Additionally, the AMPK pathway via Reg1-Snf1 is blocked. Under optimal nutrient conditions, phosphatase Reg1 and its subunit Glc7 (not depicted) are active. The complex, Reg1-Glc7, then dephosphorylates Snf1, thereby inactivating it. In the third axis, the major regulator of cell proliferation, TORC1, is activated by glucose. This leads to the activation of a variety of effectors and inactivation of Kns1. Kns1 is supposedly phosphorylated by TORC1 either directly or by another intermediate kinase. Additionally, Kns1 is most likely autophosphorylated, thereby further inhibiting itself. These phosphorylations seem to play a crucial role in protein instability, inhibition of NLSs, and thereby, nuclear translocation and auto-inhibition of the catalytic function. With this mechanism, the protein is kept inactive, unstable, and located in the cytoplasm, reducing its negative effect on RNA Pol III activity.

Once the conditions change, glucose is depleted and the network switches. Under unfavourable nutrients, global translation rates decrease. eIF2 is phosphorylated by Gcn2 and thereby diminishing the recycling of eIF2-GDP for ternary complex formation. This leads to an increase in specific translation, such as Gcn4. Gcn4 is favourably translated and can act as a transcription factor to induce the transcription of stress response genes. Gcn4 might not enhance *KNS1* transcription directly, but

indirectly regulate Kns1 protein expression and activity. Kns1 may be dephosphorylated by a phosphatase activated by Gcn4 under stress conditions. However, it is still possible that Gcn4 is directly involved in the increase in *KNS1* transcription in the ISR, as only little data was evaluated. Additionally, a change in nutrients leads to the inactivation of Reg1-Glc7 phosphatase. Through this mechanism, the AMP kinase, Snf1, is activated. Snf1 is known to phosphorylate many targets and regulate gene expression of glucose repressed genes. Regarding the Kns1 regulation, two options are available. Either Snf1 directly phosphorylates Kns1 on activating positions and thereby increases the catalytic function or stability of Kns1 protein, or *KNS1* is a glucose repressed gene that is derepressed by the Snf1-Reg1 pathway increasing the transcription rates under non-favourable conditions. Snf1 also directly phosphorylates Kog1, the regulatory subunit of TORC1, which leads to further inhibition of TORC1 activity. Furthermore, TORC1, a pro-proliferative mediator, is inhibited by non-glucose conditions, an effect that can be simulated by rapamycin treatment. When TORC1 is inactive, many effectors are inhibited. Kns1, however, becomes activated. The negative regulation of TORC1, most likely phosphorylation, is released, and Kns1 protein levels increase. The autoinhibitory function may also be reduced as a direct result of TORC1 inhibition. The activation of Kns1 is supported by its more precise localisation to the nucleus, activation of the catalytic domain, and stabilisation of the protein. This leads to an increase in the phosphorylation of Rpc53, the regulatory subunit of RNA Pol III, which contributes to the inhibition of tRNA and 5S rRNA transcription.

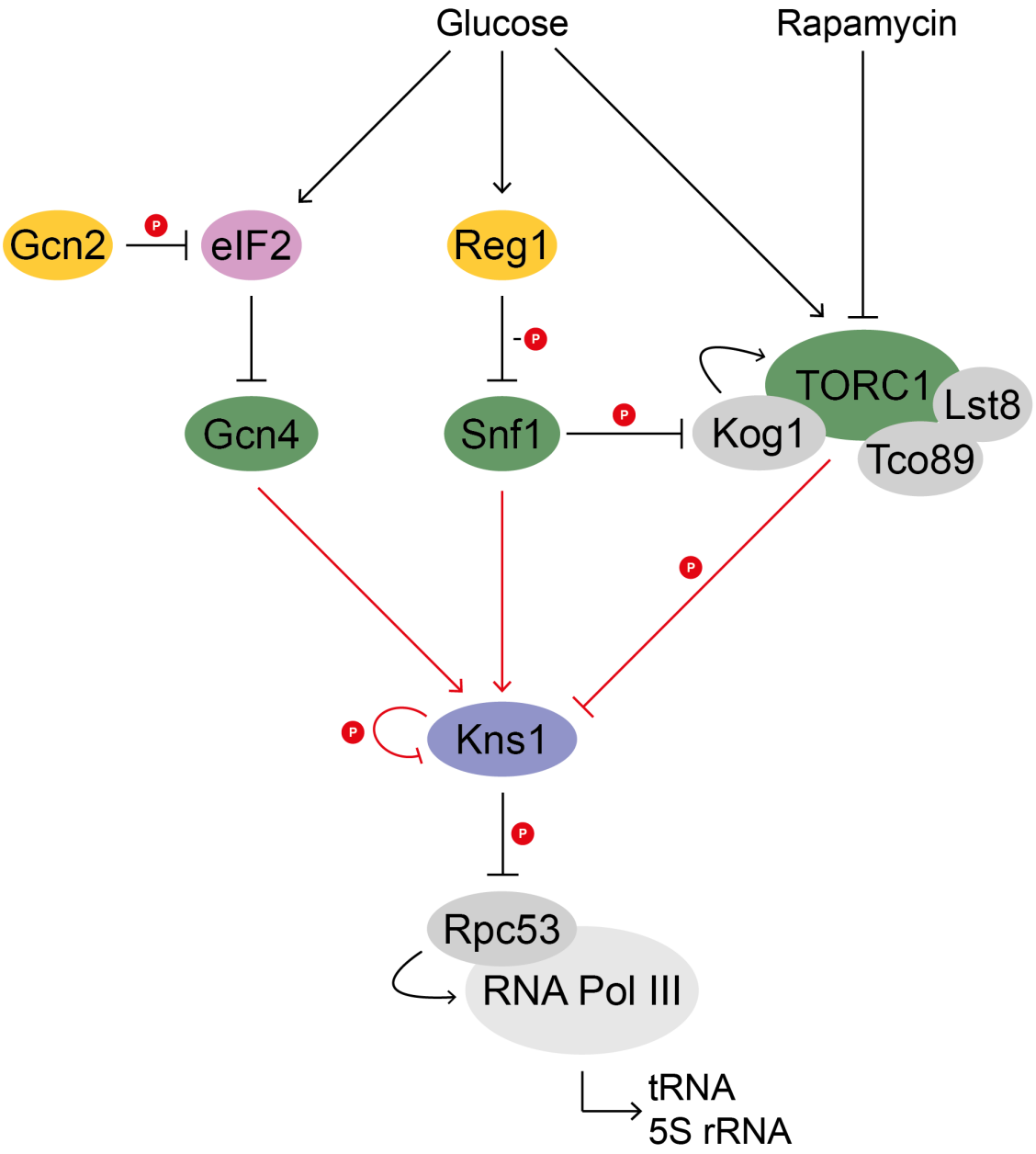

Figure 5.1 Schematic overview of Kns1 regulation.

This scheme shows that the LAMMER kinase Kns1 is the central negative effector of TORC1 that integrates glucose signals. The availability of glucose regulates three pathways that regulate the response: eIF2-mediated translational control, Reg1/Snf1 carbon source response, and TORC1 as the major regulator of cell proliferation. All pathways most likely integrate the signal via Kns1, which is inactive under favourable conditions; therefore, RNA Pol III is active. Bars show inhibitory regulation, and arrows indicate activating connections. Red connections indicate the analyses in this study. The red circles indicate phosphorylation.

6 METHODS

6.1 Working with bacteria

The *E. coli* strain DH5α was used for amplification of *E. coli*- and *S. cerevisiae* shuttle vectors. The relevant genotype is noted in Table 3.

Table 3 Relevant *E. coli* DH5α genotype.

Strain	Genotype
DH5α	*F- φ 80dlacZ ΔM15 Δ(lacZYA-argF)-U169 deoR endA1 gyrA96 hsdR17(rK-, mk+) phoA recA1 relA1 supE44 thi-1 λ-*

6.1.1 Cultivation of DH5α cells

The cultivation of bacteria was performed in LB liquid - or solid media with 100 $\frac{\mu g}{ml}$ ampicillin each at 37 °C.

6.1.2 Transformation of DH5α cells with electroporation

A short pulse of high electricity increases the permeability of the cell membrane and thereby increases the uptake of external DNA (Dower *et al.* 1988). In this project electrocompetent DH5α cells of the working group were used for electroporation.

PCR products or ligated plasmids were dialyzed for 20 min before the transformation. One aliquot of competent cells was defrosted on ice and diluted 1:2 in sterile H_2O. 5 µl of dialyzed DNA was added to half of the diluted *E. coli* suspension. The complete batch was transferred to a cooled electroporation cuvette and the electroporation took place with the following parameters: Field strength 12.5 kV/cm, Resistance 200 Ω, Capacity 25 µF, Capacitor voltage 2.5 kV. The cells were transferred to 37 °C pre-warmed SOC medium right after the electric pulse and further incubated at 37 °C for 30 – 60 min to phenotypically express the β-lactamase gene that encodes for the ampicillin resistance. The selection of positive transformants was performed on LB_{Amp}-plates over night at 37 °C.

6.2 Working with yeast

Data obtained in this work was generated with yeast strains from the W303 background only.

6.2.1 Cultivation of yeast strains in liquid media

The cultivation of yeast cells was performed in XY rich medium with 2 % carbon source (D = glucose, Raf = raffinose or Gly = glycerol for different experimental approaches). Starter cultures were prepared in 5 ml medium and incubated at 30 °C in a rotator over the day. The main cultures were inoculated of the starter cultures and volumes were chosen depending on the experiment (5 ml – 150 ml). The cultures were incubated at 25 °C, or 30 °C for glycerol samples, overnight to reach exponential growth phase (0.4 – 1.5 OD_{600}/ml) the next day.

For expression of genes under the inducible *GAL1* promoter a galactose induction was performed. These strains were inoculated in XY rich medium with 2 % raffinose (XYRaf). The promoter was then induced with addition of 2 % galactose at 25 °C for 2 h.

6.2.2 Storage and conservation of yeast strains

For the routinely use yeast strains were plated on XYD plates and stored at 4 °C. For the conservation of strains 2 ml of overnight cultures in rich medium were harvested, resuspended in 1 ml 15 % glycerol, and stored at -80 °C.

6.2.3 Yeast strain construction

6.2.3.1 Transformation of yeast with the lithium acetate method

The efficiency of DNA uptake into yeast cells is increased by a treatment with alkali-ions, e.g. lithium acetate (Ito *et al.* 1983).

For the transformation of yeast 2 ml of a growing culture were harvested at an OD_{600} of around 0.8. The supernatant was discarded, and the pellet washed in 1 ml sterile H_2O two times. The supernatant was discarded quantitatively once more, and the batch was pipetted directly onto the transformation pellet (Table 4).

Table 4 Transformation batch for lithium acetate method.

Linear DNA, diluted in H_2O	**34 µl**
Herring sperm DNA, diluted 1:5 in 1x TE	50 µl
PEG 3350 50 % (w/v)	240 µl
LiAc 1 M	36 µl
In Total	360 µl

The reaction batch was mixed for 40 sec, then incubated at RT for 20 min in a rotator and lastly incubated at 42 °C for 15 min. The cells were centrifuged at 13200 rpm for 30 sec and the pellet was resuspended in 150 µl sterile H_2O. The cells were plated on a specific selection plate and the final incubation took place at 30 °C for two to three days.

For the transformation of resistance markers, the cells have been incubated in rich medium for 6 h so that the resistance could develop, then harvested at 800 g for 3 min, the supernatant discarded, and the pellet resuspended in H_2O before the cells were plated on selection plates.

6.2.3.2 Integration of plasmid-DNA into the yeast genome

The integration of DNA into the yeast genome is based on homologous recombination. Genome material is exchanged with homologue material at the integration locus. This process is more effective when linear DNA is used. Integrative plasmids were therefore digested with restriction endonucleases to linearize them (section 6.4.6.1) and later a yeast transformation (section 6.2.3.1) was performed. Integration can take place at a specific gene locus or a marker gene. The utilised plasmid systems in this study include pFA6a-, pFA6a-link- and pUG-plasmids described by Longtine *et al.* 1998 and Sheff and Thorn 2004.

6.2.3.3 Epitope fusion and deletion of endogenous sites

Genes of interest can also be marked with epitopes to visualize the endogenous conditions in an approach as close to native as possible. For that homologous recombination is utilised. The wanted epitope is amplified with flanking sequences homologous to the exact position next to the target gene (section 6.4.4.1). The PCR product is then transformed into yeast (section 6.2.3.1) and integrated at the specific site. It is important to ensure a continuous protein synthesis of the target gene together with the epitope. Start codons can be included in the PCR product or stop codons skipped by targeting the epitope upstream of it. When the flanking regions during amplification are homologous to sequences right upstream and downstream of the target gene, the complete gene will be exchanged by the PCR product. By this means a deletion of a gene can be performed.

6.2.3.4 Crossing of haploid yeast strains

Haploid yeast strains of different mating types (*MATa* and *MATα*) can be crossed to generate a new diploid strain. To experimentally select for those diploid cells the initial strains should include different auxotrophies or resistances to antibiotics as selection markers. Then, the cells can be selected on the corresponding double selection plates and only diploid colonies are used for analyses.

For the crossing cell material from an existing colony of each strain was resuspended in 5 µl H_2O. The suspensions were carefully dropped over one another on a XYD plate and incubated at 30 °C for at least 6 h or better overnight. On the next day the diploid cells were selected on fitting double selection plates. After 2 – 4 days of incubation at 30 °C the growing single colonies could be used for sporulation. When a selection was not possible due to same markers, sporulation was started directly from the crossing plate.

6.2.3.5 Sporulation of diploid yeast cells and tetrad dissection

Diploid yeast cells can switch to a meiotic cell division when under carbon- and nitrogen deficiency. In this so-called sporulation a tetrad with four haploid spores develops surrounded by a protective shield, the ascus (Hartwell 1974).

In experimental surroundings this sporulation can be induced by inoculating diploid cells in 2 ml nutrient rich pre-sporulation medium and incubating at 30 °C for at least 6 h or 25 °C overnight. After incubation the cells have been washed in nutrient deficient sporulation medium at 2000 rpm for 3 min and resuspended in 2 ml sporulation medium. The incubation took place in a rotator at 25 °C for 3 – 4 days to complete the sporulation. To separate the single spores of the tetrads, first 50 µl of the sporulation suspension were digested with 50 µl of novozyme solution at room temperature for 19 – 21 min. The ascus was digested and the free spores in tetrads could be dissected by micromanipulation and laid down on a XYD plate. After two to four days at 30 °C the spores were grown to colonies and could be analysed regarding their genotype. For that, cell material of each spore was resuspended in 150 µl H_2O and put on corresponding selection plates of all parental markers. The mating type of the new strains were analysed with a Mating type-PCR (section 6.4.4.4).

6.2.3.6 Growth test of yeast strains using a dilution row

Analysis of growing constitutions of strains under differing conditions, like temperature or media, is important to clarify phenotypes. A 1:10 dilution row (6 dilution steps in total) was prepared in a 96-well microtiter plate starting with a concentration of 1 OD_{600} in 200 µl of an overnight culture. About 3 µl of all dilutions were replica plated on rich media or selective media plates. The plates were then incubated at 25 °C, 30 °C and 37 °C for one and two days until documentation took place.

6.2.3.7 Yeast-2-hybrid

To study physical interactions of proteins a yeast-2-hybrid (Y2H) approach can be used. Each target is fused to a split transcription factor which is used to analyse the expression of reporter genes when both targets are co-transformed.

The used plasmids for fusion of target proteins with the split transcription factor are pEG202, containing the *lexA* DNA binding domain (BD) under control of a constitutive *pADH1*, and pJG4-5, containing the B42 transcription activating domain (AD) under control of the inducible *pGAL1*. Both plasmids are 2µ plasmids which are not stably integrated into the yeast genome. The reporter strain W276 includes two reporter genes: *LEU2* and *lacZ*. Both genes are controlled by *lexA* operator sequences that are only activated by the transcription factor comprised of *lexA* binding domain and B42 transcription activator. When the target proteins bring the lexA binding domain and B42 transcription activator in proximity, a functional transcription factor is assembled. The reporter genes are correspondingly expressed. Growth on SD-Leu plates indicates the activation of the *LEU2* reporter by an intact transcription factor. The *lacZ*

gene (from *E. coli*) encodes for β-galactosidase which can hydrolyse the chromogenic substrate X-Gal and leads to a blue dye as a product (5,5'-dibromine-4,4'-dichlorine-indigo). Therefore, a blue colouring of X-Gal covered plates indicates an interaction of the target proteins, too.

The target plasmids, containing fusion constructs as described above, were transformed into the reporter strain W276 (section 6.2.3.1). Six transformants of each analysed combination (Table 5) were picked for the Y2H and spotted on SD-HT, SD-HTL, SGal-HT and SGal-HTL plates. The incubation took place at 30 °C for 2 days. After that, the colonies on the SGal plates were covered with X-Gal buffer (section 7.3.3) and incubated another day at 30 °C to receive a blue colouring. The dye is intensified when stored at 4 °C after incubation.

Table 5 Analysed combinations of Y2H used in this study.

Approach	lexA-BD fusion	B42-AD fusion
1	lexA-KNS1-NTD(1-289aa)	B42-KNS1-CTD(280-737aa)
2	lexA-KNS1-CTD(280-737aa)	B42-KNS1-NTD(1-289aa)
3	lexA	B42-KNS1-CTD(280-737aa)
4	lexA-KNS1-NTD(1-289aa)	B42
5	lexA	B42-KNS1-NTD(1-289aa)
6	lexA-KNS1-CTD(280-737aa)	B42
7	lexA	B42

The Y2H was performed by Antje Machetanz-Morokane.

6.2.4 Synchronizing the cell cycle of yeast

To study specific cell cycle dependent responses yeast cells can be arrested in the different cell cycle phases.

6.2.4.1 Synchronizing with the pheromone α-factor

The mating of two haploid yeast cells of differing mating types (*MATa* and *MATα*) leads to formation of a shmoo and thereafter fusion of the cells to form a diploid one (Herskowitz 1988). To ensure that both cells are in the required G_1-phase they secrete specific mating pheromones (a-factor or α-factor). The pheromones induce an arrest in G_1-phase in cells of the opposite mating type. Yeast cells that did not mate can degrade the pheromones with help of proteases and are released from the cell cycle arrest.

The pheromone α-factor was experimentally used to arrest *MATa* yeast cells in G_1-phase. The experimentally used strains carried a deletion of the gene *BAR1* which encodes for a pheromone protease. This deletion *(Δbar1*) increases the pheromone sensitivity as cells cannot leave the arrest by degrading the α-factor. Synchronizing experiments were performed with exponentially growing cells (0.4 – 1.5 OD_{600}/ml). The α-factor was added in a concentration of 50 $\frac{ng}{ml}$ (stock solution: 500 $\frac{\mu g}{ml}$ in H_2O) and

the culture was incubated for at least 1 h at 25 °C. Samples for flow cytometry or protein lysates were harvested before and after treatment if not mentioned otherwise.

6.2.4.2 Synchronizing with the acid hydroxyurea

Hydroxyurea functions as an inhibitor of DNA synthesis in *S. cerevisiae* (Doran and Bailey 1986). It activates the S-phase checkpoint mainly by the inhibition of DNA synthesis and therefore blocks cell cycle progression. This occurs due to the deactivation of the enzyme ribonucleotide reductase which produces dNTPs as precursors for DNA synthesis. It was also suggested that reactive oxygen species are produced that lead to cell cycle arrest independent of dNTP synthesis (Shaw *et al.* 2024).

To arrest yeast cells in S-phase 0.1 M hydroxyurea (stock solution: 2 M in H_2O) was added to exponentially growing cells (0.4 – 1.5 OD_{600}/ml). The incubation took place at 25 °C for 2 h. Samples for flow cytometry and protein lysates were harvested before and after treatment if not mentioned otherwise.

6.2.4.3 Synchronizing with the acid nocodazole

Nocodazole is known as an acid that depolymerizes microtubules and blocks nuclear division (Jacobs *et al.* 1988; Monje-Casas and Queralt 2017). Hence, the spindle control system is activated, cells cannot proceed through mitosis and arrest in the early M-phase.

Synchronizing experiments were performed with exponentially growing cells (0.4 – 1.5 OD_{600}/ml). Nocodazole was added in a concentration of 7.5 $\frac{\mu g}{ml}$ (stock solution: 1.5 $\frac{mg}{ml}$ in DMSO) and the culture was incubated for at least 2 h at 25 °C. Samples for flow cytometry and protein lysates were harvested before and after treatment if not mentioned otherwise.

6.2.5 Inhibition of yeast processes

Regulating the processes in yeast is crucial for cell viability and adaption to surrounding conditions. To study the effects of various processes different inhibitory approaches were used in this study.

6.2.5.1 Inhibition of TORC1 activity by rapamycin

The small molecule rapamycin blocks cell cycle progression and simulates a nutrient starved phenotype in *S. cerevisiae* (Hardwick *et al.* 1999; Dobrenel *et al.* 2016). The process involves a binding of rapamycin to the FK506-binding protein, Fpr1 in yeast, and the complex then binds to TOR1/2 to inactivate kinase activity of TORC1 (Dennis *et al.* 1999; Hardwick *et al.* 1999). By this, rapamycin induces a G_1-phase and translation arrest, sporulation, and autophagy and represses rRNA transcription (Hardwick *et al.* 1999; Dobrenel *et al.* 2016).

Studying influences of the master regulator TORC1 were performed by inhibiting its function via rapamycin in a concentration of 200 $\frac{ng}{ml}$ (stock solution: 200 $\frac{\mu g}{ml}$ in DMSO). Cultures were incubated at 25 °C for 1 – 2 h to ensure a full TORC1 block. Samples were harvested in even intervals (e.g. every 30 min).

6.2.5.2 Blocking protein synthesis with cycloheximide

Cycloheximide is a known inhibitor of eukaryotic translation (Cooper and Bossinger 1976; Schneider-Poetsch *et al.* 2010). The drug inhibits protein synthesis by preventing elongation of eukaryotic translation. Cycloheximide interferes with the eukaryotic elongation factor 2-mediated translocation of the ribosome by binding to it. Additionally, it was suggested that the rate of rRNA synthesis remains unaffected for some time even when protein synthesis is already blocked (Popolo *et al.* 1982).

Protein turnover rates were analysed by inhibiting re-synthesis completely with addition of 100 $\frac{\mu g}{ml}$ cycloheximide (CHX stock solution: 20 $\frac{mg}{ml}$ in EtOH). Samples were harvested in even intervals right after cycloheximide addition (e.g. every 30 min).

6.2.5.3 Inhibition of proteasomal degradation by MG132

Small hydrophobic peptide aldehydes have been identified to reversibly inhibit protein degradation by targeting the chymotryptic activity of the proteasome (Lee and Goldberg 1996; Collins *et al.* 2010). One of those is carbobenzoxyl-leucinylleucinyl-leucinal (MG132). While inhibition of the proteasomal degradation via MG132 is highly efficient in mammals, proliferation in *S. cerevisiae* is relatively resistant. Mutations, such as *Δise1*, increase the permeability and uptake of inhibitor molecules (Gaber *et al.* (1989)), but the 20S core could compensate for proteasome function (Collins *et al.* (2010)).

To study protein degradation via the 26S proteasome the inhibitor MG132 was used. To incorporate MG132 into yeast the cell wall must be permeabilized. In the present study this is achieved by using a *Δise1* mutant. To receive a complete block of proteasomal activity 100 µM MG132 (stock solution: 100 mM in DMSO) were added to the cultures and incubated for 30 min at 30 °C. After harvesting the t_0 100 $\frac{\mu g}{ml}$ cycloheximide was added to further inhibit new protein synthesis and increase the stabilising effects. Samples were harvested in even intervals (e.g. every 30 min).

6.3 Fixing, flow cytometry and microscopy of yeast cells

6.3.1 Fixing of yeast cells with ethanol

A fixing of yeast cells with ethanol is possible. 0.25 OD_{600} cells were harvested for this reason. The pellet was resuspended in 150 µl H_2O and 350 µl of 100 % ethanol was added afterwards. The fixed cells can be stored at 4 °C for 1-2 years.

6.3.2 DNA staining with Sytox Green

For an analysis with flow cytometry the DNA must be stained with the fluorochrome Sytox Green. The ethanol fixed cells (section 6.3.1) were washed in 1 ml sodium citrate buffer (50 mM, pH 7.0), resuspended in 250 µl sodium citrate buffer and treated with ultrasound (six pulses with 40 % power) to separate cell clusters. The segregated cells were treated with 10 µl RNase A (10 $\frac{mg}{ml}$) and incubated at 50 °C for 1 h in a thermoshaker with two times manual inversions. After that a treatment with 10 µl proteinase K (10 $\frac{mg}{ml}$) followed. The cells were again incubated at 50 °C for 1 h under constant shaking and inverted two times manually. The cells were then spinned down at 13200 rpm for 1 min, the supernatant was discarded quantitatively and very carefully, and finally the pellet was resuspended in 250 µl of sodium citrate buffer (50 mM, pH 7.0) mixed with 1 µM Sytox Green. The staining was executed for at least two days at 4 °C in the dark.

6.3.3 Flow cytometry

With help of flow cytometry DNA contents of ethanol fixed cells can be measured and cell cycle phases can be analysed. It is a strong tool to see influences of different factors on the cell cycle progression. The analyses were performed on the flow cytometry CyFlow Space by Partec. For that, 5 – 20 µl of a sample were diluted in 1.5 ml Tris/HCl (50 mM, pH 7.5) and about 300 events per second were measured in the channel FL1 (for DNA content) with a gain of 540 (Table 6). The speed was set to 0.6 and 20000 events in total were measured for each sample. Forward scatter (FSC) and sideward scatter (SSC) were also evaluated to check for size and shape of the cells, respectively. The DNA profiles were depicted with the software WinMDI 2.8. For quantification of the percentage of cells in the different cell cycle phases the software FCS Express 6 was used.

Table 6 Constant settings for flow cytometric analyses.

Channel	x-Axis Scale	Gain	Lower Limit	Upper Limit
FSC	log3	100	50	999.9
SSC	log3	230	10	999.9
FL1 (Sytox)	linear	540	10	999.9

6.3.4 Microscopy of living cells at the confocal microscope

To observe the localisation of fluorescently labelled proteins (mostly with GFP or mCherry) in living yeast, cells of a growing (or some cases stationary) culture were harvested for 3 min at 800 g and the supernatant discarded. The harvested cells were resuspended in the remaining medium and 4 µl spread across a cover glass (24 x 60 mm) to distribute the cells evenly. The cells were then covered with a piece of SD++–, SRaf++–, SGly++– or SRG++–agar depending on the used carbon source conditions (Table 7) and a smaller cover glass (18 x 18 mm) to keep them in living conditions during the experiment.

Table 7 Contents of different microscopy agars. The agar was chosen depending on the used carbon source conditions.

Agar	Contents	Volumes (ml)
SD++ or SGly++	0.75 % agarose in H_2O	21.0
	20 % glucose or glycerol	3.0
	10x YNB	3.0
	10x Dropout++	3.0
SRaf++	0.75 % agarose in H_2O	18.0
	10 % raffinose	6.0
	10x YNB	3.0
	10x Dropout++	3.0
SRG++	1 % agarose in H_2O	8.5
	10 % raffinose	3.0
	20 % galactose	0.5
	10x YNB	1.5
	10x Dropout++	1.5

The microscopy took place at the confocal microscope Observer Z.1 with a spinning disc system and an Axiocam MRm at 25 °C. Photos of z-stacks of 14 layers were taken with a distance of 0.6 µm between each layer. GFP-signals were detected with a laser of 488 nm and mCherry-signals were detected at 561 nm. Laser intensities and shutter speed were adjusted for each experiment depending on the signal strength.

To visualize the nucleus, the fusion protein mCherry-NLS was used. The C-terminal region of Swi5 (569 – 709 aa) with mutated Cdk1 phosphorylation sites (S646A and S664A) was used as the NLS. The mutations are important to ensure a correct nuclear import of the protein. Additionally, a MYC13-epitope was added to the C-terminus of the fusion protein, and it was expressed constitutively (*pTEF2*).

The visualization was done with the programs AxioVision LE Rel. 4.8 and ImageJ. To perform quantification analyses the signal intensities were summed up by projecting the z-stacks with maximum intensity and subtracting the background.

Nuclear enrichment levels were calculated to address the nuclear signal intensity in relation to the cytoplasmic levels. For that, the concentration of mean pixels of the

nucleus and cytoplasm were calculated in ImageJ independently. An area of 7 x 7 px was utilised to calculate the mean pixel value for each compartment. The coefficient of those values was then calculated to address the enrichment (Equation 1).

$$Enrichment = \frac{meanPixels(nucleus)}{meanPixels(cytoplasm)}$$

Equation 1 Calculation of nuclear enrichment levels of microscopic data.

The concentration of pixels (meanPixels) in a 7 x 7 px area of each compartment was measured using ImageJ. The enrichment coefficient indicates the portion of nuclear signal compared to cytoplasmic signal.

An enrichment coefficient of ≤ 1 counts for a stronger cytoplasmic signal intensity. A nuclear enrichment of > 1 suggested a stronger signal in the nucleus.

Phenotypic analyses were performed by calculating cell volume and roundness in ImageJ. The volume (V) of cells was calculated using the length (a), width (b) and height (c) of the cells (Equation 2).

$$V = a * b * c * 4/3 * \pi$$

Equation 2 Calculation of volume of cells using the length (a), width (b) and height (c).

Roundness of the cells was also calculated with the given length, width, and height of the cells. The area (A) and perimeter (P) of the cells was calculated first and then added in an equation to calculate a roundness in % (Equation 3). The closer to 100 % the calculation is, the closer to a perfect circle the cells are.

$$R = 4 * \pi * A/P^2 * 100$$

Equation 3 Calculation of the roundness of cells.

The area (A) and perimeter (P) were calculated using the length, width and height of the cells beforehand.

6.4 Genetic and molecular biology methods

6.4.1 RNA isolation from yeast

RNA was isolated with the phenol chloroform method (Holm *et al.* 1986) to study transcription levels and mapping the transcription start site of target genes.

5 OD_{600} of exponentially growing cells (OD_{600} ≈ 0.5 – 0.8) were harvested at 800 g for 3 min for total RNA isolation. The cells were washed in 1 ml cold H_2O (full speed for 30 sec) at 4 °C and the pellet was then carefully resuspended in 400 µl TES solution. 400 µl pre-warmed (65 °C) hot phenol was added to each sample, mixed and the batch was incubated at 65 °C for 1 h in a thermoshaker with manual mixing every 15 min. The samples were immediately cooled on ice for 5 min after the incubation and centrifuged at 4 °C for 5 min at full speed. The upper, aqueous phase was transferred into a new tube and 400 µl phenol was added. After intensive mixing the samples were incubated on ice again for 5 min. A centrifugation at 4 °C with full speed for 5 min took place, the aqueous phase was again transferred into a new tube and 400 µl chloroform was added. Another centrifugation step at 4 °C with full speed for 5 min was performed. The total upper phase was transferred into a new tube for RNA precipitation, 1 ml cold 100 % ethanol and 40 µl sodium acetate (3 M pH 5.3) was added and mixed thoroughly. The precipitation was conducted over night at -80 °C. The next day the samples were spined down for 30 min at 4 °C full speed. The supernatant was discarded, the cells washed with 1 ml 70 % ethanol in DEPC(diethylpyrocarbonate)-H_2O and centrifuged for 30 min at 4 °C full speed once more. The ethanol was then discarded completely, and the RNA was dried for 30 min with an open tube at room temperature. Finally, the RNA was solubilized in 50 µl DEPC-H_2O. The RNA concentration was identified in an 1:10 dilution (section 6.4.2) and the integrity checked on an agarose gel (section 6.4.5).

6.4.2 Determination of DNA and RNA concentration and purity

The concentration of double stranded DNA or RNA was analysed photometrically on a NanoDrop DS-11 FX+ (DeNovix) by measuring the extinction rate at 260 nm. Analysis of the quotient of extinction at 260 nm and 280 nm helped determine the purity level of the samples. Pure samples (with very little protein contamination) showed a value of about 1.8 – 2.0. RNA concentrations were measured in triplicates to ensure correct values for calculations.

6.4.3 Reverse transcription

For the process of reverse transcription mRNA is utilised as a template for the reverse transcriptase, an enzyme that synthesizes a complementary DNA strand (Varmus 1987; King 2010). This cDNA (complementary DNA) can then be used experimentally to study RNA levels in a PCR.

6.4.3.1 Gene-specific first strand cDNA synthesis

For a gene-specific cDNA synthesis, the reverse transcriptase Superscript IV (Invitrogen) was used. Total RNA was diluted to a final concentration of 250 $\frac{ng}{\mu l}$.

Afterwards the RNA was mixed with the gene-specific reverse primer and dNTPs (Table 8). The primer was annealed to the RNA in a thermocycler at 65 °C for 5 min and then immediately cooled on ice for at least 1 min. The reverse transcription (RT) mix was prepared as described in Table 9 and the components added to the samples. For each approach a DNA contamination control without reverse transcriptase was conducted. The reverse transcription was performed in the thermocycler (Table 10) and cDNA could be used for primer extension analysis (section 6.4.4.6).

Table 8 Mastermix for specific primer and RNA.

Contents	Volume (µl)
10 mM dNTP mix (fresh)	1
Gene-specific R-primer 1:10 diluted in H2O (10 $\frac{pmol}{\mu l}$)	1
H_2O	3
2 µg RNA	8

Table 9 Reaction contents for reverse transcription and DNA control (–RT).

Contents	Volume (µl)	Volume (µl) – RT
RNA and primer mix	13	13
5x RT buffer	4	4
Dithiothreitol (DTT) (0.1 M)	1	1
RNAsin Plus (2 $\frac{mg}{ml}$)	1	–
Superscript IV RT	1	–
H_2O	–	2

Table 10 Temperature profile for reverse transcription reaction. RT components are just added after the first incubation step.

Step	Temperature (°C)	Duration
1	65	5 min
2	50	15 min
3	80	10 min
4	8	forever

6.4.3.2 Non-specific reverse transcription

For an unspecific reverse transcription, the QuantiNova Reverse Transcription Kit by Qiagen was used. It contains a mix of oligo-dT and random primers to include cDNA synthesis from all transcript regions. The reaction and contents were utilised as described in the manufacturer's manual. gDNA was eliminated and only very little amount of RNA was applied (50 – 100 ng) to increase the specificity of the reaction. The reverse transcription step was also prolonged to 15 min at 45 °C to ensure a complete synthesis.

6.4.4 Polymerase chain reaction

The polymerase chain reaction (PCR) is a helpful tool to amplify specific DNA-fragments (Mullis *et al.* 1986). Oligonucleotide primers define the amplification region via complementary sequences. The use of a thermostable DNA-polymerase allows exponential amplification of DNA in a PCR thermocycler. Commonly used polymerases are *Taq*-polymerase from *Thermus aquaticus* for analytical purposes and *KOD*-polymerase from *Thermococcus kodakaraensis*, which has a correction reading function, for preparative purposes. As templates for PCR isolated genomic DNA, plasmid DNA (section 6.4.6.4) or yeast colonies directly from rich media plates were used. The method was used for cloning of certain genes or gene fragments in vectors and for genome manipulation (e.g. addition of C-terminal epitopes or deletion of genes). Analytically the PCR was also used to distinguish mating types of yeast cells and check for successful deletions of genes.

6.4.4.1 PCR for amplification of DNA fragments

The PCR was used as a preparative method to amplify gene fragments out of the complete yeast genome or a plasmid to prepare for further clonings. For this purpose, oligonucleotide primers with additional restriction sites at the very ends, which allow a specific cloning into the wanted vector, were used. The following reaction set-up and temperature profile were used for this approach (Table 11 and Table 12).

Table 11 Contents of the PCR amplification.

Contents	Volume (µl)
10x KOD Hot Start DNA Polymerase Buffer	5
$MgSO_4$ (25 Mm)	3
dNTP mix (2 Mm)	5
Primer Forward 1:10 diluted in H_2O (10 $\frac{pmol}{\mu l}$)	2
Primer Reverse 1:10 diluted in H_2O (10 $\frac{pmol}{\mu l}$)	2
KOD Hot Start DNA polymerase (1 $\frac{U}{\mu l}$)	1
Template DNA 1:5 diluted in H_2O	1
H_2O	Ad 50

Table 12 Temperature profile for amplification of DNA fragments.

Step	Temperature (°C)	Duration
Denaturation	95	5 min
	30 cycles	
Denaturation	95	1 min
Annealing	54-59	40 sec
Amplification	72	1 min/kb
	Cycles end	
Amplification	72	5 min
Storage	8	Forever

The annealing temperature, the amplification duration and the number of cycles were adapted to the used primers, DNA template and length of the amplification fragment.

6.4.4.2 PCR for manipulation of genomes

With help of PCR linear DNA fragments were amplified to fuse proteins with an epitope (e.g. 12FLAG) or fluorescent proteins via homologous recombination. This approach was also used to delete genes via homologous recombination with a selective marker. For C-terminal fusions or whole gene deletions the pFA6a system was used (Longtine *et al.* 1998). For fluorescent markers the optimized pFA6a-link system was utilised (Sheff and Thorn 2004). Oligonucleotides were designed with around 45 bp homologous to the integration site in the yeast genome and 20 bp homologous to the amplified region in the plasmid. The PCR took place with the following conditions (Table 13 and Table 14).

Table 13 Reaction contents for amplification of epitope fusions.

Contents	Volume (µl)
10x KOD Hot Start DNA Polymerase Buffer	5
$MgSO_4$ (25 Mm)	3
dNTP mix (2 Mm)	5
Primer Forward 1:10 diluted in H_2O (10 $\frac{pmol}{\mu l}$)	2
Primer Reverse 1:10 diluted in H_2O (10 $\frac{pmol}{\mu l}$)	2
KOD Hot Start DNA polymerase (1 $\frac{U}{\mu l}$)	1
Template DNA 1:5 diluted in H_2O	1
H_2O	Ad 50

Table 14 Temperature profiles for amplification of epitope fusions.

Step	Temperature (°C)	Duration
Denaturation	95	5 min
	30 cycles	
Denaturation	95	1 min
Annealing	54-59	40 sec
Amplification	72	1kb/min
	Cycles end	
Amplification	72	5 min
Storage	8	Forever

After the PCR was performed the yeast cells were directly transformed with 10 – 15 µl of the PCR product (section 6.2.3.1).

6.4.4.3 Site-directed mutagenesis

To insert a mutation at a specific site the site-directed mutagenesis was used. Two complementary oligonucleotides were designed to include the wanted mutation and around 20 nucleotides upstream and downstream of the mutated site. A plasmid with the gene that is being mutated was used as a template for this PCR. The PCR was conducted as described in Table 15 and Table 16. After the PCR was checked for success on an agarose gel (section 6.4.5) a *DpnI* digest to get rid of the template followed. *DpnI* digests DNA with the restriction site GATC in a methylation-dependent manner only detecting the site when position 2 on the leading strand and position 3 on the complementary strand is N6 adenine methylated. This methylation is only present on the template and not yet on the amplified PCR product which allows a purification of the sample. To perform this digest 0.5 µl *DpnI* were added to the PCR sample and incubated for 1 h at 37 °C. An *E. coli* transformation as described in section 6.1.2 followed. Isolation of the plasmid was done with the NucleoSpin Kit by Macherey-Nagel (section 6.4.6.4). The correct mutation and plasmid sequence were checked by sequencing (section 6.4.6.5).

Table 15 Contents of site-directed mutagenesis.

Contents	Volume (µl)
10x KOD buffer	5
$MgSO_4$ (25 mM)	3
25 ng DNA template	variable
dNTP mix (2 mM)	5
F-Primer (10 $\frac{pmol}{\mu l}$)	3
R-Primer (10 $\frac{pmol}{\mu l}$)	3
KOD DNA polymerase (5 $\frac{U}{\mu l}$)	1.5
H_2O	Ad 50

Table 16 Temperature profile of site-directed mutagenesis.

Step	Temperature (°C)	Duration
Denaturation	94	4 min
	20 cycles	
Denaturation	94	1 min
Annealing	55	1 min
Amplification	72	1 min/kB + 1 min
	Cycles end	
Amplification	72	5 min
Storage	8	Forever

6.4.4.4 Detection of mating types with MAT-PCR

To detect the mating type of yeast cells with a PCR (Huxley *et al.* 1990) a small volume of cells was picked directly from a full media plate and resuspended carefully in the reaction batch. An isolation of genomic DNA was not necessary as the CoralLoad buffer (containing KCl, $(NH_4)_2SO_4$ and Mg_{2+}, Qiagen) used in this PCR approach is sufficient for cell lysis. The reaction conditions and used volumes of all components are listed in Table 17 and Table 18.

Table 17 Reaction contents of MAT-PCR.

Contents	Volume (µl)
10x CoralLoad buffer (Qiagen)	2.5
dNTP mix (2 Mm)	2.5
Primer mix of WS826/827/828 (10 $\frac{pmol}{\mu l}$)	3
Taq DNA polymerase (5 $\frac{U}{\mu l}$)	1
H_2O	Ad 25

Table 18 Temperature profile for MAT-PCR.

Step	Temperature (°C)	Duration
Denaturation	94	4 min
30 cycles		
Denaturation	94	1 min
Annealing	55	1 min
Amplification	72	40 sec
Cycles end		
Amplification	72	3 min
Storage	8	Forever

The PCR products were analysed in an agarose gel (section 6.4.5). *MATa* cells show a DNA fragment of 544 bp and *MATα* cells produce a 404 bp fragment. If the cells are diploid both fragments are amplified and detected in the gel.

6.4.4.5 Colony-PCR

A special form of MAT-PCR is the Colony-PCR, which was used to check on successful deletion of genes. The forward oligonucleotide primer was designed to bind upstream of the deletion locus and the reverse oligonucleotide primers were designed to either bind in the marker cassette used to delete a gene or in the gene itself. To support the discrimination of the PCR products, the primers were chosen to produce PCR fragments of different sizes. Diploid cells or supposedly haploid spores were picked up directly from rich media plates and resuspended in the reaction batch. An isolation of genomic DNA beforehand was also not needed as the colony buffer is sufficient for cell lysis. The reaction conditions and used volumes are listed down below (Table 19 and Table 20).

Table 19 Reaction contents for Colony-PCR.

Contents	Volume (µl)
10x CoralLoad buffer (Qiagen)	2.5
dNTP mix (2 mM)	2.5
F-Primer diluted 1:10 in H_2O (10 $\frac{pmol}{\mu l}$)	1.5
R-Primer diluted 1:10 in H_2O (10 $\frac{pmol}{\mu l}$)	1.5
Taq DNA polymerase (5 $\frac{U}{\mu l}$)	1
H_2O	Ad 25

Table 20 Temperature profile for Colony-PCR.

Step	Temperature (°C)	Duration
Denaturation	94	4 min
	35 cycles	
Denaturation	94	1 min
Annealing	T_{Primer}-4	1 min
Amplification	72	1 min/kb
	Cycles end	
Amplification	72	3 min
Storage	8	Forever

The PCR products were analysed on an agarose gel. The different product sizes of a successful deleted gene or the gene itself could be distinguished and the genotype of the cell analysed.

6.4.4.6 Primer extension analysis for transcription start site mapping

To map the transcription start site of specific genes under varying conditions a modified primer extension analysis was used (Boorstein and Craig 1989; Gurr and Januszeski). For this, the transcript of a target gene is reverse transcribed into cDNA which is in turn used as input for a PCR. Within the PCR different forward primers along a possible transcript in the 5'UTR of the gene are used together with one reverse primer inside the coding region of the gene (Figure 6.1). When a primer anneals further upstream of the actual transcript no PCR product will be made. This allows a limitation of the transcript length and a rough mapping of the transcription start site.

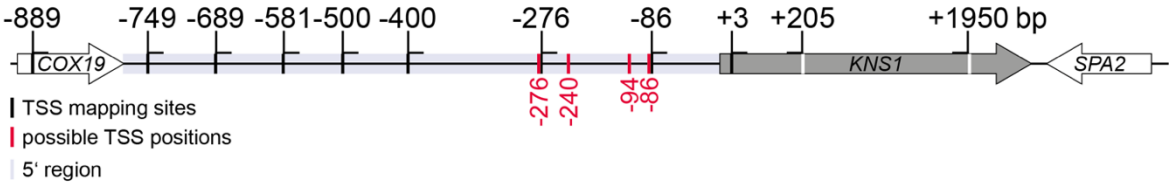

Figure 6.1 Positions of used primers for primer extension PCR of the 5'UTR of *KNS1*. Position +1950 bp was used for reverse transcription, +205 bp as a reverse primer for primer extension. Different forward primers were used to map a possible transcription start site.

RNA from cells of different conditions was isolated and reverse transcribed (as described in section 6.4.1 and section 6.4.3.1). The received cDNA was used as a template for a PCR approach which was conducted with *Taq* polymerase and Qiagen buffer. Q solution was added to the reaction to minimize side-effects by secondary structures and increase the efficiency of the PCR. The reaction set-up and temperature profile can be found in Table 21 and

Table 22. The annealing temperature was adjusted over all primer sets and the elongation time was set to fit the largest fragment so that all approaches could be performed at the same time.

Table 21 Contents of primer extension PCR.

Contents	Volume (µl)
10x Qiagen PCR buffer	2.5
Q solution	5
dNTP mix (2 mM)	2.5
F-Primer diluted 1:10 in H_2O (10 $\frac{pmol}{\mu l}$)	1.5
R-Primer diluted 1:10 in H_2O (10 $\frac{pmol}{\mu l}$)	1.5
Taq DNA polymerase (5 $\frac{U}{\mu l}$)	1
cDNA	0.5
H_2O	Ad 25

Table 22 Temperature profile of primer extension PCR.

Step	Temperature (°C)	Duration
Denaturation	94	1 min
	25 cycles	
Denaturation	94	1 min
Annealing	55	1 min
Amplification	72	1 min
	Cycles end	
Amplification	72	10 min
Storage	8	Forever

6.4.4.7 Quantitative-PCR

A quantitative real-time PCR (qPCR) is useful for analysis of starting material. The input amount can be measured with this approach (Bustin *et al.* 2009). The principle behind a real-time detection is as follows: the template DNA is amplified and duplicated each cycle. The PCR mastermix contains an intercalant fluorescent dye ("SYBR Green") that binds to double-stranded DNA. The more DNA is amplified the more fluorescent signal can be detected in real-time. The cycles of PCR can be quantified and visualized against the fluorescent intensity (Figure 6.2 A). In this quantification a certain cycle threshold (C_T value) can be detected. With this C_T value it is possible to calculate how many cycles are necessary to exceed the signal intensity threshold which in turn defines the input amount of template.

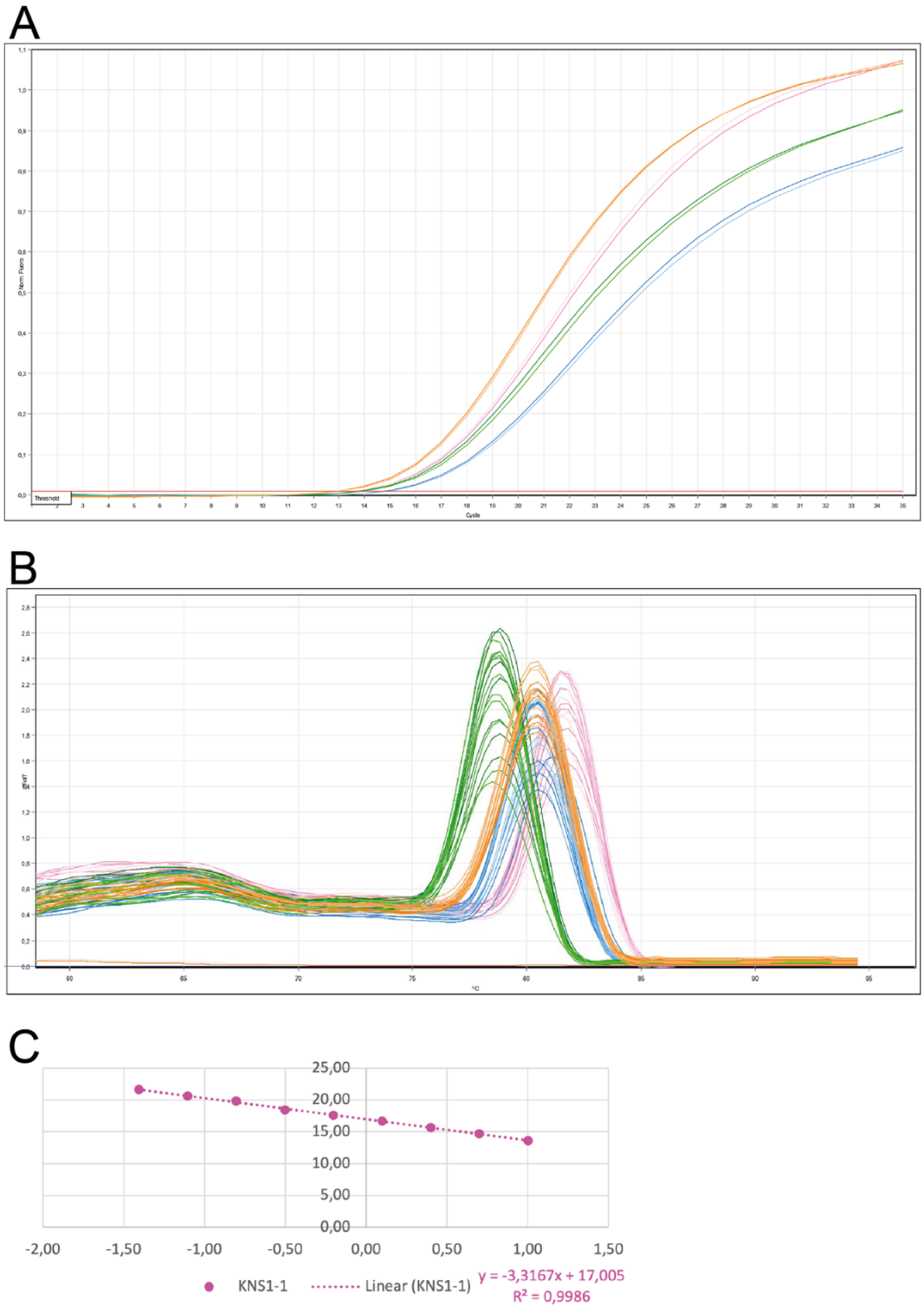

Figure 6.2 Testing primer efficiency for qPCR analysis.

A. qPCR reaction curves. The x-axis indicates the cycles and the y-axis indicates the fluorescence intensity. Shown are different primer sets in different colours. The threshold to measure the C_T values is set with a red line. B. Melting curves of different primer sets in a qPCR reaction. Different colours indicate different primer sets. The x-axis displays the temperature (in °C), while the y-axis displays the first derivative of the fluorescence signal against the temperature (dF/dT). C. Calculation of primer efficiency. The graph displays the gDNA input in logarithmic scale on the x-axis, 1:2 dilutions beginning with 10 ng DNA which equals 1 on the

graph, while the y-axis displays mean C_T values from duplicates. With this the slope of the graph can be measured to use for the calculation of primer efficiency.

For a correct quantification of the C_T values all used primer sets required validation. The primer efficiency was investigated to ensure only one duplication per cycle (Taylor 2019). To test the primer efficiencies genomic DNA (gDNA) in 1:2 dilution steps starting with 10 ng was used as a template for a qPCR. The C_T values and gDNA (in logarithmic scale) were graphically visualized (Figure 6.2 C). The slope (m) of the linear graph was used to calculate the exact efficiency (E) of each primer set with Equation 4. When the efficiency is equal to 2 a duplication of the PCR product per cycle is achieved (= 100 %). A range from 97 – 103 % is considered precise enough for qPCR.

$$E = 10^{\frac{-1}{m}}$$

Equation 4 Calculation of primer efficiency (E) for qPCR. The slope (m) of the linear graph was used for this calculation.

Primer should also bind solely to the target gene and dimers should be excluded from the analysis. Therefore, a melting curve was added after each qPCR run in which the temperature was slowly and continuously increased to denature the DNA. Unspecific primer dimers would, however, have lower melting temperatures that could be visualized in this analysis (Figure 6.2 B).

In this study the qPCR was used to investigate mRNA levels of different conditions to check for increased transcription activity. The RNA was reverse transcribed beforehand (section 0) and 5 ng of the corresponding cDNA was used as a template. For each gene of interest (GOI) a master mix was prepared and carefully loaded into the qPCR tubes (Table 23). The cDNA was directly pipetted into the reaction mix. Each GOI was at least measured in duplicates in every run. The amplification was performed in Rotor-Gene Q (Qiagen) with the program described in Table 24.

Table 23 Contents of qPCR mastermix.

Contents	Volume (µl)
2x SYBR Green master mix	10
F-Primer diluted 1:10 in H_2O (10 $\frac{pmol}{\mu l}$)	1.4
R-Primer diluted 1:10 in H_2O (10 $\frac{pmol}{\mu l}$)	1.4
RNase-free H_2O	3.2
5 ng cDNA	4

Table 24 Temperature profile used in qPCR with additional melting curve at the end of each run.

Step	Temperature (°C)	Duration
Denaturation	95	2 min
	30 cycles	
Denaturation	95	5 sec
Annealing/Elongation	57.7	10 sec
	Cycles end	
Melting curve	58 – 95	

After each run an analysis with the Rotor-Gene Q Series software was performed. The threshold was set close to the beginning of the exponential phase and the corresponding C_T values for each sample that reached the threshold could be used for further calculations. The expression of the GOI in each sample was calculated in reference to a housekeeping gene which was constantly expressed in all conditions (ΔC_T in Equation 5). The relative abundance (RA) was calculated using the $2^{-\Delta\Delta C_T}$ method and using wildtype conditions (WT) as a reference (Equation 5). The $\log_2$ of this relative abundance was used to visualize changes in the expression patterns compared to wildtype conditions.

$$\Delta C_T = C_T(GOI) - C_T(housekeeping)$$

$$\Delta\Delta C_T = \Delta C_T(condition) - \Delta C_T(WT)$$

$$RA = 2^{-\Delta\Delta C_T}$$

Equation 5 Calculation of relative abundance of genes of interest in qPCR.

First a ΔC_T value is calculated using the C_T values of the genes of interest (GOI) and the housekeeping gene. Then, the $\Delta\Delta C_T$ is calculated to address specific tested conditions in relation to WT. And finally, the relative abundance (RA) is calculated using the $\Delta\Delta C_T$ value. This indicates the changes of expression level of the genes of interest normalized to a housekeeping gene in specific tested conditions.

6.4.5 Gel electrophoresis of DNA and RNA

The agarose gel electrophoresis is an easy way to check nucleotide fragments as they are separated according to their size within an electric field. It can be used for purity checks, identification, size analysis and separation of PCR and digested fragments.

6.4.5.1 DNA samples

To prepare an agarose gel, 1 – 1.5 % agarose was heated in 1x TAE buffer until dissolved completely. Then 0.2 $\frac{\mu g}{ml}$ ethidium bromide was added, and the solution was poured into a specific tray. Together with an added comb to create pockets for the samples the gel was left to solidify. Ethidium bromide is a chemical that intercalates into the DNA which can then be made visible with UV light. After solidification of the gel, it was put into a chamber with 1x TAE buffer.

The DNA samples were mixed with a specific loading dye and pipetted into the open pockets. GeneRuler Mix by Thermo Fisher Scientific was used as DNA size reference. The separation of fragments was performed with a constant voltage of 80 – 90 V for 30 to 60 min. The DNA was then visualized with the UV detection system "UVP GelStudio PLUS" by Analytic Jena.

6.4.5.2 RNA samples

For RNA samples a 2 % agarose gel was prepared. The agarose was dissolved in 1x TAE (RNase-free), then 0.2 $\frac{\mu g}{ml}$ ethidium bromide was added, and the solution solidified in a special RNase-free tray with a comb for pockets.

The RNA samples and RiboRuler High Range standard (Thermo Scientific) were prepared as follows: 200 ng of diluted RNA and 2 µl of the RNA standard were mixed with equal volumes of 2x RNA Loading Dye (Thermo Scientific). The samples were mixed briefly and then heated at 70 °C for 10 min. After cooling down on ice for 3 min the samples were spined down prior to gel loading. The separation of RNA was performed with a constant voltage of 80 V for 45 – 60 min. The RNA was visualized with the same UV detection system as for DNA samples (section 6.4.5.1).

6.4.6 Cloning

6.4.6.1 Restriction digest of DNA

Restriction endonucleases detect specific sequences and cut double stranded DNA specifically to produce linear DNA fragments with sticky or blunt ends. For different purposes different reaction approaches were used. A preparative digest as part of a cloning process was performed at 37 °C for 2 hours (Table 25).

Table 25 Contents and volumes of preparative digest.

Contents	Volume (µl)
DNA	5-10
10x Restriction buffer	2
Restriction enzyme 1	1
Restriction enzyme 2	1
H_2O	Ad 20

A restriction digest was also used to test proper integration of inserts at various steps of the cloning process. A smaller reaction batch was used for this purpose (Table 26).

Table 26 Reaction batch for test digest.

Contents	Volume (µl)
DNA	1-5
10x Restriction buffer	1
Restriction enzyme 1	0.3
Restriction enzyme 2	0.3
H_2O	Ad 10

The incubation took place at 37 °C and 1h incubation time. If the restriction endonuclease had time saver attributes, incubation was reduced to 15 min.

Lastly, the restriction digest was used to linearize certain DNA fragments to perform yeast transformation (section 6.2.3.1), too. A linearization digest was performed at 37 °C for 1 – 2 hours and with the following reaction batch (Table 27).

Table 27 Contents and volumes for linearization digest of plasmids and vectors.

Contents	Volume (µl)
DNA	2500 ng
10x Restriction buffer	3
Restriction enzyme	2
H_2O	Ad 30

All restriction buffers and enzymes were used as described in the manufacturer's instructions (NEB).

6.4.6.2 Purification of DNA fragments

6.4.6.2.1 DNA extraction from agarose gels

DNA fragments could be cut out from agarose gels under a UV lamp. The DNA was then isolated from the small gel pieces with the QIAquik Gel Extraction Kit by Qiagen according to the manufacturer's instructions.

6.4.6.2.2 Purification of DNA fragments after PCR or restriction digest

DNA fragments could be purified after a PCR or restriction digest to purify the DNA and get rid of unwanted oligonucleotides, nucleotides, enzymes, and buffers. This was done with help of the QIAquik PCR Purification Kit by Qiagen and all steps were proceeded as noted in the manual.

6.4.6.3 Ligation

Linear DNA fragments with compatible sticky ends originating from a restriction endonuclease digest with the same enzymes (section 6.4.6.1) can be connected covalently by ligases. The fragment intensities of vector and insert were checked on an agarose gel (section 6.4.5) and the volumes were calculated considering the sizes of fragments. The general ratio of vector to insert was 1:5 and the following approach was used (Table 28).

Table 28 Approach for ligation of linear DNA fragments.

Contents	Volume
Vector DNA	50-100 ng
Insert DNA	5-times the copies of vector DNA
T4-DNA-ligase	1 U
10x Ligase buffer	2 µl
H_2O	Ad 20

The ligation was performed for 2 hours at room temperature. The ligation batch was dialyzed for 20 min against sterile water to get rid of the ligation buffers and components. To amplify the number of plasmids the ligation batch was then transformed into *E. coli* DH5α-cells (section 6.1.2). The plasmids could then be isolated in greater numbers afterwards (section 6.4.6.4).

6.4.6.4 Isolation of plasmids from *E. coli*

6.4.6.4.1 Mini preparation

The mini preparation is a quick way to isolate a large number of plasmids from *E. coli* (Berghammer and Auer 1993). The isolated DNA can be used for test restriction digests but is not suitable for sequencing or long-term storage as it is contaminated with proteins to a high degree.

2 ml of an overnight culture were harvested at 14000 rpm for 4 min in a micro tube. The supernatant was discarded, and the pellet dissolved in 40 µl EasyPrep buffer. The

solution was cooked at 100 °C for 1 min and immediately cooled on ice. The reaction batch was spined down at 14000 rpm for 15 min. The isolated plasmid DNA was included in the supernatant after this step. For a restriction digest 5 µl of the DNA were used (section 6.4.6.1).

6.4.6.4.2 Column purification of plasmid DNA

Plasmid DNA already isolated from *E. coli* could be purified in a small volume for a better result to use for sequencing. The column purification was performed with the Mini Prep NucleoSpin Kit by Macherey-Nagel and was conducted as described in the manufacturer's instruction. The purified sample yielded 30 – 50 µl DNA.

6.4.6.4.3 Midi preparation

To purify large amounts of plasmid DNA (80 ml culture, 1 ml yield) the GenElute HP Plasmid Midi Kit by Sigma-Aldrich was used. The Midi Prep was performed as noted in the manual.

6.4.6.5 Sequencing

Sequencing of plasmid DNA was used as a control to check PCR products before further steps were done. The samples were prepared as in Table 29 listed.

Table 29 Preparation of plasmid DNA samples for sequencing by Microsynth Seqlab.

Contents	Volume
Plasmid DNA	500 ng
Primer 1:10 diluted in H_2O	3 µl
H_2O	Ad 12 µl

The sequencing was done by Microsynth Seqlab and DNA sequences were analysed with the software SnapGene.

6.4.7 Marker exchange

Sometimes existing yeast strains contained selection markers not suitable for the planned experiments. In this case a marker exchange was performed. For that, a plasmid with the fitting marker was used and digested with restriction endonucleases cutting upstream of the *pTEF* region and downstream of the *tTEF* region. The digest was performed as in section 6.4.6.1 described. After a check on an agarose gel (section 6.4.5) the digested fragment was transformed into diploid yeast cells (section 6.2.3.1) and via homologous recombination of the *pTEF* and *tTEF* sites the old selection marker was exchanged with the new one.

6.5 Protein analytics

6.5.1 Preparation of protein lysates from yeast cells

Raw extracts of proteins were produced by mechanical lysis of yeast cells with help of glass beads. 10 –12 OD_{600} of yeast cells from an exponentially growing culture were harvested at 2000 rpm for 3 min. The supernatant was discarded, and the pellet was dissolved in 1 ml cold, sterile H_2O. The cells were transferred to a micro tube with 0.3 g glass beads and were spined down at 14000 rpm for 30 sec. The supernatant was discarded, and the pellet could be frozen at -70 °C for storage at this point. To lyse the cells the samples were slowly defrosted on ice and all further steps were performed on ice, too. 150 µl buffer 3 with β-glycerol phosphate (60 mM) was added to the samples and the cells were mechanically lysed in a mill (Retsch) at highest frequency for 5 – 7 min. The cell fragments were then centrifuged at 14000 rpm for 3 min at 4 °C. Immediately after that, 50 µl of the supernatant was mixed with 50 µl 2x Laemmli buffer and cooked at 100 °C for 10 min.

6.5.2 Determination of protein concentration with the Bradford method

To determine protein concentrations 5 µl of the protein lysate (section 6.5.1) was diluted 1:1000 in sterile water. 500 µl of this dilution was mixed 1:2 with Bradford reagent and incubated for 5 min at room temperature. Afterwards, the OD_{595} was measured as a value for protein concentration. Water diluted 1:2 in Bradford reagent was used as a reference for the measured extinction values. The calculated relative protein concentrations ensured a similar sample input on SDS gels.

6.5.3 SDS-polyacrylamide gel electrophoresis (SDS-PAGE)

Proteins can be separated in an electrical field due to their size with help of the SDS-PAGE (Brunelle and Green 2014). Secondary structure and protein-protein interactions must be destructed for the SDS-PAGE to work. Therefore, sodiumdodecylsulfate (SDS) and β-mercaptoethanol are added to a polyacrylamide gel and set reducing and denaturing conditions. β-mercaptoethanol reduces di-sulphide-bridges which helps to diminish secondary structures. The negatively charged SDS furthermore attaches to the proteins relative to their size which results in a general negative charge. Hence, the proteins will independently move in the electrical field. This movement is independent of protein charge and smaller proteins will move faster in a polyacrylamide gel than larger ones. The gel is divided into two parts, a stacking, and a resolving gel (discontinuous electrophoresis). Both have different concentrations of polyacrylamide and different pH values of the used buffers. This leads to a stacking effect of the proteins in the stacking gel due to the low mobility in this buffer and a simultaneous release of all proteins into the resolving gel where the separation of the proteins along their size starts.

6.5.3.1 SDS-PAGE

Firstly, a 9 % resolving gel was prepared and filled between two glass plates that were sealed with a rubber band (Table 30). The gel was overlaid with isopropanol. After

about 30 min of polymerisation the isopropanol was removed, and the stacking gel was filled on top of the resolving gel (Table 31). To prepare open pockets for the samples a comb was added to the upper part of the stacking gel. The gels were always loaded with equivalent amounts of protein (1 – 2 OD_{595} ≙ 25 – 50 $\frac{\mu g}{\mu l}$). The corresponding volumes in µl were calculated with help of the Bradford method (section 6.5.2) and the following equation: $V(1\ OD_{595}) = \frac{1}{OD_{595}}$. As a size reference 3 µl of the protein standard Color Prestained Protein Standard (Broad Range) by NEB was used in each gel. The electrophoresis was performed with an electric current of 25 mA per gel for 1.5 – 2 h until the blue front of the Laemmli buffer had left the gel. Subsequent, the stacking gel was removed, and the resolving gel was used for further analyses like western blot (section 6.5.4).

Table 30 Contents and volumes of a 9 % resolving gel to be filled into glass plates for separation of proteins in the range of 17 – 250 kDa.

Contents	Volume
H_2O	2.6 ml
1.5 M Tris/Cl pH 8.8	1.5 ml
Acrylamide solution (30 % acrylamide, 0.8 % bisacrylamide)	1.8 ml
10 % SDS	60 µl
10 % Ammoniumpersulfate (APS)	36.5 µl
Tetramethyldiamine (TEMED)	3.65 µl

Table 31 Contents and volumes of a stacking gel to be filled on top of a resolving gel. A comb was added so that pockets for the sample loading were left open.

Contents	Volume
H_2O	1.5 ml
0.5 M Tris/Cl pH 6.8	625 µl
Acrylamide solution (30 % acrylamide, 0.8 % bisacrylamide)	335 µl
10 % SDS	25 µl
10 % Ammoniumpersulfate (APS)	25 µl
Tetramethyldiamine (TEMED)	2.5 µl

6.5.3.2 Phos-tag SDS-PAGE

For characterization of phosphorylation levels, a Phos-tag SDS-PAGE was used to distinguish phosphorylated from unphosphorylated isoforms of the target protein (Kinoshita *et al.* 2009, 2022; Sugiyama and Uezato 2022). Phos-tag is a di-nuclear metal complex (1,3-bis[bis(pyridin-2-ylmethyl)amino]propan-2-olato dizinc(II) complex) that is able to bind to phosphates and thereby interferes with the migration of phosphorylated proteins.

For this study 7.5 % Phos-tag gels were used (Table 32). A SDS resolving gel with addition of Phos-tag (Sigma-Aldrich) and $MnCl_2$ was prepared. The stacking gel was prepared as described in Table 31. Both gels were handled as already described in section 6.5.3.1. Samples (section 6.5.1) as well as the protein standard had to be adjusted with $MnCl_2$ to an end concentration of 5 mM or 1 mM respectively. The SDS-PAGE was performed at 5 mA per gel for 3 – 4 hours. Before transferring the separated proteins onto a membrane in a western blot analysis the gels were washed three times with 10 mM ethylenediaminetetraacetic acid (EDTA) for 10 min on a rocker. The EDTA was discarded afterwards, and a subsequent western blot took place (section 6.5.4).

Table 32 Components and volumes of a 7.5 % resolving gel for Phos-tag SDS-PAGE to distinguish phosphorylated and unphosphorylated protein isoforms.

Component	10 µM Phos-tag (Volumes)	20 µM Phos-tag (Volumes)
H_2O	2.9 ml	2.9 ml
1.5 M Tris/Cl pH 8.8	1.5 ml	1.5 ml
Acrylamide solution	1.5 ml	1.5 ml
10 % SDS	60 µl	60 µl
10 % Ammonium persulfate	36.5 µl	36.5 µl
Tetramethyl diamine	3.65 µl	3.65 µl
5 mM Phos-tag	12 µl	24 µl
5 mM MnCl2	12 µl	24 µl

6.5.4 Western blot

Proteins can be detected in a polyacrylamide gel after their separation with help of a western blot. The separated proteins (section 6.5.1) firstly have to be transferred onto a nitrocellulose membrane (Dennis-Sykes *et al.* 1985) and will then be detected with specific antibodies (section 6.5.5). To transfer the proteins onto a nitrocellulose membrane a Whatman GB005 paper saturated with transfer buffer was put on the graphite anode of the blotting apparatus. On top of the Whatman paper the nitrocellulose membrane soaked in water and the watered resolving gel followed. To finish the stack another Whatman paper saturated with transfer buffer was added. The gadget was closed by adding the cathode. The transfer of proteins was performed at 40 mA per gel for 2 hours. Afterwards, the nitrocellulose membrane was dyed with PonceauS to check an even protein transfer onto the membrane and the dye was documented. To prevent the primary antibody to bind unspecifically, the membrane was blocked with 5 % milk (5 % skimmed milk powder in TBS-T) for 30 min.

6.5.5 Detection of proteins with antibodies

After a successful transfer of proteins to a nitrocellulose membrane the proteins can be detected with antibodies. At first, a specific primary antibody is bound to the target protein or its fused epitope. A secondary antibody with a fluorescent dye can then bind

to the primary antibody ("The Essential Guide to Successful Quantitative Western Blots" 2021). This enhances the signal intensity and specificity of the detection. The fluorescence of the secondary antibody could later be excited with lasers of an infrared imager. The fluorescence signal detected is proportional to the protein concentration which allows a quantitative analysis.

A membrane blocked with 5 % milk could be used for detection with antibodies. The primary antibody was added to 5 – 10 ml of 5 % milk in specific dilutions and the membrane was incubated with this mixture on a rocker at 4 °C overnight. On the next day the membrane was washed with TBS-T three times (shaking for 5 min at room temperature each time). Subsequently, the secondary antibody was added to 5 ml of 5 % milk and the membrane was incubated with the mixture for at least 2 hours at room temperature on a rocker in the dark to protect the fluorescent dyes. The membrane was again washed with TBS-T three times for 5 min. The specific detection of proteins could then take place via stimulation of the fluorescent dye coupled to the secondary antibody (680 nm or 800 nm) on the Odyssey Infrared Imager by LI-COR. The analysis and quantification of the signals was performed with the software ImageStudio by LI-COR.

6.6 Polysome profiling

Polysome profiles can be used to detect different protein expression levels. Measuring the number of mRNA-associated ribosomes can give insights into the activity of mRNA translation specifically for each target. These values can then be used as a basis for other analyses to evaluate regulation of protein expression. With this method mRNAs with or without attached ribosomes can be separated by a saccharose gradient in an ultracentrifugation (Chassé *et al.* 2016). To separate the different polysome species correctly, the ribosomes must be stalled by inhibiting translation elongation with cycloheximide.

6.6.1 Saccharose gradient

For the gradient, saccharose solutions (10, 20, 30, 40 and 50 %) in lysis buffer were prepared and sterile filtrated. Just before use, 100 $\frac{\mu g}{ml}$ cycloheximide (CHX stock solution: 20 $\frac{mg}{ml}$ in EtOH) was added to the saccharose solutions. To start producing the gradient 2.2 ml of 50 % saccharose with CHX were added to a centrifuge tube, spined down for 10 sec at full speed and frozen at -80 °C. After 20 min the first layer was completely frozen and the next low percentage saccharose solution was overlaid in the same manner. For each saccharose concentration the same procedure was performed until a final freeze at -80 °C took place overnight. The centrifugation tube with the final saccharose gradient was slowly defrosted at 4 °C the night before the centrifugation.

6.6.2 Cell lysis and polysome profiling

The wanted yeast strains were inoculated overnight to receive exponentially growing cells the next day. 105 OD_{600} in total were harvested at approximately 0.7 OD_{600} by

centrifuging with 1800 g for 3 min. The cells were then resuspended in 1 ml of cold lysis buffer with 100 $\frac{\mu g}{ml}$ CHX and split to four tubes with 0.6 g glass beads each. The samples were spined down for 3 min with 1000 g, the supernatant was discarded, the pellet was resuspended in 300 µl cold lysis buffer with 100 $\frac{\mu g}{ml}$ CHX and frozen over night at -80 °C. The next day the cells were carefully defrosted on ice and mechanically lysed in a mill (Retsch) at highest frequency for 10 min. Cell fragments were centrifuged at 2000 g for 5 min, two tubes were combined and again spined down at 4000 g for 5 min. An RNA concentration measurement of a 1:10 dilution in lysis buffer with 100 $\frac{\mu g}{ml}$ CHX at the NanoDrop followed (section 6.4.2). Same amounts of RNA were used to load the saccharose gradient (section 6.6.1). For that, 800 µg RNA were carefully pipetted onto the gradient and volumes were tared with lysis buffer with 100 $\frac{\mu g}{ml}$ CHX. The separation of ribosome associated RNAs within the saccharose gradient was conducted at 4 °C with 35000 rpm for 3 h in the ultra-centrifuge (Thermo Scientific Sorvall WX Ultra Series, rotor TH641). Afterwards, a detection with the Äkta start was performed. 60 % saccharose were used to push the saccharose gradient with mRNA from the bottom of the tube into the Äkta. The UV-detection at A_{260} started with the light, ribosome-free mRNAs in 10 % saccharose, towards monosomes and lastly polysomes in high density saccharose solutions. The polysome profiles were analysed on the computer at the Äkta.

7 MATERIAL

7.1 Yeast strains

Table 33 All strains used in this work were from the yeast background W303. The corresponding mating (MAT) type and genotype are given, as well as information (Info) on the origin of the strains.

Name	MAT	Genotype	Info
AG 3678	MATa	rpd3-delta-Kl-TRP1	Provided by the working group of Prof. Dr. Joachim Griesenbeck
AG 3681	MATα	rpd3-delta-Kl-TRP1	Provided by the working group of Prof. Dr. Joachim Griesenbeck
W02873	MAT a	pep4delta::URA3	Working group of Prof. Dr. Wolfgang Seufert
W08458	MATα	trp1::pTEF2-mCherry-SWI5-S/A-tCYC1-TRP1	Working group of Prof. Dr. Wolfgang Seufert
W08459	MATα	ura3::pTEF2-mCherry-SWI5-S/A-tCYC1-URA3	Working group of Prof. Dr. Wolfgang Seufert
W08785	MATa	gcn2-delta::natNT2	Working group of Prof. Dr. Wolfgang Seufert
W08786	MATα	gcn2-delta::natNT2	Working group of Prof. Dr. Wolfgang Seufert
W10526	MATa	HMO1-3mCherry-tCYC1-TRP1	Working group of Prof. Dr. Wolfgang Seufert
W10527	MATα	HMO1-3mCherry-tCYC1-TRP1	Working group of Prof. Dr. Wolfgang Seufert
W14785	MATa	gcn4-delta::natNT2	Working group of Prof. Dr. Wolfgang Seufert
W14786	MATα	gcn4-delta::natNT2	Working group of Prof. Dr. Wolfgang Seufert
W15827	MATa	trp1::pTEF2-mCherry-SWI5-S/A-tCYC1-TRP1 pTEF2-GFP-SSO1-tCYC1-URA3	Working group of Prof. Dr. Wolfgang Seufert
W15828	MATα	trp1::pTEF2-mCherry-SWI5-S/A-tCYC1-TRP1 pTEF2-GFP-SSO1-tCYC1-URA3	Working group of Prof. Dr. Wolfgang Seufert
W15829	MATa	trp1::pTEF2-mCherry-SWI5-S/A-tCYC1-TRP1 pTEF2-GFP-SSO1-tCYC1-URA3 cdc123-delta326-HA3-His	Working group of Prof. Dr. Wolfgang Seufert
W15830	MATα	trp1::pTEF2-mCherry-SWI5-S/A-tCYC1-TRP1 pTEF2-GFP-SSO1-	Working group of Prof. Dr. Wolfgang Seufert

		tCYC1-URA3 cdc123-delta326-HA3-His	
W15595	MATα	cdc123-delta326-HA3-His	Working group of Prof. Dr. Wolfgang Seufert
W15596	MATa	cdc123-delta326-HA3-His	Working group of Prof. Dr. Wolfgang Seufert
W16736	MATa	snf1-delta::LEU2	Working group of Prof. Dr. Wolfgang Seufert
W16737	MATα	snf1-delta::LEU2	Working group of Prof. Dr. Wolfgang Seufert
W16774	MATa	snf1-delta::LEU2 cdc123-deltaC(1-326)-HA3-HIS3MX6	Working group of Prof. Dr. Wolfgang Seufert
W16775	MATα	snf1-delta::LEU2 cdc123-deltaC(1-326)-HA3-HIS3MX6	Working group of Prof. Dr. Wolfgang Seufert
W17204	MATa	hxk2-delta::LEU2	Working group of Prof. Dr. Wolfgang Seufert
W17205	MATα	hxk2-delta::LEU2	Working group of Prof. Dr. Wolfgang Seufert
W17529	MATa	FOB1-ytdTomato-TRP1	Working group of Prof. Dr. Wolfgang Seufert
W17530	MATa	FOB1-ytdTomato-TRP1	Working group of Prof. Dr. Wolfgang Seufert
W17638	MATa	hmo1-delta::kanMX4	Working group of Prof. Dr. Wolfgang Seufert
W17639	MATα	hmo1-delta::kanMX4	Working group of Prof. Dr. Wolfgang Seufert
W17835	MATa	pfk2-delta::KanMX6	Working group of Prof. Dr. Wolfgang Seufert
W17835	MATa	pfk2-delta::KanMX6	Working group of Prof. Dr. Wolfgang Seufert
W17836	MATα	pfk2-delta::KanMX6	Working group of Prof. Dr. Wolfgang Seufert
W17836	MATα	pfk2-delta::KanMX6	Working group of Prof. Dr. Wolfgang Seufert
W17847	MATa	reg1-delta::KanMX6	Working group of Prof. Dr. Wolfgang Seufert
W18091	MATa	reg1-delta::KanMX6 snf1-delta::LEU2 trp1::pTEF2-mCherry-SWI5-S/A-tCYC1-TRP1	Working group of Prof. Dr. Wolfgang Seufert
W18093	MATa	reg1-delta::KanMX6 snf1-delta::LEU2 trp1::pTEF2-mCherry-SWI5-S/A-tCYC1-TRP1 cdc123-deltaC(1-326)-HA3-HIS3	Working group of Prof. Dr. Wolfgang Seufert

W18095	MATa	reg1-delta::KanMX6 gcn2-delta::natNT2	Working group of Prof. Dr. Wolfgang Seufert
W18096	MATa	reg1-delta::KanMX6 gcn2-delta::natNT2 cdc123-deltaC(1-326)-HA3-HIS3	Working group of Prof. Dr. Wolfgang Seufert
W18097	MATa	gcn2-delta::natNT2 cdc123-deltaC(1-326)-HA3-HIS3	Working group of Prof. Dr. Wolfgang Seufert
W18158	MATα	KNS1-GFP-URA3 trp1::pTEF2-mCherry-SWI5-S/A-tCYC1-TRP1	Johannes Klier for this work
W18159	MATa	RPC53-3HA-TRP1	Johannes Klier for this work
W18160	MATα	RPC53-3HA-TRP1	Johannes Klier for this work
W18170	MATα	KNS1-12xFLAG-KanMX6	Johannes Klier for this work
W18226	MATa	KNS1-GFP-URA3 trp1::pTEF2-mCherry-SWI5-S/A-tCYC1-TRP1	Johannes Klier for this work
W18227	MATα	KNS1-GFP-URA3 trp1::pTEF2-mCherry-SWI5-S/A-tCYC1-TRP1 cdc123-delta326-HA3-His	Johannes Klier for this work
W18228	MATa	KNS1-GFP-URA3 trp1::pTEF2-mCherry-SWI5-S/A-tCYC1-TRP1 cdc123-delta326-HA3-His	Johannes Klier for this work
W18229	MATα	RPC53-3HA-TRP1 cdc123-delta326-HA3-His	Johannes Klier for this work
W18230	MATa	RPC53-3HA-TRP1 cdc123-delta326-HA3-His	Johannes Klier for this work
W18286	MATa	KNS1-12xFLAG-KanMX6 cdc123-delta326-HA3-His	Johannes Klier for this work
W18287	MATα	KNS1-12xFLAG-KanMX6 cdc123-delta326-HA3-His	Johannes Klier for this work
W18288	MATα	kns1-delta::KanMX6	Johannes Klier for this work
W18289	MATa	kns1-delta::KanMX6	Johannes Klier for this work
W18290	MATa	KNS1-12xFLAG-KanMX6	Johannes Klier for this work
W18453	MATa	tCYC1::pTEF2-MYC3-KNS1-tCYC-LEU2	Johannes Klier for this work
W18454	MATα	tCYC1::pTEF2-MYC3-KNS1-tCYC-LEU2	Johannes Klier for this work
W18455	MATa	tCYC1::pTEF2-MYC3-KNS1-tCYC-LEU2 RPC53-3HA-TRP1	Johannes Klier for this work
W18456	MATα	tCYC1::pTEF2-MYC3-KNS1-tCYC-LEU2 RPC53-3HA-TRP1	Johannes Klier for this work
W18457	MATa	RPC53-3HA-TRP1 GCD11(1-521)-KanMX6	Johannes Klier for this work

W18458	MATα	RPC53-3HA-TRP1 GCD11(1-521)-KanMX6	Johannes Klier for this work
W18459	MATa	RPC53-3HA-TRP1 kns1-delta::KanMX6 cdc123-delta326-HA3-His	Johannes Klier for this work
W18460	MATα	RPC53-3HA-TRP1 kns1-delta::KanMX6 cdc123-delta326-HA3-His	Johannes Klier for this work
W18461	MATa	RPC53-3HA-TRP1 kns1-delta::KanMX6	Johannes Klier for this work
W18462	MATα	RPC53-3HA-TRP1 kns1-delta::KanMX6	Johannes Klier for this work
W18463	MATa	kns1-delta::KanMX6 cdc123-delta326-HA3-His	Johannes Klier for this work
W18464	MATα	kns1-delta::KanMX6 cdc123-delta326-HA3-His	Johannes Klier for this work
W18465	MATα	RPC53-GFP-URA3 trp1::pTEF2-mCherry-SWI5-S/A-tCYC1-TRP1	Veronika Waas for this work
W18470	MATa	RPC53-GFP-URA3 trp1::pTEF2-mCherry-SWI5-S/A-tCYC1-TRP1	Veronika Waas for this work
W18471	MATa	RPC53-GFP-URA3 trp1::pTEF2-mCherry-SWI5-S/A-tCYC1-TRP1 cdc123-delta326-HA3-His	Veronika Waas for this work
W18472	MATα	RPC53-GFP-URA3 trp1::pTEF2-mCherry-SWI5-S/A-tCYC1-TRP1 cdc123-delta326-HA3-His	Veronika Waas for this work
W18473	MATa	KNS1-3xFLAG-KanMX6	Veronika Waas for this work
W18474	MATα	KNS1-3xFLAG-KanMX6	Veronika Waas for this work
W18485	MATa	tCYC1::pTEF2-MYC3-KNS1-tCYC-LEU2 cdc123-deltaC(1-326)-HA3-HIS3MX6	This work
W18486	MATα	tCYC1::pTEF2-MYC3-KNS1-tCYC-LEU2 cdc123-deltaC(1-326)-HA3-HIS3MX6	This work
W18487	MATa	tCYC1::pTEF2-MYC3-KNS1-tCYC-LEU2 RPC53-3HA-TRP1 cdc123-deltaC(1-326)-HA3-HIS3MX6	This work
W18488	MATα	tCYC1::pTEF2-MYC3-KNS1-tCYC-LEU2 RPC53-3HA-TRP1 cdc123-deltaC(1-326)-HA3-HIS3MX6	This work
W18549	MATa	tCYC1::pTEF2-MYC3-KNS1-tCYC-LEU2 trp1::pTEF2-mCherry-SWI5-S/A-tCYC1-TRP1 CDC19-GFP-URA3	This work

W18550	MATα	tCYC1::pTEF2-MYC3-KNS1-tCYC-LEU2 trp1::pTEF2-mCherry-SWI5-S/A-tCYC1-TRP1 CDC19-GFP-URA3	This work
W18551	MATa	RPC53-GFP-URA3 cdc123-deltaC(1-326)-HA3-HIS3MX6	This work
W18552	MATα	RPC53-GFP-URA3 cdc123-deltaC(1-326)-HA3-HIS3MX6	This work
W18553	MATa	RPC53-GFP-URA3	This work
W18554	MATα	RPC53-GFP-URA3	This work
W18572	MATα	KNS1-3HA-TRP1	This work
W18573	MATα	KNS1-13MYC-TRP1	This work
W18574	MATa	ura3::5'UTR-KNS1(1-9)-GFP-SWI5-S/A-myc13-URA3	This work
W18575	MATα	ura3::5'UTR-KNS1(1-9)-GFP-SWI5-S/A-myc13-URA3	This work
W18576	MATa/α	KNS1/kns1-delta::TRP1	This work
W18577	MATa/α	HXK2/hxk2-delta::HIS3	This work
W18595	MATa	ura3::5'UTR-KNS1(1-9)-GFP-SWI5-S/A-myc13-URA3 cdc123-delta326-HA3-His	Carina Mayr for this work
W18596	MATα	ura3::5'UTR-KNS1(1-9)-GFP-SWI5-S/A-myc13-URA3 cdc123-delta326-HA3-His	Carina Mayr for this work
W18598	MATa	KNS1-12xFLAG-KanMX6 pep4delta::URA3	Carina Mayr for this work
W18599	MATα	KNS1-12xFLAG-KanMX6 pep4delta::URA3	Carina Mayr for this work
W18600	MATa	hxk2-delta::HIS3	This work
W18601	MATα	hxk2-delta::HIS3	This work
W18602	MATa	HMO1-3mCherry-tCYC1-TRP1 RPC53-GFP-URA3 cdc123-deltaC(1-326)-HA3-HIS3MX6	This work
W18603	MATα	HMO1-3mCherry-tCYC1-TRP1 RPC53-GFP-URA3 cdc123-deltaC(1-326)-HA3-HIS3MX6	This work
W18604	MATa	HMO1-3mCherry-tCYC1-TRP1 RPC53-GFP-URA3	This work
W18605	MATα	HMO1-3mCherry-tCYC1-TRP1 RPC53-GFP-URA3	This work
W18606	MATα	reg1-delta::His3MX6	Carina Mayr for this work
W18607	MATa	reg1-delta::His3MX6	Carina Mayr for this work

W18659	MATa	KNS1-12xFLAG-KanMX6 RPC53-3HA-TRP1	Carina Mayr for this work
W18660	MATα	KNS1-12xFLAG-KanMX6 RPC53-3HA-TRP1	Carina Mayr for this work
W18661	MATa	KNS1-12xFLAG-KanMX6 cdc123-delta326-HA3-His RPC53-3HA-TRP1	Carina Mayr for this work
W18662	MATα	KNS1-12xFLAG-KanMX6 cdc123-delta326-HA3-His RPC53-3HA-TRP1	Carina Mayr for this work
W18670	MATa	KNS1-12xFLAG-KanMX6 reg1-delta::His3MX6	Carina Mayr for this work
W18671	MATα	KNS1-12xFLAG-KanMX6 reg1-delta::His3MX6	Carina Mayr for this work
W18672	MATa	snf1-delta::LEU2 reg1-delta::His3MX6	Carina Mayr for this work
W18673	MATα	snf1-delta::LEU2 reg1-delta::His3MX6	Carina Mayr for this work
W18825	MATa	hmo1-delta::kanMX4 KNS1-12xFLAG-KanMX6	Antje Machetanz-Morokane for this work
W18826	MATα	hmo1-delta::kanMX4 KNS1-12xFLAG-KanMX6	Antje Machetanz-Morokane for this work
W18827	MATa	hmo1-delta::kanMX4 RPC53-3HA-TRP1	Antje Machetanz-Morokane for this work
W18828	MATα	hmo1-delta::kanMX4 RPC53-3HA-TRP1	Antje Machetanz-Morokane for this work
W18829	MATa	RPC53-3HA-TRP1 snf1-delta::LEU2 reg1-delta::HIS3MX6	Ferdinand Schmid for this work
W18829	MATa	RPC53-3HA-TRP1 snf1-delta::LEU2 reg1-delta::HIS3MX6	Ferdinand Schmid for this work
W18830	MATα	RPC53-3HA-TRP1 snf1-delta::LEU2 reg1-delta::HIS3MX6	Ferdinand Schmid for this work
W18830	MATα	RPC53-3HA-TRP1 snf1-delta::LEU2 reg1-delta::HIS3MX6	Ferdinand Schmid for this work
W18831	MATa	RPC53-3HA-TRP1 snf1-delta::LEU2	Ferdinand Schmid for this work
W18831	MATa	RPC53-3HA-TRP1 snf1-delta::LEU2	Ferdinand Schmid for this work
W18832	MATα	RPC53-3HA-TRP1 snf1-delta::LEU2	Ferdinand Schmid for this work
W18832	MATα	RPC53-3HA-TRP1 snf1-delta::LEU2	Ferdinand Schmid for this work
W18833	MATa	RPC53-3HA-TRP1 reg1-delta::HIS3MX6	Ferdinand Schmid for this work

W18833	MATa	RPC53-3HA-TRP1 reg1-delta::HIS3MX6	Ferdinand Schmid for this work
W18834	MATα	RPC53-3HA-TRP1 reg1-delta::HIS3MX6	Ferdinand Schmid for this work
W18834	MATα	RPC53-3HA-TRP1 reg1-delta::HIS3MX6	Ferdinand Schmid for this work
W18835	MATα	KNS1-12xFLAG-KanMX6 snf1-delta::LEU2 reg1-delta::HIS3MX6	Ferdinand Schmid for this work
W18835	MATα	KNS1-12xFLAG-KanMX6 snf1-delta::LEU2 reg1-delta::HIS3MX6	Ferdinand Schmid for this work
W18836	MATa	KNS1-12xFLAG-KanMX6 snf1-delta::LEU2	Ferdinand Schmid for this work
W18836	MATα	KNS1-12xFLAG-KanMX6 snf1-delta::LEU2	Ferdinand Schmid for this work
W18837	MATα	KNS1-12xFLAG-KanMX6 snf1-delta::LEU2	Ferdinand Schmid for this work
W18837	MATa	KNS1-12xFLAG-KanMX6 snf1-delta::LEU2	Ferdinand Schmid for this work
W18838	MATa	RPC53-GFP-URA3 tCYC1::pTEF2-MYC3-KNS1-tCYC-LEU2	Ferdinand Schmid for this work
W18838	MATa	RPC53-GFP-URA3 tCYC1::pTEF2-MYC3-KNS1-tCYC-LEU2	Ferdinand Schmid for this work
W18839	MATα	RPC53-GFP-URA3 tCYC1::pTEF2-MYC3-KNS1-tCYC-LEU2	Ferdinand Schmid for this work
W18839	MATα	RPC53-GFP-URA3 tCYC1::pTEF2-MYC3-KNS1-tCYC-LEU2	Ferdinand Schmid for this work
W18967	MATα	RPC53-GFP-URA3 tCYC1::pTEF2-MYC3-KNS1-tCYC-LEU2 HMO1-3mCherry-tCYC1-TRP1	Ferdinand Schmid for this work
W18967	MATα	RPC53-GFP-URA3 tCYC1::pTEF2-MYC3-KNS1-tCYC-LEU2 HMO1-3mCherry-tCYC1-TRP1	Ferdinand Schmid for this work
W18968	MATa	RPC53-GFP-URA3 tCYC1::pTEF2-MYC3-KNS1-tCYC-LEU2 HMO1-3mCherry-tCYC1-TRP1	Ferdinand Schmid for this work
W18968	MATa	RPC53-GFP-URA3 tCYC1::pTEF2-MYC3-KNS1-tCYC-LEU2 HMO1-3mCherry-tCYC1-TRP1	Ferdinand Schmid for this work
W18969	MATα	RPC53-3HA-TRP1 snf1-delta::LEU2 cdc123-delta326-HA3-His	Ferdinand Schmid for this work
W18969	MATα	RPC53-3HA-TRP1 snf1-delta::LEU2 cdc123-delta326-HA3-His	Ferdinand Schmid for this work

W18970	MATa	RPC53-3HA-TRP1 snf1-delta::LEU2 cdc123-delta326-HA3-His	Ferdinand Schmid for this work
W18970	MATa	RPC53-3HA-TRP1 snf1-delta::LEU2 cdc123-delta326-HA3-His	Ferdinand Schmid for this work
W18971	MATa	RPC53-GFP-URA3 HTA1-yEmRFP-Kan	Antje Machetanz-Morokane for this work
W18972	MATα	RPC53-GFP-URA3 HTA1-yEmRFP-Kan	Antje Machetanz-Morokane for this work
W18973	MATa	RPC53-GFP-URA3 HTA2-yEmRFP-Kan	Antje Machetanz-Morokane for this work
W18974	MATα	RPC53-GFP-URA3 HTA2-yEmRFP-Kann	Antje Machetanz-Morokane for this work
W18975	MATa	RPC53-GFP-URA3 NOP56-3mCherry-tCYC1-TRP1	Antje Machetanz-Morokane for this work
W18976	MATα	RPC53-GFP-URA3 NOP56-3mCherry-tCYC1-TRP1	Antje Machetanz-Morokane for this work
W18977	MATa	RPC53-GFP-URA3 FOB1-ytdTomato-TRP1	Antje Machetanz-Morokane for this work
W18978	MATα	RPC53-GFP-URA3 FOB1-ytdTomato-TRP1	Antje Machetanz-Morokane for this work
W19026	MATa	KNS1-GFP-URA3	Jannis Winter for this work
W19027	MATα	KNS1-GFP-URA3	Jannis Winter for this work
W19028	MATa	KNS1-NTD(1-289 aa)-GFP-URA3	Jannis Winter for this work
W19029	MATα	KNS1-NTD(1-289 aa)-GFP-URA3	Jannis Winter for this work
W19109	MATa	KNS1-NTD(1-289 aa)-FLAG-URA3	Jannis Winter for this work
W19110	MATα	KNS1-NTD(1-289 aa)-FLAG-URA3	Jannis Winter for this work
W19111	MATα	tcyc::pTEF2-MYC3-KNS1-CTD(278-737 aa)-tCYC-LEU2	Jannis Winter for this work
W19112	MATα	tcyc1::pTEF2-GFP-KNS1-NTD(1-289aa)-tCYC1-URA3 trp1::pTEF2-mCherry-SWI5-S/A-tCYC1-TRP1	Jannis Winter for this work
W19113	MATα	tcyc1::pTEF2-GFP-KNS1-CTD(278-737aa)-tCYC1-URA3 trp1::pTEF2-mCherry-SWI5-S/A-tCYC1-TRP1	Jannis Winter for this work
W19114	MATα	tcyc1::pTEF2-GFP-KNS1(D440A)-tCYC1-URA3 trp1::pTEF2-mCherry-SWI5-S/A-tCYC1-TRP1	Jannis Winter for this work
W19115	MATa	KNS1-GFP-URA3 trp1::pTEF2-mCherry-SWI5-S/A-tCYC1-TRP1 cdc123-deltaC(1-326)-HA3-HIS3MX6	Jannis Winter for this work

W19123	MATa	KNS1-NTD(1-289 aa)-12xFLAG-URA3 cdc123-deltaC(1-326)-HA3-HIS3MX6	Jannis Winter for this work
W19124	MATα	KNS1-NTD(1-289 aa)-12xFLAG-URA3 cdc123-deltaC(1-326)-HA3-HIS3MX6	Jannis Winter for this work
W19125	MATa	KNS1-3HA-TRP1	This work
W19126	MATa	KNS1-13MYC-TRP1	This work
W19127	MATa	KNS1-3HA-TRP1 cdc123-deltaC(1-326)-HA3-HIS3MX6	This work
W19128	MATα	KNS1-3HA-TRP1 cdc123-deltaC(1-326)-HA3-HIS3MX6	This work
W19129	MATa	KNS1-13MYC-TRP1 cdc123-deltaC(1-326)-HA3-HIS3MX6	This work
W19130	MATα	KNS1-13MYC-TRP1 cdc123-deltaC(1-326)-HA3-HIS3MX6	This work
W19132	MATa	KNS1-GFP-URA3 trp1::pTEF2-mCherry-SWI5-S/A-tCYC1-TRP1	Jannis Winter for this work
W19133	MATα	KNS1-GFP-URA3 trp1::pTEF2-mCherry-SWI5-S/A-tCYC1-TRP1	Jannis Winter for this work
W19134	MATa	KNS1-12xFLAG-KanMX6 tif4631-delta::HIS3MX6	This work
W19135	MATα	KNS1-12xFLAG-KanMX6 tif4631-delta::HIS3MX6	This work
W19136	MATa	KNS1-12xFLAG-KanMX6 pep4delta::URA3 cdc123-deltaC(1-326)-HA3-HIS3MX6	This work
W19137	MATα	KNS1-12xFLAG-KanMX6 pep4delta::URA3 cdc123-deltaC(1-326)-HA3-HIS3MX6	This work
W19138	MATa	RPC53-GFP-URA3 NOP56-3mCherry-tCYC1-TRP1 cdc123-deltaC(1-326)-HA3-HIS3MX6	This work
W19139	MATa	RPC53-GFP-URA3 FOB1-ytdTomato-TRP1 cdc123-deltaC(1-326)-HA3-HIS3MX6	This work
W19140	MATα	RPC53-GFP-URA3 FOB1-ytdTomato-TRP1 cdc123-deltaC(1-326)-HA3-HIS3MX6	This work
W19141	MATa	RPC53-3HA-TRP1 tif4631-delta::HIS3MX6	This work
W19142	MATα	RPC53-3HA-TRP1 tif4631-delta::HIS3MX6	This work

W19143	MATa	KNS1-NTD(1-289 aa)-GFP trp1::pTEF2-mCherry-SWI5-S/A-tCYC1-TRP1	Jannis Winter for this work
W19144	MATα	KNS1-NTD(1-289 aa)-GFP trp1::pTEF2-mCherry-SWI5-S/A-tCYC1-TRP1	Jannis Winter for this work
W19157	MATa	tcyc::pTEF2-MYC3-KNS1-CTD(278-737 aa)-tCYC-LEU2 cdc123-deltaC(1-326)-HA3-HIS3MX6	Jannis Winter for this work
W19158	MATα	tcyc::pTEF2-MYC3-KNS1-CTD(278-737 aa)-tCYC-LEU2 cdc123-deltaC(1-326)-HA3-HIS3MX6	Jannis Winter for this work
W19159	MATa	tcyc1::pTEF-GFP-KNS1-CTD(278-737 aa)-tCYC1-URA3 cdc123-deltaC(1-326)-HA3-HIS3MX6 trp1::pTEF2-mCherry-SWI5-S/A-tCYC1-TRP1	Jannis Winter for this work
W19160	MATα	tcyc1::pTEF-GFP-KNS1-CTD(278-737 aa)-tCYC1-URA3 cdc123-deltaC(1-326)-HA3-HIS3MX6 trp1::pTEF2-mCherry-SWI5-S/A-tCYC1-TRP1	Jannis Winter for this work
W19161	MATa	tcyc1::pTEF-GFP-KNS1-CTD(278-737 aa)-tCYC1-URA3 trp1::pTEF2-mCherry-SWI5-S/A-tCYC1-TRP1	Jannis Winter for this work
W19162	MATa	tcyc1::pTEF-GFP-KNS1(D440A)-tCYC1-URA3 cdc123-deltaC(1-326)-HA3-HIS3MX6 trp1::pTEF2-mCherry-SWI5-S/A-tCYC1-TRP1	Jannis Winter for this work
W19163	MATα	tcyc1::pTEF-GFP-KNS1(D440A)-tCYC1-URA3 cdc123-deltaC(1-326)-HA3-HIS3MX6 trp1::pTEF2-mCherry-SWI5-S/A-tCYC1-TRP1	Jannis Winter for this work
W19164	MATa	tcyc1::pTEF-GFP-KNS1(D440A)-tCYC1-URA3 trp1::pTEF2-mCherry-SWI5-S/A-tCYC1-TRP1	Jannis Winter for this work
W19249	MATα	trp1::pTEF2-mCherry-SWI5-S/A-tCYC1-TRP1 pTEF2-GFP-SSO1-tCYC1-URA3 tif4631-delta::HIS3MX6	This work
W19250	MATα	trp1::pTEF2-mCherry-SWI5-S/A-tCYC1-TRP1 pTEF2-GFP-SSO1-tCYC1-URA3 tif4631-delta::HIS3MX6	This work
W19255	MATα	RPC53-GFP-URA3 HTA1-yEmRFP-Kan cdc123-deltaC(1-326)-HA3-HIS3MX6	This work

W19256	MATα	RPC53-GFP-URA3 HTA2-yEmRFP-Kan cdc123-deltaC(1-326)-HA3-HIS3MX6	This work
W19257	MATα	tcyc::pTEF2-MYC3-KNS1-NTD(1-289 aa)-tCYC-LEU2	Jannis Winter for this work
W19258	MATα	tcyc::pTEF2-MYC3-KNS1-(D440A)-tCYC-LEU2	Jannis Winter for this work
W19259	MATα	ura3::pGAL1-GFP-KNS1(D440A)-tCYC-URA3	Jannis Winter for this work
W19260	MATα	tcyc::pGAL1-GFP-KNS1-tCYC-URA3	Jannis Winter for this work
W19261	MATa	tcyc::pTEF-MYC3-KNS1(D440A)-tCYC-LEU2 cdc123-deltaC(1-326)-HA3-HIS3MX6	Jannis Winter for this work
W19262	MATα	tcyc::pTEF-MYC3-KNS1(D440A)-tCYC-LEU2 cdc123-deltaC(1-326)-HA3-HIS3MX6	Jannis Winter for this work
W19265	MATa	tcyc::pTEF-MYC3-KNS1(D440A)-tCYC-LEU2	Jannis Winter for this work
W19266	MATa	tcyc::pTEF-MYC3-KNS1-CTD(278-737 aa)-tCYC-LEU2	Jannis Winter for this work
W19267	MATα	KNS1-NTD(1-289 aa)-GFP trp1::pTEF2-mCherry-SWI5-S/A-tCYC1-TRP1 cdc123-deltaC(1-326)-HA3-HIS3MX6	Jannis Winter for this work
W19269	MATα	tcyc1::pTEF-GFP-KNS1-NTD(1-289 aa)-URA3-tCYC1 trp1::pTEF2-mCherry-SWI5-S/A-tCYC1-TRP1 cdc123-deltaC(1-326)-HA3-HIS3MX6	Jannis Winter for this work
W19284	MATα	tcyc1::pTEF-GFP-KNS1-CTD(278-737 aa D440A)-URA3-tCYC1 trp1::pTEF2-mCherry-SWI5-S/A-tCYC1-TRP1	Jannis Winter for this work
W19285	MATα	tcyc::pTEF-MYC3-KNS1-CTD(278-737 aa D440A)-URA3-tCYC	Jannis Winter for this work
W19330	MATa	RPC53-3HA-TRP1 bar1-delta::LEU2	This work
W19331	MATα	RPC53-3HA-TRP1 bar1-delta::LEU2	This work
W19332	MATa	KNS1-12xFLAG-KanMX6 bar1-delta::LEU2	This work
W19333	MATα	KNS1-12xFLAG-KanMX6 bar1-delta::LEU2	This work

W19334	MATa	KNS1-12xFLAG-KanMX6 snf1-delta::LEU2 cdc123-deltaC(1-326)-HA3-HIS3MX6	This work
W19335	MATα	KNS1-12xFLAG-KanMX6 snf1-delta::LEU2 cdc123-deltaC(1-326)-HA3-HIS3MX6	This work
W19336	MATa	RPC53-3HA-TRP1 gcn2-delta::natNT2	This work
W19337	MATα	RPC53-3HA-TRP1 gcn2-delta::natNT2	This work
W19338	MATa	RPC53-3HA-TRP1 gcn2-delta::natNT2 cdc123-deltaC(1-326)-HA3-HIS3MX6	This work
W19339	MATα	RPC53-3HA-TRP1 gcn2-delta::natNT2 cdc123-deltaC(1-326)-HA3-HIS3MX6	This work
W19340	MATα	KNS1-12xFLAG-KanMX6 gcn2-delta::natNT2	This work
W19341	MATα	KNS1-12xFLAG-KanMX6 gcn2-delta::natNT2	This work
W19342	MATα	KNS1-12xFLAG-KanMX6 gcn2-delta::natNT2 cdc123-deltaC(1-326)-HA3-HIS3MX6	This work
W19343	MATα	KNS1-12xFLAG-KanMX6 gcn2-delta::natNT2 cdc123-deltaC(1-326)-HA3-HIS3MX6	This work
W19344	MATa	RPC53-3HA-TRP1 gcn4-delta::natNT2	This work
W19345	MATα	RPC53-3HA-TRP1 gcn4-delta::natNT2	This work
W19346	MATa	RPC53-3HA-TRP1 gcn4-delta::natNT2 cdc123-deltaC(1-326)-HA3-HIS3MX6	This work
W19347	MATα	RPC53-3HA-TRP1 gcn4-delta::natNT2 cdc123-deltaC(1-326)-HA3-HIS3MX6	This work
W19348	MATa	KNS1-12xFLAG-KanMX6 gcn4-delta::natNT2	This work
W19349	MATα	KNS1-12xFLAG-KanMX6 gcn4-delta::natNT2	This work
W19350	MATa	KNS1-12xFLAG-KanMX6 gcn4-delta::natNT2 cdc123-deltaC(1-326)-HA3-HIS3MX6	This work

W19351	MATα	KNS1-12xFLAG-KanMX6 gcn4-delta::natNT2 cdc123-deltaC(1-326)-HA3-HIS3MX6	This work
W19380	MATa	RPC53-3HA-TRP1 cdc123-delta326-HA3-His gcn3-delta::natNT2	Kathrin Preußel Danger for this work
W19381	MATα	RPC53-3HA-TRP1 cdc123-delta326-HA3-His gcn3-delta::natNT2	Kathrin Preußel Danger for this work
W19382	MATa	RPC53-3HA-TRP1 pfk2-delta::KanMX6	Kathrin Preußel Danger for this work
W19383	MATα	RPC53-3HA-TRP1 pfk2-delta::KanMX6	Kathrin Preußel Danger for this work
W19384	MATa	RPC53-3HA-TRP1 hxk2-delta::LEU2	Kathrin Preußel Danger for this work
W19385	MATα	RPC53-3HA-TRP1 hxk2-delta::LEU2	Kathrin Preußel Danger for this work
W19386	MATa	KNS1-12xFLAG-KanMX6 hxk2-delta::LEU2	Kathrin Preußel Danger for this work
W19387	MATα	KNS1-12xFLAG-KanMX6 hxk2-delta::LEU2	Kathrin Preußel Danger for this work
W19388	MATa	RPC53-3HA-TRP1 gcn3-delta::natNT2	Kathrin Preußel Danger for this work
W19389	MATα	RPC53-3HA-TRP1 gcn3-delta::natNT2	Kathrin Preußel Danger for this work
W19390	MATa	tcyc1::pTEF2-HA4-KNS1-tCYC1-LEU2	Kathrin Preußel Danger for this work
W19391	MATα	tcyc1::pTEF2-HA4-KNS1-tCYC1-LEU2	Kathrin Preußel Danger for this work
W19392	MATa	tcyc1::pTEF2-HA4-KNS1(D440A)-tCYC1-LEU2	Kathrin Preußel Danger for this work
W19393	MATα	tcyc1::pTEF2-HA4-KNS1(D440A)-tCYC1-LEU2	Kathrin Preußel Danger for this work
W19454	MATa	tCYC1::pTEF2-MYC3-KNS1-tCYC-LEU2 RPC53-3HA-TRP1 gcn4-delta::natNT2	This work
W19455	MATα	tCYC1::pTEF2-MYC3-KNS1-tCYC-LEU2 RPC53-3HA-TRP1 gcn4-delta::natNT2	This work
W19456	MATa	KNS1-12xFLAG-KanMX6 reg1-delta::His3MX6 gcn4-delta::natNT2	This work
W19457	MATα	KNS1-12xFLAG-KanMX6 reg1-delta::His3MX6 gcn4-delta::natNT2	This work
W19458	MATα	KNS1-12xFLAG-KanMX6 pfk2-delta::NATMX4	Kathrin Preußel Danger for this work

W19459	MATα	KNS1-12xFLAG-KanMX6 pfk2-delta::NATMX4	Kathrin Preußel Danger for this work
W19460	MATa	KNS1-12xFLAG-KanMX6 cdc123-deltaC(1-326)-HA3-HIS3MX6 gcn3-delta::natNT2	Kathrin Preußel Danger for this work
W19461	MATα	KNS1-12xFLAG-KanMX6 cdc123-deltaC(1-326)-HA3-HIS3MX6 gcn3-delta::natNT2	Kathrin Preußel Danger for this work
W19462	MATa	KNS1-12xFLAG-KanMX6 gcn3-delta::natNT2	Kathrin Preußel Danger for this work
W19463	MATα	KNS1-12xFLAG-KanMX6 gcn3-delta::natNT2	Kathrin Preußel Danger for this work
W19464	MATa	RPC53-3HA-TRP1 pfk2-delta::NATMX4 kns1-delta::KanMX6	Kathrin Preußel Danger for this work
W19465	MATα	RPC53-3HA-TRP1 pfk2-delta::NATMX4 kns1-delta::KanMX6	Kathrin Preußel Danger for this work
W19466	MATa	RPC53-3HA-TRP1 hxk2-delta::LEU2 kns1-delta::KanMX6	Kathrin Preußel Danger for this work
W19467	MATα	RPC53-3HA-TRP1 hxk2-delta::LEU2 kns1-delta::KanMX6	Kathrin Preußel Danger for this work
W19468	MATa	RPC53-3HA-TRP1 gcn4-delta::natNT2 kns1-delta::KanMX6 cdc123-deltaC(1-326)-HA3-HIS3MX6	Kathrin Preußel Danger for this work
W19469	MATα	RPC53-3HA-TRP1 gcn4-delta::natNT2 kns1-delta::KanMX6 cdc123-deltaC(1-326)-HA3-HIS3MX6	Kathrin Preußel Danger for this work
W19470	MATa	RPC53-3HA-TRP1 gcn4-delta::natNT2 kns1-delta::KanMX6	Kathrin Preußel Danger for this work
W19471	MATα	RPC53-3HA-TRP1 gcn4-delta::natNT2 kns1-delta::KanMX6	Kathrin Preußel Danger for this work
W19472	MATa	tcyc1::pTEF2-HA4-KNS1-tCYC1-LEU2 kns1-delta::KanMX6	Kathrin Preußel Danger for this work
W19473	MATα	tcyc1::pTEF2-HA4-KNS1-tCYC1-LEU2 kns1-delta::KanMX6	Kathrin Preußel Danger for this work
W19474	MATa	tcyc1::pTEF2-HA4-KNS1-tCYC1-LEU2 RPC53-3HA-TRP1 kns1-delta::KanMX6	Kathrin Preußel Danger for this work
W19475	MATa	tcyc1::pTEF2-HA4-KNS1(D440A)-tCYC1-LEU2 kns1-delta::KanMX6	Kathrin Preußel Danger for this work
W19476	MATα	tcyc1::pTEF2-HA4-KNS1(D440A)-tCYC1-LEU2 kns1-delta::KanMX6	Kathrin Preußel Danger for this work

W19477	MATa	tcyc1::pTEF2-HA4-KNS1(D440A)-tCYC1-LEU2 RPC53-3HA-TRP1 kns1-delta::KanMX6	Kathrin Preußel Danger for this work
W19478	MATα	trp1::pTEF2-mCherry-SWI5-S/A-tCYC1-TRP1 ura3::pTEF2-KNS1-YEGFP-tCYC1-URA3	Adelheid Weissgerber for this work
W19479	MATα	trp1::pTEF2-mCherry-SWI5-S/A-tCYC1-TRP1 ura3::pTEF2-KNS1-YEGFP-tCYC1-URA3	Adelheid Weissgerber for this work
W19480	MATα	trp1::pTEF2-mCherry-SWI5-S/A-tCYC1-TRP1 ura3::pTEF2-KNS1(D440A)-YEGFP-tCYC1-URA3	Adelheid Weissgerber for this work
W19481	MATα	trp1::pTEF2-mCherry-SWI5-S/A-tCYC1-TRP1 ura3::pTEF2-KNS1(D440A)-YEGFP-tCYC1-URA3	Adelheid Weissgerber for this work
W19545	MATa	RPC53-3HA-TRP1 kns1-delta::KanMX6 cdc123-delta326-HA3-His tcyc::pTEF2-MYC3-KNS1(D440A)-tCYC-LEU2	Severin Graml for this work
W19546	MATα	RPC53-3HA-TRP1 kns1-delta::KanMX6 cdc123-delta326-HA3-His tcyc::pTEF2-MYC3-KNS1(D440A)-tCYC-LEU2	Severin Graml for this work
W19547	MATa	RPC53-3HA-TRP1 cdc123-delta326-HA3-His tcyc::pTEF2-MYC3-KNS1(D440A)-tCYC-LEU2	Severin Graml for this work
W19548	MATα	RPC53-3HA-TRP1 cdc123-delta326-HA3-His tcyc::pTEF2-MYC3-KNS1(D440A)-tCYC-LEU2	Severin Graml for this work
W19549	MATa	RPC53-3HA-TRP1 kns1-delta::KanMX6 tcyc::pTEF2-MYC3-KNS1(D440A)-tCYC-LEU2	Severin Graml for this work
W19550	MATα	RPC53-3HA-TRP1 kns1-delta::KanMX6 tcyc::pTEF2-MYC3-KNS1(D440A)-tCYC-LEU2	Severin Graml for this work
W19551	MATa	RPC53-3HA-TRP1 tcyc::pTEF2-MYC3-KNS1(D440A)-tCYC-LEU2	Severin Graml for this work
W19552	MATa	RPC53-3HA-TRP1 tcyc::pTEF2-MYC3-KNS1(D440A)-tCYC-LEU2	Severin Graml for this work
W19584	MATa	RPC53-GFP-URA3 HTA2-yEmRFP-Kan tCYC1::pTEF2-MYC3-KNS1-tCYC-LEU2	This work

W19585	MATα	RPC53-GFP-URA3 HTA2-yEmRFP-Kan tCYC1::pTEF2-MYC3-KNS1-tCYC-LEU2	This work
W19586	MATa	RPC53-GFP-URA3 HTA2-yEmRFP-Kan cdc123-deltaC(1-326)-HA3-HIS3MX6	This work
W19587	MATα	ura3::pTEF2-GFP-KNS1-tCYC1-URA3 trp1::pTEF2-mCherry-SWI5-S/A-tCYC1-TRP1	This work
W19588	MATα	ura3::pTEF2-GFP-KNS1(D440A)-tCYC1-URA3 trp1::pTEF2-mCherry-SWI5-S/A-tCYC1-TRP1	This work
W19589	MATα	ura3::pTEF2-GFP-KNS1-NTD(1-289aa)-tCYC1-URA3 trp1::pTEF2-mCherry-SWI5-S/A-tCYC1-TRP1	This work
W19590	MATα	ura3::pTEF2-GFP-KNS1-CTD(278-737aa)-tCYC1-URA3 trp1::pTEF2-mCherry-SWI5-S/A-tCYC1-TRP1	This work
W19591	MATα	ura3:.pTEF2-GFP-KNS1-CTD(278-737aa D440A)-tCYC1-URA3 trp1::pTEF2-mCherry-SWI5-S/A-tCYC1-TRP1	This work
W19614	MATa	ura3::pTEF2-KNS1-NTD(1-289aa)-YEGFP-tCYC1-URA3 trp1::pTEF2-mCherry-SWI5-S/A-tCYC1-TRP1	This work
W19615	MATα	ura3::pTEF2-KNS1-NTD(1-289aa)-YEGFP-tCYC1-URA3 trp1::pTEF2-mCherry-SWI5-S/A-tCYC1-TRP1	This work
W19616	MATα	tcyc1::pTEF2-MYC3-KNS1-tCYC-LEU2 ura3::pGAL1-HA3-HCT1-m11-URA3	This work
W19617	MATα	tcyc1::pTEF2-MYC3-KNS1-tCYC-LEU2 ura3::pGAL1-HA3-HCT1-m11-URA3	This work
W19618	MATα	tcyc1::pTEF2-HA4-KNS1-tCYC1-LEU2 ura3::pGAL1-MYC3-HCT1-m11-URA3	This work
W19619	MATα	tcyc1::pTEF2-HA4-KNS1-tCYC1-LEU2 ura3::pGAL1-MYC3-HCT1-m11-URA3	This work
W19620	MATa	tcyc1::pTEF2-MYC3-KNS1-tCYC-LEU2 hct1-delta::kanMX4	This work
W19621	MATα	tcyc1::pTEF2-MYC3-KNS1-tCYC-LEU2 hct1-delta::kanMX4	This work

W19622	MATa	tcyc1::pTEF2-MYC3-KNS1-NTD(1-289aa)-tCYC-LEU2 hct1-delta::kanMX4	This work
W19623	MATα	tcyc1::pTEF2-MYC3-KNS1-NTD(1-289aa)-tCYC-LEU2 hct1-delta::kanMX4	This work
W19624	MATa	tcyc1::pTEF2-MYC3-KNS1-NTD(1-289aa)-tCYC-LEU2	This work
W19637	MATa	ura3::pTEF2-KNS1-NTDshort(1-174aa)-YEGFP-tCYC1-URA3 trp1::pTEF2-mCherry-SWI5-S/A-tCYC1-TRP1	This work
W19638	MATα	ura3::pTEF2-KNS1-NTDshort(1-174aa)-YEGFP-tCYC1-URA3 trp1::pTEF2-mCherry-SWI5-S/A-tCYC1-TRP1	This work
W19641	MATa	ura3::pTEF2-KNS1-YEGFP-tCYC1-URA3 trp1::pTEF2-mCherry-SWI5-S/A-tCYC1-TRP1 hct1-delta::kanMX4	This work
W19642	MATα	ura3::pTEF2-KNS1-YEGFP-tCYC1-URA3 trp1::pTEF2-mCherry-SWI5-S/A-tCYC1-TRP1 hct1-delta::kanMX4	This work
W19643	MATa	ura3::pTEF2-GFP-KNS1-NTD(1-289aa)-tCYC1-URA3 trp1::pTEF2-mCherry-SWI5-S/A-tCYC1-TRP1 hct1-delta::kanMX4	This work
W19644	MATα	ura3::pTEF2-GFP-KNS1-NTD(1-289aa)-tCYC1-URA3 trp1::pTEF2-mCherry-SWI5-S/A-tCYC1-TRP1 hct1-delta::kanMX4	This work
W19687	MATα	ura3::pTEF2-GFP-KNS1-CTDlong(166-737aa)-tCYC1-URA3 trp1::pTEF2-mCherry-SWI5-S/A-tCYC1-TRP1	This work
W19694	MATa	RPC53-3HA-TRP1 gcn4-delta::natNT2 hxk2-delta::LEU2	Antje Machetanz-Morokane for this work
W19695	MATα	RPC53-3HA-TRP1 gcn4-delta::natNT2 hxk2-delta::LEU2	Antje Machetanz-Morokane for this work
W19696	MATa	RPC53-3HA-TRP1 gcn4-delta::natNT2 pfk2delta::KanMX6	Antje Machetanz-Morokane for this work
W19697	MATα	RPC53-3HA-TRP1 gcn4-delta::natNT2 pfk2delta::KanMX6	Antje Machetanz-Morokane for this work

W19698	MATa	pTEF2-KNS1-YEGFP-tCYC1-URA3 pTEF2-mCherry-SWI5-S/A-tCYC1-TRP msn5-delta::HisMX	Antje Machetanz-Morokane for this work
W19699	MATα	pTEF2-KNS1-YEGFP-tCYC1-URA3 pTEF2-mCherry-SWI5-S/A-tCYC1-TRP msn5-delta::HisMX	Antje Machetanz-Morokane for this work
W19700	MATa	pTEF2-KNS1-YEGFP-tCYC1-URA3 pTEF2-mCherry-SWI5-S/A-tCYC1-TRP cdc55-delta::natNT2	Antje Machetanz-Morokane for this work
W19701	MATα	pTEF2-KNS1-YEGFP-tCYC1-URA3 pTEF2-mCherry-SWI5-S/A-tCYC1-TRP cdc55-delta::natNT2	Antje Machetanz-Morokane for this work
W19714	MATα	ura3::pGAL1-GFP-KNS1-CTD(280-737aa)-tCYC1-URA3 trp1::pTEF2-mCherry-SWI5-S/A-tCYC1-TRP1	This work
W19715	MATα	ura3::pGAL1-GFP-KNS1-CTD(280-737aa)-tCYC1-URA3 trp1::pTEF2-mCherry-SWI5-S/A-tCYC1-TRP1	This work
W19716	MATα	ura3::pGAL1-GFP-KNS1-CTDlong(166-737aa)-tCYC1-URA3 trp1::pTEF2-mCherry-SWI5-S/A-tCYC1-TRP1	This work
W19717	MATα	ura3::pGAL1-GFP-KNS1-CTDlong(166-737aa)-tCYC1-URA3 trp1::pTEF2-mCherry-SWI5-S/A-tCYC1-TRP1	This work
W19718	MATα	ura3::pGAL1-GFP-KNS1-tCYC1-URA3 trp1::pTEF2-mCherry-SWI5-S/A-tCYC1-TRP1	This work
W19719	MATα	ura3::pGAL1-GFP-KNS1(D440A)-tCYC1-URA3 trp1::pTEF2-mCherry-SWI5-S/A-tCYC1-TRP1	This work
W19720	MAT a	RPC53-3HA-TRP1 gcn4-delta::natNT2 reg1delta::His3MX6	This work
W19721	MATα	RPC53-3HA-TRP1 gcn4-delta::natNT2 reg1delta::His3MX6	Antje Machetanz-Morokane for this work
W19740	MATa	ura3::5'UTR-KNS1(1-9)-GFP-SWI5-S/A-myc13-URA3 hxk2-delta::LEU2	This work
W19741	MATα	ura3::5'UTR-KNS1(1-9)-GFP-SWI5-S/A-myc13-URA3 hxk2-delta::LEU2	This work
W19742	MATa	ura3::5'UTR-KNS1(1-9)-GFP-SWI5-S/A-myc13-URA3 pfk2-delta::NATMX4	This work

W19743	MATα	ura3::5'UTR-KNS1(1-9)-GFP-SWI5-S/A-myc13-URA3 pfk2-delta::NATMX4	This work
W19747	MATa	hxk2-delta::LEU2 ura3::pTEF2-KNS1-NTD(1-289aa)-YEGFP-tCYC1-URA3 trp1::pTEF2-mCherry-SWI5-S/A-tCYC1-TRP1	Jannis Winter for this work
W19748	MATa	hxk2-delta::LEU2 ura3::pTEF2-KNS1-NTD(1-289aa)-YEGFP-tCYC1-URA3 trp1::pTEF2-mCherry-SWI5-S/A-tCYC1-TRP1	Jannis Winter for this work
W19749	MATα	hxk2-delta::LEU2 ura3::pTEF2-KNS1-YEGFP-tCYC1-URA3 trp1::pTEF2-mCherry-SWI5-S/A-tCYC1-TRP1	Jannis Winter for this work
W19750	MATα	hxk2-delta::LEU2 ura3::pTEF2-KNS1-YEGFP-tCYC1-URA3 trp1::pTEF2-mCherry-SWI5-S/A-tCYC1-TRP1	Jannis Winter for this work
W19759	MATa	RPC53-3HA-TRP pfk2delta::KanMX6 gcn2-delta::natNT2	Antje Machetanz-Morokane for this work
W19760	MATα	RPC53-3HA-TRP pfk2delta::KanMX6 gcn2-delta::natNT2	Antje Machetanz-Morokane for this work
W19761	MATa	RPC53-3HA-TRP hxk2-delta::LEU2 gcn2-delta::natNT2	Antje Machetanz-Morokane for this work
W19762	MATα	RPC53-3HA-TRP hxk2-delta::LEU2 gcn2-delta::natNT2	Antje Machetanz-Morokane for this work
W19772	MATa	tor1delta::HIS3MX6	Antje Machetanz-Morokane for this work
W19773	MATα	tor1delta::HIS3MX6	Antje Machetanz-Morokane for this work
W19799	MATa	tor1delta::HIS3MX6 RPC53-3HA-TRP1	Antje Machetanz-Morokane for this work
W19800	MATα	tor1delta::HIS3MX6 RPC53-3HA-TRP1	Antje Machetanz-Morokane for this work
W19802	MATa	ise1delta::Kan	Antje Machetanz-Morokane for this work
W19803	MATα	ise1delta::Kan	Antje Machetanz-Morokane for this work
W19842	MATα	ura3::pTEF2-GFP-KNS1-NTDshort2(166-289aa)-URA3	Kathrin Preußel Danger for this work
W19843	MATα	ura3::pTEF2-GFP-KNS1-NTDshort2(166-289aa)-URA3	Kathrin Preußel Danger for this work

W19844	MATa	ise1delta::Kan leu::pTEF-myc-KNS1-NTD(1-289)-LEU	Antje Machetanz-Morokane for this work
W19845	MATα	ise1delta::Kan leu::pTEF-myc-KNS1-NTD(1-289)-LEU	Antje Machetanz-Morokane for this work
W19846	MATa	RPC53-3HA-TRP1 pep4-delta::URA3	Kathrin Preußel Danger for this work
W19847	MATα	RPC53-3HA-TRP1 pep4-delta::URA3	Kathrin Preußel Danger for this work
W19848	MATa	RPC53-3HA-TRP1 pep4-delta::URA3 pTEF-MYC-KNS1-NTD(1-289aa)-LEU2	Kathrin Preußel Danger for this work
W19849	MATa	RPC53-3HA-TRP1 pep4-delta::URA3 pTEF-MYC-KNS1-NTD(1-289aa)-LEU2	Kathrin Preußel Danger for this work
W19865	MATa	KNS1-12xFLAG-KanMX6 rpd3-delta-Kl-TRP1	This work
W19866	MATα	KNS1-12xFLAG-KanMX6 rpd3-delta-Kl-TRP1	This work
W19867	MATa	cat8-delta::HIS3	This work
W19868	MATa	pep4delta::HIS3 ura3::pTEF2-KNS1-YEGFP-tCYC1-URA3	Antje Machetanz-Morokane for this work
W19869	MATα	pep4delta::HIS3 ura3::pTEF2-KNS1-YEGFP-tCYC1-URA3	Antje Machetanz-Morokane for this work
W19870	MATa	pep4delta::HIS3 ura3::pTEF2-KNS1(D440A)-YEGFP-tCYC1-URA3	Antje Machetanz-Morokane for this work
W19871	MATα	pep4delta::HIS3 ura3::pTEF2-KNS1(D440A)-YEGFP-tCYC1-URA3	Antje Machetanz-Morokane for this work
W19872	MATa/α	KNS1-12xFLAG-KanMX6/KNS1-13MYC-TRP	Antje Machetanz-Morokane for this work
W19873	MATa/α	bar1-delta::KanMX/BAR1 KNS1-13MYC-TRP/KNS1	Antje Machetanz-Morokane for this work
W19874	MATa/α	KNS1-12xFLAG-KanMX6/KNS1 tCYC1::pTEF2-MYC3-KNS1-tCYC-LEU2/tCYC1	Antje Machetanz-Morokane for this work
W19875	MATa/α	bar1-delta::KanMX/BAR1 tCYC1::pTEF2-MYC3-KNS1-tCYC-LEU2/tCYC	Antje Machetanz-Morokane for this work
W19876	MATα	cat8-delta::HIS3	This work
W19877	MATa	RPC53-3HA-TRP1 cat8-delta::HIS3	This work
W19878	MATα	RPC53-3HA-TRP1 cat8-delta::HIS3	This work
W19879	MATa	KNS1-12xFLAG-KanMX6 cat8-delta::HIS3	This work

W19880	MATα	KNS1-12xFLAG-KanMX6 cat8-delta::HIS3	This work
W19881	MATa	RPC53-3HA-TRP1 rpd3-delta-Kl-TRP1	This work
W19882	MATα	RPC53-3HA-TRP1 rpd3-delta-Kl-TRP1	This work
W19883	MATa	KNS1-12xFLAG-KanMX6 tor1delta::HIS3MX6	This work
W19884	MATα	KNS1-12xFLAG-KanMX6 tor1delta::HIS3MX6	This work
W19970	MATa	KNS1-12xFLAG-KanMX6 ise1delta::Kan	This work
W19971	MATα	KNS1-12xFLAG-KanMX6 ise1delta::Kan	This work

7.2 Plasmids and vectors

Table 34 Plasmids and vectors used in this work. Given are name, construct and information (Info) of the plasmids.

Name	Construct	Info
pBluescript KS II +	-	Working group of Prof. Dr. Wolfgang Seufert
pFA6a-3HA-His3MX6		Longtine *et al.* 1998
pFA6a-3HA-kanMX6		Longtine *et al.* 1998
pFA6a-3xFLAG-KanMX6	pFA6a-3xFLAG-KanMX6	Working group of Prof. Dr. Wolfgang Seufert
pFA6a-KanMX6		Working group of Prof. Dr. Wolfgang Seufert
pWS2222	pFA6a-12xFLAG-KanMX6	Working group of Prof. Dr. Wolfgang Seufert
pWS2223	pFA6a-12xFLAG-His3MX6	Working group of Prof. Dr. Wolfgang Seufert
pWS2699	pFA6a-3xFLAG-His3MX6	Working group of Prof. Dr. Wolfgang Seufert
pWS2731	YEGFP	Working group of Prof. Dr. Wolfgang Seufert
pWS2741	pGAL1-MYC3-YEGFP-tCYC1	Working group of Prof. Dr. Wolfgang Seufert
pWS2872	pTEF2-GFP-SWI5-S/A-tCYC1-LEU2	Working group of Prof. Dr. Wolfgang Seufert
pWS2873	pTEF2-GFP-SWI5-S/A-tCYC1-TRP1	Working group of Prof. Dr. Wolfgang Seufert
pWS2874	pTEF2-GFP-SWI5-S/A-tCYC1-HIS3	Working group of Prof. Dr. Wolfgang Seufert
pWS2875	pTEF2-GFP-SWI5-S/A-tCYC1-URA3	Working group of Prof. Dr. Wolfgang Seufert
pWS3232	pTEF2-MYC3-tCYC	Working group of Prof. Dr. Wolfgang Seufert
pWS3631	pTEF2-flag3-tCYC1	Working group of Prof. Dr. Wolfgang Seufert
pWS5852	KNS1	Johannes Klier for this work
pWS5853	pTEF2-MYC3-KNS1-tCYC	Johannes Klier for this work
pWS5903	GFP(A206K)	Veronika Waas for this work
pWS5908	GFP(A206K) (217-715)	This work
pWS5909	GFP(A206K) (217-704)	This work

pWS5910	5'UTR-KNS1(1-9)	This work
pWS5911	5'UTR-KNS1(1-9)-GFP-SWI5-S/A-myc13	This work
pWS5920	pTEF2-GFP-KNS1-tCYC1-URA3	This work
pWS5967	KNS1(D440A)	Jannis Winter for this work
pWS5968	KNS1-NTD(1-289aa)	Jannis Winter for this work
pWS5969	KNS1-CTD(278-737aa)	Jannis Winter for this work
pWS5971	pTEF2-GFP-KNS1(D440A)-tCYC1	Jannis Winter for this work
pWS5972	pTEF2-MYC3-KNS1(D440A)-tCYC	Jannis Winter for this work
pWS5973	pTEF2-GFP-KNS1-NTD(1-289aa)-tCYC1	Jannis Winter for this work
pWS5974	pTEF2-MYC3-KNS1-NTD(1-289aa)-tCYC	Jannis Winter for this work
pWS5975	pTEF2-GFP-KNS1-CTD(278-737aa)-tCYC1	Jannis Winter for this work
pWS5976	pTEF2-MYC3-KNS1-CTD(278-737aa)-tCYC	Jannis Winter for this work
pWS6005	pGAL1-GFP-KNS1-tCYC1	Jannis Winter for this work
pWS6006	pGAL1-GFP-KNS1(D440A)-tCYC1	Jannis Winter for this work
pWS6009	KNS1-CTD(278-737aa, D440A)	Jannis Winter for this work
pWS6010	pTEF2-GFP-KNS1-CTD(278-737aa, D440A)-tCYC1	Jannis Winter for this work
pWS6011	pTEF2-MYC3-KNS1-CTD(278-737aa, D440A)-tCYC	Jannis Winter for this work
pWS6024	pTEF2-HA4-KNS1-tCYC1	Kathrin Preußel Danger for this work
pWS6025	pTEF2-HA4-KNS1(D440A)-tCYC1	Kathrin Preußel Danger for this work
pWS6032	pBS-KNS1 wt	Adelheid Weissgerber for this work
pWS6033	pB-KNS1(D440A)	Adelheid Weissgerber for this work
pWS6034	pTEF2-KNS1-YEGFP-tCYC1	Adelheid Weissgerber for this work
pWS6035	pTEF2-KNS1(D440A)-YEGFP-tCYC1	Adelheid Weissgerber for this work
pWS6063	pBS-KNS1-NTD(1-289aa)	Severin Graml for this work
pWS6064	pBS-KNS1-NTDshort(1-174aa)	Severin Graml for this work
pWS6065	pTEF2-KNS1-NTD(1-289aa)-YEGFP-tCYC1	Severin Graml for this work
pWS6066	pTEF2-KNS1-NTDshort(1-174aa)-YEGFP-tCYC1	Severin Graml for this work
pWS6068	pTEF2-KNS1(166-737aa)-GFP-tCYC1	Adelheid Weissgerber for this work
pWS6080	pGAL-GFP-KNS1-CTDlong(166-737aa)	Antje Machetanz-Morokane for this work

pWS6081	pBS-KNS1-NTD(1-289aa)	Antje Machetanz-Morokane for this work
pWS6082	pBS-KNS1-CTD(280-737aa)	Antje Machetanz-Morokane for this work
pWS6083	pJG4-5-KNS1-CTD(280-737aa)	Antje Machetanz-Morokane for this work
pWS6084	pEG202-KNS1-CTD(280-737aa)	Antje Machetanz-Morokane for this work
pWS6085	pEG-KNS1-NTD(1-289aa)	Antje Machetanz-Morokane for this work
pWS6086	pJG 4-5-KNS1-NTD(1-289aa)	Antje Machetanz-Morokane for this work
pWS6092	pBS-KNS1-NTDshort2(166-289)	Kathrin Preußel Danger for this work
pWS6093	pTEF2-GFP-KNS1short2(166-289)-tCYC1	Kathrin Preußel Danger for this work

7.3 Media, buffers and solutions

7.3.1 Bacterial media

Table 35 Bacterial media used for this work.

Medium	Contents
LB Liquid Medium	10 g/l Bacto Tryptone 5 g/l Bacto Yeast Extract 10 g/l NaCl 0.3 mM NaOH Antibiotics
LB Solid Medium	LB Medium 17 g/l Euro agar
SOC Medium	20 g/l Bacto Tryptone 5 g/l Bacto Yeast Extract 10 mM NaCl 2.5 mM KCl 10 mM $MgCl_2$ 20 mM glucose

A selection on a resistance of ampicillin was performed by adding 100 $\frac{\mu g}{ml}$ ampicillin to the medium.

7.3.2 Yeast media

Table 36 Yeast media used for this work.

Medium	Contents
Pre-Sporulation Medium (Pre-Spo)	3 g/l Bacto Peptone 8 g/l Bacto Yeast Extract 100 g/l glucose 50 mg/l adenine sulfate
SD Liquid Medium	100 ml/l Yeast Nitrogen Base 100 ml/l 10x Dropout -5 Carbon source (e.g. glucose) 50 mg/l adenine 50 mg/l histidine 100 mg/l leucine 100 mg/l tryptophan 50 mg/l uracil
SD Solid Medium	SD Liquid Medium 17 g/l Bacto agar
Sporulation Medium (Spo)	1 g/l Bacto Yeast Extract 10 g/l potassium acetate 0.5 g/l glucose 10 ml/l 10x Dropout++
XY Liquid Medium	20 g/l Bacto Peptone 10 g/l Bacto Yeast Extract 200 mg/l tryptophan 100 mg/l adenine sulfate 10 mM KH_2PO_4 Carbon source (e.g. glucose)
XY Solid Medium	XY Liquid Medium 17 g/l Bacto agar

The following autoclaved sugars were used as carbon source and added to the medium: glucose 20 %, galactose 20 %, raffinose 10 % and glycerol 20 %. To select auxotrophic markers of the used strains the correlating amino acid was not added to selective media (adenine, histidine, leucin, tryptophan or uracil). To select for resistances of toxins G418 in a concentration of 500 $\frac{\mu g}{ml}$ (W303) and clonNAT in a concentration of 100 $\frac{\mu g}{ml}$ were added to the medium.

7.3.3 Buffers and solutions

Table 37 All buffers and solutions used for this work and prepared in the lab.

Buffer/Solution	Contents
Buffer 3	150 mM NaCl 50 mM Tris/HCl pH 7.5 50 mM NaF 5 mM EDTA 0.1 % Igepal CA-630 60 mM β-glycerol phosphate
Colony Buffer (10x) + $MgCl_2$	125 mM Tris/HCl pH 8.5 560 mM KCl 15 mM $MgCl_2$
DEPC-H_2O	0,01 % (v/v) diethylpyrocarbonate
DNA Running Buffer	0.25 % bromophenol blue 50 % glycerine 1 mM EDTA 10 mM Tris/HCl pH 7.8
Dropout -5 (10x)	0.5 g/l alanine 0.5 g/l arginine 0.5 g/l asparagine 1 g/l aspartic acid 0.5 g/l cysteine 0.5 g/l glutamine 1 g/l glutamic acid 0.5 g/l glycine 0.5 g/l (myo-)inositol 0.5 g/l isoleucine 0.5 g/l lysine 0.5 g/l methionine 50 mg/l p-aminobenzoic acid 0.5 g/l phenylalanine 0.5 g/l proline 1 g/l serine 1 g/l threonine 0.5 g/l tyrosine 1 g/l valine
Dropout++ (10x)	10x Dropout -5 0.5 g/l adenine 0.5 g/l histidine 1 g/l leucine 1 g/l tryptophan 0.5 g/l uracil

EasyPrep Buffer	10 mM Tris/HCl pH 8.0 1 mM EDTA 15 % (w/v) saccharose 2 mg/ml lysozyme 0.2 mg/ml RNase A 0.1 mg/ml BSA
Ligase Buffer (10x)	50 mM Tris/HCl 10 mM MgCl2 10 mM DTT 1 mM ATP Set to pH 7.5
LSB (Laemmli Sample Dye 2x)	120 mM Tris/HCl pH 6.8 40 mg/ml SDS 200 mg/ml glycerine 400 µg/ml bromophenol blue
Lysis Buffer	100 mM NaCl 30 mM $MgCl_2$ 10 mM Tris/HCl pH 7,5
5 % Milk TBS-T	25 g skimmed milk powder 50 ml TBS-T 450 ml H_2O
Novozyme Solution	1 M sorbitol 10 mM Tris/HCl pH 7.5 1 mM EDTA 50 mM DTT 2 mg/ml novozyme
PEG/LiAc (Polyethylene Glycol/Lithium Acetate)	100 ml/l 10x TE 100 ml/l 1M LiAc pH 7.5 800 ml/l 50 % polyethylene glycol
PonceauS	1 g PonceauS 50 ml glacial acetic acid Ad 1 l water
Proteinase K	10 mg/ml Proteinase K 10 mM Tris/HCl pH 7.5 1 mM calcium acetate
RNase A	10 mg/ml RNase A 10 mM Tris/HCl pH 7.5 15 mM NaCl
TAE (50x)	2 M Tris-Base 50 mM EDTA Set pH 8.0 with glacial acetic acid

TBS (10x)	200 mM Tris-Base 1.37 M NaCl Set pH 7.6 with HCl
TBS-T	100 ml/l TBS (10x) 10 ml/l Tween 20 (10 %)
TE (10x)	100 mM Tris/HCl pH 7.5 10 mM EDTA
TES Solution	10 mM Tris/HCl pH 7,5 10 mM EDTA 0.5 % SDS
Transfer Buffer	2.9 g/l glycine 5.8 g/l Tris-Base 3.7 ml/l SDS (10 %) 100 ml/l methanol
Turbo-LRB (Laemmli Running Buffer 10x)	250 mM Tris-Base 9.46 M glycine 10 g/l SDS
X-Gal Buffer	5 ml 1 M Na-phosphate buffer pH 7.0 600 µl N,N-Dimethylformamid (DMFA) 100 µl 10 % SDS 100 µl X-Gal 5 ml Liquid agar
YNB (10x)	17 g/l Yeast Nitrogen Base 50 g/l ammonium sulfate

7.4 Nucleic acids, enzymes and antibodies

7.4.1 Oligonucleotides

Table 38 Oligonucleotides used for this work with annotated name, sequence in 5' – 3' direction and information (Info) on source and purpose.

Name	Sequence (5' – 3' direction)	Info
WS0821	ATGTGATGTGAGAACTGTATCCTAG	R-Primer in *pTEF*, verification of a deletion with pFA6-constructs, working group of Prof. Dr. Wolfgang Seufert
WS1663	CATCTCGAGTTATTTGTACAATTCATC CATACCAT	R-Primer, amplification of GFP (XhoI site), working group of Prof. Dr. Wolfgang Seufert
WS2376	CCGTAAGTAGCATCACCTTC	R-Primer in GFP, verification of GFP containing constructs, working group of Prof. Dr. Wolfgang Seufert
WS2404	TTAACATCACCATCTAATTC	R-Primer, sequencing only, binds in GFP, working group of Prof. Dr. Wolfgang Seufert
WS3631	GTTGTAGGAATATAATTCTCCACACAT AATAAGTACGCTAATTAAATAAACAGC TGAAGCTTCGTACGC	F-Primer, deletion of *HXK2*, working group of Prof. Dr. Wolfgang Seufert
WS3632	GTAGAAAAAGGGCACCTTCTTGTTGT TCAAACTTAATTTACAAATTAAGTGCA TAGGCCACTAGTGGATCTG	R-Primer, deletion of *HXK2*, working group of Prof. Dr. Wolfgang Seufert
WS3633	AACCTCCTCGCACATTGGTA	F-Primer, verification of intact *HXK2*, working group of Prof. Dr. Wolfgang Seufert
WS3634	AATGGCCAAGAAATCACCGG	R-Primer, verification of intact *HXK2*, working group of Prof. Dr. Wolfgang Seufert
WS3870	CTTCTAGGCCGTGTGGACGGTAAAATA GTAGTCACACCTCAAATCCGGATCCCC GGGTTAATTAA	F-Primer, tagging of *RPC53*, this work
WS3871	ATGACTGTGTATATTCATTTATATACTC GACAGATGCGAGTGCGAGAATTCGAGC TCGTTTAAAC	R-Primer, tagging of *RPC53*, this work
WS3872	GGCATACTGGATGATGGTATTGCAACT TATAATAATACCCAAGGACGGATCCCC GGGTTAATTAA	F-Primer, tagging of *KNS1*, this work
WS3873	AAAAGATGTGAAAAAAAGAAGAGAAA AGTAGAACGAGAACACCCAGAATTCGA GCTCGTTTAAAC	R-Primer, tagging of *KNS1*, this work
WS3874	TACTGCTCTTCTTCATTATTGCTTTAT CTTCCGCGTACCTTAGTTCGGATCCCC GGGTTAATTAA	F-Primer, deletion of *KNS1*, this work
WS3875	GCCGGAGTTAAAGTTGCGAGGAAAC	F-Primer, verification of a deletion of *KNS1*, this work

WS3876	GGTCTAGACTGTTCCTCAGATTGTC	R-Primer, verification of a deletion of *KNS1*, this work
WS3877	GGCATACTGGATGATGGTATTGCAACT TATAATAATACCCAAGGAGGTGACGGT GCTGGTTTA	F-Primer, GFP-tagging of *KNS1*, this work
WS3878	AAAAGATGTGAAAAAAAGAAGAGAAA AGTAGAACGAGAACACCCATCGATGAA TTCGAGCTCG	R-Primer, GFP-tagging of *KNS1*, this work
WS3879	ACGTGGATCCATGTCACAGAATATTCA AATTGG	F-Primer, cloning of *KNS1* (BamHI site), this work
WS3889	ACGTCTCGAGCTATCCTTGGGTATTAT TATAAGTT	R-Primer, cloning of *KNS1* (XhoI site), this work
WS3910	CTCACTGCCTCAGTTGCC	F1-Primer, sequencing only, binds in *KNS1*, this work
WS3911	GTGCTCCAACGGCATTGC	F2-Primer, sequencing only, binds in *KNS1*, this work
WS3912	CTTCTAGGCCGTGTGGACGGTAAAATA GTAGTCACACCTCAAATCGGTGACGGT GCTGGTTTA	F-Primer, GFP-tagging of *RPC53*, this work
WS3913	ATGACTGTGTATATTCATTTATATACTC GACAGATGCGAGTGCGATCGATGAATT CGAGCTCG	R-Primer, GFP-tagging of *RPC53*, this work
WS3916	CATTACTTATCCACTCAATCTAAGTTA TCCAAAGATCCAAACGA	F-Primer, mutagenesis of GFP (A206K), this work
WS3917	TCGTTTGGATCTTTGGATAACTTAGAT TGAGTGGATAAGTAATG	R-Primer, mutagenesis of GFP (A206K), this work
WS3918	CAGTGAGCTCGCCGCCCACATCGGAAT ATC	F-Primer, cloning of *5'-UTR-KNS1* (SacI site), this work
WS3919	CTGATCTAGACTGTGACATAACTAAGG TACGCGG	R-Primer, cloning of *5'-UTR-KNS1* (XbaI site), this work
WS3920	AGCTTCTAGATACCCAGATCATATGAA ACAAC	F-Primer, sequencing only, binds in GFP, this work
WS4001	ACGTCTCGAGCTATGATTTATTGGATG ATGCGCTTTC	R-Primer, cloning of *KNS1-NTD(1-289aa)* (XhoI site), this work
WS4002	ACGTGGATCCATGTCTTCAGAAAGCGC ATCATCCAAT	F-Primer, cloning of *KNS1-CTD(280-737aa)* (BamHI site), this work
WS4003	TTTACATCAAACGGCTCTTCAGAAAGC GCATCATCCAATAAATCAGGTGACGGT GCTGGTTTA	F-Primer, tagging of *KNS1-NTD(1-289aa)*, this work
WS4004	GATTTGGGCATAATACACACGGCTTTG AAACCAGAAAATATCCTGATTTG	F-Primer, mutagenesis of *KNS1 (D440A)*, this work
WS4005	CAAATCAGGATATTTTCTGGTTTCAAA GCCGTGTGTATTATGCCCAAATC	R-Primer, mutagenesis of *KNS1 (D440A)*, this work

WS4060	ACGTACTAGTATGTCACAGAATATTCAAATTGGCA	F-Primer, amplification of *KNS1* (SpeI site), Kathrin Preußel Danger for this work
WS4061	ACGTGGATCCTCCTTGGGTATTATTATAAGTTGCAAT	R-Primer, amplification of *KNS1* (BamHI site), Kathrin Preußel Danger for this work
WS4098	ACGTGAATTCTGATTTATTGGATGATGCGCTTTCTGAAGAG	R-Primer, cloning of *KNS1-NTD(1-289aa)* (EcoRI site), this work
WS4099	ACGTGAATTCTGTCGTGATATACGTACTATTGCTTGTAGCT	R-Primer, cloning of *KNS1-NTDshort1(1-174aa)* (EcoRI site), this work
WS4109	ACGTGAATTCATGTCACAGAATATTCAAATTGGCAC	F-Primer, cloning of *KNS1-NTD(1-289aa)* (EcoRI site), this work
WS4110	ACGTGGATCCGGTCTCGAATTCATGTCTTCAGAAAGCGCATCATCCAAT	F-Primer, cloning of *KNS1-CTD(280-737aa)* (BamHI-BsaI-EcoRI site), this work
WS4112	CTAGACCTGAATCAAGCAGAC	F-Primer, qPCR, in *KNS1* (pos 199-219), this work
WS4113	CAACTGAGGCAGTGAGATGG	R-Primer qPCR, in *KNS1* (pos 567-548), this work
WS4116	CAGAATATTCAAATTGGCACTAGAAAACGT	F1-Primer, TSS mapping of *KNS1*, binds in KNS1 (+7 bp), this work
WS4117	CAAGTCGAAGATTTAGCACAACAAAGAC	F2-Primer, TSS mapping of *KNS1*, binds upstream of *KNS1* (-86 bp), this work
WS4118	CAAAGTATTGTTACCTCACCACCAAG	F3-Primer, TSS mapping of *KNS1*, binds upstream of *KNS1* (-276 bp), this work
WS4119	GAATCCTGGCTCCACATCTC	F4-Primer, TSS mapping of *KNS1*, binds upstream of *KNS1* (-400 bp), this work
WS4120	GGAAACACACAGCGAAGGGAAA	F5-Primer, TSS mapping of *KNS1*, binds upstream of *KNS1* (-500 bp), this work
WS4121	CGTGATTGGGCGGTTTTCCA	F6-Primer, TSS mapping of *KNS1*, binds upstream of *KNS1* (-581 bp), this work
WS4122	GAAATAGCCGCCGATATGGC	F7-Primer, TSS mapping of *KNS1*, binds upstream of *KNS1* (-689 bp), this work
WS4123	GCTAGACGCTGTTGGTAATATCATAC	F8-Primer, TSS mapping of *KNS1*, binds upstream of *KNS1* (-749 bp), this work
WS4124	GCAGGATGGACCACCAATTG	F9-Primer, TSS mapping of *KNS1*, binds in *COX19* (-889 bp), this work
WS4125	CCAATTGATGCTTAAGCTATCGC	R-Primer, Reverse Transcription of *KNS1*, binds in *KNS1* (+1950 bp), this work
WS4126	AACACCCTAAAGAGAATTTACAAGTTGAGTAAAAGACAAGACACAAAATTCGGATCCCCGGGTTAATTAA	F-Primer, deletion of *CAT8*, this work
WS4127	GAATATTTAGAGGATTCCGTTTTGAATATATTACACTATGAAATAAAGAAGAATTCGAGCTCGTTTAAAC	R-Primer, deletion of *CAT8*, this work

WS4128	GCGATAACCGAGACATGCATG	F-Primer, verification of a deletion of *CAT8*, this work
WS4129	CGACACCTGTCACAAGCTTG	R-Primer, verification of a deletion of *CAT8*, this work
WS4137	TGCCTCAGTTGCCTCTATCG	F1-Primer, qPCR, in *KNS1* (pos 557), this work
WS4138	CCCTCCAGAGTCTTTGCACA	R1-Primer, qPCR, in *KNS1* (pos 701), this work
WS4139	GGTCAGTTCCAGTGCCTCTT	F2-Primer, qPCR, in *KNS1* (pos 1114), this work
WS4140	CCTGAATATGAGAGCCGGGG	R2-Primer, qPCR, in *KNS1* (pos 1255), this work
WS4141	CGTTCCCCTGCGACATTTG	F3-Primer, qPCR, in *KNS1* (pos 1564), this work
WS4142	AATGTCTGTGGGGAAAGGGG	R3-Primer, qPCR, in *KNS1* (pos 1704), this work
WS4143	CAAATGGAAAGGAGTTGAGCCG	F1-Primer, qPCR, in *CDC10* (pos 455), this work
WS4144	AGCTCCCTAAACTCCGTTCT	R1-Primer, qPCR, in *CDC10* (pos 584), this work
WS4145	CTCATACTCTTGTGGAGGACCG	F2-Primer, qPCR, in *CDC10* (pos 241), this work
WS4146	CCTTTCACGTTGGGCTGTC	R2-Primer, qPCR, in *CDC10* (pos 408), this work
WS4147	TAAGGCGCTTTTCAAGGACG	F1-Primer, qPCR, in *MRP7* (pos 903), this work
WS4148	TGACTTCTTCCCGCTTTTGG	R1-Primer, qPCR, in *MRP7* (pos 1032), this work
WS4149	GAGGCGTGATTTGAAACTGC	F2-Primer, qPCR, in *MRP7* (pos 333), this work
WS4150	CCCTGACCTCTAACTGCTTCA	R2-Primer, qPCR, in *MRP7* (pos 496), this work

7.4.2 Nucleic acids

Table 39 Nucleic acids used for this work and their corresponding company.

Nucleic acids	Company
dNTPs	New England Biolabs, Ipswich (USA)
GeneRuler DNA Ladder Mix	Thermo Fisher Scientific, Waltham (USA)
Herringsperm DNA	Roche Diagnostics GmbH, Mannheim
RiboRuler High Range RNA Ladder	Thermo Fisher Scientific, Waltham (USA)

7.4.3 Enzymes and solutions

Table 40 Enzymes and other solutions used in this work and their company of acquisition.

Enzymes and solutions	Company
Color Prestained Protein Standard	New England Biolabs, Ipswich (USA)
CoralLoad Buffer	QIAGEN GmbH, Hilden
KOD Hot Start DNA Polymerase	Novagen (Merck), Darmstadt
MG132	Selleck Chemicals LLC, Houston (USA)
Novozym 234	NovoBiolabs, Bagsværd (Dänemark)
10x PCR Buffer	QIAGEN GmbH, Hilden
Phos-Tag	Sigma-Aldrich (Merck), St. Louis (USA)
Proteinase K	AppliChem GmbH, Darmstadt
Q Solution	QIAGEN GmbH, Hilden
Restrictionendonucelases	New England Biolabs, Ipswich (USA)
RNase A	Roche Diagnostics GmbH, Mannheim
RNAsin Plus	Medenbach Lab, University of Regensburg
SuperScript IV Reverse Transcriptase	Invitrogen (Thermo Fisher Scientific), Waltham (USA)
T4 DNA Ligase	New England Biolabs, Ipswich (USA)
Taq DNA Polymerase	Biomaster GmbH, Windeck

7.4.4 Antibodies

Table 41 Primary antibodies (AB) used in this work.

Name	Dilution	Type	Company
12CA5	1:50	Monoclonal AB (mouse) against the HA epitope	Field *et al.* 1988
9E10	1:50	Monoclonal AB (mouse) against the c-MYC epitope	Evan et al. 1985
α-GFP	1:2000	Monoclonal AB (mouse) against GFP	Roche Diagnostics GmbH, Mannheim
α-Tub2	1:5000	Polyclonal AB (rabbit) against β-tubulin	Eurogentec Deutschland GmbH, Köln
M2	1:20000	Monoclonal AB (mouse) against the FLAG epitope	Sigma-Aldrich (Merck), St. Louis (USA)
α-Phospho-eIF2α	1:500	Polyclonal AB (rabbit) against phosphorylated eIF2α (Ser51)	Cell Signaling Technology, Massachusetts (USA)

Table 42 Secondary antibodies (AB) used in this work.

Name	Dilution	Type	Company
α-mouse IRDye 680	1:15000	Secondary AB (goat) against mouse primary AB	Li-COR Biosciences GmbH, Bad Homburg
α-mouse IRDye 800	1:15000	Secondary AB (goat) against mouse primary AB	Li-COR Biosciences GmbH, Bad Homburg
α-rabbit IRDye 680	1:15000	Secondary AB (goat) against rabbit primary AB	Li-COR Biosciences GmbH, Bad Homburg
α-rabbit IRDye 800	1:15000	Secondary AB (goat) against rabbit primary AB	Li-COR Biosciences GmbH, Bad Homburg

7.5 Kits

Table 43 Kits used in this work.

Kit	Company
GenElute HP Plasmid Midiprep Kit	Sigma-Aldrich (Merck), St. Louis (USA)
NucleoSpin Kit	Macherey-Nagel GmbH & Co. KG, Düren
QiAquick Gel Extraction Kit	QIAGEN GmbH, Hilden
QiAquick PCR Purification Kit	QIAGEN GmbH, Hilden
QuantiNova Reverse Transcription Kit	QIAGEN GmbH, Hilden
QuantiNova „SYBRGreen" PCR Kit	QIAGEN GmbH, Hilden

7.6 Software and online databases

Table 44 Software and databases used in this work with corresponding company, citation or website.

Software/Database	Company/website
Adobe Illustrator 2024	Adobe Systems Software Ireland Limited, Dublin (Ireland)
Adobe Photoshop 2024	Adobe Systems Software Ireland Limited, Dublin (Ireland)
AlphaFold	Jumper *et al.* (2021), Varadi *et al.* (2022)
AxioVision LE Rel. 4.8	Carl Zeiss Vision, Göttingen
cNLS Mapper	Kosugi *et al.* (2009)
FCS Express 6 Flow Research Edition	De Novo Software, Los Angeles (USA)
ImageJ	Rasband, W.S., U.S. National Institutes of Health, Bethesda (USA)
Image Studio 5.5	Li-COR Biosciences GmbH, Bad Homburg
Microsoft Office 365	Microsoft Corporation, Redmond (USA)
NCBI Database	www.ncbi.nlm.nih.gov
PaperPal	www.paperpal.com
Reverse Compliment	www.bioinformatics.org/SMS/rev.comp.html
Rotor Gene Q 2.3.4	QIAGEN GmbH, Hilden
Saccharomyces Genome Database	www.yeastgenome.org
SnapGene Vers. 4.3.2	GSL Biotech LLC, Chicago (USA)
VisionWorks 8.21	Analytik Jena GmbH & Co. KG, Jena
Windows FloMax Software	Sysmex Partec GmbH, Goerlitz
WinMDI 2.8	Joe Trotter

8 BIBLIOGRAPHY

Alberghina L., R. L. Rossi, L. Querin, V. Wanke, and M. Vanoni, 2004 A cell sizer network involving Cln3 and Far1 controls entrance into S phase in the mitotic cycle of budding yeast. Journal of Cell Biology **167**: 433–443.

Albuquerque C. P., M. B. Smolka, S. H. Payne, V. Bafna, J. Eng, H. Zhou, 2008 A Multidimensional Chromatography Technology for In-depth Phosphoproteome Analysis. Molecular & Cellular Proteomics **7**: 1389–1396.

Ashe M. P., S. K. De Long, and A. B. Sachs, 2000 Glucose Depletion Rapidly Inhibits Translation Initiation in Yeast, (M. P. Wickens, Ed.). Molecular Biology of the Cell **11**: 833–848.

Atiyeh H., and Z. Duvnjak, 2003 Utilization of raffinose and melibiose by a mutant of *Saccharomyces cerevisiae*. Journal of Chemical Technology & Biotechnology **78**: 1068–1074.

Balch W. E., R. I. Morimoto, A. Dillin, and J. W. Kelly, 2008 Adapting Proteostasis for Disease Intervention. Science **319**: 916–919.

Bard J. A. M., E. A. Goodall, E. R. Greene, E. Jonsson, K. C. Dong, and A. Martin, 2018 Structure and Function of the 26S Proteasome. Annual Review of Biochemistry **87**: 697–724.

Barnett J. A., 2003 A history of research on yeasts 5: the fermentation pathway. Yeast **20**: 509–543.

Battaglioni S., D. Benjamin, M. Wälchli, T. Maier, and M. N. Hall, 2022 mTOR substrate phosphorylation in growth control. Cell **185**: 1814–1836.

Belle A., A. Tanay, L. Bitincka, R. Shamir, and E. K. O'Shea, 2006 Quantification of protein half-lives in the budding yeast proteome. Proceedings of the National Academy of Sciences of the United States of America. **103**: 13004–13009.

Ben-David Y., K. Letwin, L. Tannock, A. Bernstein, and T. Pawson, 1991 A mammalian protein kinase with potential for serine/threonine and tyrosine phosphorylation is related to cell cycle regulators. The EMBO Journal **10**: 317–325.

Bender J., and G. R. Fink, 1994 AFC1, a LAMMER kinase from *Arabidopsis thaliana*, activates STE12-dependent processes in yeast. Proceedings of the National Academy of Sciences of the United States of America **91**: 12105–12109.

Berghammer H., and B. Auer, 1993 Easypreps: fast and easy plasmid minipreparation for analysis of recombinant clones in *E. coli*. BioTechniques **14**: 524–528.

Biggar K. K., and S. S.-C. Li, 2015 Non-histone protein methylation as a regulator of cellular signalling and function. Nature Reviews Molecular Cell Biology **16**: 5–17.

Binda M., M.-P. Péli-Gulli, G. Bonfils, N. Panchaud, J. Urban, T. W. Sturgill, R. Loewith, and C. De Virgilio., 2009 The Vam6 GEF Controls TORC1 by Activating the EGO Complex. Molecular Cell **35**: 563–573.

Boguta M., and D. Graczyk, 2011 RNA polymerase III under control: repression and de-repression. Trends in Biochemical Sciences **36**: 451–456.

Boorstein W. R., and E. A. Craig, 1989 [25] Primer extension analysis of RNA, pp. 347–369 in *RNA Processing Part A: General Methods*, Methods in Enzymology. Academic Press.

Breitkreutz A., H. Choi, J. R. Sharom, L. Boucher, V. Neduva, B. Larsen, Z.-Y- Lin, B.-J. Breitkreutz, C. Stark, G. Liu, J. Ahn, D. Dewar-Darch, T. Reguly, X. Tang, R. Almeida, Z. S.

Qin, T. Pawson, A.-C. Gingras, A. I. Nesvizhskii, and M. Tyers, 2010 A Global Protein Kinase and Phosphatase Interaction Network in Yeast. Science **328**: 1043–1046.

Broach J. R., 2012 Nutritional Control of Growth and Development in Yeast. Genetics **192**: 73–105.

Brunelle J. L., and R. Green, 2014 One-dimensional SDS-Polyacrylamide Gel Electrophoresis (1D SDS-PAGE), pp. 151–159 in *Methods in Enzymology*, Elsevier.

Budenholzer L., C. L. Cheng, Y. Li, and M. Hochstrasser, 2017 Proteasome Structure and Assembly. Journal of Molecular Biology **429**: 3500–3524.

Bullock A. N., S. Das, J. É. Debreczeni, P. Rellos, O. Fedorov, F. H. Nielsen, K. Guo, E. Papagrigoriou, A. L. Amos, S. Cho, B. E. Turk, G. Ghosh, and S. Knapp, 2009 Kinase Domain Insertions Define Distinct Roles of CLK Kinases in SR Protein Phosphorylation. Structure **17**: 352–362.

Busti S., P. Coccetti, L. Alberghina, and M. Vanoni, 2010 Glucose Signalling-Mediated Coordination of Cell Growth and Cell Cycle in *Saccharomyces cerevisiae*. Sensors **10**: 6195–6240.

Bustin S. A., V. Benes, J. A. Garson, J. Hellemans, J. Huggett, M. Kubista, R. Mueller, T. Nolan, M. W. Pfaffl, G. L. Shipley, J. Vandersompele, and C. T. Wittwer, 2009 The MIQE Guidelines: Minimum Information for Publication of Quantitative Real-Time PCR Experiments. Clinical Chemistry **55**: 611–622.

Caligaris M., B. Sampaio-Marques, R. Hatakeyama, B. Pillet, P. Ludovico, C. De Virgilio, J. Winderickx, and R. Nicastro, 2023 The Yeast Protein Kinase Sch9 Functions as a Central Nutrient-Responsive Hub That Calibrates Metabolic and Stress-Related Responses. Journal of Fungus **9**: 787.

Carlson M., 1999 Glucose repression in yeast. Current Opinion in Microbiology **2**: 202–207.

Castilho B. A., R. Shanmugam, R. C. Silva, R. Ramesh, B. M. Himme, and E. Sattlegger, 2014 Keeping the eIF2 alpha kinase Gcn2 in check. Biochimica et Biophysica Acta - Molecular Cell Research **1843**: 1948–1968.

Chassé H., S. Boulben, V. Costache, P. Cormier, and J. Morales, 2016 Analysis of translation using polysome profiling. Nucleic Acids Research **45**: 1–9.

Chen X.-Q., T. Shen, S.-J. Fang, X.-M. Sun, G.-Y. Li, and Y.-F. Li, 2023 Protein homeostasis in aging and cancer. Frontiers in Cell and Developmental Biology **11**: 1143532.

Cherkasova V. A., and A. G. Hinnebusch, 2003 Translational control by TOR and TAP42 through dephosphorylation of eIF2α kinase GCN2. Genes & Development **17**: 859–872.

Choudhary K., and M. Kupiec, 2022 The cohesin complex of yeasts: sister chromatid cohesion and beyond. FEMS Microbiology Reviews **47**: 1–22.

Cohen P., and S. Frame, 2001 The renaissance of GSK3. Nature Reviews Molecular Cell Biology **2**: 769–776.

Collins G. A., T. A. Gomez, R. J. Deshaies, and W. P. Tansey, 2010 Combined chemical and genetic approach to inhibit proteolysis by the proteasome. Yeast **27**: 965–974.

Colwill K., T. Pawson, B. Andrews, J. Prasad, J. L. Manley, J. C. Bell, and P. I. Duncan, 1996 The Clk/Sty protein kinase phosphorylates SR splicing factors and regulates their intranuclear distribution. The EMBO Journal **15**: 265–275.

Conlon I., and M. Raff, 2003 Differences in the way a mammalian cell and yeast cells coordinate cell growth and cell-cycle progression. Journal of Biology **2**: 1–10.

Connelly S., and J. L. Manley, 1988 A functional mRNA polyadenylation signal is required for transcnpnon termination by RNA polymerase II. Genes & Development **2**: 440–452.

Conrad M., J. Schothorst, H. N. Kankipati, G. Van Zeebroeck, M. Rubio-Texeira, and J. : Thevelein, 2014 Nutrient sensing and signalling in the yeast *Saccharomyces cerevisiae*. FEMS Microbiology Reviews **38**: 254–299.

Cooper T. G., and J. Bossinger, 1976 Selective inhibition of protein synthesis initiation in *Saccharomyces cerevisiae* by low concentrations of cycloheximide. Journal of Biological Chemistry **251**: 7278–7280.

Costa-Mattioli M., and P. Walter, 2020 The integrated stress response: From mechanism to disease. Science **368**: 1–11.

Crawford R. A., and G. D. Pavitt, 2019 Translational regulation in response to stress in *Saccharomyces cerevisiae*. Yeast **36**: 5–21.

Das S., and B. Das, 2013 mRNA quality control pathways in *Saccharomyces cerevisiae*. Journal of Biosciences **38**: 615–640.

Davey N. E., and D. O. Morgan, 2016 Building a Regulatory Network with Short Linear Sequence Motifs: Lessons from the Degrons of the Anaphase-Promoting Complex. Molecular Cell **64**: 12–23.

De Alteriis E., F. Cartenì, P. Parascandola, J. Serpa, and S. Mazzoleni, 2018 Revisiting the Crabtree/Warburg effect in a dynamic perspective: a fitness advantage against sugar-induced cell death. Cell Cycle **17**: 688–701.

De Deken R. H., 1966 The Crabtree Effect: A Regulatory System in Yeast. Journal of General Microbiology **44**: 149–156.

DeBerardinis R. J., J. J. Lum, G. Hatzivassiliou, and C. B. Thompson, 2008 The Biology of Cancer: Metabolic Reprogramming Fuels Cell Growth and Proliferation. Cell Metabolism **7**: 11–20.

Deng H., Z. Du, S. Lu, Z. Wang, and X. He, 2023 Regulation of Cat8 in energy metabolic balance and glucose tolerance in *Saccharomyces cerevisiae*. Applied Microbiology and Biotechnology **107**: 4605–4619.

Dennis P. B., S. Fumagalli, and G. Thomas, 1999 Target of rapamycin (TOR): balancing the opposing forces of protein synthesis and degradation. Current Opinion in Genetics & Development **9**: 49–54.

Dennis-Sykes C. A., W. J. Miller, and W. J. McAleer, 1985 A quantitative Western Blot method for protein measurement. Journal of Biological Standardization **13**: 309–314.

Deprez M.-A., E. Eskes, J. Winderickx, and T. Wilms, 2018 The TORC1-Sch9 pathway as a crucial mediator of chronological lifespan in the yeast *Saccharomyces cerevisiae*. FEMS Yeast Research **18**: 1–15.

Deutscher D., I. Meilijson, M. Kupiec, and E. Ruppin, 2006 Multiple knockout analysis of genetic robustness in the yeast metabolic network. Nature Genetics **38**: 993–998.

Devare M. N., Y. H. Kim, J. Jung, W. K. Kang, K.-S. Kwon, and J.-Y. Kim, 2020 TORC1 signalling regulates cytoplasmic pH through Sir2 in yeast. Aging Cell **19**: 1–15.

Dever T. E., 2002 Gene-Specific Regulation by General Translation Factors. Cell **108**: 545–556.

Dever T. E., T. G. Kinzy, and G. D. Pavitt, 2016 Mechanism and Regulation of Protein Synthesis in *Saccharomyces cerevisiae*. Genetics **203**: 65–107.

DeVit M. J., and M. Johnston, 1999 The nuclear exportin Msn5 is required for nuclear export of the Mig1 glucose repressor of *Saccharomyces cerevisiae*. Current Biology **9**: 1231–1241.

Dickinson J. R., and M. Schweizer, 1999 The metabolism and molecular physiology of *Saccharomyces cerevisiae*. Taylor & Francis, London.

Dirick L., T. Böhm, and K. Nasmyth, 1995 Roles and regulation of Cln-Cdc28 kinases at the start of the cell cycle of *Saccharomyces cerevisiae*. The EMBO Journal **14**: 4803–4813.

Dobrenel T., C. Caldana, J. Hanson, C. Robaglia, M. Vincentz, B. Veit, and C. Meyer, 2016 TOR Signalling and Nutrient Sensing. Annual Review of Plant Biology **67**: 261–285.

Doran P. M., and J. E. Bailey, 1986 Effects of Hydroxyurea on immobilized and suspended yeast fermentation rates and cell cycle operation. Biotechnology & Bioengineering **28**: 1814–1831.

Dower W. J., J. F. Miller, and C. W. Ragsdale, 1988 High efficiency transformation of *E. coli* by high voltage electroporation. Nucleic Acids Research **16**: 6127–6145.

Duncan P. I., B. W. Howell, R. M. Marius, S. Drmanic, E. M. J. Douville, and J. C. Bell, 1995 Alternative Splicing of STY, a Nuclear Dual Specificity Kinase. Journal of Biological Chemistry **270**: 21524–21531.

Dvir A., J. W. Conaway, and R. C. Conaway, 2001 Mechanism of transcription initiation and promoter escape by RNA polymerase II. Current Opinion in Genetics & Development **11**: 209–214.

Enenkel C., R. W. Kang, F. Wilfling, and O. P. Ernst, 2022 Intracellular localization of the proteasome in response to stress conditions. Journal of Biological Chemistry **298**: 1–10.

Engel C., S. Neyer, and P. Cramer, 2018 Distinct Mechanisms of Transcription Initiation by RNA Polymerases I and II. Annual Review of Biophysics **47**: 425–446.

Erb I., and E. Van Nimwegen, 2011 Transcription Factor Binding Site Positioning in Yeast: Proximal Promoter Motifs Characterize TATA-Less Promoters. PLoS ONE **6**: 1–12.

Evan G. I., G. K. Lewis, G. Ramsay, and J. M. Bishop, 1985 Isolation of Monoclonal Antibodies Specific for Human c-myc Proto-Oncogene Product. Molecular and Cellular Biology **5**: 3610–3616.

Field J., J.-I. Nikawa, D. Broek, B. MacDonald, L. Rodgers, I. A. Wilson, R. A. Lerner, and M. Wigler, 1988 Purification of a RAS-Responsive Adenylyl Cyclase Complex from *Saccharomyces cerevisiae* by Use of an Epitope Addition Method. Molecular and Cellular Biology **8**: 2159–2165.

Finley D., H. D. Ulrich, T. Sommer, and P. Kaiser, 2012 The Ubiquitin–Proteasome System of *Saccharomyces cerevisiae*. Genetics **192**: 319–360.

Futcher A. B., 1990 Yeast cell cycle. Current Opinion in Cell Biology **2**: 246–251.

Gaber R. F., D. M. Copple, B. K. Kennedy, M. Vidal, and M. Bard, 1989 The Yeast Gene *ERG6* Is Required for Normal Membrane Function but Is Not Essential for Biosynthesis of the Cell-Cycle-Sparking Sterol. Molecular and Cellular Biology **9**: 3447–3456.

Galdieri L., S. Mehrotra, S. Yu, and A. Vancura, 2010 Transcriptional Regulation in Yeast during Diauxic Shift and Stationary Phase. OMICS: A Journal of Integrative Biology **14**: 629–638.

Gancedo J. M., 1998 Yeast Carbon Catabolite Repression. Microbiology and Molecular Biology Reviews **62**: 334–361.

Gancedo J. M., 2008 The early steps of glucose signalling in yeast. FEMS Microbiology Reviews **32**: 673–704.

García-Sacristán A., M. J. Fernández-Nestosa, P. Hernández, J. B. Schvartzman, and D. B. Krimer, 2005 Protein kinase clk/STY is differentially regulated during erythroleukemia cell differentiation: a bias towards the skipped splice variant characterizes postcommitment stages. Cell Research **15**: 495–503.

Gasmi N., P.-E. Jacques, N. Klimova, X. Guo, A. Ricciardi, F. Robert, and B. Turcotte, 2014 The Switch from Fermentation to Respiration in *Saccharomyces cerevisiae* Is Regulated by the Ert1 Transcriptional Activator/Repressor. Genetics **198**: 547–560.

Gebauer F., and M. W. Hentze, 2004 Molecular mechanisms of translational control. Nature Reviews Molecular Cell Biology **5**: 827–835.

Glatz D. C., D. Rujescu, Y. Tang, F. J. Berendt, A. M. Hartmann, F. Faltraco, C. Rosenberg, C. Hulette, K. Jellinger, H. Hampel, P. Riederer, H.-J. Möller, A. Andreadis, K. Henkel, and S. Stamm, 2006 The alternative splicing of tau exon 10 and its regulatory proteins CLK2 and TRA2-BETA1 changes in sporadic Alzheimer's disease. Journal of Neurochemistry **96**: 635–644.

Goffeau A., B. G. Barrell, H. Bussey, R. W. Davis, B. Dujon, H. Feldmann, F. Galibert, J. D. Hoheisel, C. Jacq, M. Johnston, E. J. Louis, H. W. Mewes, Y. Murakami, P. Philippsen, H. Tettelin, and S. G. Oliver, 1996 Life with 6000 genes. Science **274**: 546–567.

González A., and M. N. Hall, 2017 Nutrient sensing and TOR signalling in yeast and mammals. The EMBO Journal **36**: 397–408.

Grandi P., and M. Bantscheff, 2019 Advanced proteomics approaches to unravel protein homeostasis. Drug Discovery Today: Technologies **31**: 99–108.

Gu Z., L. M. Steinmetz, X. Gu, C. Scharfe, R. W. Davis, and W.-H. Li, 2003 Role of duplicate genes in genetic robustness against null mutations. Nature **421**: 63–66.

Guertin D. A., and D. M. Sabatini, 2007 Defining the Role of mTOR in Cancer. Cancer Cell **12**: 9–22.

Gurr J. A., M. M. Januszeski, I. M. Tidikis, J. J. Norcross, and I. A. Kourides, 1990 Thyroid hormone regulates expression of the thyrotropin beta-subunit gene from both transcription start sites in the mouse and rat. Molecular and Cellular Endocrinology **71**:185–193.

Gutiérrez-Santiago F., and F. Navarro, 2023 Transcription by the Three RNA Polymerases under the Control of the TOR Signalling Pathway in *Saccharomyces cerevisiae*. Biomolecules **13**: 1–21.

Hahn S., and E. T. Young, 2011 Transcriptional Regulation in *Saccharomyces cerevisiae*: Transcription Factor Regulation and Function, Mechanisms of Initiation, and Roles of Activators and Coactivators. Genetics **189**: 705–736.

Hall M. N., 1996 The TOR signalling pathway and growth control in yeast. Biochemical Society Transactions **24**: 234–239.

Hampsey M., 1998 Molecular Genetics of the RNA Polymerase II General Transcriptional Machinery. Microbiology and Molecular Biology Reviews **62**: 465–503.

Hanes J., H. von der Kammer, J. Klaudiny, and K. H. Scheit, 1994 Characterization by cDNA cloning of two new human protein kinases. Journal of Molecular Biology **244**: 665–672.

Hardwick J. S., F. G. Kuruvilla, J. K. Tong, A. F. Shamji, and S. L. Schreiber, 1999 Rapamycin-modulated transcription defines the subset of nutrient-sensitive signalling pathways directly controlled by the Tor proteins. Proceedings of the National Academy of Sciences of the United States of America **96**: 14866–14870.

Hartmann Y., 2024 Regulation of the yeast Kns1 kinase.

Hartwell L. H., 1974 *Saccharomyces cerevisiae* cell cycle. Bacteriological Reviews **38**: 164–198.

Hayles J., and P. Nurse, 1986 Cell Cycle Regulation in Yeast. Journal of Cell Science **4**: 155–170.

Hecht K., J. Bailey, and W. Minas, 2002 Polycistronic gene expression in yeast versus cryptic promoter elements. FEMS Yeast Research **2**: 215–224.

Hedges D., M. Proft, and K.-D. Entian, 1995 *CAT8* , a New Zinc Cluster-Encoding Gene Necessary for Derepression of Gluconeogenic Enzymes in the Yeast *Saccharomyces cerevisiae*. Molecular and Cellular Biology **15**: 1915–1922.

Hellen C. U. T., and P. Sarnow, 2001 Internal ribosome entry sites in eukaryotic mRNA molecules. Genes & Development **15**: 1593–1612.

Henriksen P., S. A. Wagner, B. T. Weinert, S. Sharma, G. Bačinskaja, M. Rehman, A. H. Juffer, T. C. Walther, M. Lisby, and C. Choudhary, 2012 Proteome-wide Analysis of Lysine Acetylation Suggests its Broad Regulatory Scope in *Saccharomyces cerevisiae*. Molecular & Cellular Proteomics **11**: 1510–1522.

Hershey J. W. B., N. Sonenberg, and M. B. Mathews, 2019 Principles of Translational Control. Cold Spring Harbor Perspectives in Biology **11**: 1–6.

Hershko A., and A. Ciechanover, 1998 The Ubiquitin System. Annual Review of Biochemistry **67**: 425–479.

Herskowitz I., 1988 Life cycle of the budding yeast *Saccharomyces cerevisiae*. Microbiology Reviews **52**: 536–553.

Hiesinger M., S. Roth, E. Meissner, and H.-J. Schüller, 2001 Contribution of Cat8 and Sip4 to the transcriptional activation of yeast gluconeogenic genes by carbon source-responsive elements. Current Genetics **39**: 68–76.

Hindupur S. K., A. González, and M. N. Hall, 2015 The Opposing Actions of Target of Rapamycin and AMP-Activated Protein Kinase in Cell Growth Control. Cold Spring Harbor Perspectives in Biology **7**: 1–20.

Hinnebusch A. G., 1997 Translational Regulation of Yeast *GCN4*. Journal of Biological Chemistry **272:** 21661–21664.

Hinnebusch A. G., and K. Natarajan, 2002 Gcn4p, a Master Regulator of Gene Expression, Is Controlled at Multiple Levels by Diverse Signals of Starvation and Stress. Eukaryotic Cell **1**: 22–32.

Hinnebusch A. G., 2011 Molecular Mechanism of Scanning and Start Codon Selection in Eukaryotes. Microbiology and Molecular Biology Reviews **75**: 434–467.

Hinnebusch A. G., 2014 The Scanning Mechanism of Eukaryotic Translation Initiation. Annual Review of Biochemistry **83**: 779–812.

Hinnebusch A. G., I. P. Ivanov, and N. Sonenberg, 2016 Translational control by 5′-untranslated regions of eukaryotic mRNAs. Science **352**: 1413–1416.

Ho Y., A. Gruhler, A. Heilbut, G. D. Bader, L. Moore, S.-L. Adams, A. Millar, P. Taylor, K. Bennett, K. Boutilier, L. Yang, C. Wolting, I. Donaldson, S. Schandorff, J. Shewnarane, M. Vo, J. Taggart, M. Goudreault, B. Muskat, C. Alfarano, D. Dewar, Z. Lin, K. Michalickova, A. R. Willems, H. Sassi, P. A. Nielsen, K. J. Rasmussen, J. R. Andersen, L. E. Johansen, L. H. Hansen, H. Jespersen, A. Podtelejnikov, E. Nielsen, J. Crawford, V. Poulsen, B. D. Sorensen, J. Matthiesen, R. C. Hendrickson, C. W. V. Hogue, D. Figeys, and M. Tyers, 2002 Systematic identification of protein complexes in *Saccharomyces cerevisiae* by mass spectrometry. Nature **415**: 180–183.

Hochstrasser M., 2009 Origin and function of ubiquitin-like proteins. Nature **458:** 422–429.

Holm C., D. W. Meeks-Wagner, W. L. Fangman, and D. Botstein, 1986 A rapid, efficient method for isolating DNA from yeast. Gene **42**: 169–173.

Holt L. J., B. B. Tuch, J. Villén, A. D. Johnson, S. P. Gygi, and D. O. Morgan, 2009 Global Analysis of Cdk1 Substrate Phosphorylation Sites Provides Insights into Evolution. Science **325**: 1682–1686.

Howell J. J., S. J. H. Ricoult, I. Ben-Sahra, and B. D. Manning, 2013 A growing role for mTOR in promoting anabolic metabolism. Biochemical Society Transactions **41**: 906–912.

Hsieh W.-C., B. M. Sutter, H. Ruess, S. D. Barnes, V. S. Malladi, and B. P. Tu, 2022 Glucose starvation induces a switch in the histone acetylome for activation of gluconeogenic and fat metabolism genes. Molecular Cell **82**: 60-74.

Hughes Hallett J. E., X. Luo, and A. P. Capaldi, 2014 State Transitions in the TORC1 Signalling Pathway and Information Processing in *Saccharomyces cerevisiae*. Genetics **198**: 773–786.

Hughes Hallett J. E., X. Luo, and A. P. Capaldi, 2015 Snf1/AMPK promotes the formation of Kog1/Raptor-bodies to increase the activation threshold of TORC1 in budding yeast. eLife **4**: 1–19.

Huxley C., E. D. Green, and I. Dunham, 1990 Rapid assessment of *S. cerevisiae* mating type by PCR. Trends in Genetics **6**: 236.

Ito H., Y. Fukuda, K. Murata, and A. Kimura, 1983 Transformation of intact yeast cells treated with alkali cations. Journal of Bacteriology **153**: 163–168.

Jackson J. C., and J. M. Lopes, 1996 The Yeast *UME6* Gene Is Required for Both Negative and Positive Transcriptional Regulation of Phospholipid Biosynthetic Gene Expression. Nucleic Acids Research **24:** 1322–1329.

Jackson R. J., C. U. T. Hellen, and T. V. Pestova, 2010 The mechanism of eukaryotic translation initiation and principles of its regulation. Nature Reviews Molecular Cell Biology **11**: 113–127.

Jacobs C. W., A. E. Adams, P. J. Szaniszlo, and J. R. Pringle, 1988 Functions of microtubules in the *Saccharomyces cerevisiae* cell cycle. The Journal of Cell Biology **107**: 1409–1426.

Jadhav T., and M. W. Wooten, 2009 Defining an Embedded Code for Protein Ubiquitination. Journal of Proteomics & Bioinformatics **02**: 316–333.

James B. P., W. D. Staatz, S. T. Wilkinson, E. Meuillet, and G. Powis, 2009 Superoxide dismutase is regulated by LAMMER kinase in Drosophila and human cells. Free Radical Biology and Medicine **46**: 821–827.

Jiménez J., S. Bru, M. P. Ribeiro, and J. Clotet, 2015 Live fast, die soon: cell cycle progression and lifespan in yeast cells. Microbial Cell **2**: 62–67.

Johnson K. W., and K. A. Smith, 1991 Molecular cloning of a novel human cdc2/CDC28-like protein kinase. Journal of Biological Chemistry **266**: 3402–3407.

Jumper J., R. Evans, A. Pritzel, T. Green, M. Figurnov, O. Ronneberger, K. Tunyasuvunakool, R. Bates, A. Zidek, A. Potapenko, A. Bridgland, C. Meyer, S. A. A. Kohl, A. J. Ballard, A. Cowie, B. Romera-Paredes, S. Nikolov, R. Jain, J. Adler, T. Back, S. Petersen, D. Reiman, E. Clancy, M. Zielinski, M. Steinegger, M. Pacholska, T. Berghammer, S. Bodenstein, D. Silver, O. Vinyals, A. W. Senior, K. Kavukcuoglu, P. Kohli, and D. Hassabis, 2021 Highly accurate protein structure prediction with AlphaFold. Nature **596**: 583–589.

Kadosh D., and K. Struhl, 1997 Repression by Ume6 Involves Recruitment of a Complex Containing Sin3 Corepressor and Rpd3 Histone Deacetylase to Target Promoters. Cell **89**: 365–371.

Kadosh D., and K. Struhl, 1998 Targeted Recruitment of the Sin3-Rpd3 Histone Deacetylase Complex Generates a Highly Localized Domain of Repressed Chromatin *In Vivo*. Molecular and Cellular Biology **18**: 5121–5127.

Kaffman A., N. M. Rank, E. M. O'Neill, L. S. Huang, and E. K. O'Shea, 1998 The receptor Msn5 exports the phosphorylated transcription factor Pho4 out of the nucleus. Nature **396**: 482–486.

Kalitsis P., T. Zhang, K. M. Marshall, C. F. Nielsen, and D. F. Hudson, 2017 Condensin, master organizer of the genome. Chromosome Research **25**: 61–76.

Kayikci Ö., and J. Nielsen, 2015 Glucose repression in *Saccharomyces cerevisiae*. FEMS Yeast Research **15**: 1–8.

Kim K.-H., Y.-M. Cho, W.-H. Kang, J.-H. Kim, K.-H. Byun, Y. D. Park, K. S. Bae, and H. M. Park, 2001 Negative Regulation of Filamentous Growth and Flocculation by Lkh1, a Fission Yeast LAMMER Kinase Homologue. Biochemical and Biophysical Research Communications **289**: 1237–1242.

Kim J.-H., A. Roy, D. Jouandot, and K. H. Cho, 2013 The glucose signalling network in yeast. Biochimica et Biophysica Acta - General Subjects **1830**: 5204–5210.

King N. (Ed.), 2010 *RT-PCR Protocols*. Humana Press, Totowa, NJ.

Kinoshita E., E. Kinoshita-Kikuta, and T. Koike, 2009 Separation and detection of large phosphoproteins using Phos-tag SDS-PAGE. Nature Protocols **4**: 1513–1521.

Kinoshita E., E. Kinoshita-Kikuta, and T. Koike, 2022 History of Phos-tag technology for phosphoproteomics. Journal of Proteomics **252**: 1–8.

Klein M., S. Swinnen, J. M. Thevelein, and E. Nevoigt, 2017 Glycerol metabolism and transport in yeast and fungi: established knowledge and ambiguities. Environmental Microbiology **19**: 878–893.

Kosugi S., M. Hasebe, M. Tomita, and H. Yanagawa, 2009 Systematic identification of cell cycle-dependent yeast nucleocytoplasmic shuttling proteins by prediction of composite motifs. Proceedings of the National Academy of Sciences of the United States of America **106**: 10171–10176.

Kozak M., 1986 Point mutations define a sequence flanking the AUG initiator codon that modulates translation by eukaryotic ribosomes. Cell **44**: 283–292.

Kozak M., 2005 Regulation of translation via mRNA structure in prokaryotes and eukaryotes. Gene **361**: 13–37.

Kraft C., M. Peter, and K. Hofmann, 2010 Selective autophagy: ubiquitin-mediated recognition and beyond. Nature Cell Biology **12**: 836–841.

Krogan N. J., G. Cagney, H. Yu, G. Zhong, X. Guo, A. Ignatchenko, J. Li, S. Pu, N. Datta, A. P. Tikuisis, T. Punna, J. M. Peregrin-Alvarez, M. Shales, X. Zhang, M. Davey, M. D. Robinson, A. Paccanaro, J. E. Bray, A. Sheung, B. Beattie, D. P. Richards, V. Canadien, A. Lalev, F. Mena, P. Wong, A. Starostine, M. M. Canete, J. Vlasblom, S. Wu, C. Orsi, S. R. Collins, S. Chandran, R. Haw, M. H. Y. Lam, G. Butland, A. M. Altaf-Ul, S. Kanaya, A. Shilatifard, E. O'Shea, J. S. Weissman, C. J. Ingles, T. R. Hughes, J. Parkinson, M. Gerstein, S. J. Wodak, A. Emili, and J. F. Greenblatt, 2006 Global landscape of protein complexes in the yeast Saccharomyces cerevisiae. Nature **440**: 637–643.

Kruckeberg A. L., 1996 The hexose transporter family of *Saccharomyces cerevisiae*. Archives of Microbiology **166**: 283–292.

Kumar A., S. Agarwal, J. A. Heyman, S. Matson, M. Heidtman, S. Piccirillo, L. Umansky, A. Drawid, R. Jansen, Y. Liu, K.-H. Cheung, P. Miller, M. Gerstein, G. Shirleen Roeder, and M. Snyder, 2002 Subcellular localization of the yeast proteome. Genes & Development **16**: 707–719.

Kwak H., and J. T. Lis, 2013 Control of Transcriptional Elongation. Annual Review of Genetics **47**: 483–508.

Landrieux E., N. Alic, C. Ducrot, J. Acker, M. Riva, and C. Carles, 2006 A subcomplex of RNA polymerase III subunits involved in transcription termination and reinitiation. EMBO Journal **25**: 118–128.

Lanz M. C., K. Yugandhar, S. Gupta, E. J. Sanford, V. M. Faça, S. Vega, A. M. N. Joiner, J. C. Fromme, H. Yu, and M. B. Smolka, 2021 In-depth and 3-dimensional exploration of the budding yeast phosphoproteome. EMBO Reports **22**: 1–17.

Laplante M., and D. M. Sabatini, 2012 mTOR Signalling in Growth Control and Disease. Cell **149**: 274–293.

Lee D. H., and A. L. Goldberg, 1996 Selective Inhibitors of the Proteasome-dependent and Vacuolar Pathways of Protein Degradation in *Saccharomyces cerevisiae*. Journal of Biological Chemistry **271**: 27280–27284.

Lee K., C. Du, M. Horn, and L. Rabinow, 1996 Activity and Autophosphorylation of LAMMER Protein Kinases. Journal of Biological Chemistry **271**: 27299–27303.

Lee P., B.-R. Cho, H.-S. Joo, and J.-S. Hahn, 2008 Yeast Yak1 kinase, a bridge between PKA and stress-responsive transcription factors, Hsf1 and Msn2/Msn4. Molecular Microbiology **70**: 882–895.

Lee J., R. D. Moir, and I. M. Willis, 2009 Regulation of RNA Polymerase III Transcription Involves SCH9-dependent and SCH9-independent Branches of the Target of Rapamycin (TOR) Pathway. Journal of Biological Chemistry **284**: 12604–12608.

Lee J., R. D. Moir, K. B. McIntosh, and I. M. Willis, 2012 TOR Signalling Regulates Ribosome and tRNA Synthesis via LAMMER/Clk and GSK-3 Family Kinases. Molecular Cell **45**: 836–843.

Lee J., R. D. Moir, and I. M. Willis, 2015 Differential Phosphorylation of RNA Polymerase III and the Initiation Factor TFIIIB in *Saccharomyces cerevisiae*. PLoS ONE **10**: 1–19.

Li X., Q. Mei, Q. Yu, M. Wang, F. He, D. Xiao, H. Liu, F. Ge, X. Yu, and S. Li, 2023 The TORC1 activates Rpd3L complex to deacetylate Ino80 and H2A.Z and repress autophagy. Science Advances **9**: 1–17.

Lim J.-Y., and H.-M. Park, 2019 The Dual-Specificity LAMMER Kinase Affects Stress-Response and Morphological Plasticity in Fungi. Frontiers in Cellular and Infection Microbiology **9**: 213.

Lindberg R. A., A. M. Quinn, and T. Hunter, 1992 Dual-specificity protein kinases: will any hydroxyl do? Trends in Biochemical Sciences **17**: 114–119.

Liu C., J. Apodaca, L. E. Davis, and H. Rao, 2007 Proteasome inhibition in wild-type yeast *Saccharomyces cerevisiae* cells. BioTechniques **42**: 158–162.

Lockshon D., L. E. Surface, E. O. Kerr, M. Kaeberlein, and B. K. Kennedy, 2007 The Sensitivity of Yeast Mutants to Oleic Acid Implicates the Peroxisome and Other Processes in Membrane Function. Genetics **175**: 77–91.

Loewith R., and M. N. Hall, 2011 Target of Rapamycin (TOR) in Nutrient Signalling and Growth Control. Genetics **189**: 1177–1201.

Longtine M. S., A. Mckenzie Iii, D. J. Demarini, N. G. Shah, A. Wach, A. Brachat, P. Philippsen, and J. R. Pringle, 1998 Additional modules for versatile and economical PCR-based gene deletion and modification in *Saccharomyces cerevisiae*. Yeast **14**: 953–961.

Lu K., F. Den Brave, and S. Jentsch, 2017 Pathway choice between proteasomal and autophagic degradation. Autophagy **13**: 1799–1800.

Ludin K., R. Jiang, and M. Carlson, 1998 Glucose-regulated interaction of a regulatory subunit of protein phosphatase 1 with the Snf1 protein kinase in *Saccharomyces cerevisiae*. Proceedings of the National Academy of Sciences of the United States of America **95**: 6245–6250.

Lunt S. Y., and M. G. Vander Heiden, 2011 Aerobic Glycolysis: Meeting the Metabolic Requirements of Cell Proliferation. Annual Review of Cell and Developmental Biology **27**: 441–464.

MacGilvray M. E., E. Shishkova, M. Place, E. R. Wagner, J. J. Coon, and A. P. Gasch, 2020 Phosphoproteome Response to Dithiothreitol Reveals Unique *Versus* Shared Features of *Saccharomyces cerevisiae* Stress Responses. Journal of Proteome Research **19**: 3405–3417.

Manthey G. M., and J. E. McEwen, 1995 The product of the nuclear gene PET309 is required for translation of mature mRNA and stability or production of intron-containing RNAs derived from the mitochondrial COX1 locus of *Saccharomyces cerevisiae*. The EMBO Journal **14**: 4031–4043.

Martinez Marshall M. N., 2011 The role of LAMMER kinase Kns1 and the calcium/calmodulin-dependent kinase Cmk2 in the adaptation of *Saccharomyces cerevisiae* to alkaline pH stress.

McIntosh J. R., 2016 Mitosis. Cold Spring Harbor Perspectives in Biology **8**: 1–16.

Menegay H. J., M. P. Myers, F. M. Moeslein, and G. E. Landreth, 2000 Biochemical characterization and localization of the dual specificity kinase CLK1. Journal of Cell Science **113**: 3241–3253.

Mitchell A. P., 1994 Control of meiotic gene expression in *Saccharomyces cerevisiae*. Microbiological Reviews **58**: 56–70.

Mizushima N., 2007 Autophagy: process and function. Genes & Development **21**: 2861–2873.

Moeslein F. M., M. P. Myers, and G. E. Landreth, 1999 The CLK Family Kinases, CLK1 and CLK2, Phosphorylate and Activate the Tyrosine Phosphatase, PTP-1B. Journal of Biological Chemistry **274**: 26697–26704.

Moir R. D., J. Lee, R. A. Haeusler, N. Desai, D. R. Engelke, and I. M. Willis, 2006 Protein kinase A regulates RNA polymerase III transcription through the nuclear localization of Maf1. Proceedings of the National Academy of Sciences of the United States of America **103**: 15044–15049.

Moir R. D., and I. M. Willis, 2013 Regulation of pol III transcription by nutrient and stress signalling pathways. Biochimica et Biophysica Acta - Gene Regulatory Mechanisms **1829**: 361–375.

Monje-Casas F., and E. Queralt (Eds.), 2017 *The Mitotic Exit Network: Methods and Protocols*. Springer New York, New York, NY.

Monteiro P. T., J. Oliveira, P. Pais, M. Antunes, M. Palma, M. Cavalheiro, M. Galocha, C. P. Godinho, L. C. Martins, N. Bourbon, M. N. Mota, R. A. Ribeiro, R. Viana, I. Sa-Correia, and M. C. Teixeira, 2020 YEASTRACT+: a portal for cross-species comparative genomics of transcription regulation in yeasts. Nucleic Acids Research **48**: D642–D649.

Moore M. J., and N. J. Proudfoot, 2009 Pre-mRNA Processing Reaches Back toTranscription and Ahead to Translation. Cell **136**: 688–700.

Morano K. A., C. M. Grant, and W. S. Moye-Rowley, 2012 The Response to Heat Shock and Oxidative Stress in *Saccharomyces cerevisiae*. Genetics **190**: 1157–1195.

Morozumi Y., and K. Shiozaki, 2021 Conserved and Divergent Mechanisms That Control TORC1 in Yeasts and Mammals. Genes **12**: 88.

Mullis K., F. Faloona, S. Scharf, R. Saiki, G. Horn, H. Erlich, 1986 Specific Enzymatic Amplification of DNA In Vitro: The Polymerase Chain Reaction. Cold Spring Harbor Symposia on Quantitative Biology **51**: 263–273.

Muraki M., B. Ohkawara, T. Hosoya, H. Onogi, J. Koizumi, T. Koizumi, K. Sumi, J.-I. Yomoda, M. V. Murray, H. Kimura, k. Furuichi, H. Shibuya, A. R. Krainer, M. Suzuki, and M. Hagiwara, 2004 Manipulation of Alternative Splicing by a Newly Developed Inhibitor of Clks. Journal of Biological Chemistry **279**: 24246–24254.

Myers M. P., M. B. Murphy, and G. Landreth, 1994 The Dual-Specificity CLK Kinase Induces Neuronal Differentiation of PC12 Cells. Molecular and Cellular Biology **14**: 6954–6961.

Nagalakshmi U., Z. Wang, K. Waern, C. Shou, D. Raha, M. Gerstein, and M. Snyder, 2008 The Transcriptional Landscape of the Yeast Genome Defined by RNA Sequencing. Science **320**: 1344–1349.

Nakatogawa H., K. Suzuki, Y. Kamada, and Y. Ohsumi, 2009 Dynamics and diversity in autophagy mechanisms: lessons from yeast. Nature Reviews Molecular Cell Biology **10**: 458–467.

Nayler O., F. Schnorrer, S. Stamm, and A. Ullrich, 1998 The Cellular Localization of the Murine Serine/Arginine-rich Protein Kinase CLK2 Is Regulated by Serine 141 Autophosphorylation. Journal of Biological Chemistry **273**: 34341–34348.

Nguyen Ba A. N., A. Pogoutse, N. Provart, and A. M. Moses, 2009 NLStradamus: a simple Hidden Markov Model for nuclear localization signal prediction. BMC Bioinformatics **10**: 202.

Nightingale D. J., A. Geladaki, L. M. Breckels, S. G. Oliver, and K. S. Lilley, 2019 The subcellular organisation of *Saccharomyces cerevisiae*. Current Opinion in Chemical Biology **48**: 86–95.

O´Conalláin C., M.-T. Doolin, C. Taggart, F. Thornton, and G. Butler, 1999 Regulated nuclear localisation of the yeast transcription factor Ace2p controls expression of chitinase (*CTS1*) in *Saccharomyces cerevisiae*. Molecular Genetics and Genomics **262**: 275–282.

Orioli A., C. Pascali, A. Pagano, M. Teichmann, and G. Dieci, 2012 RNA polymerase III transcription control elements: Themes and variations. Gene **493**: 185–194.

Padmanabha R., S. Gehrung, and M. Snyder, 1991 The *KNS1* gene of *Saccharomyces cerevisiae* encodes a non-essential protein kinase bomologue that is distantly related to members of the CDC28/cdc2 gene family. Molecular Genetics and Genomics **229**: 1–9.

Pakos-Zebrucka K., I. Koryga, K. Mnich, M. Ljujic, A. Samali, and A. M. Gorman, 2016 The integrated stress response. EMBO Reports **17**: 1374–1395.

Panvert M., E. Dubiez, L. Arnold, J. Perez, Y. Mechulam, W. Seufert, and E. Schmitt, 2015 Cdc123, a Cell Cycle Regulator Needed for eIF2 Assembly, Is an ATP-Grasp Protein with Unique Features. Structure **23**: 1596–1608.

Papp B., C. Pál, and L. D. Hurst, 2004 Metabolic network analysis of the causes and evolution of enzyme dispensability in yeast. Nature **429**: 661–664.

Park Y.-D., W.-H. Kang, W.-S. Yang, K.-S. Shin, K. Sook Bae, H.-M. Park, 2003 LAMMER kinase homologue, Lkh1, is involved in oxidative-stress response of fission yeast. Biochemical and Biophysical Research Communications **311**: 1078–1083.

Pavitt G. D., 2018 Regulation of translation initiation factor eIF2B at the hub of the integrated stress response. WIREs RNA **9**: 1–22.

Pearce L. R., D. Komander, and D. R. Alessi, 2010 The nuts and bolts of AGC protein kinases. Nature Reviews Molecular Cell Biology **11**: 9–22.

Peeters K., F. Van Leemputte, B. Fischer, B. M. Bonini, H. Quezada, M. Tsytlonok, D. Haesen, W. Vanthienen, N. Bernardes, C. B. Gonzalez-Blas, V. Janssens, P. Tompa, W. Versées, and J. M. Thevelein, 2017 Fructose-1,6-bisphosphate couples glycolytic flux to activation of Ras. Nature Communications **8**: 922.

Perzlmaier A. F., F. Richter, and W. Seufert, 2013 Translation Initiation Requires Cell Division Cycle 123 (Cdc123) to Facilitate Biogenesis of the Eukaryotic Initiation Factor 2 (eIF2). Journal of Biological Chemistry **288**: 21537–21546

Pfeiffer T., and A. Morley, 2014 An evolutionary perspective on the Crabtree effect. Frontiers in Molecular Biosciences **1**: 1–6.

Pilla E., K. Schneider, and A. Bertolotti, 2017 Coping with Protein Quality Control Failure. Annual Review of Cell and Developmental Biology **33**: 439–465.

Pluta K., O. Lefebvre, N. C. Martin, W. J. Smagowicz, D. R. Stanford, S. R. Ellis, A. K. Hopper, A. Sentenac, and M. Boguta, 2001 Maf1p, a Negative Effector of RNA Polymerase III in *Saccharomyces cerevisiae*. Molecular and Cellular Biology **21**: 5031–5040.

Pohl C., and I. Dikic, 2019 Cellular quality control by the ubiquitin-proteasome system and autophagy. Science **366**: 818–822.

Polymenis M., and R. Aramayo, 2015 Translate to divide: control of the cell cycle by protein synthesis. Microbial Cell **2**: 94–104.

Popolo L., M. Vanoni, and L. Alberghina, 1982 Control of the Yeast Cell Cycle by Protein Synthesis. Experimental Cell Research **142**: 69–78.

Porrua O., and D. Libri, 2015 Transcription termination and the control of the transcriptome: why, where and how to stop. Nature Reviews Molecular Cell Biology **16**: 190–202.

Postnikoff S. D. L., J. E. Johnson, and J. K. Tyler, 2017 The integrated stress response in budding yeast lifespan extension. Microbial Cell **4**: 368–375.

Prouteau M., A. Desfosses, C. Sieben, C. Bourgoint, N. Lydia Mozaffari, D. Demurtas, A. K. Mitra, P. Guichard, S. Manley, and R. Loewith, 2017 TORC1 organized in inhibited domains (TOROIDs) regulate TORC1 activity. Nature **550**: 265–269.

Ptacek J., G. Devgan, G. Michaud, H. Zhu, X. Zhu, J. Fasolo, H. Guo, G. Jona, A. Breitkreutz, R. Sopko, R. R. McCartney, M. C. Schmidt, N. Rachidi, S.-J. Lee, A. S. Mah, L. Meng, M. J. R. Stark, D. F. Stern, C. De Virgilio, M. Tyers, B. Andrews, M. Gerstein, B. Schweitzer, P. F. Predki, and M. Snyder, 2005 Global analysis of protein phosphorylation in yeast. Nature **438**: 679–684.

Randez-Gil F., N. Bojunga, M. Proft, and K.-D. Entian, 1997 Glucose Derepression of Gluconeogenic Enzymes in *Saccharomyces cerevisiae* Correlates with Phosphorylation of the Gene Activator Cat8p. Molecular and Cellular Biology **17**: 2502–2510.

Richard P., 2003 The rhythm of yeast. FEMS Microbiology Reviews **27**: 547–557.

Rodgers J. T., W. Haas, S. P. Gygi, and P. Puigserver, 2010 Cdc2-like Kinase 2 Is an Insulin-Regulated Suppressor of Hepatic Gluconeogenesis. Cell Metabolism **11**: 23–34.

Rojas-Duran M. F., and W. V. Gilbert, 2012 Alternative transcription start site selection leads to large differences in translation activity in yeast. RNA **18**: 2299–2305.

Romano A. H., and T. Conway, 1996 Evolution of carbohydrate metabolic pathways. Research in Microbiology **147**: 448–455.

Rønnow B., and M. C. Kielland-Brandt, 1993 *GUT2* , a gene for mitochondrial glycerol 3-phosphate dehydrogenase of *Saccharomyces cerevisiae*. Yeast **9**: 1121–1130.

Roosen J., C. Oesterhelt, K. Pardons, E. Swinnen, and J. Winderickx, 2004 11 Integration of nutrient signalling pathways in the yeast *Saccharomyces cerevisiae*, pp. 277–318 in *Nutrient-Induced Responses in Eukaryotic Cells*, Topics in Current Genetics. edited by Winderickx J. G., Taylor P. M. Springer Berlin Heidelberg, Berlin, Heidelberg.

Rosa C., and P. Gábor (Eds.), 2006 *Biodiversity and ecophysiology of yeasts*. Springer, Berlin ; London.

Roth S., J. Kumme, and H.-J. Schüller, 2004 Transcriptional activators Cat8 and Sip4 discriminate between sequence variants of the carbon source-responsive promoter element in the yeast *Saccharomyces cerevisiae*. Current Genetics **45**: 121–128.

Rundlett S. E., A. A. Carmen, R. Kobayashi, S. Bavykin, B. M. Turner, and M. Grunstein, 1996 HDA1 and RPD3 are members of distinct yeast histone deacetylase complexes that regulate silencing and transcription. Proceedings in the National Academy of Sciences of the United States of America **93**: 14503–14508.

Sampaio-Marques B., and P. Ludovico, 2018 Linking cellular proteostasis to yeast longevity. FEMS Yeast Research **18**: 1–11.

Sanchez-Casalongue M. E., J. Lee, A. Diamond, S. Shuldiner, R. D. Moir, and I. M. Willis, 2015 Differential Phosphorylation of a Regulatory Subunit of Protein Kinase CK2 by Target of Rapamycin Complex 1 Signalling and the Cdc-like Kinase Kns1. Journal of Biological Chemistry **290**: 7221–7233.

Santangelo G. M., 2006 Glucose Signalling in *Saccharomyces cerevisiae*. Microbiology and Molecular Biology Reviews **70**: 253–282.

Savaldi-Goldstein S., D. Aviv, O. Davydov, and R. Fluhr, 2003 Alternative Splicing Modulation by a LAMMER Kinase Impinges on Developmental and Transcriptome Expression. Plant Cell **15**: 926–938.

Schmeing T. M., and V. Ramakrishnan, 2009 What recent ribosome structures have revealed about the mechanism of translation. Nature **461**: 1234–1242.

Schmitt E., M. Naveau, and Y. Mechulam, 2010 Eukaryotic and archaeal translation initiation factor 2: A heterotrimeric tRNA carrier. FEBS Letters **584**: 405–412.

Schmitt K., N. Smolinski, P. Neumann, S. Schmaul, V. Hofer-Pretz, G. H. Braus, and O. Valerius, 2017 Asc1p/RACK1 Connects Ribosomes to Eukaryotic Phosphosignaling. Molecular and Cellular Biology **37**: 1–23.

Schneider-Poetsch T., J. Ju, D. E. Eyler, Y. Dang, S. Bhat, W. C. Merrick, R. Green, B. Shen, and J. O. Liu, 2010 Inhibition of eukaryotic translation elongation by cycloheximide and lactimidomycin. Nature Chemical Biology **6**: 209–217.

Schramm L., and N. Hernandez, 2002 Recruitment of RNA polymerase III to its target promoters. Genes & Development **16**: 2593–2620.

Schüller H.-J., 2003 Transcriptional control of non-fermentative metabolism in the yeast *Saccharomyces cerevisiae*. Current Genetics **43**: 139–160.

Sessa G., V. Raz, S. Savaldi, and R. Fluhr, 1996 PK12, a plant dual-specificity protein kinase of the LAMMER family, is regulated by the hormone ethylene. The Plant Cell **8**: 2223–2234.

Shaw A. E., J. E. Whitted, M. N. Mihelich, H. J. Reitman, A. J. Timmerman, and G. D. Schauer, 2024 Revised Mechanism of Hydroxyurea Induced Cell Cycle Arrest and an Improved Alternative. bioRxiv. Preprint.

Sheff M. A., and K. S. Thorn, 2004 Optimized cassettes for fluorescent protein tagging in *Saccharomyces cerevisiae*. Yeast **21**: 661–670.

Shekhar A. C., W.-J. Wu, and H.-T. Chen, 2023 Mutational and biophysical analyses reveal a TFIIIC binding region in the TFIIF-related Rpc53 subunit of RNA polymerase III. Journal of Biological Chemistry **299**: 1–13.

Sidorova J. M., G. E. Mikesell, and L. L. Breeden, 1995 Cell cycle-regulated phosphorylation of Swi6 controls its nuclear localization. Molecular Biology of the Cell **6**: 1641–1658.

Sidorova J. M., and L. L. Breeden, 2003 Rad53 Checkpoint Kinase Phosphorylation Site Preference Identified in the Swi6 Protein of *Saccharomyces cerevisiae*. Molecular and Cellular Biology **23**: 3405–3416.

Sonenberg N., and A. G. Hinnebusch, 2009 Regulation of Translation Initiation in Eukaryotes: Mechanisms and Biological Targets. Cell **136**: 731–745.

Strich R., R. T. Surosky, C. Steber, E. Dubois, F. Messenguy, and R. E. Esposito, 1994 *UME6* is a key regulator of nitrogen repression and meiotic development. Genes & Development **8**: 796–810.

Sugiyama Y., and Y. Uezato, 2022 Analysis of protein kinases by Phos-tag SDS-PAGE. Journal of Proteomics **255**: 1–6.

Suryadinata R., M. Sadowski, and B. Sarcevic, 2010 Control of cell cycle progression by phosphorylation of cyclin-dependent kinase (CDK) substrates. Bioscience Reports **30**: 243–255.

Swaney D. L., P. Beltrao, L. Starita, A. Guo, J. Rush, S. Fields, N. J. Krogan, and J. Villén, 2013 Global analysis of phosphorylation and ubiquitylation cross-talk in protein degradation. Nature Methods **10**: 676–682.

Swatek K. N., and D. Komander, 2016 Ubiquitin modifications. Cell Research **26**: 399–422.

Szatkowska R., M. Garcia-Albornoz, K. Roszkowska, S. W. Holman, E. Furmanek, S. J. Hubbard, R. J. Beynon, and M. Adamczyk, 2019 Glycolytic flux in *Saccharomyces cerevisiae* is dependent on RNA polymerase III and its negative regulator Maf1. Biochemical Journal **476**: 1053–1082.

Tabba S., S. Mangat, R. McCartney, and M. C. Schmidt, 2010 PP1 phosphatase-binding motif in Reg1 protein of *Saccharomyces cerevisiae* is required for interaction with both the PP1 phosphatase Glc7 and the Snf1 protein kinase. Cellular Signalling **22**: 1013–1021.

Takeda E., and A. Matsuura, 2018 A substrate localization model for the selective regulation of TORC1 downstream pathways. Communicative & Integrative Biology **11**: 1–4.

Tang Z., L. L. Mandel, S.-L. Yean, C. X. Lin, T. Chen, M. Yanagida, and R.-J. Lin, 2003 The Kic1 kinase of *Schizosaccharomyces pombe* is a CLK/STY orthologue that regulates cell–cell separation. Experimental Cell Research **283**: 101–115.

Tang Z., M. Luca, J. Portillio, B. Ngo, C. Chang, T. Wen, J. Murray, and A. Carr., 2011 LAMMER kinase Kic1 is involved in pre-mRNA processing. Experimental Cell Research **317**: 2308–2320.

Taylor S. C., 2019 End the Cycle of Repeated, Failed Experiments with a Robust Field Guide to qPCR. Bioradiations **1**: 1–5.

Teixeira M. C., R. Viana, M. Palma, J. Oliveira, M. Galocha, M. N. Mota, D. Couceiro, M. G. Pereira, M. Antunes, I. V. Costa, P. Pais, C. Parada, C. Chaouiya, I. Sa-Correia, and P. T. Monteiro, 2023 YEASTRACT+: a portal for the exploitation of global transcription regulation and metabolic model data in yeast biotechnology and pathogenesis. Nucleic Acids Research **51**: D785–D791.

Thadani R., F. Uhlmann, and S. Heeger, 2012 Condensin, Chromatin Crossbarring and Chromosome Condensation. Current Biology **22**: R1012–R1021.

The Essential Guide to Successful Quantitative Western Blots, 2021

Timón-Gómez A., E. Nývltová, L. A. Abriata, A. J. Vila, J. Hosler, and A. Barrientos, 2018 Mitochondrial cytochrome c oxidase biogenesis: Recent developments. Seminars in Cell & Developmental Biology **76**: 163–178.

Toffaletti D. L., M. Del Poeta, T. H. Rude, F. Dietrich, and J. R. Perfect, 2003 Regulation of cytochrome c oxidase subunit 1 (COX1) expression in *Cryptococcus neoformans* by temperature and host environment. Microbiology **149**: 1041–1049.

Treitel M. A., S. Kuchin, and M. Carlson, 1998 Snf1 Protein Kinase Regulates Phosphorylation of the Mig1 Repressor in *Saccharomyces cerevisiae*. Molecular and Cellular Biology **18**: 6273–6280.

Tschochner H., and E. Hurt, 2003 Pre-ribosomes on the road from the nucleolus to the cytoplasm. Trends in Cell Biology **13**: 255–263.

Turcotte B., X. B. Liang, F. Robert, and N. Soontorngun, 2010 Transcriptional regulation of non-fermentable carbon utilization in budding yeast. FEMS Yeast Research **10**: 2–13.

Turowski T. W., and D. Tollervey, 2016 Transcription by RNA polymerase III: insights into mechanism and regulation. Biochemical Society Transactions **44**: 1367–1375.

Turowski T. W., and M. Boguta, 2021 Specific Features of RNA Polymerases I and III: Structure and Assembly. Frontiers in Molecular Biosciences **8**: 1–8.

Urban J., A. Soulard, A. Huber, S. Lippman, D. Mukhopadhyay, O. Deloche, V. Wanke, D. Anrather, G. Ammerer, H. Riezman, J. R. Broach, C. De Virgilio, M. N. Hall, and R. Loewith,

2007 Sch9 Is a Major Target of TORC1 in *Saccharomyces cerevisiae*. Molecular Cell **26**: 663–674.

Van Ende M., S. Wijnants, and P. Van Dijck, 2019 Sugar Sensing and Signalling in *Candida albicans* and *Candida glabrata*. Frontiers in Microbiology **10**: 1–16.

Van Rossum H. M., B. U. Kozak, M. S. Niemeijer, H. J. Duine, M. A. H. Luttik, V. M. Boer, P. Kötter, J.-M. G. Daran, A. J. A. van Maris, and J. T. Pronk, 2016 Alternative reactions at the interface of glycolysis and citric acid cycle in *Saccharomyces cerevisiae*. FEMS Yeast Research **16**: 1–13.

Vander Heiden M. G., L. C. Cantley, and C. B. Thompson, 2009 Understanding the Warburg Effect: The Metabolic Requirements of Cell Proliferation. Science **324**: 1029–1033.

Varadi M., S. Anyango, M. Deshpande, S. Nair, C. Natassia, G. Yordanova, D. Yuan, O. Stroe, G. Wood, A. Laydon, A. Zidek, T. Green, K. Tunyasuvunakool, S. Petersen, J. Jumper, E. Clancy, R. Green, A. Vora, M. Lutfi, M. Figurnov, A. Cowie, N. Hobbs, P. Kohli, G. Kleywegt, E. Birney, D. Hassabis, and S. Velankar, 2022 AlphaFold Protein Structure Database: massively expanding the structural coverage of protein-sequence space with high-accuracy models. Nucleic Acids Research **50**: D439–D444.

Varmus H., 1987 Reverse Transcription. Scientific American **257**: 56–59.

Vershon A. K., and M. Pierce, 2000 Transcriptional regulation of meiosis in yeast. Current Opinion in Cell Biology **12**: 334–339.

Vershon A. K., and M. Pierce, 2000 Transcriptional regulation of meiosis in yeast. Current Opinion in Cell Biology **12**: 334–339.

Voorhees R. M., and V. Ramakrishnan, 2013 Structural Basis of the Translational Elongation Cycle. Annual Review of Biochemistry **82:** 203–236.

Wade J. T., and K. Struhl, 2008 The transition from transcriptional initiation to elongation. Current Opinion in Genetics & Development **18**: 130–136.

Walter P., and D. Ron, 2011 The Unfolded Protein Response: From Stress Pathway to Homeostatic Regulation. Science **334**: 1081–1086.

Warburg O., 1956 On the Origin of Cancer Cells. Science **123**: 309–314.

Wei Y., C. K. Tsang, and X. F. S. Zheng, 2009 Mechanisms of regulation of RNA polymerase III-dependent transcription by TORC1. EMBO Journal **28**: 2220–2230.

Wei Y., and X. F. S. Zheng, 2010 Maf1 regulation - A model of signal transduction inside the nucleus. Nucleus **1**: 162–165.

Williams R. M., M. Primig, B. K. Washburn, E. A. Winzeler, M. Bellis, C. Sarrauste de Menthiere, R. W. Davis, and R. E. Esposito, 2002 The Ume6 regulon coordinates metabolic and meiotic gene expression in yeast. Proceedings of the National Academy of Sciences of the United States of America **99**: 13431–13436.

Willis I. M., 1993 RNA polymerase III: Genes, factors and transcriptional specificity. European Journal of Biochemistry **212**: 1–11.

Wojciech F., 2020 Eine eIF2 verursachte Störung der Translationsinitiation verändert Glukose-gesteuerte Prozesse in der Hefe *Saccharomyces cerevisiae*.

Wullschleger S., R. Loewith, and M. N. Hall, 2006 TOR Signalling in Growth and Metabolism. Cell **124**: 471–484.

Xiberras J., M. Klein, and E. Nevoigt, 2019 Glycerol as a substrate for *Saccharomyces cerevisiae* based bioprocesses – Knowledge gaps regarding the central carbon catabolism of this 'non-fermentable' carbon source. Biotechnology Advances **37**: 1–15.

Yanagida M., 2014 The Role of Model Organisms in the History of Mitosis Research. Cold Spring Harbor Perspectives in Biology **6**: 1–14.

Yang X.-J., and E. Seto, 2008 The Rpd3/Hda1 family of lysine deacetylases: from bacteria and yeast to mice and men. Nature Reviews Molecular Cell Biology **9**: 206–218.

Yu H., P. Braun, M. A. Yıldırım, I. Lemmens, K. Venkatesan, J. Sahalie, T. Hirozane-Kishikawa, F. Gebreab, N. Li, N. Simonis, T. Hao, J.-F. Rual, A. Dricot, A. Vazquez, R. R. Murray, C. Simon, L. Tardivo, S. Tam, N. Svrzikapa, C. Fan, A.-S. de Smet, A. Motyl, M. E. Hudson, J. Park, X. Xin, M. E. Cusick, T. Moore, C. Boone, M. Snyder, F. P. Roth, A.-L. Barabasi, J. Tavernier, D. E. Hill, and M. Vidal, 2008 High-Quality Binary Protein Interaction Map of the Yeast Interactome Network. Science **322**: 104–110.

Yuan W., S. Guo, J. Gao, M. Zhong, G. Yan, W. Wu, Y. Chao, and Y. Jiang, 2017 General Control Non-derepressible 2 (GCN2) Kinase Inhibits Target of Rapamycin Complex 1 in Response to Amino Acid Starvation in *Saccharomyces cerevisiae*. Journal of Biological Chemistry **292**: 2660–2669.

Yun B., R. Farkas, K. Lee, and L. Rabinow, 1994 The Doa locus encodes a member of a new protein kinase family and is essential for eye and embryonic development in *Drosophila melanogaster*. Genes & Development **8**: 1160–1173.

Zeyl C., 2000 Budding yeast as a model organism for population genetics. Yeast **16**: 773–784.

Zhou Y., Y. Zhu, L. Dai, Y. Men, J. Wu, J. Zhang, and Y. Sun, 2017a Efficiency Analysis and Mechanism Insight of that Whole-Cell Biocatalytic Production of Melibiose from Raffinose with *Saccharomyces cerevisiae*. Applied Biochemistry and Biotechnology **181**: 407–423.

Zhou Y., Y. Zhu, Y. Men, C. Dong, Y. Sun, and J. Zhang, 2017b Construction of engineered *Saccharomyces cerevisiae* strain to improve that whole-cell biocatalytic production of melibiose from raffinose. Journal of Industrial Microbiology and Biotechnology **44**: 489–501.

Zhou X., W. Li, Y. Liu, and A. Amon, 2021 Cross-compartment signal propagation in the mitotic exit network. eLife **10**: 1–30.

Zimmermann F. K., and I. Scheel, 1977 Mutants of *Saccharomyces cerevisiae* resistant to carbon catabolite repression. Molecular & General Genetics **154**: 75–82.

Zimmermann C., P. Chymkowitch, V. Eldholm, C. D. Putnam, J. M. Lindvall, M. Omerzu, M. Bjoras, R. D. Kolodner, and J. M. Enserink, 2011 A chemical-genetic screen to unravel the genetic network of *CDC28/CDK1* links ubiquitin and Rad6–Bre1 to cell cycle progression. Proceedings of the National Academy of Sciences of the United States of America **108**: 18748–18753.

9 APPENDIX

9.1 Supplementary information

9.1.1 Characterization of Kns1-dependent Rpc53 phosphorylation in the diauxic shift

Section 4.2.1 revealed an increase in Kns1 expression and activity in the diauxic shift. This led to a shift in Rpc53 phosphorylation. However, it is not clear whether Kns1 is the only kinase required for this phosphorylation under these conditions. Therefore, a growth curve analysis of Rpc53 phosphorylation in a *Δkns1* background was performed (Figure S 1 A). The analysis revealed that Kns1 was indeed sufficient to phosphorylate Rpc53 under diauxic shift conditions, as the phosphorylation was lost in *Δkns1* (Figure S 1 B). Rpc53 phosphorylation remained at a minimum level of < 20 % during the diauxic shift, similar to the control measurement (Figure S 1 C).

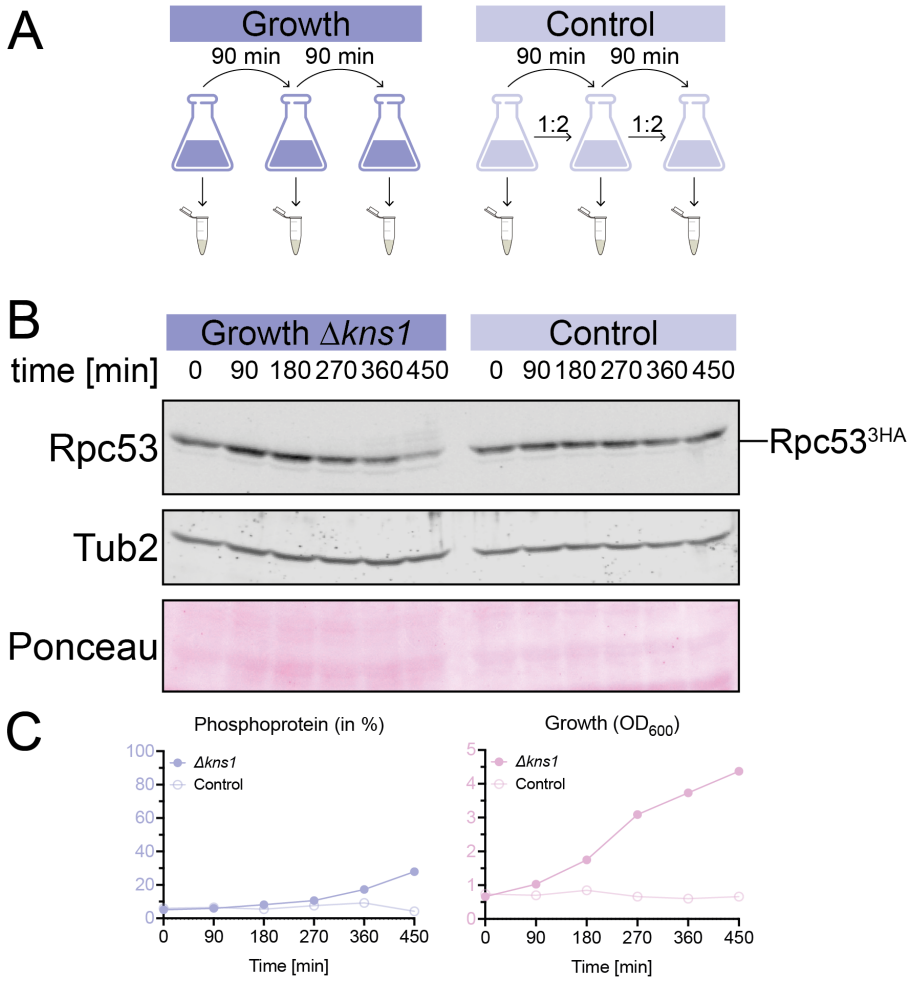

Figure S 1 Increased Rpc53 phosphorylation within the diauxic shift is dependent on Kns1.

A. Schematic overview of the experimental setup. Growth in *Δkns1* background was measured every 90 min and a control was maintained in exponential growth phase by diluting it 1:2 every 90 min. B. Western blot analysis of Rpc53 expression in a growth curve. The samples were collected every 90 min. Rpc53-3HA was detected using an α-HA antibody. Tub2 was used as a reference and proper loading was controlled using Ponceau staining. C. Graphical visualization

of Rpc53 phosphorylation in relation to total protein in % (growth: blue filled circles, control: blue open circles). OD_{600} was used to determine the growth phases (growth: pink filled circles; control: pink open circles).

The ISR is involved in the activation of Kns1 under diauxic shift conditions, as section 4.2.1 revealed. Rpc53 phosphorylation depends on the availability of Gcn4. The ISR may also be activated by blocking eIF2 recycling via eIF2B artificially. This can be achieved by deleting one of the subunits of eIF2B, e.g. Gcn3. In this *Δgcn3* background, the phosphorylation of Rpc53 was evaluated to analyse its potential effects on Kns1 activity. Growth curve analysis (Figure S 2 A) revealed that Gcn3 did not play a role in the activation of Kns1 under the diauxic shift. Rpc53 phosphorylation increased during the diauxic shift, reaching the maximum phosphorylated portion after 360 min (Figure S 2 B). Rpc53 phosphorylation started at a basal level of 20 % and increased to approximately 70 % after 360 min (Figure S 2 C). This significant change compared to the control confirmed that Gcn3 was not necessary for the activation of Kns1 under diauxic conditions.

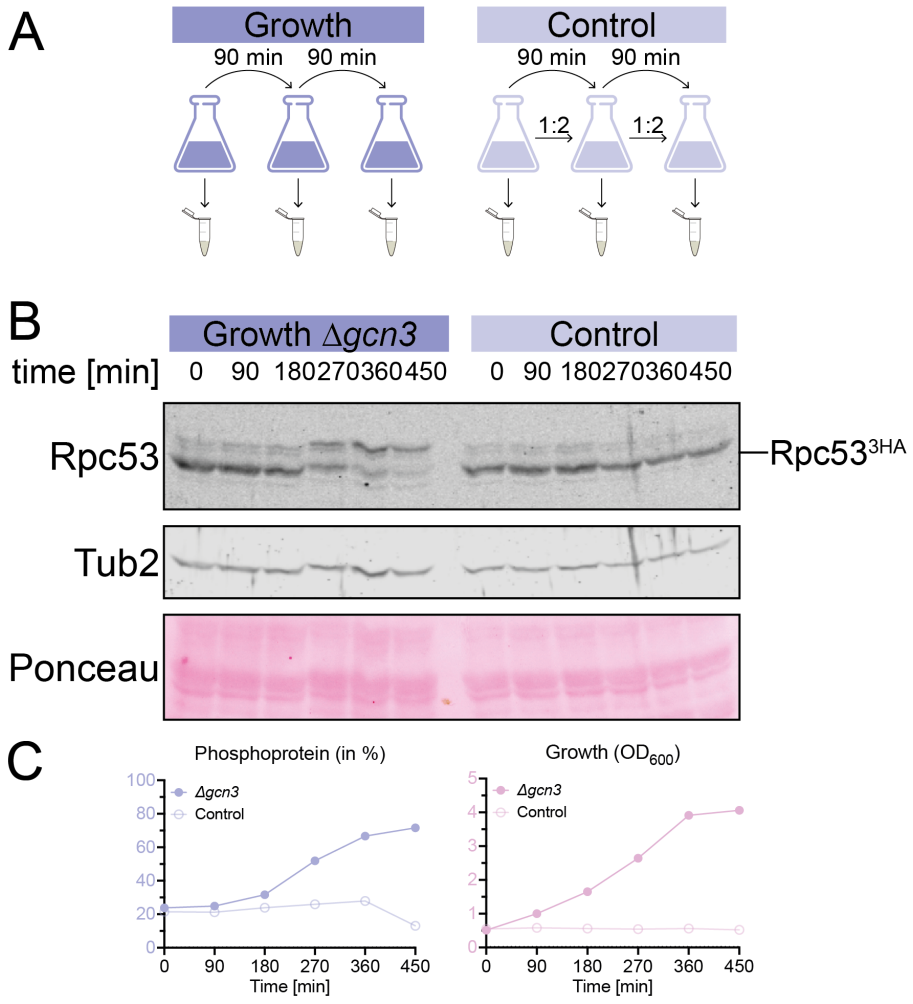

Figure S 2 Rpc53 phosphorylation increases during diauxic shift, independent of Gcn3.

A. Schematic overview of the experimental setup. Growth in *Δgcn3* background was measured every 90 min, and a control was maintained in exponential growth phase by diluting it 1:2

every 90 min. B. Western blot analysis of Rpc53 expression in a growth curve. The samples were collected every 90 min. Rpc53-3HA was detected using an α-HA antibody. Slower migrating bands resembled the phosphorylated isoforms of Rpc53. Tub2 was used as a reference and proper loading was controlled using Ponceau staining. C. Graphical visualization of Rpc53 phosphorylation in relation to total protein (%) (growth: blue filled circles, control: blue open circles). OD_{600} was used to determine the growth phases (growth: pink filled circles; control: pink open circles).

9.1.2 Kns1-dependency of carbon source specific Rpc53 phosphorylation

As described in section 4.2.2, the data showed a significant increase in Kns1 protein levels and Rpc53 phosphorylation in a carbon source-dependent manner. The correlation between Kns1 protein increase and its activity, however, has not been verified. Therefore, Rpc53 phosphorylation was evaluated in a *Δkns1* background using different carbon sources (Figure S 3 A). The analysis showed a strong Kns1-dependent increase in Rpc53 phosphorylation in the presence of raffinose and glycerol (Figure S 3 B). In the *Δkns1* background only minimal phosphorylation signals were detected. As expected, Rpc53 showed an increase in the phosphorylated proportion, from 30 % in glucose to approximately 90 % in raffinose and glycerol (Figure S 3 C). When *KNS1* was deleted, this effect was significantly reduced. The *Δkns1* cells in glucose showed 10 % phosphorylated Rpc53, which only increased to 30 – 40 % in raffinose and glycerol, respectively (Figure S 3 C). This confirmed the assumption that Kns1 is the only kinase necessary for a carbon source-dependent increase in Rpc53 phosphorylation.

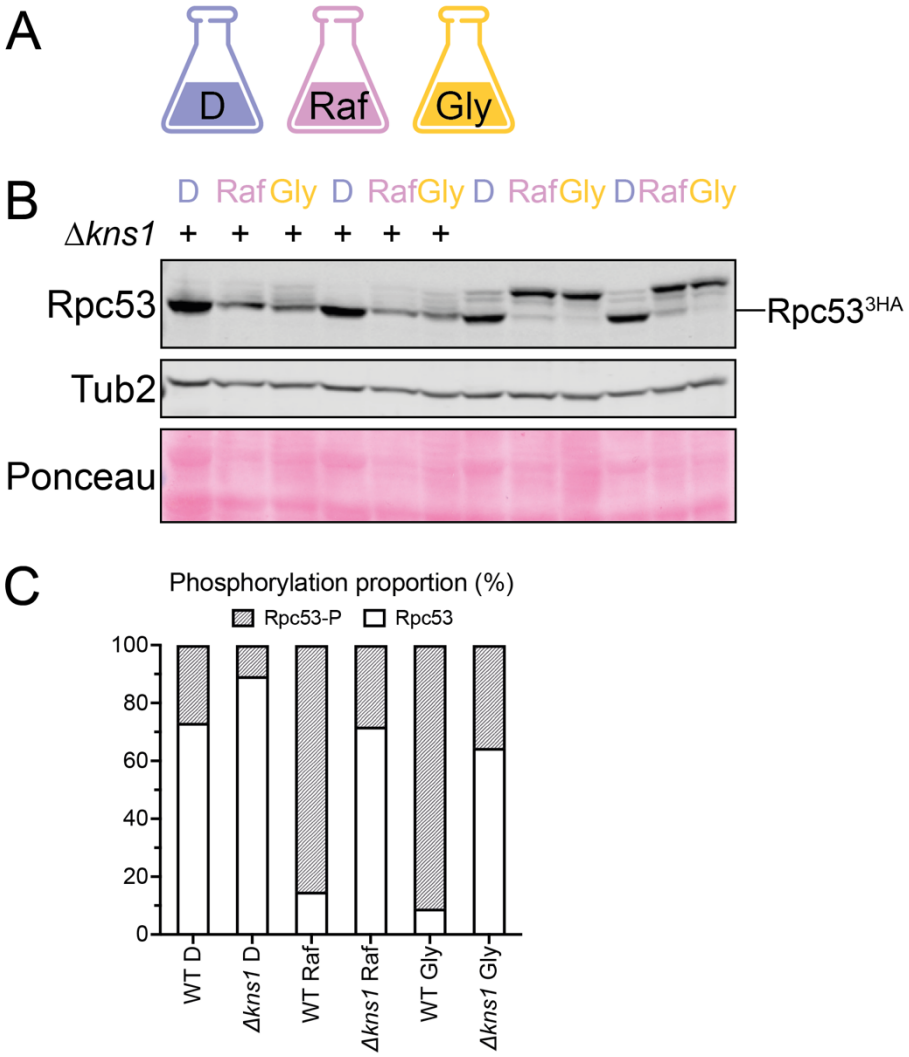

Figure S 3 Rpc53 phosphorylation increase under unfavourable conditions is Kns1-dependent.

A. Used carbon sources for this experiment were glucose (D), raffinose (Raf) and glycerol (Gly). B. Western blot analysis of Rpc53 expression and phosphorylation levels in different carbon sources comparing WT and *Δkns1* background. Slower migrating bands represent phosphorylated Rpc53 isoforms. Rcp53-3HA was detected by using an α-HA antibody. Tub2 was used as a reference and proper loading was controlled using Ponceau staining. C. Phosphorylated and unphosphorylated signals from B were calculated in proportion to total Rpc53 levels. The mean relative proportion is expressed as a percentage (n = 2). Grey portions indicate phosphorylated values and white boxes indicate unphosphorylated proportions.

The dynamics of Kns1 expression and activity in response to nutrient changes are evaluated in section 4.2.3. The data revealed a gradual increase in Kns1 expression over time upon shifting to unfavourable conditions (Figure S 4 B, C). Rpc53 phosphorylation levels increased correspondingly, reaching a maximum phosphorylation level earlier (Figure S 5 B, C). To rule out potential stress due to experimental conduction that leads to the activation of Kns1, a control was conducted. The medium was exchanged from glucose- to glucose-containing medium but treated the same as in the experiment. An increase In Kns1 expression and activity due to technical issues would lead to a similar increase in Kns1 levels in the control. The

control, however, showed constant Kns1 expression over time and no phosphorylation shift of Rpc53 (Figure S 4 B, C and Figure S 5 B, C).

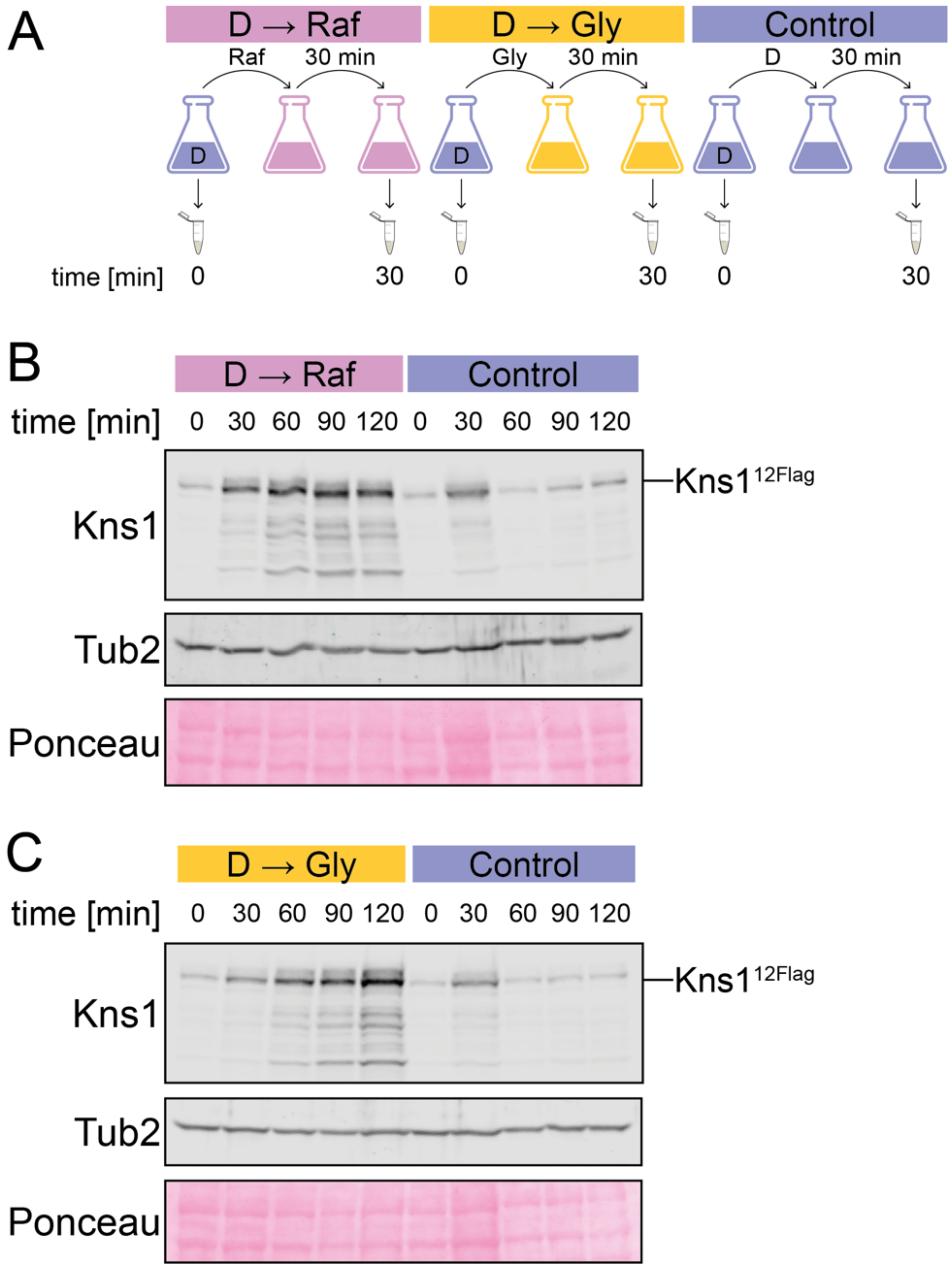

Figure S 4 Increasing Kns1 expression upon carbon source shift from favourable to unfavourable conditions.

A. Experimental setup of the carbon source shift. Starting cultures included glucose (D) and served as a time point 0. The medium was then replaced with either raffinose (Raf)- or glycerol (Gly)-containing media and incubated for 30 min. Samples were then taken every 30 min for 2 h. The medium was changed from glucose- to glucose-containing medium as a control and was treated in the same manner as the shifts. B. Western blot analysis of endogenous Kns1 levels in a carbon source shift from D to Raf. Kns1-12xFlag was detected using an α-Flag antibody. Tub2 was used as a reference, and proper loading was controlled using Ponceau staining. The sampling intervals are indicated in min. C. Western blot analysis of endogenous Kns1 levels in a carbon source shift from D to Gly. Kns1-12xFlag was detected using an α-Flag antibody. Tub2 was used as a reference, and Ponceau staining controlled the proper protein loading. The sample intervals are given in min.

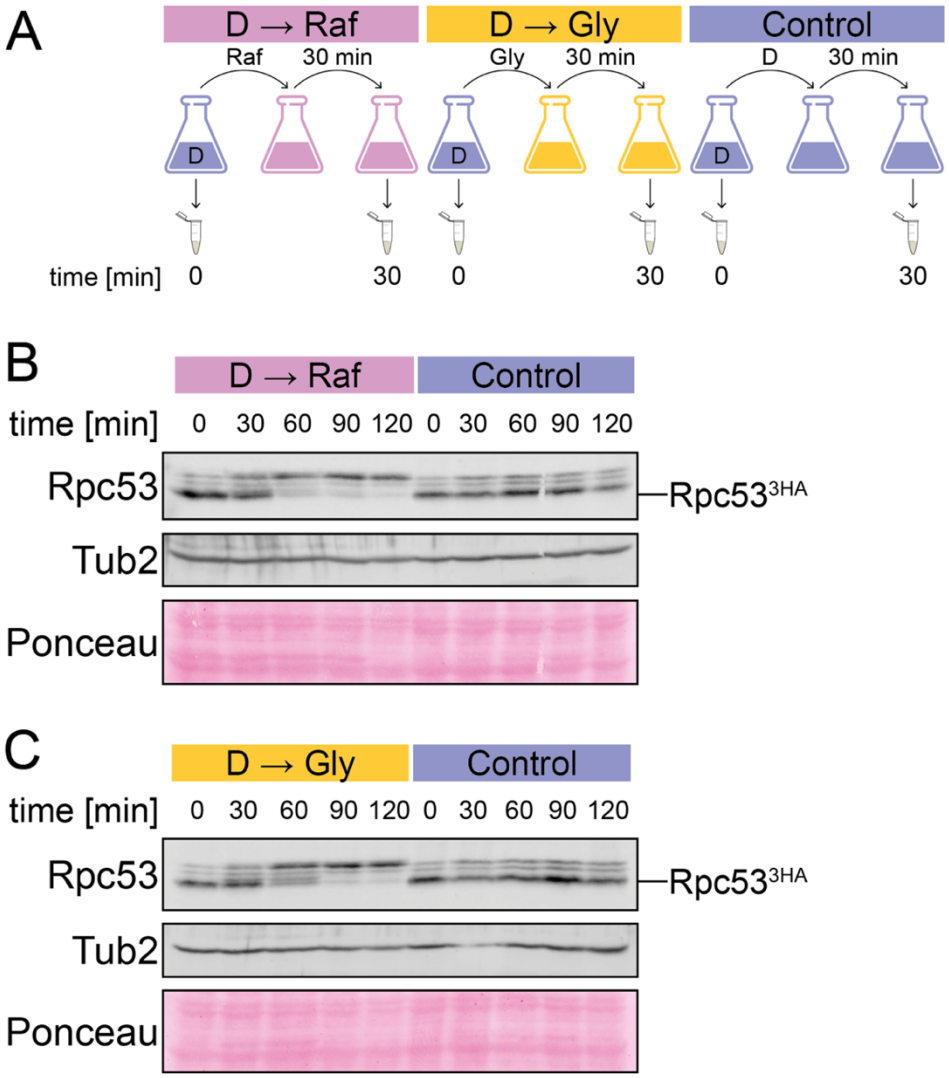

Figure S 5 Rising Rpc53 phosphorylation levels upon carbon source shift from favourable to unfavourable conditions.

A. Experimental setup of the carbon source shift. Starting cultures included glucose (D) and served as a time point 0. The medium was then replaced with either raffinose (Raf)- or glycerol (Gly)-containing media and incubated for 30 min. Sampling was performed every 30 minutes for 2 hours. The medium was changed from glucose- to glucose-containing medium as a control and was treated in the same manner as the shifts. B. Western blot analysis of Rpc53 expression and phosphorylation levels in a carbon source shift from D to Raf. Rpc53-3HA was detected using an α-HA antibody. Slower migrating bands represent phosphorylated Rpc53 isoforms. Tub2 was used as a reference, and proper loading was controlled using Ponceau staining. The sample intervals are given in min. C. Western blot analysis of Rpc53 expression and phosphorylation levels in the presence of a carbon source shift from D to Gly. Rpc53-3HA was detected using an α-HA antibody. Slower migrating bands reveal phosphorylated Rpc53 isoforms. Tub2 was used as a reference, and Ponceau staining controlled the proper protein loading. The sampling intervals are indicated in min.

9.1.3 TORC1-mediated regulation of promoter activity

In section 4.3.1, the data suggested that Kns1 expression and activity increased after TORC1 inhibition. As a negative effector kinase of TORC1, Kns1 regulates RNA Pol III activity under non-proliferative conditions. The question of how this increase is achieved under the TORC1 block was evaluated with an analysis of the reporter system, first described in section 4.1.4. The reporter that showed promoter activity was used under TORC1 active and inactive conditions, and the expression levels were compared (Figure S 6 A). The data revealed that TORC1 inhibition led to a decrease in reporter protein levels (Figure S 6 B). The protein levels dropped to approximately 50 % after blocking TORC1 activity compared to WT conditions, which indicated a strong negative influence of inhibited TORC1 function on promoter activity (Figure S 6 C). These data are in contrast to the increase in Kns1 protein levels under the inhibition of TORC1.

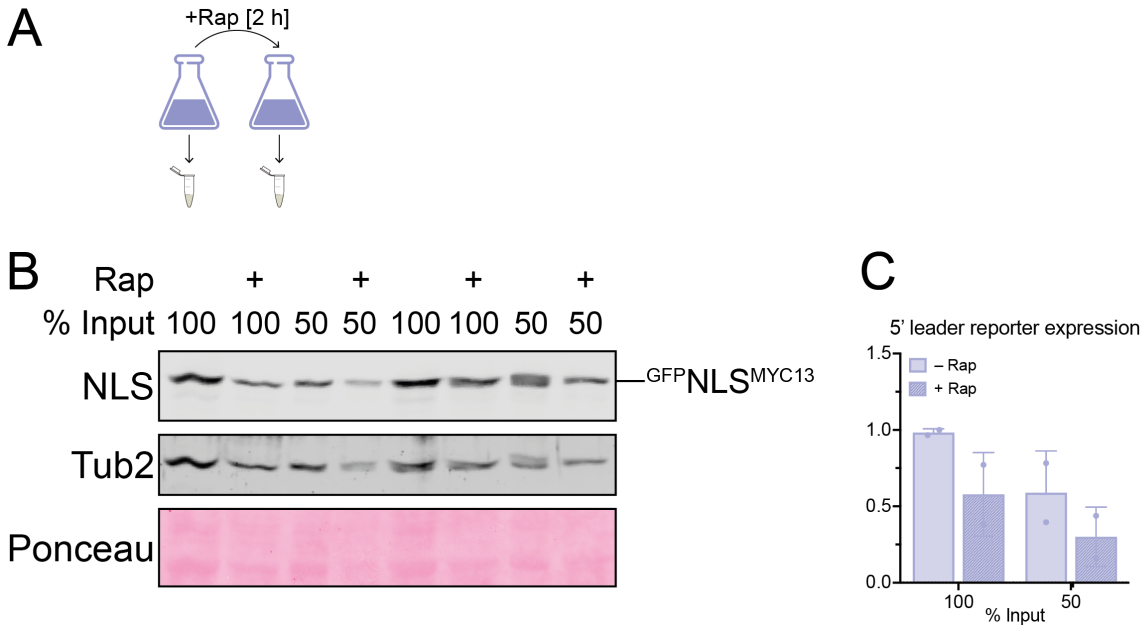

Figure S 6 Increase of Kns1 protein upon TORC1 block independent of the regulatory region.

A. Experimental conditions included a sample before treatment, used as WT conditions, and a sample after 2 hours of rapamycin treatment to fully block TORC1 activity. B. Western blot analysis of the reporter (GFP-NLS-MYC13) under conditions of TORC1 activity and TORC1 block (indicated by +). The reporter protein NLS was detected using an α-MYC antibody and different inputs were applied (annotated in %). Tub2 was used as a reference, and Ponceau staining was used to control protein levels. C. Quantification of the signals of B. Mean values of two technical replicates normalized to Tub2 are given. The individual values are depicted as dots, and the standard deviation (SD) is given in bars. The % inputs are visualized on the x-axis. The conditions analysed were as follows: no rapamycin treatment (- Rap) and rapamycin treatment (+ Rap).

9.1.4 Quantification of Kns1 fragment expression for localisation analyses

Kns1's localisation is dependent on its N-terminal domain and the two distinct nuclear localisation sequences (NLSs) within, as section 4.5.1 revealed. The different fragments used in this analysis exhibited varying signal strength. To verify that this is due to a differentiated expression and not due to technical reasons, the protein levels were measured under steady-state conditions by western blotting. Full-length Kns1 showed very low protein levels, although it was overexpressed by the constitutive promoter *TEF* (Figure S 7 A). Using only the catalytically active CTD, the protein levels drastically increased by almost 10-fold (Figure S 7 A, B). The short N-terminal fragment NTD(1-174) showed stronger expression compared to the WT full-length construct (Figure S 7 A, B). The NTD, however, was rather low in expression, similar to that of full-length variants, indicating a destabilizing effect of the N-terminus (Figure S 7 B).

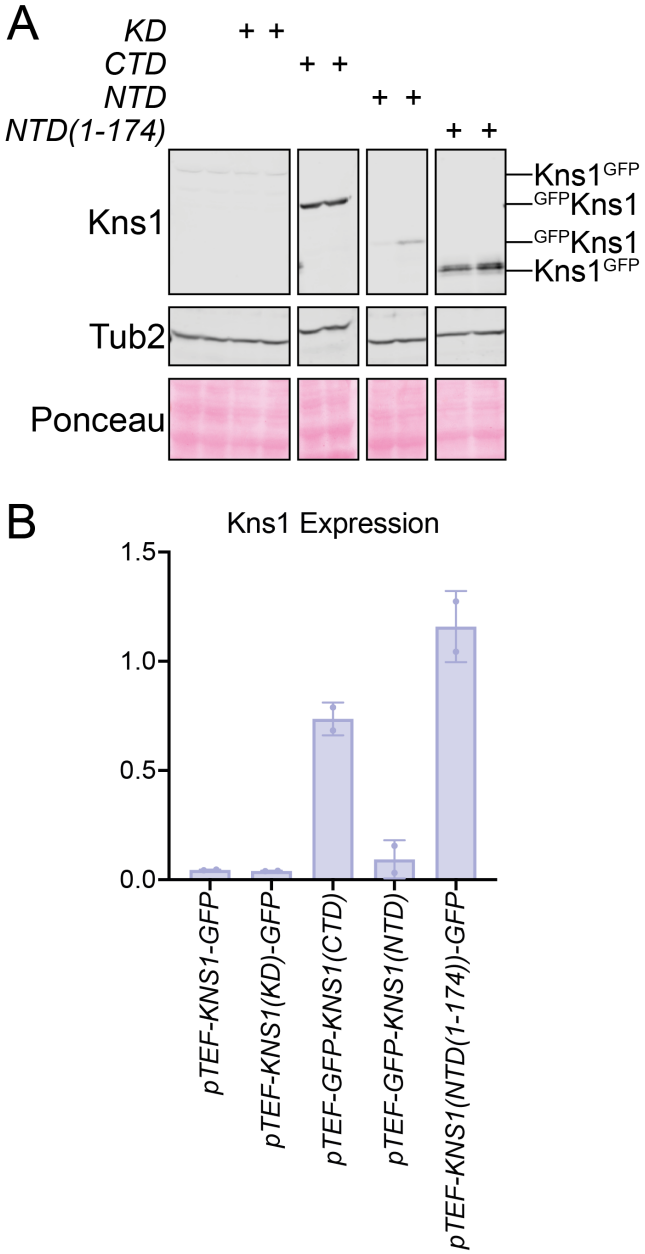

Figure S 7 Expression levels of used *pTEF*-overexpression fragments for localisation analysis.

A. Western blot analysis of constitutively overexpressed Kns1 including full-length (WT), kinase dead mutant (KD, D440A mutation), the C-terminal domain of Kns1 (CTD), the N-terminal domain of Kns1 (NTD) and a fragment of the NTD (NTD(1-174)). All different genotypes are indicated by +. Biological duplicates of GFP-marked Kns1 were detected using an α-GFP antibody. Tub2 was used as a reference, and proper loading was controlled with Ponceau staining. The analysis was performed by Kathrin Preußel Danger. B. The mean signal intensities from A were calculated and normalized to Tub2. Single values are given as dots, and standard deviation (SD) is given in bars.

Furthermore, similar experiments regarding the localisation of Kns1 and the involvement of different domains were conducted with the inducible promoter *GAL* for an even stronger overexpression (section 4.5.1). The expression of these constructs was also evaluated under steady-state conditions with the simultaneous induction of *pGAL* for 2 h for all fragments. The differences in protein levels were not as strong as those of the *pTEF* variants but were clearly distinguishable (Figure S 8 A). The full-length variant, independent of its catalytic function, showed rather low protein levels even under strong overexpression conditions (Figure S 8 A). The C-terminal domain showed strong expression, similar to the *pTEF*-overexpressed variant, and protein levels were increased approximately 5-fold compared to the WT (Figure S 8 A, B). The protein levels of CTD(166-737) were slightly lower than those of the CTD yet still strongly increased compared to the WT (Figure S 8 A, B).

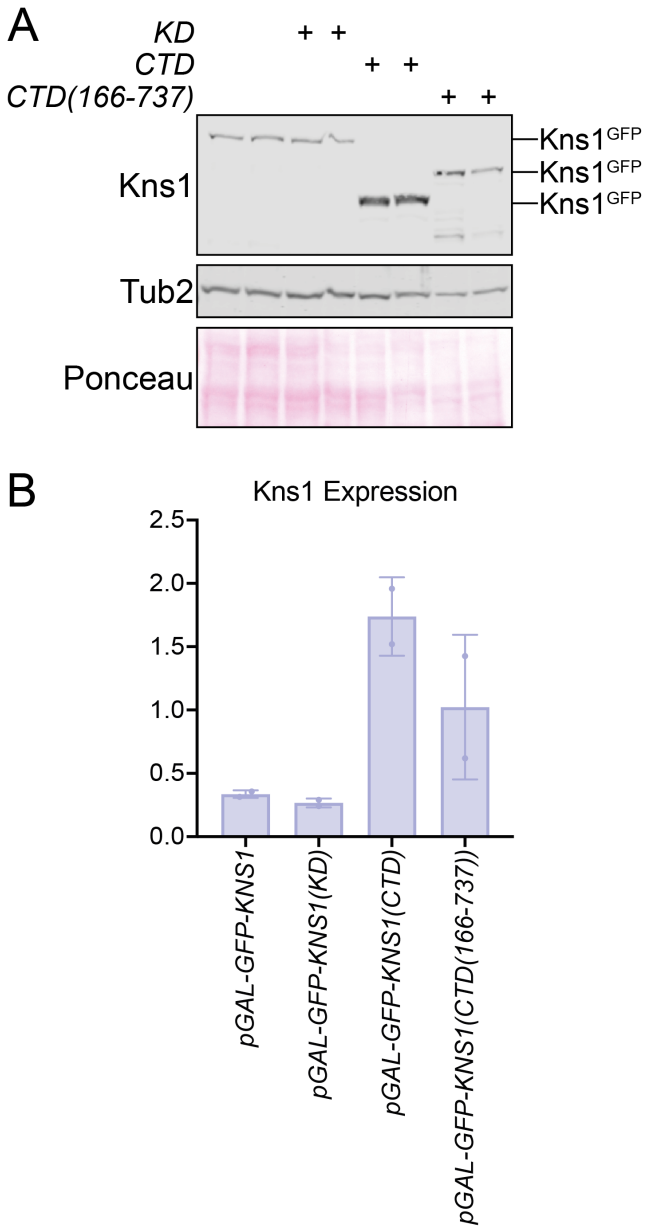

Figure S 8 Expression levels of *pGAL*-overexpression fragments used for localisation analysis. (Description on next page)

A. Western blot analysis of inducible overexpressed Kns1 including full-length (WT), kinase dead mutant (KD, D440A mutation), the C-terminal domain of Kns1 (CTD) and a long version of the CTD (CTD(166-737)). All different genotypes are indicated by +. Biological duplicates of GFP-marked Kns1 were applied and detected with an α-GFP antibody. Tub2 was used as a reference, and proper loading was controlled with Ponceau staining. The analysis was performed by Kathrin Preußel Danger. B. The mean signal intensities from A were calculated and normalized to Tub2. Single values are given as dots, and standard deviation (SD) is given in bars.

9.1.5 Growth defect of *Δise1* strain background

The 26S proteasome is a key player in the regulation of proteolysis, as demonstrated in numerous studies (Liu *et al.* 2007; Budenholzer *et al.* 2017; Bard *et al.* 2018). In this context, Kns1 underwent rapid degradation, as described in section 4.5.5, which was further elucidated by investigating the influence of the 26S proteasome on its degradation. To accomplish this, proteasomal activity was inhibited using MG132, a substance that effectively blocks 26S proteasomal active sites (Liu *et al.* 2007). To facilitate the uptake of MG132, the membrane was made permeable by deleting *ISE1*, a membrane component. However, *Δise1* exhibits reduced growth at 22 – 30 °C (Gaber *et al.* 1989). To determine the suitable conditions for the MG132 block in this study, a growth test was conducted, comparing the *Δise1* mutant with the WT strain on glucose-, raffinose-, and glycerol-containing media (Figure S 9). Strains with and without Flag-marked Kns1 were analysed at 25, 30, and 37 °C. *Δise1* displayed a strong growth deficit under all carbon source conditions at 25 °C, which was slightly reduced at 30 °C (Figure S 9). The phenotype at 37 °C was only visible under glycerol conditions, confirming temperature-dependent growth deficiency (Figure S 9). Because the effect was minimised at 30 °C for all conditions, this temperature was chosen as a compromise between slower growth and practical considerations.

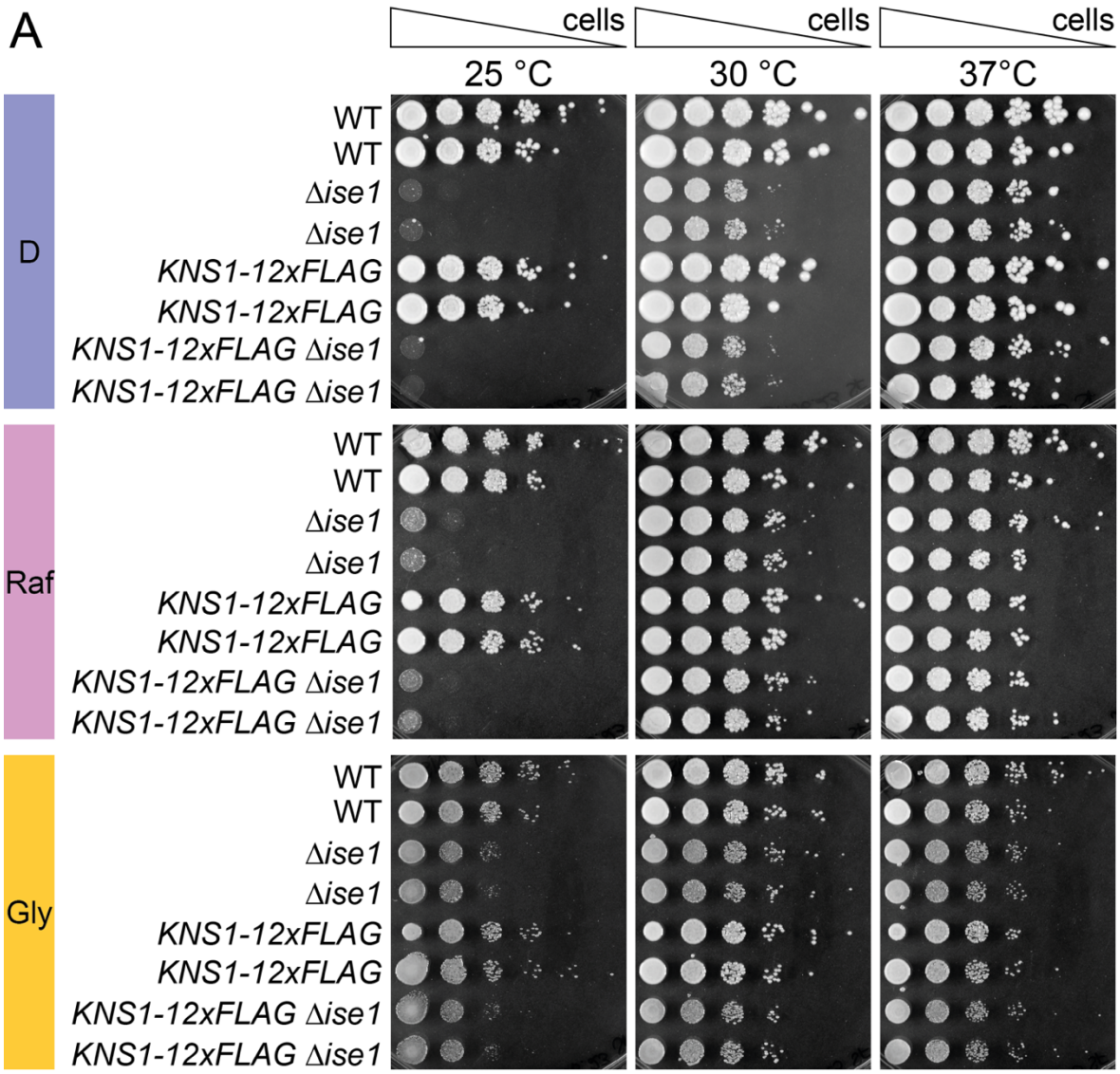

Figure S 9 Phenotypic analysis of *Δ*ise1 mutant under different carbon source conditions and temperatures.

A. The mutant *Δise1* was compared with the WT yeast strains. Additionally, strains with epitope-marked Kns1 (*KNS1-12xFLAG*) were analysed. Glucose (D), raffinose (Raf), and glycerol (Gly) were the carbon sources tested. The spot test of a dilution row was performed at 25, 30, and 37 °C, and the plates were incubated for two days.

9.1.6 Amino acid enrichment analysis

The N-terminal domains (NTDs) of proteins are often unstructured and important for protein stability and regulation. The potential destabilising function of NTDs is dependent on the amino acid composition within this domain compared to that of the total protein (Jadhav and Wooten 2009). This N-end rule distinguishes between stabilising and destabilising amino acid residues. Met, Ser, Ala, Thr, Val, or Gly in the N-terminus are known to stabilise and proteins usually have half-lives greater than 20 h. N-terminal Phe, Leu, Asp, Lys, and Arg are known to destabilise, and the half-life of these proteins is usually less than 3 min. High levels of destabilising residues in the NTD are called N-degrons and target proteins for proteasomal degradation. As Kns1 showed a half-life of less than 10 min in section 4.5.5, it was assumed that this could be due to an N-degron in Kns1's NTD. The destabilising effect was analysed by calculating the amino acid composition of the N-terminus compared to the total protein. To evaluate the amino acid composition of the proteins, their corresponding occurrences were counted (Table 45). Potentially destabilising amino acid residues (Phe, Leu, Asp, Lys, Arg) were counted in the NTD (1 – 279 aa) and total protein (1 – 737 aa)

Then, the amino acid frequency (F) was calculated for the NTD and full-length protein using Equation 6 in the respective regions.

$$\mathrm{F} = \frac{\text{number of destabilising aa}}{\text{number of total aa}}$$

Equation 6 Amino acid frequency (F) calculation using the number of destabilising aa residues and total number of amino acids (aa) in a specific region.

Using these frequencies, an enrichment ratio can be calculated. The value of this ratio (Equation 7) either supports or denies the presence of an N-degron. When the enrichment ratio was higher than 1, the destabilising amino acid residues in the NTD were enriched compared with the total protein. When the ratio equals 1, the residues have the same frequency as the total protein in a specific region. When the enrichment ratio was < 1, destabilising residues were less frequent in the specific region than in the total protein.

$$\text{Enrichment} = \frac{\mathrm{F(NTD)}}{\mathrm{F(total)}}$$

Equation 7 Calculation of the amino acid enrichment ratio.

The frequencies (F) of the specific region, the N-terminal domain (NTD), and total protein were used to calculate the possible enrichment of destabilising amino acids in the NTD.

All residues showed an enrichment of less than 1, suggesting that these residues were not enriched in the N-terminus compared with the full protein, and the N-end rule likely does not apply to Kns1 degradation (Table 45).

Table 45 Calculation of enrichment ratios of destabilising amino acids in Kns1(NTD).

The amino acids (aa) Phe, Leu, Asp, Lys and Arg were counted in the NTD (1-279 aa) and full-length (1-737 aa) proteins. The corresponding amino acid frequencies (F) were calculated for both regions using Equation 6 and are given in %. The enrichment ration was then calculated using Equation 7.

aa	1-279 aa	1-737 aa	F(total) (%)	F(NTD) (%)	Enrichment ratio
Phe	11	32	4.34	3.94	0.91
Leu	25	69	9.36	8.96	0.96
Asp	13	45	6.11	4.66	0.76
Lys	14	52	7.06	5.02	0.71
Arg	13	37	5.02	4.66	0.93

9.1.7 Delay in eIF2α phosphorylation in diauxic shift response

Ashe *et al.* (2000) stated that glucose deficiency leads to translational inhibition, which occurs without the need for eIF2α phosphorylation. This process takes less than a minute and only later on, eIF2α phosphorylation increases. A similar pattern was observed during the diauxic shift in this study. In the diauxic shift, Rpc53 phosphorylation, mediated by an increase in Kns1 expression, most likely in response to reduced translation initiation and changed nutrient availability, occurred before eIF2α phosphorylation (Figure S 10). Rpc53 phosphorylation increases from 180 min on and reaches its maximum level at 270 min of the growth analysis (Figure S 10 B). The phosphorylation of eIF2α, however, only appears after 360 min. The response of Kns1 activity, visible through Rpc53 phosphorylation shifts, is thus faster than the Gcn2 activity. A change in carbon source availability during diauxic shift is mediated more rapidly by Kns1 than eIF2, which also indicates that Kns1 response via altered carbon sources are independent of eIF2α phosphorylation. A Kns1 regulation via the ISR is still conceivable, as changes in metabolism could lead to decreased translation initiation without eIF2α phosphorylation.

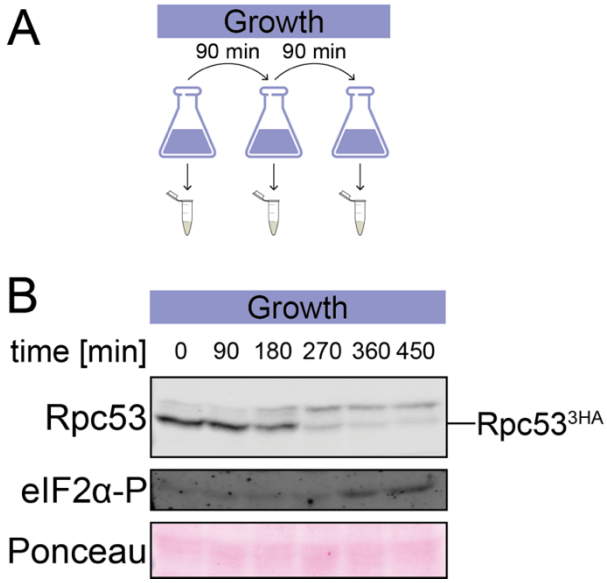

Figure S 10 Delay in eIF2α phosphorylation during diauxic shift.

A. Schematic overview of the experimental setup. Growth in WT cells was measured every 90 min. B. Western blot analysis of Rpc53 expression in a growth curve. The samples were collected every 90 min. Rpc53-3HA was detected using an α-HA antibody. Slower migrating bands resembled the phosphorylated isoforms of Rpc53. Phosphorylation of eIF2α was detected using an eIF2α-P-specific antibody that recognises phosphorylation on Ser51. Proper loading was controlled using Ponceau staining.

9.2 List of Abbreviations

%	percent
°C	degrees Celsius
++	medium with all amino acids
1C	single DNA content
2C	double DNA content
α	anti (antibodies)
Δ	deletion
Δ326	C-terminal truncation of Cdc123 at amino acid 326
µ	micro
µF	micro farad, electric capacity

A

a	length
A	area
aa	amino acids
AAP	arginine attenuator peptide
AB	antibody
acetyl-CoA	acetyl-coenzyme A
AD	transcription activating domain
Amp	ampicillin
AMP	adenosine monophosphate
AMPK	adenosine monophosphate kinase
APC/C	anaphase promoting complex/cyclosome
APS	ammonium persulfate
ATP	adenosine triphosphate

B

b	width
BD	binding domain
bp	base pair
BSA	bovine serum albumin

C

c	height
C	cytokinesis
C-terminus	carboxy-terminus
cAMP	cyclic adenosine monophosphate
CDC	cell division cycle genes
CDK	cyclin-dependent kinase
cDNA	complementary DNA
CHX	cycloheximide

clonNAT	nourseothricin
CP	core particle
CSRE	carbon source-responsive element
C_T	cycle threshold
CTD	C-terminal domain

D

D	glucose
Da	Dalton
DEPC	diethylpyrocarbonate
DHAP	dihydroxyacetone phosphate
DIC	differential interference contrast
DMSO	dimethyl sulfoxide
dNTP	deoxyribonucleoside triphosphate
DTT	dithiothreitol
DUB	deubiquitinating enzyme

E

E	primer efficiency
E. coli	*Escherichia coli*
EDTA	ethylenediaminetetraacetic acid
eEF	eukaryotic elongation factor
EGOC	EGO complex
eIF	eukaryotic initiation factor
ER	endoplasmic reticulum
EtBr	ethidium bromide
EtOH	ethanol

F

F	amino acid frequency
F-primer	forward primer
FAD	flavin adenine dinucleotide
FADH	flavin adenine dinucleotide (hydroquinone), reduced
FAT	FRAP-ATM-TRRAP domain
FC	fold change
FKBP	FK506-binding protein
FRB	FKBP12-rapamycin-binding
FSC	forward scatter

G

g	gram or relative centrifugal force (g-force)
G	gap phase
G3P	L-glycerol-3-phosphate
G418	kanamycin
GAAC	General amino acid control

GAP	GTPase-activating protein
GCN	General control non-derepressible
gDNA	genomic DNA
GDP	guanosine diphosphate
GEF	guanine nucleotide exchange factor
GFP	green fluorescent protein
Gly	glycerol
GOI	gene of interest
GSK3	glycogen synthase kinase 3
GTP	guanosine triphosphate

H

h	hours
H_2O	water
HA	haemagglutinin
HDAC	histone deacetylase complex
HU	hydroxyurea

I

IC	initiation complex
ICR	internal control region
IHRES	internal ribosome entry site
ISR	integrated stress response

K

KD	kinase dead mutation
kV	kilo volt

L

l	litre
LB	Luria broth
LiAc	lithium acetate
LSB	Laemmli sample buffer

M

m	slope or milli
M	mitosis or molar (mol/l)
m7G	7-methylguanosine cap
mA	milli ampere
MAT	mating type
MFC	multifactor complex
MG132	carbobenzoxyl-leucinylleucinyl-leucinal
min	minutes
ml	milli litre
mm	milli metre

mtRNA	mitochondrial RNA
MYC	c-myc-epitope

N

n	number of samples
N-terminus	amino-terminus
NAD	nicotinamide adenine dinucleotide
NADH	nicotinamide adenine dinucleotide, reduced
ng	nano gram
NLS	nuclear localisation sequence
nm	nano metre
Noc	Nocodazole
ns	not significant
nt	nucleotides
NTD	N-terminal domain

O

OD	optical density
ONPG	ortho-nitrophenyl-beta-D-galactopyranoside
ORF	open reading frame

P

p	promoter
P	perimeter or phosphate
PABP	poly(A) binding protein
PAC	polymerase A and C sites
PAGE	polyacrylamide gel electrophoresis
PCR	polymerase chain reaction
PEG	polyethylene glycol
PFK	phosphofructokinase
Phos-tag	1,3-bis(bis(pyridin-2-ylmethyl)amino)propan-2-olato dizinc(II)
phospho	phosphorylation
PIC	pre-initiation complex
PIKK	PI kinase related protein kinase
PKA	protein kinase A
pLDDT	score prediction of local distance difference test
PP	protein phosphatase
PQC	protein quality control
PTM	post-translational modification
px	pixel

Q

qPCR	quantitative PCR

R

R	roundness
r	ribosomal
R-primer	reverse primer
RA	relative abundance qPCR
Raf	raffinose
RHEB	Ras homolog enriched in brain
RiBi	ribosome biogenesis factors
RNA Pol I-III	RNA polymerase I-III
RP	regulatory particle
rpm	rounds per minute
RRPE	ribosomal RNA processing element
RT	room temperature

S

S	synthesis phase
S. cerevisiae	*Saccharomyces cerevisiae*
SD	selective medium with dextrose or standard deviation
SDS	sodium dodecyl sulfate
sec	seconds
SMC	structural maintenance of chromosomes
SOC	super optimal broth with catabolite repression
SSC	sideward scatter
SU	subunit

T

t	time interval
TAE	Tris acetate EDTA
TBP	TATA-binding protein
TBS	Tris buffered saline
TBS-T	Tris buffered saline with Tween
TC	ternary complex
TCA	tricarboxylic acid
TE	Tris EDTA
TEMED	N,N,N´,N´-tetramethylethylendiamine
TES	Tris EDTA SDS buffer
TOR	Target of Rapamycin
TORC	Target of Rapamycin Complex
TOROID	TORC1 organized in inhibited domains
Tris	Tris(hydroxymethyl)aminomethane
$tRNA_i^{Met}$	initiation methionyl tRNA
TSC	tuberous sclerosis complex
TSS	transcription start site
Turbo-LRB	Turbo Laemmli running buffer

U

U	unit (beta-galactosidase activity)
uORF	upstream ORF
UPR	unfolded protein response
UPS	ubiquitin-proteasome system
UTR	untranslated region

V

V	volume
V-ATPase	vacuolar proton pump
w/v	weight per volume
WT	wildtype

X

XY	yeast optimal medium

Y

Y2H	yeast-2-hybrid
YNB	Yeast nitrogen base

Z

z	layer
ZBD	zinc binding domain

9.3 Index of Figures

9.4 Index of Tables

9.5 Index of Equations

10 ACKNOWLEDGEMENTS

"No one who achieves success does so without acknowledging the help of others.
The wise and confident acknowledge this help with gratitude."

– Alfred North Whitehead

I would like to express my gratitude to the multitude of people involved in this doctoral thesis.

First, I would like to thank Prof. Dr. Wolfgang Seufert. Thank you for the opportunity to stay in your group and work on this PhD thesis, Wolfgang. Thank you for the continuous support over the last few years, the many fruitful discussions we had, and the technical advice and knowledge you shared with me during this time. I enjoyed working in your group and learned a lot.

I would also like to thank my two mentors, Prof. Dr. Joachim Griesenbeck and Prof. Dr. Boris Pfander, for their continuous support and scientific input on my work over the last five years. I would also like to thank Achim for supporting my mental health. You helped me calm down and encouraged me to keep fighting for what I love. I also cannot thank you enough for all the discussions on my data and their potential meaning, as well as the figure layout, not only in my annual reports but also in meetings in between. Thank you for agreeing to be the second referee to this thesis, too.

Thank you Prof. Dr. Frank Sprenger for your technical support over the years and the great atmosphere of the group. I will definitely remember the cocktail parties and fun summer days. I would also like to thank you for agreeing to be my 3rd examiner for this thesis, Frank.

It was also a pleasure to work with many great people in this group. First, thank you Franzi for guiding me at the start of this thesis and helping me with my research proposals and ideas for the first poster sessions. It was great to have your expertise on daily tasks and the structure of my PhD work. Second, thank you, Julia, for quickly becoming a friend after joining this group. You supported me during the last phase of my thesis, were a great office companion ("Teamwork makes the dream work") and helped me with my figures for posters and this thesis. I am grateful for the distractions you initiated with many fun game nights. In addition, thank you so much for correcting my thesis. A big thank you also goes to Andrea, Antje and Adelheid. You are not only the technical assistance behind this work, but also the women with magic hands. While I tried to do as much of cloning and yeast strain generation myself, there are moments where you must accept that others are simply more practiced in these tasks. In addition, thank you for your patience with my many questions on buffers and solutions and how to prepare them correctly. Thank you, Andrea, for many years of easy

communication and reliable preparation for the practical courses. Thank you for your emotional support and discussions on private topics. It was my pleasure to work with you. Thank you, Philipp, for your support with the confocal microscope, and your tips and tricks for editing and quantifying the images in ImageJ. A huge thank you goes to Arlett. You are the good soul of the group and the heart that keeps everything together. Thank you for your continuous support on all tasks, buying pink lab equipment to brighten my mood, searching for the right chemicals, and fighting for my contracts. Thank you for your emotional support. You are the reason why I am still sane and had a place to load all my mental issues. Thank you for thinking about others first, even when your own life is full of challenges. Thank you to everyone else in our group and the Sprenger group, too. I always enjoyed working with you, and our joint lunches were a great way to have scheduled breaks every day.

I would also like to thank all my super-motivated students who helped me shape this project along the way. Thank you, Veronika, Carina, Johannes, Jannis, Ferdinand, Severin, Kathrin and Yannick. I had a great time teaching you, and I enjoyed working with you all a lot. You all helped me with my project, suggested your own ideas, did a lot of testing on hypotheses, and generated a lot of data for me. Special thanks go to Ferdi, who helped me back on track during my mid-PhD crisis. Your positive energy is contagious. You took over a huge workload in your student helper's job with so much passion. Thank you to Jannis and Kathi for trusting me so much that you joined me and the project twice. That means a lot to me. Thank you for all your suggestions on my work. Special thanks go to Kathi for correcting my thesis, even though you are no longer part of the group. I cannot say thank you to you often enough. Finally, thank you, Yannick, for your great energy, all the fun we had, and all the struggles we fought together last year. Your passion and motivation have greatly pushed this project. I really enjoyed all our little breaks with music, memes, and pokémon hunting, and your stress chocolate was highly appreciated.

I would also like to thank a couple of people who helped me work on my future and keep my mental health on track during this PhD thesis. Thank you to the RIGeL team, Kinga and Caro, for helping me with my career plans, my mental issues and problems, pushing me to stay strong, encouraging my sometimes insecure soul, and supporting me with connections and information so that I someday might achieve what I am working for. Additionally, it was my great pleasure to develop and work on the MINT Labs projects, brainstorming ideas, making science accessible for children, and organising our courses. I also want to thank Sandra and Fabian and the entire MINT Labs Regensburg e.V. team. Thank you for the opportunity to share my passion for microorganisms (and plants) with you and the children. I had so much fun, improving our courses and adapting the content to different age groups. Thank you for supporting my work outside academia and for the easy communication on all topics. Thank you, Sandra, for all our coffee breaks or Christmas market evenings with lots and lots of talking about our futures, careers, and personal lives. Of course, I would also like to thank my friends for keeping in touch for a long time. Thank you for your mental support, although our paths have become very different. In particular, I would like to

thank you, Vroni, for correcting part of this thesis while being occupied with your own scientific work. It means a lot to me. Thank you.

And last but not least, I would like to thank my family. Thank you, Mum, Dad, and Tanja, for supporting me all this way. Thank you for your ongoing encouragement over the years, for listening to my problems and struggles, and for letting me choose whatever path I think works best for me. Thank you, Matze, for always having my back, understanding that this is what I love to do, and for your genuine support over all those years. Thank you for accepting all my mental breakdowns and high-stress phases, and caring for me when I sometimes cannot do it myself. Thank you for helping me figure out my life and career along the way, and for being there for me all the time, despite having your own career.

I would not be here today, if not for all your support. Thank you so much!